

Design of an inspection robot for
small diameter gas distribution mains

Edwin Dertien



Design of an inspection robot for small diameter gas distribution mains

Edwin Dertien

Promotiecommissie

Voorzitter, secretaris	prof. dr. ir. P. M. G. Apers	Universiteit Twente
Promotoren	prof. dr. ir. S. Stramigioli	Universiteit Twente
	prof. dr. ir. J. van Amerongen	Universiteit Twente
Leden	prof. dr. A. A. Schäffer	Technische Univ. München
	prof. dr. ir. P. P. Jonker	Technische Univ. Delft
	prof. dr. ir. P. P. L. Regtien	Universiteit Twente
	prof. dr. ir. A. O. Eger	Universiteit Twente
Referenten	dr. ir. C.J.A. Pulles	KIWA Nederland B.V.
	dr. E. Zwicker	ALSTOM Inspection Robotics
Paranimfen	Gijs van Oort	
	Dennis Reidsma	

The research described in this thesis has been conducted at the Department of Electrical Engineering, Math and Computer Science at the University of Twente, and has been financially supported by a consortium consisting of KIWA Nederland B.V., Enexis, Liander, Cogas and Endinet. DEMCON and ALSTOM Inspection Robotics participated in the engineering of this project. More information can be found on <http://www.inspectierobot.nl>

CTIT Ph.D. thesis series no 14-318
Centre for Telematics and Information Technology
P.O. Box 217, 7500 AE Enschede, the Netherlands

Cover picture: the Objet Eden printer printing a series of parts for the robot. Inside cover: gas network of Arnhem by Liander documentation software. Cartoon at the back by Nozzman: <http://www.nozzman.com>

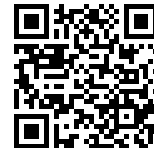
ISBN 978-90-365-3681-3
ISSN 1381-3618
DOI <http://dx.doi.org/10.3990/1.9789036536813>

Copyright ©2014 by E. Dertien, Enschede, The Netherlands.

No part of this work may be reproduced by print, photocopy or any other means without the permission in writing from the publisher. All pictures in this thesis have been reproduced with permission of the respective copyright holders.

Printed by Asbreuk, Enschede

CTIT



DESIGN OF AN INSPECTION ROBOT FOR SMALL DIAMETER GAS DISTRIBUTION
MAINS

PROEFONTWERP

ter verkrijging van
de graad van doctor aan de Universiteit Twente,
op gezag van de rector magnificus,
prof. dr. H. Brinksma,
volgens besluit van het College voor Promoties
in het openbaar te verdedigen
op donderdag 3 juli 2014 om 16:45 uur

door

Edwin Christian Dertien
geboren op 19 april 1979
te Smallerland

Dit proefschrift is goedgekeurd door:

prof. dr. ir. Stefano Stramigioli, promotor

prof. dr. ir. Job van Amerongen, promotor

Samenvatting

In ons land ligt ongeveer 100 000 km gasnet in stedelijk gebied. Dit gasnet wordt goed in de gaten gehouden, en moet worden vervangen zodra de kans op lekken toeneemt. Vervangen van het netwerk is duur, dus hoe langer de veiligheid nog gegarandeerd kan worden, hoe beter.

De oplossing die in deze thesis wordt onderzocht is een *serie autonome robots die zelfstandig door het netwerk bewegen en daarbij continu de kwaliteit van het netwerk monitoren en zwakke plekken in kaart brengen*. Vanuit deze context kan dit project gezien worden als een haalbaarheidsstudie voor deze oplossing: kan een robot überhaupt (zelfstandig) opereren in het gasnetwerk? Er wordt hierbij een antwoord gezocht op vijf deelvragen:

- Wat is, gegeven het netwerk, de beste methode voor een robot om zich voort te bewegen?
- Waar haalt deze robot zijn energie vandaan?
- Welke sensoren kunnen het beste door de robot gebruikt worden om iets over het gasnetwerk te vertellen?
- Hoe kan de robot het beste communiceren met de buitenwereld?
- Hoe kan de robot het beste bestuurd worden?

Om een antwoord te vinden op deze deelvragen zijn een drietal prototypes van een robotsysteem gemaakt. Het ontwerp van het voortbewegingsmechanisme is sterk afhankelijk van het gegeven gasdistributienetwerk. De belangrijkste (en meest bepalende) daarin zijn lange buissegmenten met een uitwendige diameter van 63 mm tot 125 mm, (haakse) bochten, T-splitsingen en hellingen van 30°.

Mechanisch ontwerp

De meest bepalende factor voor het ontwerp is de minimale buisdiameter (63 mm). Het ontwerp dat ten grondslag ligt aan alle beschreven prototypes bestaat uit een robot 'slang' op wielen, bestaande uit een aantal modules waarmee twee klemmende V-vormen gemaakt kunnen worden. In het midden bevindt zich een rotatiegewricht om de hele robot in de buis te kunnen laten draaien.

Elektronica

De elektronica voor het gebruik op een mobiele robot moet klein en energiezuinig zijn. Omdat het ontwerp over veel vrijheidsgraden beschikt, is bedrading een serieus ontwerpprobleem. Om dit te ondervangen is de elektronica zoveel mogelijk over de segmenten verdeeld. Hiermee is een gedistribueerd regelsysteem gebouwd

bestaande uit een 'master' controller en een 'slave' node per robot segment. Om de bedrading verder tot een minimum te beperken communiceren de slaves met de master via een seriële bus die ook voor de energievoorziening gebruikt wordt. De energie wordt geleverd door batterijen of via een kabel.

Sensoren

Er is een camerasysteem ontworpen dat informatie geeft over de buiskwaliteit en gebruikt kan worden voor navigatie. Het camerasysteem maakt gebruik van een laser die een cirkel projecteert op de binnenkant van de buiswand. Afwijkingen van de cirkelvorm duiden op vervormingen van de buis (b.v. door buigen, druk van buitenaf) of op obstakels. De beeldbewerkingstappen zijn geoptimaliseerd om uitgevoerd te kunnen worden op een kleine, zuinige computer die met het camerasysteem op de robot geplaatst kan worden.

Er is een 'lekluisteraar' ontworpen bestaande uit een ultrasone microfoon die het geluid van weglekkend gas opvangt. Hoewel de bruikbaarheid van deze meetgegevens erg afhankelijk is van de condities rondom een lek (gasdruk, grootte van het lek, materiaal rond de buis) is het een relatief simpele en goedkope toevoeging aan de set sensoren die in veel gevallen een extra indicatie van een gaslek kan geven.

Door de hoeken tussen de verschillende segmenten te meten terwijl de robot in een buis geklemd is kan de diameter en aard van de buis bepaald worden. Door middel van de accelerometer (of een meer uitgebreidere IMU) kan vervolgens de oriëntatie van de buis bepaald worden waar de robot zich in bevindt.

Communicatie

De master controller van het eerste prototype beschikt over een 2.4 GHz radioverbinding die op korte afstand gebruikt kan worden, bijvoorbeeld tussen de robot en een nabij gelegen ondergronds basisstation. Voor verdere experimenten is vooral naar het gebruik van kabels (tether) gekeken. Behalve dat kabels kunnen worden gebruikt voor communicatie kunnen ze ook worden gebruikt voor stroomvoorziening. Ook is het handig om in geval van storing de robot te kunnen terugtrekken.

Besturing

De wielen worden snelheidsgestuurd, het rotatiegewricht positiegestuurd en de klemmende V-vormen worden bestuurd met een combinatie van positie en stijfheid. De besturing is uitgevoerd met gangbare PID controllers en geïmplementeerd op de 'slave' nodes in iedere module.

Hoewel bij het systeemontwerp is uitgegaan van een autonome robot is de aandacht in eerste instantie gericht op de ontwikkeling van een systeem dat überhaupt door het netwerk kan bewegen. De robot heeft te veel vrijheidsgraden om allemaal

individueel door een operator te laten besturen (tenminste 11 motoren) dus is gezocht naar een bruikbare combinatie (mapping) van vrijheidsgraden naar een besturingspaneel.

Het is gebleken dat andere bewegingen nodig zijn om de robot door een bocht of T-splitsing te laten gaan dan gedacht. In simulatie en op papier (2D) wordt uitgegaan van een robot die zich strak gecentreerd in een buis kan klemmen. In de praktijk blijkt zich in een bocht veel op de bodem van de buis of zelfs diagonaal geklemd af te spelen. Het rotatiegewricht blijkt een goede extra krachtbron om de robot over richels en hoeken heen te 'wriemelen'. Een vervolgstap zal zijn om deze inzichten te formaliseren tot een algoritme dat zelfstandig door een besturingscomputer kan worden uitgevoerd.

Productiemethode

De productiemethode heeft een grote invloed gehad op het ontwerpproces. Het eerste prototype is op 'conventionele' manier ontworpen en geproduceerd. Het tweede prototype is bij wijze van experiment ontworpen met gebruik van een 3D printer. Deze werkwijze bleek in zeer korte tijd een aantal deelontwerpen op te leveren die goed genoeg bleken te zijn voor fysieke testen. Met name de besparing in gewicht door het gekozen (3D geprinte) materiaal hebben in korte tijd een prototype opgeleverd dat (in plaats van de gevraagde 30°) loodrecht in een buis omhoog kan klimmen. Ook bij het ontwerpen en produceren van de elektronica is dankbaar gebruik gemaakt van de ontwikkelingen in open hardware en open software van de afgelopen jaren.

Hoewel de beschreven technieken voor digitale fabricage (3D printer, lasersnijder) al veel langer bekend zijn, zijn ze de afgelopen jaren veel toegankelijker geworden. Met de beschrijving van het verschil in ontwerpproces van het eerste prototype (klassiek) en het tweede prototype (digitale fabricage) wordt beargumenteerd dat voor deze (gunstige) ontwikkeling de *toegankelijkheid*, *beschikbaarheid* en *zichtbaarheid* van de gebruikte technieken van groot belang zijn.

The gas distribution network in the Netherlands has a length of roughly 100 000 km in urban areas. This network needs to be monitored constantly and segments need to be replaced when the risks of leaks increase. Since replacement is expensive it is important to know how long a segment of the network is still expected to offer reliable service.

In this thesis a solution for the lack of ‘inside information’ is explored: *the realisation of a swarm of autonomous robots that move constantly through the network, while collecting and storing data. The robots surface now and then for maintenance and exchange of data with the network operators.* This project can be seen as a feasibility study of a part of this goal: Is it possible to design a robot which can move (autonomously) through the gas distribution network? Five partial questions need to be answered:

- What is the best mechanism for *propulsion* for the system?
- What is the best way of providing *energy* to the system?
- Which *sensing methods* can be used for assessing the quality of the pipes?
- What is the best method for *communication* with the system?
- How to *control* the designed mechanism? Which steps are necessary for autonomous or operator-based control?

In order to answer these questions, three prototypes have been realised. The design of a propulsion mechanism depends strongly on the layout of the gas distribution network. Based on data available on a number of representative urban distribution networks a description has been made of the environment in which the robot has to operate. The most important aspects are long stretches of pipe (tens of metres), a diameter range of 63 mm to 125 mm, (mitre) bends, T-joints and inclinations up to 30°.

Mechanical design

The most demanding requirement is that in 63 mm pipes with thick walls the robot has to move through an inner diameter as small as 51.5 mm. Most of the design requirements follow directly from the given network environment. The design which is the basis of all of the realised prototypes is a wheeled robot ‘snake’ consisting of a number of modules which can be used as two clamping V-shapes. The central module is a rotation joint which can be used to change the orientation of the robot in a pipe.

Electronics

The design has many actuated degrees of freedom, so wiring is a serious issue. To reduce the amount of wiring, the electronic system has been distributed over the robot segments. A master controller is added which communicates to these distributed 'slave nodes' via a serial bus. Also energy for propulsion is provided through this bus. Energy is supplied through batteries or a tether cable.

Sensors

A camera system has been developed which can be used for both pipe assessment and navigation. The camera system uses a laser projector which projects a cone (circle) on the inside of the pipe. Deformations of the pipe and obstacles such as bends and T-joints show up as deviations of the captured circle shape. The vision processing algorithms have been optimised so that they can be executed on a small, energy efficient computer which can be placed with the camera system on the robot.

An acoustic leak detector has been developed using an ultrasonic microphone which captures the noise of gas leaking out of a pipe. Although the relevance of this data is strongly dependent on the conditions of the leak (size, gas pressure, material surrounding the pipe), it is a relatively simple and inexpensive addition to the existing sensory system as extra indication of leaks.

An accurate map of the inspected network is important for navigation of the robot and also valuable data for network operators. By measuring the angles between the modules while the robot is clamping inside a pipe, the diameter and shape of this pipe can be determined. Using an accelerometer also the orientation of the pipe can be determined.

Communication

The first prototype has been equipped with a short-range 2.4GHz radio link which can be used, for example, for communication between the robot and a nearby docking station. During experiments the robot has been mostly operated using a tether cable, which can be used both for communication and power supply. The tether can also be used mechanical fail-save, for pulling the robot back in case of a technical failure.

Control

The wheels are velocity controlled, the rotation joint is position controlled and the clamping V-shapes are controlled using a combination of position and force (stiffness). These controllers are implemented on the slave nodes as conventional PID controllers.

Although the overall goal of the project is to realise an autonomous robot, the focus during the project has shifted to creating a system that is capable of manoeuvring in the given network altogether. Because it is difficult to control the large number of degrees of freedom individually by an operator (at least 11 motors) a mapping has been designed, combining degrees of freedom to a reduced control set.

Where in simulation or in (2D) drawing the robot is always clamped in the centre of the pipe, in practice complex manoeuvres are taking place on the bottom of the pipe or even diagonally clamped. The rotation joint, which was primarily intended for axial rotation inside the pipe of one clamping V-shape with respect to the other) appears to be a very useful source for 'wriggling' the robot over edges and bumps (ones that hardly show up in simulations). A next step in the research will be formalising these insights and adapting them for (autonomous) control.

Production

A special place in this project is reserved for the chosen production methods which had a large impact on the design process. The first prototype has been designed and produced in a 'conventional' way which took a long time and missed some crucial steps in integration. The second prototype has been designed and produced using a 3D printer. This approach has yielded a number of iterations in a short time, suitable for physical tests. The reduction of weight due to the printed material with respect to the first prototype, yielded a prototype capable of a vertical climb (instead of the requested 30°). Also in the design and production of the electronic systems extensive use of the developments in open hardware and open software in recent years has been made.

Although the described technologies for digital fabrication (3D printing, laser cutting) have been in use for a long time, the development in recent years allowed these tools to become increasingly accessible. The difference in design and production between the first prototype and the subsequent prototypes can be used to describe the importance of *accessibility*, *visibility* and *availability* of these tools as condition for fruitful usage.

Contents

1	Introduction	1
1.1	Introduction	1
1.2	PIRATE project	1
1.3	Problem Statement	2
1.3.1	Network	2
1.3.2	Current methodology for inspection	3
1.3.3	Economic boundaries	3
1.3.4	Proposed solution	4
1.4	Mechatronic Design Project	5
1.5	Organisation of this Thesis	5
2	System Specification	7
2.1	Introduction	7
2.2	Requirements and Specifications	7
2.2.1	Proposed solution	7
2.2.2	Economic boundaries	8
2.3	Operational requirements	10
2.3.1	Distribution and deployment	10
2.3.2	Mission profile	11
2.3.3	Performance criteria	11
2.3.4	Utilisation requirements	12
2.3.5	Effectiveness requirements	13
2.3.6	Operational life cycle	13
2.3.7	Environment	14
2.4	Design requirements	21
2.4.1	Maintenance concept	21
2.4.2	Safety	23
2.4.3	Disposal	23
2.5	Summary	24
3	Conceptual Design	25
3.1	Introduction	25
3.2	Ideation	25
3.3	Related research	27
3.3.1	Introduction	27
3.3.2	NDT quality inspection	27
3.3.3	In pipe inspection methods	28
3.3.4	Robot systems	29
3.4	Design Considerations	35
3.4.1	Technical performance measures	35
3.4.2	Modular Design	35

3.5	Conclusion	47
4	Mechanical Design: Prototype I	49
4.1	Introduction	49
4.2	Requirements	51
4.2.1	Goal	51
4.2.2	Environment	51
4.3	Design	52
4.3.1	Design concept	52
4.3.2	Modular Design	53
4.3.3	Payload	60
4.4	Control	62
4.5	Results	64
4.6	Conclusions	66
4.6.1	System design	66
4.6.2	Discussion	67
5	Mechanical Design: Prototype II	71
5.1	Introduction	71
5.2	Analysis	72
5.2.1	Clamping	72
5.2.2	All wheel drive	75
5.2.3	full modular concept	75
5.2.4	position sensing	77
5.3	Implementation	77
5.3.1	Clamp system	78
5.3.2	Drive motor	80
5.3.3	Design iterations	80
5.3.4	Material	81
5.4	Results	81
5.5	Conclusion	85
6	Mechanical Design: Omniwheel Prototype	87
6.1	Introduction	87
6.2	Analysis	89
6.2.1	Orientation	89
6.2.2	Wheel choice	90
6.2.3	Clamping	90
6.2.4	Orientation control	90
6.3	Implementation	91
6.3.1	Mechanical design	91
6.3.2	Electronics	92
6.3.3	User interface	92
6.3.4	Orientation control	94

6.4	Results	95
6.4.1	Straight section	95
6.5	Conclusion	96
7	Electronic (embedded) system Design	99
7.1	Introduction	99
7.2	Embedded system design	99
7.2.1	Master Slave setup	100
7.2.2	RS485 bus	101
7.2.3	Slave node design	103
7.2.4	Master node design	108
7.3	Power system	113
7.3.1	Battery considerations	113
7.3.2	Tethered power supply considerations	114
7.4	Conclusion	114
8	Sensing	115
8.1	Introduction	115
8.2	Stereo Camera System	115
8.2.1	Introduction	115
8.2.2	Analysis	117
8.2.3	Implementation	127
8.2.4	Results	130
8.2.5	Conclusion	131
8.3	Acoustic sensor	132
8.3.1	Introduction	132
8.3.2	Analysis	132
8.3.3	Implementation	133
8.3.4	Results	133
8.3.5	Conclusion	133
8.4	Internal state sensing	135
8.5	Conclusion	138
9	Communication	139
9.1	Introduction	139
9.2	Wireless communication	139
9.3	Tether system	140
9.3.1	Spooling system	141
9.3.2	Single use coil	142
9.4	Ethernet cable	144
9.5	Conclusion	144

10 Control	147
10.1 Introduction	147
10.2 Slave nodes	147
10.2.1 Velocity control	153
10.2.2 Position control	154
10.3 World Model	154
10.4 Operator interface	157
10.4.1 Control software	159
10.5 Conclusion	161
11 Prototyping and development	163
11.1 Introduction	163
11.2 Additive Manufacturing	166
11.2.1 Design iteration through 3D print	167
11.2.2 Printed metal parts	168
11.2.3 Body material	173
11.3 Design for laser cutter	173
11.4 Open micro controller design	174
11.5 PCB manufacturing	176
11.6 Reflow oven	177
11.7 MEMS sensors	178
11.8 Conclusion	180
12 Evaluation	183
12.1 Introduction	183
12.2 The complete robot	183
12.3 Tests	185
12.3.1 Axial rotation in 110 mm	187
12.3.2 Climb in 63 mm pipe	190
12.3.3 T-joint	192
12.3.4 Wriggle and Squeeze	193
12.3.5 Reverse clamp	196
12.3.6 Other manoeuvres	196
12.4 Conclusion	198
13 Conclusion	199
13.1 Introduction	199
13.2 Conclusion	200
13.2.1 Mechanical design	200
13.2.2 Electronics	201
13.2.3 Sensors	202
13.2.4 Communication	202
13.2.5 Control	203
13.2.6 Production	203

13.3 Future Work 204

The introduction chapter summarises the research question as posed by KIWA and gives an outline for the remainder of this thesis.



Introduction

1.1 Introduction

The main focus of the work described in this thesis is the *design and development of a mechatronic system for inspecting small diameter gas distribution mains*. This project, initiated in 2006 by KIWA¹, has as aim to realise a robot capable of autonomous non-destructive qualitative and quantitative inspection of live gas distribution mains, targeting the small (63-120 mm) pipes in the Dutch network. The research goal has been formulated originally as a set of requirements by Pulles et.al. [72].

KIWA

This introduction chapter starts with a brief outline of the project. Section 1.3 describes the research aim as proposed by KIWA [72]. The following section will continue with the project description, followed by the problem statement, the current network and inspection methodology and economic context. In the last section an overview of the remainder of this thesis will be given.

1.2 PIRATE project

The project was given the acronym '*PIRATE*' which stands for Pipe Inspection Robot for AuTonomous Exploration. The project can be considered as a response to a report by the Dutch Transportation Security Council chaired by mr. Pieter van Vollenhoven [103] in which the details and figures of safety of the gas-transportation in the Netherlands have been given. Direct cause for this report being a large explosion in one of the older grey cast iron distribution mains in Amsterdam, 2001. A later report by the same council stressed the importance of acquiring detailed information on the quality and status of the current network [107].

PIRATE

This thesis describes the project and design as realised and tested up to the end of 2013. In 2013 ALSTOM inspection robotics (AIR)² has expressed interest in the

ALSTOM

¹KIWA (gastec), Apeldoorn, <http://www.kiwa.nl>



FIGURE 1.1 Result of the explosion in the Tsaar Peterstraat, Amsterdam, 2001 - *image from [103]*

project and has continued the development of the robot system with as aim the development of an inspection tool for pipes in power plants, expanding their existing suite of robotic inspection tools as described by Zwicker et al. [12][116].

1.3 Problem Statement

1.3.1 Network

*transmission
distribution*

The national network of gas mains consist of a national distribution network (>40 bar) and a number of networks for national distribution. The national distribution net consists of a high-mid pressure network (1-8 bar) of *transmission* mains stretching 20 000 km and a low-pressure network (30-100 mbar) of *distribution* mains stretching 100 000 km [102]. The low-pressure network extends into all of the urban areas. Therefore this network has the fullest attention with regard to the risks for public health and safety. Replacement of pipe-lines in an urban area is expensive, so it is important to have accurate data on the locations of leaks or damaged pieces.

PE

PVC

The pipes of *grey cast iron* and *asbestos cement* create the largest risk for leakage. Grey cast iron is sensitive to corrosion. Historically joints in grey cast iron are constructed using rope (with cast lead) and are relatively susceptible to leakage too. Polyethylene (PE) is less sensitive for degradation in time. It is however sensitive to point-loads (stones), tension (bend, stretch) for example by tree roots. Unmodified ('hard') PVC can be brittle and prone to breaking during nearby digging activities. Modern PE (2nd and 3rd generation) is very resilient, but the quality of of welds is

²ALSTOM Inspection Robotics, <http://www.inspection-robotics.com>

occasionally a cause of concern. Summarising the most common causes for leakage: bending, creep, tension, brittleness, impacts, inferior connections, porous rubber sealing and corrosion [72].

The existing network is occasionally incompletely documented [107]. Although most of the network is within 0.5 m of the mapped or 'known' route, improving the accuracy and mapping, especially regarding the depth of the pipes is important. Based on data provided by KIWA³ [53] it can be said that one-third of the leaks is caused by badly constructed lines, one third by deterioration over time and one third by actions of third parties (excavations, road works).

1.3.2 Current methodology for inspection

Currently, the low pressure distribution networks are only inspected by conventional leakage searching above ground. This is a labour-intensive process and does not yield any information about layout and quality of the pipe, only leaks that can be 'smelled' can be detected. The worst case accuracy of above ground detection is several metres. By (Dutch) law, every segment of the gas pipe network has to be inspected every 5 years⁴. It is hard to determine the necessary amount of sample inspections of a network, necessary to acquire accurate judgement on the quality. According to KIWA, every year 2 000 leaks are being found with the conventional leak inspection methods, 6 000 are reported by the public [72]. Continuum has had 9 000 public leak reports in 2005, from which 1 000 not correct, 2 000 in home and 6 000 about the distribution network [103].

Although there are many developments in the area of inspection of high pressure mains, for example by companies like ROSEN⁵, fully autonomous inspection is not an available option yet. The systems in operation are more passive data loggers than autonomous robots. A more elaborate overview of the systems currently available for in-pipe inspection will be given in chapter 3.

1.3.3 Economic boundaries

Economic aspects of the proposed pipe inspection system are discussed in the problem description by KIWA [72]. In order to design the system to be economically feasible, the costs of the system should outweigh the costs of conventional above ground leak detection. Apart from that, a certain added value might be attributed to the system due to:

- detection of more, and possibly smaller leaks
- more accurate positional data of leaks (centimetre accuracy instead of metre)

³<http://www.netbeheernederland.nl/publicaties/onderzoek/>

⁴Besluit externe veiligheid buisleidingen, <http://wetten.overheid.nl>

⁵ROSEN - Rosen Inspection Robotics, <http://www.rosen.com>

- data about position, orientation, material and quality of the pipe
- preventive indication of risk areas due to corrosion and deformation.

In the economic discussion of the system, the following aspects are important for design of the system:

- system costs: the system itself, equipment, personnel, maintenance and development
- the amount of data yielded by the system (try to attribute an economic value to the detection of the location of a leak, depending on the accuracy of this data, the public risk in the searched area)
- the speed with which data can be acquired from a given (subset) of the gas distribution network
- life span and life cycle of the system.

These criteria will be translated into design requirements in chapter 2.

1.3.4 Proposed solution

The proposed solution for obtaining information about the quality of the gas distribution mains has been limited to the *design and development of a mechatronic system for in-pipe inspection*. In this thesis this proposed solution will be explored. The project goal described in [72] aims at developing a totally *autonomous* system. The image sketched is

a (series of) robots, moving day and night through the network autonomously, while collecting and storing data. The robots surface now and then for maintenance and exchange of data

The design and development of this mechatronic system can be reformulated into a set of *research questions* relating to a method of propulsion inside the pipes, control and navigation, communication and quality assessment.

propulsion

1. What is the best mechanism for *propulsion* given the intended environment?

energy

2. What is the best way of providing *energy* to the system?

sensing methods

3. Which *sensing methods* can be used for assessing the quality of the inspected pipes? How to represent and visualise the resulting measurement?

control

4. How to *control* the designed mechanism? Which steps are necessary for autonomous or operator-based control?

5. What is the best method for *communication* with the system?

communication

One important aspect of the proposed system is the level of *autonomy*. The level of autonomy of the system determines to a large extent the type of *scenario* in which the system can be used. A tethered user operated robot might have a huge economic potential if sections can be inspected which cannot be inspected by conventional means. However, when the situation is taken into account where the whole network needs to be inspected annually, a fully autonomous system might be a more viable solution by comparison.

autonomy
scenario

In this thesis a number of use scenarios will be explored with increasing complexity and increasing level of autonomy. The design and realisation of a fully autonomous system consisting of multiple robots will be beyond the scope of this work.

1.4 Mechatronic Design Project

The thesis describes a *mechatronic* design process which resembles in many ways the *MART* project by Schipper et al. [86]: a multidisciplinary design project carried out by a design team consisting of electrical engineers, mechanical engineers and software engineers. As described in chapter 3 of his thesis, a mechatronics design project benefits from a 'one room approach', in case of the *MART* a large group of master's and PhD students. A similar approach has been used in the *PI-RATE* project. Over a period of 7 years a large number of bachelor's and master's projects have been completed on realising parts of the design. The most productive phases of the project were when a design team with diverse expertise was housed in one room. From 2006 to 2008 as a design team housed at DEMCON⁶, from 2013 - onwards as a team at the University of Twente.

mechatronic
MART

1.5 Organisation of this Thesis

In chapter 2 detailed requirements for the system will be given. In chapter 3 a number of existing robots for in-pipe inspection will be discussed, as well as current inspection methods, sensors and equipment. The development project can be subdivided in five main topics: the *mechanical* system, *control* electronics, *communication* system, *sensing* system and *power* system. Three subsequent mechanical prototypes will be discussed (chapters 4, 5, 6) after which the electronics, sensing, communication and control system are treated in separate chapters (7, 8, 9, 10). After a chapter discussing the used development methodology using rapid prototyping (chapter 11) the thesis will be concluded with an evaluation and discussion of the presented work (chapters 12 and 13).

⁶DEMCON is a spinoff company of the University of Twente, which has its roots in the *MART* project - <http://www.demcon.nl>

This chapter treats the system specifications based on discussions and brainstorm sessions with KIWA, Demcon and network operator Alliander at the start of the project.

2

System Specification

2.1 Introduction

This chapter formulates the specifications for the realisation of a prototype of an autonomous pipe inspection system. The primary focus lies on the *propulsion system, energy supply, communication system, sensing and control*. Most of the requirements are summarised in this chapter in tables 2.1, 2.5 and 3.1. Input for the requirements were a number of brainstorm sessions (discussed with the conceptual designs in chapter 3) and data provided by KIWA [72] and *Continuon*¹. This chapter discusses the requirements and specifications based on *Blanchard & Fabricy's* method of Systems Engineering [6].

2.2 Requirements and Specifications

2.2.1 Proposed solution

Although a much wider space for solutions can be explored, such as above ground vehicles, new arial and satellite monitoring, ground penetration radar systems (GPR) or changing pipes with build-in sensors, using smart sensor nodes embedded in distribution points etc., the choice has been made to design a mechatronic system (or *robot*) which inspects the pipe from *inside* the pipe for three main reasons. For the intended system it should be possible to:

robot

- inspect the existing network - no redesign of pipe elements
- inspect (nondestructive) from the *inside* of the network - give a life prediction rather than just the presence of leaks
- inspect with as many quantitative and qualitative tools (sensors) as possible.

¹Continuon has been renamed 'Liander' as part of 'Alliander' - <http://www.liander.nl>

docking stations

The system that is to be designed must be capable of autonomously inspecting a certain area of the gas pipe network, detecting leaks and recording the exact location and status of the pipe. The system must be capable of measuring its position relative to one or more entry-points and *docking stations*. Every registration (pipe layout, pipe status, location of a leak) has to be recorded alongside an accurate position measurement. In case of a fully autonomous realisation, the system must be capable of navigating through the network, localising docking stations and performing a docking operation for exchange of information and a refill of the energy-supply.

The ideal situation (and initial aim of the project) is a fully *autonomous* system. A *swarm* of robots that performs a continuous inspection of the current net, feeding status information through docking stations to a central server. The focus in this thesis has been primarily on the capability to move through the network and measure pipe deformation - and less on the software necessary to operate the system without operator intervention. So everywhere it reads 'autonomous' in this thesis, different levels of autonomy might apply for different scenarios and missions for the robot. This will be discussed in chapter 10.

2.2.2 Economic boundaries

As a reference for comparison of the costs of the system, the costs of the current methodologies for inspection can be taken. An autonomous system would be economically feasible when it is cheaper than the current labour-intensive leak detecting methods. On the other side, increased accuracy and the increased amount of available data on the networks have an added value. It is difficult to value this extra information, however, every segment of the network that does not need to be replaced has an economic value (i.e. a saving on replacement). An economic analysis by KIWA as described by Pulles et al. [71] is being discussed in the following section.

Analysis

The autonomous system can potentially save costs for the network operator because of two reasons:

- It can replace the current methodology for searching leaks.
- It can, while maintaining, or even increasing the safety levels, postpone the instalment of new pipes.

Leak detection at normative prescribed frequency costs, roughly estimated, 20 €/ (km year). An average extension of the life span of a segment of the network of 5% yields a saving of 100 €/ (km year). Calculated for the Dutch situation, with 100 000 km of low pressure mains, a saving of 12 M€/year could be possible.

When operating at a speed of 0.04 m/s and an availability of 50 % (because of charging, docking, communication) and considering a life span of 5 year, one robot can inspect 3 500 km. The value of these measurements, when they replace the standard leak detection, and when they prevent 5 % of unnecessary replacements, is 420 000€ per year.

Using this operating speed, availability and the given size of the network and required inspection frequency, the following estimates can be given for the size of the fully autonomous inspection system:

- a total distance of 100 000 km should be inspected in 5 year. Each robot is capable of inspecting 3 500 km in 5 year, so you need 30 robots, 6 need to be replaced annually based on their expected life span
- docking stations: when the range which one robot can inspect on one battery charge is 10 km, 10 000 docking stations need to be placed. When a docking station has a life span of 15 years, 700 stations need to be replaced annually
- launch valves: minimal 1 launch system is necessary per robot's life span distance, requiring a total of 30 launch systems. When they have a life span of 30 years, 1 needs to be replaced annually.

The hypothetical value of the quality assessment by a robotic inspection system inside the pipes justifies the feasibility study such as being carried out in this thesis. Based on this (Dutch) situation, an autonomous inspection system would need 30 robots, 10 000 docking stations and 30 launch systems. This is a rough initial estimation, especially the possible operation speed, availability and life span have to be verified after the design and engineering stage of this project.

Regarding logistics this scheme seems feasible. The system could be restricted to the most dense (urban) areas. The largest costs are drawn by the docking stations. Two possible solutions for increasing the feasibility could be proposed: Increase the *range* of a robot (very difficult, as will be pointed out in the rest of this study) or finding a simple solution for a cheap docking station. With that respect a mobile docking system from a home will be considered. *range*

For calculating the total costs of the system some assumptions need to be made. Especially the costs for hardware, material and build are difficult to estimate in an initial phase. The used figures are based on previous robotic projects with comparable complexity such as the walking robots designed previously by the same

team [19] and previous experience at KIWA. Using these estimates the total costs of the system can be calculated as follows:

- build and material for the robots: 10 000 € per robot; 60 000 € /year total
- build, material and installation of a docking station 1 000 € per docking station; 70 000 € /year total
- build, material and installation of a launch valve: 2 000 € per valve; 2 000 € /year total.

The total outline of the costs sums up to 762 000 €/year, which is small compared with the expected saving of 12 M€/year of extra life time. The costs also outweigh the yearly costs of traditional leak searching. With the onetime costs for development and startup (7 M€), the costs of a total operational system can be gained back from the system within one year.

2.3 Operational requirements

2.3.1 Distribution and deployment

field operator

The system will be used in the existing network within existing infrastructure and maintenance facilities. A *field operator* will insert the robot using a specially designed launching system. The robot will crawl through the network for a certain period, recording data about pipe structure, status, layout and leaks. At certain locations within the network docking stations will be placed for interchanging information and refilling the energy supply. Depending on the required speed of assessment of a range of the network one or more robots can be deployed simultaneously.

A couple of scenarios can be thought of beforehand:

- continuous (permanent) deployment: Distributed over the complete network, a certain number of robots will be deployed at all times
- segmented deployment: According to a certain time schedule and planning a certain number of robots will be deployed in a specifically denoted target area, being for instance a certain urban area. After an inspection period, all robots will be retrieved and released for a certain period into another area
- single mission deployment: In a specific situation one robot will inspect a segment of the network or one special component and return after inspection.

The first scenario requires a permanent distributed system of facilities (launch systems, docking stations), the second and third scenario requires more mobile facilities.

2.3.2 Mission profile

The *primary mission* of the system can be described as follows: After launch, the robot will move through the network while collecting data. At certain times the robot will dock at a station for interchange of information and refill of its energy supplies. At certain intervals (as long as possible) the robot has to be retrieved from the network for maintenance. The tasks the system needs to carry out during these missions are:

- simultaneously localising and mapping (SLAM) covering a pre-defined set of way-points
- autonomous navigation, taking (or avoiding) obstacles
- entering and exiting the network using a launch valve prior to the mission
- docking at a station for recharge and data exchange.

The *secondary mission* tasks are considered the dedicated inspection tasks or short missions directed by an operator. These missions consist of:

- execution of a *rendez-vous*: at a certain point in time the robot has to be at a specified point in the network, for instance for retrieval, maintenance or an emergency docking operation (energy shortage)
- execution of an *inspection round*: starting from a launch pipe the system travels to a certain specified spot in the network, inspects a certain area and returns to the launch pipe. This mission is only 'economically valuable' when the required data cannot be obtained by conventional leak searching above ground
- *emergency procedures*: when certain(sub)systems in the robot fail, appropriate action has to be taken: back to the closest launch pipe or docking station. When rendered in-manoeuvrable, sending an emergency localisation signal (acoustic, mechanic or by radio) or, in case of tethered operation, become passive and be pulled back.

2.3.3 Performance criteria

The following performance criteria follow from the chosen primary and secondary mission tasks. These are generic criteria that will be translated in requirements and can be used to compare design options.

- Range, radius of action (energy capacity and data storage capacity)
- Energy consumption (depending on speed and weight)

- Speed (Driving speed, speed during measurements, during special manoeuvres (corners) and docking)
- Size (Determined by the environment: the minimal pipe diameter and minimal corner radius)
- Weight (related to size and the necessary energy capacity)

2.3.4 Utilisation requirements

duty-cycle

The utilisation of the system is related to the desired mission profiles. The mission profile can be broken down into operation cycles. The most important cycle is the *duty-cycle* of the system. An example could be a 24-hour cycle with 16 hours of autonomous operation and 8 hours of recharging. For autonomous systems operating in an environment where human intervention is necessary from time to time, a 24-hour cycle seems a logical choice. Also disturbances from outside (traffic, ground-work activities, use of water drains and sewers) occur with a 24-hour cycle. The battery requirements and charging time are being defined by this cycle.

MTBF

A different cycle is the maintenance cycle: the time the system can operate without intervention, calibration or maintenance. The length of this cycle is determined by the *MTBF* (Mean Time Between Failure). An example could be a work period of a month, after which a checkup and cleanup are performed during a week. Then the system can be launched again for another month's cycle.

Let A [m] be the size of an urban district in metre (pipe length), P [s] the length of autonomous operation on one single battery charge, S [m/s] the travel speed and D [%] the duty cycle, then the required number of charging stations in that area is n :

$$n = \frac{A}{PS}$$

The amount of time necessary to cover this urban district is:

$$t = \frac{A}{SD}$$

With conventional leak detection an urban district (10 km, 1 000 households) can be covered in three days. A robot covering the same area in the same time, with an availability of 50 % (remainder of the time is necessary for recharging and communication) has to travel 10 km in 36 hours. Average speed should at least be $10000/(36 * 3600) = 8$ cm/s. If the robot has an autonomous period P of 6 hour, $(10/6 * 0.08 * 3.6) = 6$ docking stations (for recharging) are necessary.

2.3.5 Effectiveness requirements

Because the system needs to operate in an inaccessible location it is important that the system is very reliable in order to be able to operate without intervention as long as possible. Based on the utilisation it can be said that a cycle of days would not work for any of the specified missions, a cycle of weeks would work for most of the specified secondary missions to be completed and a cycle of months would be necessary for the primary mission. A month of continuous operation requires a very high level of reliability and robustness, or MTBF, having a severe impact on the level of engineering and the allowed system costs.

Existing autonomous robot systems coming close to a MTBF in the order of magnitude of weeks or even months, can be found in applications like planetary research missions. Research in the area of autonomous (lab)robots and autonomous museum guide robots gives however not a very promising view of the current state of affairs in technology. A study by Carlson et al. [13] gives an average MTBF of 8 hours and an availability rate of 50 % for an inspected group of 15 different autonomous robot systems. On the other hand the Mars mission from 2003 discussed in this context by Stancliff et al. [92] is an example that it is still possible to operate an inaccessible autonomous robot system for a long period of time in a harsh environment.

It is possible to predict the MTBF of a certain system by multiplying all known failure rates of the subparts of that system. The problem is that this can only be calculated for a known design with all parts specified. In the study on mars-rovers an example is given for the calculation of the failure rates for all single modules on a Mars rover. Also standard derivations for temperature shifts are being calculated. It is however hard to compare these calculated risks to the results of real missions. A further study by the same author was aimed at (robot) competitions involving similar design decisions [93].

The possible reasons for a robotic system to fail during operation are abundant, therefore it is necessary to make a detailed risk assessment. A risk inventory has been made and updated throughout the project following the specifications by ALSTOM. For every (sub)system the risks have been listed and possible fall-back options discussed.

2.3.6 Operational life cycle

In the economic discussion an expected life-span of five years has been used. It is necessary that the system can operate and can end its operational life with as little harmful effect to the environment as possible. A *modular design* can lengthen the operational life by making it easy to replace defective parts and modules.

2.3.7 Environment

The design requirements for the mechanical system are determined by the environment in which the robot has to operate. The mechanical properties of this environment (tubular sections, arcs, bends) are determining the shape of the robot. Besides that, the environmental temperature, moisture and contamination are also important with respect to robustness. Figure 2.1 gives a schematic overview of the necessary *obstacles* the robot needs to navigate through. In the following section these obstacles will be dealt with in detail.

obstacles

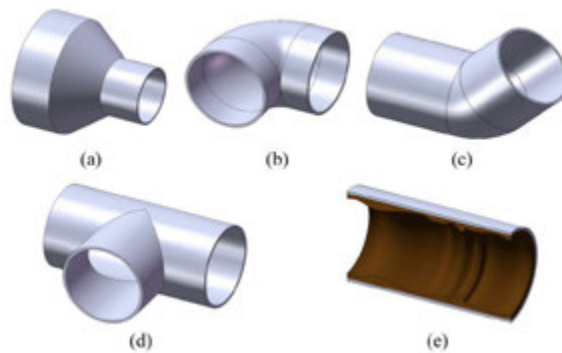


FIGURE 2.1 Schematic overview of different obstacle types (a) diameter reduction, (b) 90° corner, (c) angle, (d) T-joint and (e) welds - *image from [68]*

The number of leaks in the network varies from 1 leak per 100 km to 1 leak per km - strongly depending on age, type of material used, population density and soil consistency. Because sensors are being used for monitoring the network, it is important to take a closer look at disturbances (vibrations, noise) from the direct environment of the pipe. The vicinity of other pipes with water (sewers), electric mains (electric noise), communication lines, traffic above ground, work in the ground (excavation and digging) might have an influence on sensor readings.

The mechanical properties of the environment regarding size and shape can be listed in order of increasing complexity for a mobile robot system. Table 2.1 lists these properties.

Pipes

The environment consists of different types of pipes. Two materials are mainly used in the Dutch gas network: plastics such as PE or PVC and (older) grey cast iron. If the system has to operate in an average urban area, it has to be capable of moving in both types, including connections between both sorts. The diameters of the used pipes are listed in table 2.2.

TABLE 2.1 Summary of the environment

Property	Parametrization
straight pipe	63 mm to 125 mm
inclination of the pipe	+/- 30°
gradual diameter change	63 to 125 mm, 45°
sudden diameter change by obstacle	-10 to +5 mm
deformation from outside (dent, bend)	10% increase/decrease
bends	$R \in [D/2, \rightarrow]$
T or Y joint	choose direction[L,R,straight]
Valves or shutters	10% diameter change
Contaminants	dust, sand, oil, water

TABLE 2.2 Used pipes, outside diameters

PVC (SDR41)		PE (SDR17.6)		Grey cast Iron	
outside	inside	outside	inside	outside	inside
63 mm	59 mm	63 mm	57 mm		
75 mm	71 mm	75 mm	69 mm	76 mm	66 mm
				80 mm	70 mm
90 mm	85 mm	90 mm	80 mm	98 mm	84 mm
110 mm	106 mm	110 mm	100 mm	118 mm	98 mm
125 mm	119 mm	125 mm	115 mm		

Surface

In general the robot has to move around in a PE or PVC pipe of 63 mm with a smooth surface and in a pipe of grey cast iron of 100 mm with possible corrosion (which can be seen as a random scattered profile of 1 mm height max). These two inner surfaces are very different. In the PE or PVC situation it is likely for the robot propulsion module to loose traction because of excessive slip due to the smooth material properties. In the case of a grey cast iron pipe, it is likely for a propulsion module to loose traction because of contaminants (rust, dust). *slip*

Connection

Connections occur in the network with an average frequency of once per 12 m. In general methods for connecting pipes are used: by *welding* and with *sleeves*. PE pipes mostly welded together by heating the pipe edges and melting them together (butt heat fusion) although this technology is mainly used in larger diameters. Electrofusion is the preferred technique for the smaller diameter PE pipes. At the inside of the pipe two ridges will remain with a certain height. In the PE pipe of 63 mm the welds have a height of 3 mm. In PE pipes of 125 mm heights of 5 mm are possible. The welds have a length varying from 6 - 12 mm. These welds, together with the allowed external deformation (dents) of the pipe, specify the maximal height and

width of the robot system. Since the occurrence frequency of the connections is very high it is necessary for the system to negotiate them with minimum delay and minimum control effort.

The other method used for connecting pipes is by means of sleeves - which are mainly used as transitions to other materials in the PE network. The connection with fixed corner-pieces, T-joints and adapter pieces for unequal diameters use this method: A sleeve with a larger diameter than the pipe is fitted over the pipe, using glue, rubber gaskets or other sealing material to make a gas-tight connection. For the grey cast iron system sleeves are used with a clamping mechanism. Also *rope*, *leaded rope* and *tar* are being used as sealants and might protrude inside the pipe. It is difficult to predict to what extent they prove to be obstacles for the system. They are listed in table 2.1 as 'sudden diameter change'.

At connection sleeves and T-joints uneven or irregular connections can occur, as displayed schematically in figure 2.2. At the inside of the pipe, these sleeves can cause dents with a depth d up to 10 mm and a length L up to 140 mm depending on the used pipe diameter D_p . Also differences in design and fitting methods might cause a different layout inside a given joint.

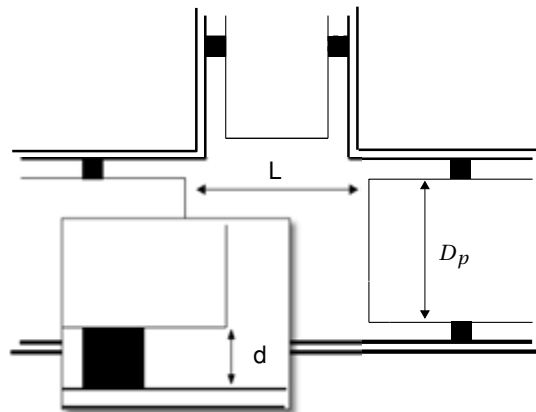


FIGURE 2.2 Schematic drawing of the inside of a T-joint - the bottom part is magnified

T-joints and corners

Although the somewhat flexible PE or PVC pipe allow (gentle) curves, normally for corners and bends special connection pieces with varying radius (curvature) are being used. They are connected to the pipes with sleeved connection pieces. Also T joints are mostly connected with sleeves.

The home-connections in PE or PVC pipes are using *drilling connectors*, see figure 2.3: a T-joint consisting of two halves is clamped over an existing pipe, after which a hole is drilled through the pipe wall to make a connection. This hole can leave splinters and slight dents inside the PE/PVC main pipe. A detailed overview of possible connection pieces, sleeves and obstacles which have been used for the summary in table 2.3 is given in [22].

*drilling
connector*



FIGURE 2.3 Drilling connector (picture by Wavin, 2013)

Network layout

In table 2.4 a summary is given of a couple of typical (averaged) network components such as shown in figure 2.4. Figure 2.5 shows the type of materials and amounts that have been used throughout the history of the Dutch network based on data provided by Brouns and Poorts [9]. This data has been used in estimating the energy budget for special moves (moving over obstacles) and standard operation (driving through a straight pipe). In the network every corner piece contributes two 'sleeved' transitions (with possible dent or unequal connection). Every T-joint contributes three 'sleeved' connections. The PE or PVC pipes are connected mainly by welding, the grey cast iron part are connected by sleeves, sometimes by flange. The Home-connection pieces are T-joints that are being clamped over the PE or PVC pipe, with a smaller (20 mm) hole drilled into the pipe.

TABLE 2.3 Overview of network elements


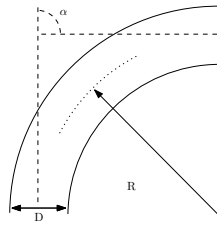
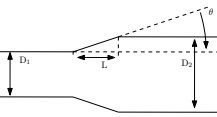
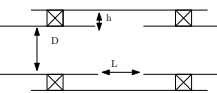
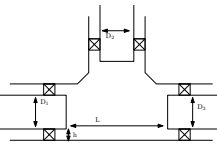

	type (wall) PE63 (SDR 11) PE63 (SDR 17.3) PVC63 (SDR 41) PE100 110 (SDR 11) PE80 110 (SDR 17.6) PE80 125 (SDR 17.6) PVC110 (SDR 41) CI 4" CI 6"	D(inner) 51.5 mm 57 mm 59 mm 90 mm 97 mm 110 mm 104.6 mm 80 mm 120 mm	connection 4 mm weld 3 mm weld sleeve 5 mm weld 5 mm weld 8 mm weld sleeve sleeve sleeve
	type (wall) D PVC (2.0) 63,75,90,110 PE80 (SDR13.6) 63,75,90,110 PE80 (SDR17) 63,75,90,110	radius R/D > 1 R/D > 1 R/D > 1	angles α 11 ° 22.5 ° 30 ° 45 ° 90 °
	type (wall) PVC (sleeve) PE80 (SDR13.6) PE80 (SDR17.6)	D1-D2 available: 63-75 63-90 63-110 75-90 75-110 90-110	L, θ n.a.
	type PE80 PVC	D 63,75,90,110 63,75,90,110	L,h n.a.
	type (wall) PE80 (SDR 17.6) PVC (D1=D3=sleeve) PVC (D2 = (2.1))	(D1=D3)-D2 110-110 63,75,90,110 63-75,63-90,63-110 75-90,75-110,90-110	L,h n.a.
	type rust grease rope	h 1mm 3mm	



FIGURE 2.4 Schematic image of a part of the gas distribution grid in Arnhem -
screenshot from KIWA documentation software

TABLE 2.4 Summary of obstacles in a quarter in Arnhem (figure 2.4)

Summary of network obstacles			
		Urban area 1 km²	Countryside 1 km²
PE/PVC pipe			
	63 mm	20 km	2 km
	75 mm	5 km	
	110 mm	5 km	
Total length		30 km	2 km
Welds			
	63 mm (3mm)	2000	200
	75 mm (4mm)	500	
	110 mm (5mm)	500	
Total welds		3000	100
'Sleeved' connection pieces			
	Corners	600	10
	T-joints	100	6
	Home-connection	1000	12
Total 'sleeved' connections		1500	38
Grey cast iron pipe			
	98 mm	2 km	1 km
	118 mm	3 km	1 km
Total length		5 km	2 km
'Sleeved' connection pieces			
	Corners	100	10
	Connection sleeves	500	10
	T-joints	20	6
Total 'sleeved' connections		310	38

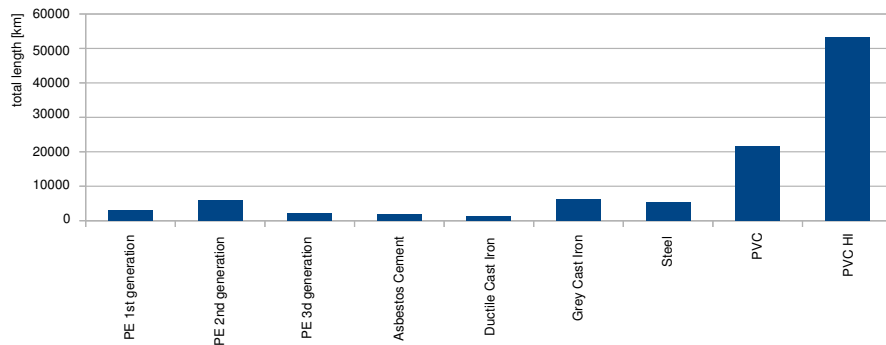


FIGURE 2.5 Materials used in the Dutch distribution network - *based on data from [9]*

2.4 Design requirements

A major part of the requirements for the design follow from the ability to move around in the specified network (section 4.2.2). In table 2.5 the requirements following from the critical aspects of the environment (obstacle height, pipe diameter) are being summarised. The first priorities listed are absolutely necessary for operation of the system. The second priorities could increase the economic potential even further.

2.4.1 Maintenance concept

For the maintenance policy of the system the following items need to be specified:

1. Levels of maintenance (frequency, task complexity, personnel skill level requirements, special facility needs)
2. repair-policies (when, where, if at all)
3. organisational (responsibility, customer, producer, third party, user)
4. logistic (spare parts, replacement models)
5. effectiveness requirements (skill, transportation, repair time)
6. environment (needed environment for repair, facilities)

TABLE 2.5 Requirements summary

requirement	first priority	second priority
size	fitting a 51 mm diameter cylindrical shape	..
clamp range	57-114 mm	57-300 mm
taking obstacles	diameter changes, elbow joints, T-joints inclination +/- 30° diameter change (slope) 45°	vertical pipes, sinks +/- 90° diameter change no slope
taking obstacles without active con- trol	bends $R \in [D/2, \rightarrow]$ contaminants: vaseline, tar, dust, sand 3 mm welds in 63 mm pipe	.. beer-lids, mummified rabbits 3 mm weld + 10% pipe deformation
clamp force	withstanding internal gas velocity of max 30 m/s	..
operation tempera- ture	0-25° C	..
range (24h)	2.4 km	10 km
velocity	0.04 m/s	0.08 m/s
defects to detect	leaks, min size 0.1 m ³ /h	
positional accuracy	500 mm for defects (dig- ging)	10 mm for characteri- sation
characterization	layout, orientation, deforma- tion deformation of 5% is critical for PE/PVC detect dent of 10 mm over 100 mm length detect dent of 2 mm over 20 mm length	material, thickness
operation	operator controlled, (semi) autonomous	fully autonomous
control	tethered	untethered
power	tethered	untethered
modularity	..	interchangeable, ex- pandable fully modu- lar system
communication	tethered, wireless short- range (docking station) emergency audio, mechani- cal	wireless long range ..
launch facilities	stationary system	mobile system

Maintenance should take place as little as possible. A defect in the system should be traceable by a field crew up to the level of a functional part or module. A replacement part should be easy to swap with the defective current version, without advanced system knowledge.

2.4.2 Safety

Safety is an important issue in the design of the robot system. No influence on gas flow in the net and on composition of the gas mixture and quality can be permitted. Therefore it is not allowed for the robot to exhaust fumes or anything else in the the pipe network. This is relevant for the development of the power system.

The safety of the operators and environment of the gas inspection system, especially at the launch system which has a possible connection with the gas network and outside air is important.

When a robot gets 'out of sight' or out of reach of its operators, it is important that it does not interfere with the existing control, measurement and safety systems in the net.

For inspections of the Dutch gas network a number of regulations are in relevant. Relevant system standards are NEN7244-1 to 10², NEN 1059 and to a lesser extent 3650. For the older network parts the rules of the KVG³ are relevant since the formally the network has to comply with the rules valid at the time that the network was constructed. Furthermore the legislation regarding safety with respect to explosive material and labour-legislation are to be considered in the design process.

2.4.3 Disposal

It is important to take a minimal impact on environment into account. In a wide sense the design should be socially responsible regarding choice of material and energy. The device is going to operate in urban areas. Human safety and health should be the primary concern, the more because the sole purpose of the system is to increase the safety of the gas network. The leakage of gas may seem an economic waste, however the primary goal is an increase of safety. Therefore it is vitally important that the system does not introduce new risks to public health and safety. For all parts it is important to choose components that are not harmful for the environment. One of the most recent additions to the set of safety norms is the RoHS⁴ legislation which restricts the usage of hazardous substances. These rules have influence on battery choice and manufacturing process (lead-free) of the electronic system.

²NEN, Dutch institute for Standardisation, <http://www.nen.nl>

³KVG, Royal Gas Network operators Association, <http://www.kvg.nl>

⁴<http://www.rohs.eu>

2.5 Summary

The aim of this project is to design a mechatronic system for (autonomous) inspection of live gas distribution mains. This aim can be summarised in the following design questions (repeated from section 1.3.4):

1. What is the best mechanism for *propulsion* given the intended environment?
2. What is the best way of providing *energy* to the system?
3. Which *sensing methods* can be used for assessing the quality of the inspected pipes? How to represent and visualise the resulting measurement?
4. How to *control* the designed mechanism? Which steps are necessary for autonomous or operator-based control?
5. What is the best method for *communication* with the system?

The research questions are presented with a hierarchy with strong dependencies. The first question is directed by the specified environment, summarised in table 2.5. The second question is directed by the necessary range of the system, inspection velocity and necessary budget for sensing and control. The chosen sensing methodology has to satisfy the requirements for detecting obstacles (navigation) and pipe quality (deformations of 5 %). Control and communication depend on the desired level of autonomy and will have a strong impact on the available energy budget.

This section describes literature, preceding work and the results of the first ideation sessions leading to the conceptual design.

3

Conceptual Design

3.1 Introduction

In order to explore the design space a number of concepts, thoughts and mock-ups have been generated. First the results of this ideation process will be given, followed by an overview of the state of the art in pipe inspection systems. After that an overview per topic (propulsion, power, communication, sensing, control) of design choices will be given, resulting in a set of detailed requirements for the design chapters. This conceptual design, together with the analysis in chapter 2, has been presented at the IGRC 2008 [71].

3.2 Ideation

The first ideas as a result of the posed question as outlined in chapter 1 are briefly presented here as they form a 'leitmotif' for the chosen design principle and the design choices that have been made during the process. In a number of brainstorm sessions including representatives of Demcon, KIWA, Liander and University of Twente ideas and an outline for the project were sketched focussing mostly on the propulsion mechanism. The section on the state of the art will also mostly discuss complete robots or propulsion mechanisms. The state of the art in vision, communication, control and power systems for pipe-inspection robots will be discussed in chapters (8 - 10).

Figure 3.1 shows one of the initial ideas based on an active clamping system. Wheels¹ have been proven as an invention for moving efficiently in structured environments. A *wheeled clamping mechanism* has been the inset of the project from the start. The rationale here is that the *ratio between obstacles and long stretches of pipes is small* (see table 2.4). Most of the time the robot will be driving in a straight pipe, occasionally alternated by a T-joint, bend or diameter change.

*wheeled
clamping
mechanism*

¹The original reference to the invention of the wheel has been considered outside the scope of this Thesis

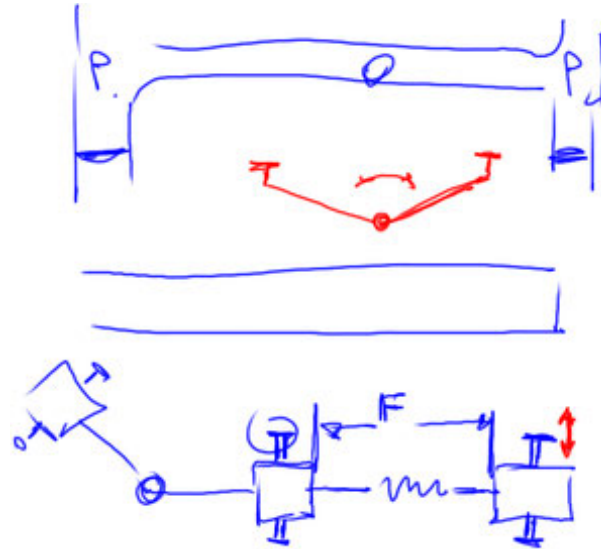


FIGURE 3.1 sketch of first idea, clamping system

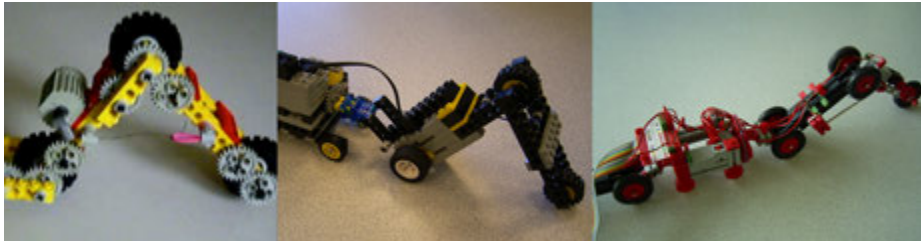


FIGURE 3.2 LEGO™ and Fischertechnik™ models of the robot concept

A number of models with LEGO and other rapid prototyping tools (see chapter 11) have been made as ‘conversation’ pieces during the first brainstorm sessions and design discussions². A number of suggestions to satisfy the design requirements emerged from these discussions:

- the majority of the network consists of *long, straight pipe*. In order to inspect this at a reasonable speed, covering a long range (action radius), *wheeled* locomotion is the most feasible option.
- in order to take obstacles in the vertical plane, a *clamping* mechanism is necessary

²In hindsight it is nice to see how many of the explored concepts (clamping V-shape, rotation joint, modular robot train) have been used in the realised prototypes

- the robot should be able to move and *select branches* in a T-junction
- spreading factor: the robots should be able to move in a *range of pipe diameters* in a single mission

In the following literature review the main emphasis lies on wheeled, clamping vehicles - capable of taking junctions. This reduces the focus on inch-worm and snake type robots which are also capable of moving in pipes, but are typically not capable of selecting branches of joints or taking sharp (mitre) joint. With a *mitre joint* a joint is meant which is made by bevelling each of two parts to be joined, usually at a 45° angle, to form a corner, usually a 90° angle³. This in contrast with the 90° bends with an inner radius

mitre joint

3.3 Related research

3.3.1 Introduction

The related work for this project consists of many research projects on qualitative testing methods for pipe systems, current methods for in-pipe inspection and the design and development of (robot) vehicles for in-pipe navigation.

3.3.2 NDT quality inspection

The preferred method of inspection of live distribution systems is an *NDT*- or Non Destructive Testing method. KIWA is specialised in both destructive and non-destructive testing. Currently used methods (deployed by robots, remote probes and endoscopes) are *optical*, *US* (ultra sound) or *EC* (eddy current). On pipe inspection gauges (PIG's) also a large variety of calliper tools (size/diameter) and inertial measurement systems are being deployed.

NDT

KIWA uses stress-strain tests executed in their laboratory facilities in Apeldoorn for predicting service life of network components, mainly being PVC, PE and grey cast iron pipes. Roy Visser [106] uses a hybrid technology: technically, a pipe is damaged using a needle (micro indenture), but since the indenture is very shallow and small (micro scale) the pipe can still be in operation.

The most common method for assessment is searching for leaks using gas detection sensors above ground. They are used to '*sniff*' the leaks, using a tiny cart containing sensors as shown in figure 3.3. By law - as mentioned in section 1.3 - every segment of the distribution network has to be inspected in this manner every 5 years.

sniffing

A different method for assessment of pipelines above ground is the use of ground penetration radar (*GPR*) or pipe penetration radar, as described in texts by Conyers

GPR

³See Wikipedia: http://en.wikipedia.org/wiki/Miter_joint



FIGURE 3.3 Leak searching using ‘sniffing’ equipment - *image courtesy of KIWA*

et al. [17]. This technology is widespread amongst archeologists⁴ and has successfully been used to detect orientation and position of pipes from the outside. The technology is under attention of network operators and is being developed and refined, a.o. in the ORFEUS project by Parrini et al. [69]. A recent development is the use of ground penetration radar from the inside of pipes as described by Ekes et al. [31], which is commercially used by the firm SerwerVue⁵.

More recently above ground also (autonomous) flying vehicles or drones have been applied to monitor integrity (road works, excavation works) around pipelines. Detailed measurements and imaging techniques can give information about stress and strain to known pipes by comparing images over time [114].

3.3.3 In pipe inspection methods

pan-tilt

The most common surveillance and inspection method for small diameter pipes is using camera systems. Either using a passive, stiff tether with a *pan-tilt* camera at the end, such as employed by SyntoCam, a branch of SynthoTech Inspection Systems⁶, or tethered camera’s on tractor vehicles with tracks or wheels - figure 3.6 categories (b) and (c) - such as employed by IBAK Inspection Systems⁷ shown in figure 3.4.

PIG

The most common surveillance and inspection method for large diameter pipes is using Pipe Inspection Gauges or *PIGs*, in figure 3.6 shown as category (a). Compa-

⁴http://en.wikipedia.org/wiki/Ground-penetrating_radar

⁵<http://www.sewervue.com>

⁶<http://www.synthotech.com>

⁷<http://www.ibak.de>



FIGURE 3.4 Industrial endoscope system for pipe inspection

nies like ROSEN Inspection Robotics⁸ employ PIGs with a variety of sensors (US, EC, Calliper) and perform regular measurements of big (oil) transportation mains. An example is shown in figure 3.5.



FIGURE 3.5 Geometry (or caliper) PIG by ROSEN- *image courtesy of ROSEN Inspection Systems*

3.3.4 Robot systems

A number of very detailed state of the art overviews of in-pipe inspection robots have been written in the past years. The most noticeable and complete are articles by Roh et al. [36] which includes the much quoted propulsion mechanism

⁸<http://www.rosen.com>

overview (figure 3.6) and Mirats Tur et al.[63] which discusses systems aimed at (submerged) water pipe inspection, and more recently by Ismail et al. [46] giving a general overview and Roslin et al. [82] which discuss a 'hybrid' breed of robot systems. Most of the complete systems for pipe inspection are either wheeled robots, category (b) in figure 3.6, clamping robots, category (d), or a combination of both. Neunbauer et al.[66] showed some examples of this combination in their work on a legged robot, category (e), for in-pipe inspection, reproduced in figure 3.7.

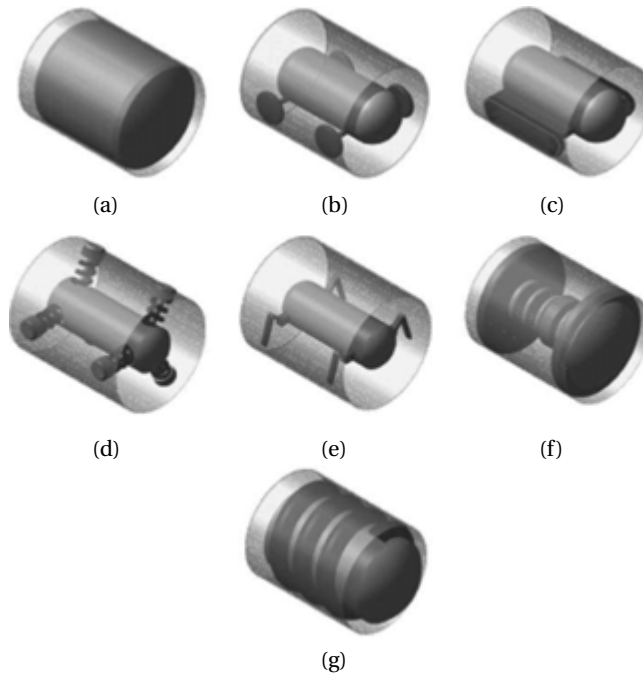


FIGURE 3.6 overview of propulsion mechanisms - *image from [36]*

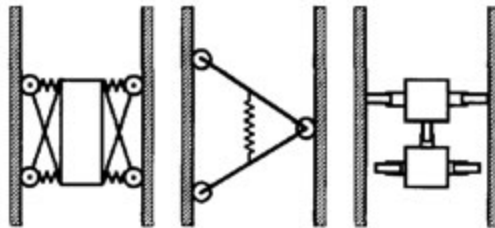


FIGURE 3.7 overview of clamping propulsion systems - *image from [66]*

The amount of literature available on designs for in-pipe inspection, navigation

and sensing is large. Different diameters, materials, conditions and, more importantly, different aspects of in-pipe robot design are being addressed in these. In the following section an overview of complete systems will be given. Literature covering one single aspect of a design (such as a propulsion system, actuator or sensing system) is addressed in their respective design chapters. Two systems, the *CMU Explorer* and the *RoboScan* by FosterMiller have been used for a comparison regarding performance and specification in section 3.4.1. They will also be discussed in this section.

Wheeled robots

The most conventional (and industrialised) concept for in-pipe navigation is a wheeled vehicle such as shown in figure 3.8. Robot designs like KARO [56] and MAKRO [38][54][96] use this principle, where the MAKRO has also articulated joints in between a number of wheeled modules. The volume of these vehicles is optimised for manoeuvring in pipes (so they have basically a cylindrical shape), they are heavy (so they can pull a tether, providing the wheels with enough traction) and they have been equipped with cameras or other sensors.

For this type of robot it is only possible to move through mitre bends and T-joints in pipes much wider than the robot's diameter. Depending on the chosen shape, the length of the robot cannot exceed the pipe diameter too much, see figure 3.17 for a sketch of the maximum volume that can pass through a mitre bend in a given diameter.



FIGURE 3.8 MAKRO robot - image from [54]

In steel pipes often magnetic wheels are used to increase traction force. One of the fundamental issues is how to switch the magnetic force on or off. The robot design by Kawaguchi et al. [50] uses a wheel-in-wheel design. Robots designed by EPFL

together with ALSTOM by Tache et al. [97][98][116] use a variety of clutch mechanisms and other designs such as additional lifters for this purpose. A good overview of this type of systems is given in the work by Caprari et al. [12].

Wheeled robot KANTARO [65] uses differential drive to select branches in (smooth) T-joints. This robot drives *sideways* through the pipe, avoiding the bottom.

Explorer-II

Explorer-II (figure 3.9) is an autonomous pipe inspection robot built by CMU (Carnegie Mellon University). This research project is in an advanced stage. The first field trials of the system have been conducted at the end of 2005. The project started with the name GRISLEE [85]. Results have been published in 2010 by Schempf et al. [84]. The system can carry out an autonomous visual inspection of 1 km length of pipeline.



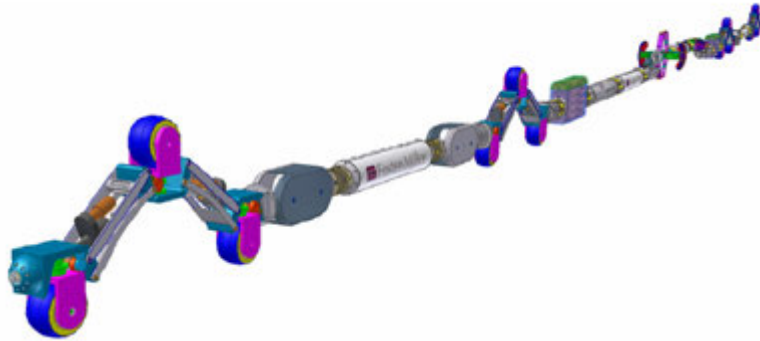
FIGURE 3.9 CMU Explorer II - *image from [84]*

RoboScan

RoboScan (figure 3.10) is a conceptual design by Foster-Miller [108], based on their previously built prototype called 'Pipe-mouse'. A number of study models have been investigated, and the system is well documented (detailed specifications are, however, classified). There is no data available on field trials.

MRINSPECT

The MRINSPECT series of robots has been developed over the past decade. The robot also falls into the category of wheeled-clamping vehicles capable of taking turns in T-joints. At large number of incarnations have been published by Roh et al. [15] [16] [36] [37] [51] [79] [80]. The current model is MRINSPECT VI. Comparable systems have been realised by Gambao et al. [10] and Sato et al. [83].

FIGURE 3.10 RoboScan - *image from [108]*FIGURE 3.11 MRINSPECT IV - *image from [16]*

Screw type robots

Screw-type wheeled mechanisms can also be considered in the category of clamped wheeled platforms. According to their website, the Houston based company itRobotics [48] has produced a small pipe inspection robot system called SPI 774. This system can autonomously carry out a visual inspection of coiled pipe (same diameter, no bumps, no T-junctions). The propulsion system looks similar to models by Hirose [43] and derived works such as the robots by Horodincea et al. [45] and more recently by Yabe et al. [113].



FIGURE 3.12 itRobotics' autonomous inspection system - *image from [48]*

Snake type robots

Snake type robots have a high agility, flexibility and can move through T-joints and obstacles. A recent (industrialised) snake robots for in-pipe inspection has been designed at CMU by Wright et al. after a series of prototypes discussed in [109][110]. The system is shown in figure 3.13. A good overview and comparison of snake-type robots is given in a survey article by Hopkins et al. [44].

Also the recently revealed Pipetron⁹ by HiBot consists of a robot snake using a modular wheeled clamping structure. This robot can manoeuvre through pipes in a range of 70 - 80 mm and take smooth bends and t-joints.



FIGURE 3.13 CMU modular robot snake - *image from [109]*

⁹http://www.hibot.co.jp/en/products/robots_1/pipetron_30

Inchworm type robots

A good overview of all (mostly pneumatic) inch-worm type robots, in figure 3.6 shown as category (f), is given by Ono et al. [67]. Although inch-worm designs are very flexible and agile, they lack the necessary velocity and dexterity for the environment that needs to be inspected.

3.4 Design Considerations

3.4.1 Technical performance measures

In this section the performance measures resulting from the requirements in the previous chapter will be compared with two existing systems. Goal is to estimate how important it is for a certain measure to outperform the competing designs (and by doing so estimate the feasibility of the design). Table 3.1 lists a number of performance measures of RoboScan and ExplorerII compared with the required specifications for the PIRATE design. Specifications have been obtained from [108] and [84].

TABLE 3.1 Technical Performance measures

specification	RoboScan	ExplorerII	PIRATE	weight(%)
clamping	250-500 mm	150-200 mm	55-114 mm	40%
weight	–	30 kg	1 kg	20%
range	8 km	1.8 km	2.4 km	10%
autonomy	–	8 hour	8 hour	10%
speed	0.15 m/s	0.1 m/s	0.08 m/s	5%
size(length)	12 m	2.4 m	–	5%
gas speed	6 m/s	minimal	30 m/s	5%
cycle	–	24 hour	24 hour	5%
total				100%

3.4.2 Modular Design

The system design can be divided into modules with their own specific function such as propulsion, clamping, sensing, power supply, etc. An even better approach would be to use many similar modules to achieve a certain performance. Snake robots as discussed in section 3.3.4 have this benefit. Also for repair and maintenance a modular approach has many benefits: replacing a module can be more effective than having to repair a system at component level.

Module Size

The maximum module size determines the shape of the mechanical system. The module has to travel through the pipe, so at least at one of the surface planes, the size of its shape cannot exceed the size of the minimal pipe diameter. Besides going through the pipe itself, also sharp (mitre) joints and elbow joints need to be taken.

The thickness of pipes is often given in SDR ratio¹⁰: $SDR = D/s$, where D = pipe outside diameter (mm) and s = pipe wall thickness (mm). The inner diameter of a 63 mm pipe with SDR 17.6 is 57 mm. In a worst case situation it might contain welds of roughly the wall thickness, being two 3 mm welds, resulting in an inner diameter to pass through of 51 mm, see also table 2.3.

The restricting element in the network determining the maximum module volume and shape is the mitre joint. When rigid module shapes are considered, the symmetrical volume that can pass through is in this case limited to a 'pill' shape: a cylinder with hemispheres at both ends. The maximum volume which could pass through is a curved cylinder (*banana shape*) as drawn in figure 3.17, which can be determined graphically. However, when a symmetrical shape is necessary (or allowed) this pill-shape is sufficient to indicate the upper limit of space per module, for example for battery storage.

banana shape

The configuration for which the optimum is being calculated is when the module is at a 45° angle inside the elbow joint. This situation is displayed in figure 3.14. The maximum length l_{max} of any object going through this joint cannot exceed the cross-section width at 45°, in case of the banana shape the maximum distance between the end-points. The maximum radius r an object going through a joint can have is half the pipe diameter D .

In figure 3.14, the maximum volume for a pill shape fitting in the mitre joint consists of two half spheres with radius r and a cylinder with radius r and length l :

$$l = 2D\sqrt{2} - 2r(1 + \sqrt{2})$$

$$V = \pi r^2 l + 4/3\pi r^3$$

$$l_{max} = 2D\sqrt{2}, r_{max} = 1/2D$$

where l is the length of the cylindrical piece and r is the radius of the cylinder and sphere, D the radius of the pipe and V the module volume.

¹⁰SDR tables can be found on <http://www.revaho.nl>

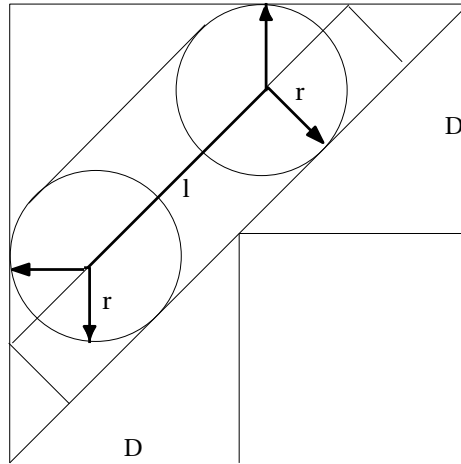


FIGURE 3.14 Pill shape in elbow joint

Given the situation shown in figure 3.14 in a pipe with diameter 60 mm, the volume that can pass through can be calculated with respect to the module diameter r as shown in figure 3.15. The maximum volume that can pass through is a pill-shape with a sphere radius of 29.5 mm and a length l of 27.2 mm and a total module length of 86 mm. When the minimum pipe diameter is chosen (including welds etc) at 51 mm, the maximum module radius would be 24.5 mm resulting in a module length of 74.9 mm and a volume of 95 cm³.

Propulsion mechanism

The propulsion mechanism is one of the most defining parts of the system design. Not only has the robot to move into two directions inside the pipe, also direction has to be chosen at T- and Y-junctions. Theoretically a minimum of two actuators is necessary: one for propulsion (forward and backward) and one for selection between two directions.

The weight of the robot together with the clamping or normal forces required to get the necessary amount of traction determine the actuator force necessary. For the traction force holds (see figure 3.16):

$$F_{traction} = F_{drag} + F_{friction} + F_{gravity}$$

The $F_{friction}$ depends on the exerted clamping force. The clamping force should be minimal, but large enough to prevent the robot from slipping. This interplay will require attention when designing a mechanism for simultaneously generating traction and clamping force.

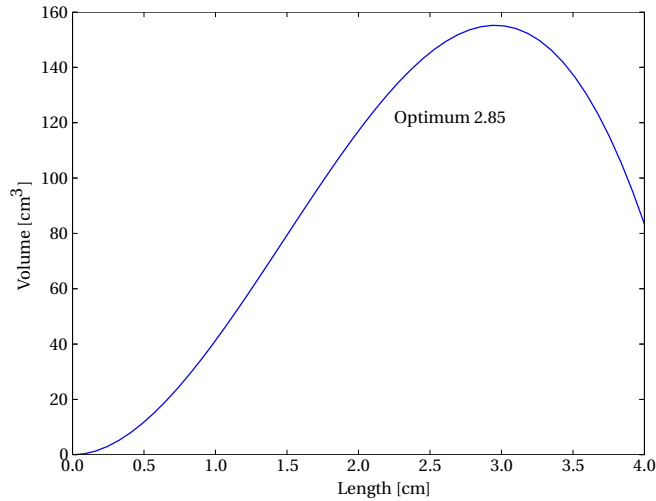


FIGURE 3.15 Volume of a pill shape fitting in a mitre bend with radius 60 mm, varying pill length l

An analysis of the volume of a pill shape that can pass through a mitre joint is shown in the previous section. The module size requirements do apply for a symmetrical shape such as might be used for a passive (battery) module. For driving and taking (selecting) corners also a curved shape can be used, especially for a module containing two wheels as discussed in section 3.2. See figure 3.17 for an estimate of this shape (2D only).

Control

A large number of propulsion mechanisms for manoeuvring in pipes need just one actuator (or a series of actuators doing the same thing, which is similar from a control point of view). The helical screw-type mechanisms such as designed by Hirose et al. [43] can move back and forward in a tube with just a single actuator. Systems that can select a direction based on differential drive such as KANTARO [65] typically need two actuators. Systems that also incorporate clamping such as the MRINSPECT series [16] typically use a differential drive for selection of the direction (mostly with more than one actuator) and also incorporate a separate actuator system for clamping inside the pipe.

The clamping V-shape, as discussed in [66], has the advantage that it can be used for both providing the clamping force on the pipe wall and for selection of a branch (in a T- or Y-junction). This selection can be made by aligning the clamp in the correct orientation and actively moving through the selected branch.

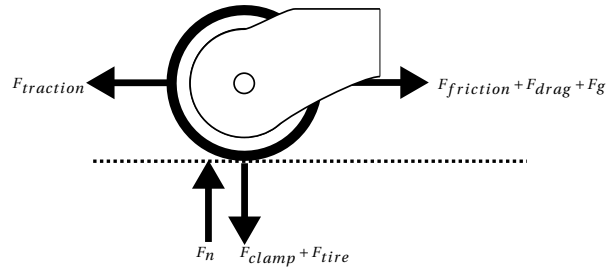


FIGURE 3.16 Traction force

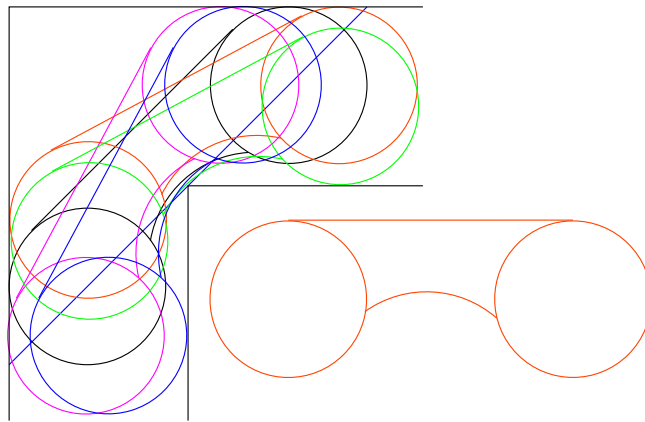


FIGURE 3.17 Sketch of the space available for a curved module in 2D

The conceptual design starts with a single clamping module shown in figure 3.18 - (a). Since selection of a branch would require the clamping V-shape to lose traction, at least one other clamping V-shape is necessary to maintain traction force (b). Since the V-shape has a preferred orientation for passing through a joint, a rotation joint is necessary for aligning the module which selects the joint with respect to the one maintaining the clamping force (c).

One of the questions to answer in this research is whether this clamping V-shape is capable of executing the necessary manoeuvres for navigation in the selected environment. It is difficult to verify this based on sketches of sizes and diameters in 2D as shown in section 3.4.2. Similar to research on passive dynamic walking robots [19], the translation of ideas from an 'ideal' world in 2D on paper and in analytical models to the real 3D world is complex. Especially since the translation is twofold: from 2D to 3D and from simulation/paper to the real physical world.

2D to 3D

In this project the choice has been made to make the transition from 2D on paper to 3D real world. Simple simulations of the 2D system have been animated in Work-

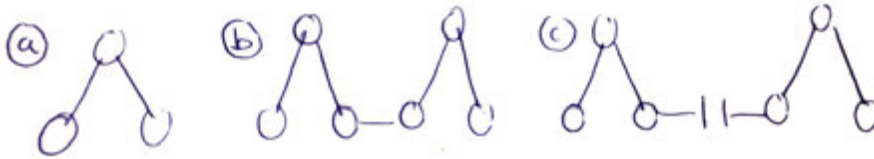


FIGURE 3.18 Sketch drawing of increasing amount of articulation necessary

ing Model (see figure 3.19). Simulations of the full system in 3D have been made in Adams¹¹ by Vennegoor [104] and later in 20sim's¹² 3D toolbox.

Although these simulations have been insightful for evaluating the structure and shape of the robot system, they did not yield detailed additional requirements. In the Adams simulation using the standard components, an animation has been made of the robot passing a joint. The contact interaction between wheels and pipe wall was modelled such that the robot was able to clamp itself sideways in the pipe in the vertical plane, starting at the bottom of the pipe. The prototype (and detailed modelling of the contact interaction) has shown that this is impossible in practice.

prototype

Since much is depending on the exact contact interaction between robot wheels and pipe wall, between clamping force and traction, the choice has been made not to spend too much effort on simulation, but to move on to a *real world prototype* as quickly as possible. The used engineering methodology is described further in chapter 11. Since many aspects of the real world are hard to capture in simulation such as all the available dents, irregularities and contamination of the pipe wall, detailed contact interaction, deformation and elasticity of the various materials used.

Power System

The power system should supply the system with its energy for the length of the autonomous operation specified in its duty cycle. A number of methods have been discussed which might be suitable, miniaturised enough, safe and accessible.

- batteries and accumulators (NiCd, NiMh, Li-Po, Li-Ion)
- fuel cell technology
- chemical energy (HO₃) - *used by Fukuda et al. in a pipe robot [34]*

¹¹<http://www.mscsoftware.com/product/adams>

¹²<http://www.20sim.com>

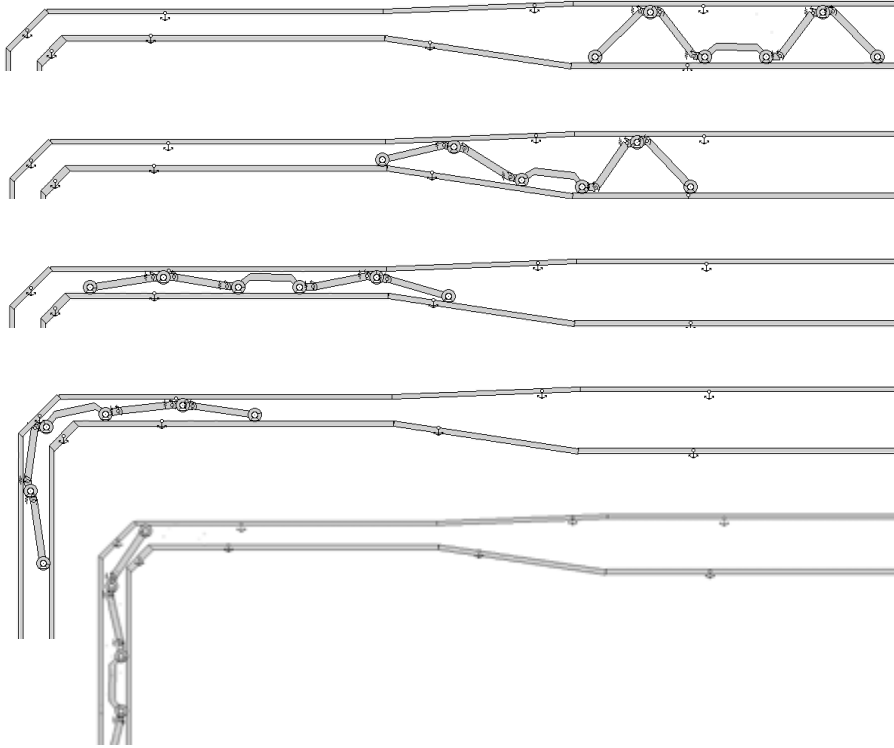


FIGURE 3.19 Sketch in 2D in WorkingModel

- mechanical energy from gas-flow
- compressed air - *used in many peristaltic inch-worm type robots [52] [41]*

A power source main function is to store a certain amount of energy in as little space as possible, and release that energy gently over time, preferably not all at once. Especially the possibility of that last event occurring should be ruled out by the chosen system. Demands regarding safety and contamination of the network rule out the options which produce (possibly) excessive heat or contaminants. Also risk of explosion should be zero (or as close to zero as possible). Therefore fuel cell, nuclear energy and combustion engines can be ruled out. (non-mature technology, possibility for contaminants, production of heat). Although batteries provide the risk of explosion (when shorted) they are mature and standard technology, used in many safety critical systems today.

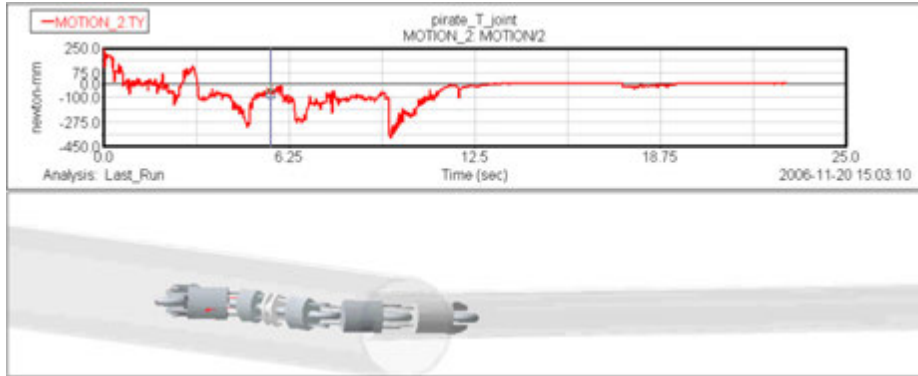


FIGURE 3.20 Simulation in Adams of the robot taking a corner

Unlike the PIGs that operate on oil pressure in the pipelines, the amount of energy that can be obtained by the mechanical gas flow is according to the following back-of-the-envelope calculations¹³ too small to be useful for a mobile robot. Due to the meshing of the network and the fact that gas will always choose the path of the lowest resistance, it is not feasible to obtain enough gas flow through or around the robot in order to produce a sufficient amount of energy.

The density of natural gas ρ is 0.781 kg/m^3 (101325 Pa and 273.15 K) with a typical flow to a household of 1 m^3 per hour. In a network using 63 mm pipes with a pressure of 100 mbar, the maximum pressure margin is 60 mbar allowing a required minimum of 40 mbar at a home connection.

The maximum gas velocity is 20 m/s (audible noise being the limiting factor). The kinetic energy is too small to be relevant: $1/2\rho v^2 = 156.2 \text{ Pa}$. The available pressure margin (6000 Pa) might yield more power.

Considering a situation where you have a gas flow from point to point, disregarding heat transfer ($\Delta Q = 0$, no other interactions that require work ($\Delta W = 0$), kinetic energy can be neglected and no elevation is present so no change in potential energy should be considered ($\Delta pe = 0$) the available power $W_{max} = \Delta P Q = \Delta P \frac{1}{4} \pi D^2 v_{max} = 230 \text{ W}$.

Although this looks promising, this power cannot be achieved due to three factors in the design of the network. First the network is designed such that the pressure difference is used for facilitating gas flow, which means that the pressure difference is proportional to the gas velocity squared. The available pressure at the robot is therefore $\Delta P_{robot} = \Delta P (1 - (v/v_{max})^2)$ and therefore the power at the robot $W_{robot} = \Delta P (1 - (v/v_{max})^2) \frac{1}{4} \pi D^2 v$. With a maximum gas flow at the robot of $\frac{1}{\sqrt{3}} v_{max}$ this will cause a factor 0.57 lower power.

¹³This calculation are based on a report by Pulles [72] and chapter 4 of [62]

Besides the pressure difference, although the network is technically capable of supplying 20 m/s, the normal consumption of a household is 1000 m^3 per year, which will average to (0.11 m^3 per hour). The average flow will be far less than the maximum, i.e. 10% of the maximum flow depending on the amount of connections to the distribution line.

The third aspect is the meshing of the grid. The stated calculations consider the situation where there is one supplier, one pipe and one home connection (with a robot located somewhere in between harvesting energy). The real situation is, however, that there are many branches, parallel routes and round-trips possible so it is impossible to state the pressure difference and the resulting flow in the vicinity of the robot, let alone design a way to turn this efficiently into energy for the robot.

Note that the PIGs are normally powered by pressured by gas or water. The environment they have to operate in can tolerate higher pressures than the discussed network, and, most importantly, are always used in a situation where a pipe has one entry and one exit (no meshing).

The battery technique with the highest energy density is the *Lithium-Polymer* or *LiPo* cell. These cells can store up to 0.3 Wh/cm³ with a weight of just 2 gram¹⁴. Current advances in battery technology can be found in the area of mobile computing and equipment. Publications can be found in the area of electric vehicles, such as [26], or robot vehicles such as the Mars Rover [74].

LiPo

The size of a battery cannot exceed the maximum module size. According to the previous section on module sizes, the maximal volume of a pill-shaped module is 95 cm³ (a module with 24.5 mm radius and a total length = 74.9 mm). The assumption that all of this volume can be used for energy storage is quite optimistic. This pure volume would allow for 45 Wh storage. A storage of 30 Wh is more realistic.

If the robot-train would be able to carry two battery modules, (like the CMU-Explorer and the RoboScan) the total usable energy storage would be 60 Wh. For an autonomous operation cycle of 8 hours, a total average consumption of 7 W is available. Note that battery technology is under rapid development at present time and capacity will increase in coming years.

Electronics

For the robot it is necessary to control position and possibly force control of all actuators. Therefore a number of control loops needs to be closed. In order to relieve the central processor of this real-time demand, a *distributed system* with one mas-

distributed system

¹⁴http://en.wikipedia.org/wiki/Energy_density

ter controller and several small local motion controllers (slaves) is proposed. Also the amount of wiring necessary for a centralised control system would likely have a severe impact on the design. Using a standard communication bus the master controller can give set-points and query the status of an actuator, while the slave controller executes the control loop. The requirements for the local control hardware are:

- position/force control of actuators used in the robot
- Small size i.e. 4 cm²
- Hardware for bus (CAN, I²C, RS485, ProfiBus) communication protocol
- Capable of executing PID control loops at 1 kHz (estimate)
- interfacing necessary sensors for motor current (torque) and position
- low power requirements, low voltage requirements i.e. LiPo cells

The master controller (or main controller) has to execute the (autonomous) control of the robot. Interfacing the sensors, vision processing, communication with an external operator. This requires more computational capacity and power than the slave controllers:

- tracking robot position: inertial measurement, (visual) odometry
- navigation based on maps, simultaneously localising and mapping the network (SLAM)
- recording and logging of sensor data
- recognising (emergency) situations
- operator control

Sensing

The sensing system has to be developed for both *assessment* of the pipe and *navigation*. A number of sensors is proposed on the robot, so that by combining sensor data (sensor fusion) qualitative and quantitative assessment of the pipe can be made.

assessment

navigation

For navigation the robot needs to know orientation, traveled distance in the pipe and its relative position with respect to a priori known landmarks such as branches and junctions. A positional accuracy of 0.5 meter is required regarding the detection of leaks (see table 2.5) above ground since a pipe has to be excavated for at least a section of 3 meter, so accuracy beyond cm-range is not necessary for localising the leaks. However, for the localisation inside the pipe for navigation, a higher

accuracy is necessary, typically in the millimetre range depending on the robustness of the procedures for manoeuvring through junctions.

During operation it is important to know where the robot is in the network, especially in case of emergencies. Also when communication from inside the pipe to the outside is not possible (or necessary, since the robot can store the relevant data), it might be important to know where a robot is located.

Because of the subterranean operation, it is not possible to use *GPS* for navigation, because *GPS* relies on receiving radio signals broadcasted by satellites on a wavelength that does not penetrate the ground (or buildings). Dead reckoning¹⁵ by using odometry data combined with a magnetic compass (only if in non-ferro material pipes) might be a feasible solution. Odometry data is normally collected using wheels with rotary sensors that move over the pipe wall. Other solutions are using visual (flow) data as employed by Hansen et al. [40]. *GPS*

IMU's or inertial measurement units combine data from accelerometers (measuring the direction of gravity) and gyroscopes (measuring rotational velocity). Also in some cases magnetometers (as compass sensor) and pressure sensors (barometric pressure varies with height) are used. Although they can give accurate orientation data, translation measurement (by integrating the linear acceleration sensor data twice) is highly susceptible to drift. Fusion of vision data with sensors for *inertial measurement* have been used for simultaneously localisation and mapping inside a pipe, as demonstrated by Kryš et al. [55]. *IMU*

Radio systems have been used for localising robots from the outside of a pipe. For PIGs this is common practice. Using ultra-long radio waves transmitted from inside the (metal) pipe, above ground the PIG can be located using an array of antennas, up to 10 meter in depth as shown by Haiming et al. [39]. However, it might be that the required power for transmission is too high for the portable power source.

Other methods for localisation inside pipes include using radioactive sources such as deployed by Xue-Mei et al. [112] or (ultrasonic) RFID beacons as shown by Chen et al. [14].

Data on the *diameter and shape* of the pipe is necessary for two main reasons: Determining pipe status and navigation. For the first the data is used to give an indication of bend, tension, corrosion, holes, dents and other strong deformation of the pipe, which can be used to predict future life of the pipe. For the navigation part, sensing the pipe diameter (in front of the robot) is necessary to detect upcoming diameter changes, welds, (T-)joints, valves, etc.

For detecting leaks the addition of an acoustic sensor is proposed. By measuring the acoustic noise of a leak (in the ultrasonic range) introduced by the (small) gas flow out of the pipe a leak can be detected [73]

¹⁵[wikipedia on Dead Reckoning, http://en.wikipedia.org/wiki/Dead_reckoning](http://en.wikipedia.org/wiki/Dead_reckoning)

Based on the requirements stated in table 2.5 for the first prototype the following set of sensors (with possible implementation) is proposed:

- inertial orientation measurement (accelerometer, gyroscope)
- position (internal state) measurement (angle sensors, torque sensors)
- relative traveled distance (odometry sensors, magnetic compass)
- leak sensor (acoustic)
- diameter (vision system)
- landmarks (vision system)
- visual inspection (camera system with additional light source)
- obstacle sensors (vision system).

Communication

For semi-autonomous or full operator controlled operation is continuous communication necessary. Tether systems have to be evaluated, as well as possibilities for other means of long-distance communication suitable for pipes. Also for (emergency) communication a short-distance radio link through the soil to the surface should be investigated.

Since path-damping for radio waves underground is very high it is unlikely that it will be possible to communicate with the robot for the entire duration of an *autonomous* mission. The underground network will sparsely allow communication using radio signals, and it is very unlikely that acoustic communication will work over large distances. Therefore all important communication has to take place while in dock. For communication at a docking station practically any short-distance communication method (Infrared (IrDA), short range radio (Bluetooth, WIFI) or physical electrical wire (Ethernet, RS232) can be used.

Although it is convenient to have a data-transfer at a reasonable rate, time is not really an issue when an autonomous robot is scheduled to be in dock for at least eight hours for recharging its batteries. Even at the relatively slow standard speed of 115.200 bps (RS232, IrDA) it is possible to exchange 40 Mb in one hour. That will make it possible to do a complete software-update and memory exchange within less than one quarter of the recharging time.

Docking station

Two docking station systems can be distinguished. First an entry-lock attached to a live gas mains system capable of launching and retrieving a robot and (tethered) communication with the robot. Secondly an underground docking station should be developed for (autonomous) missions. This docking station has two main functions: *recharging* the robots batteries and *exchange* of information: receive data from the investigated area, upload new data, a new map, perhaps new software. Additional features such as repair and cleaning of the robot are for further research. The connection at the docking station should be a simple and straightforward procedure. The robot should be able to automatically dock, make connections and start energy and data exchange.

recharging

exchange

The docking stations will have to be connected to the existing gas mains. They will need an external power connection for the charging electronics and their own operation. They also need a communication link to where the data is collected, either to a central point or in a mobile field operation post.

One of the options mentioned in the economic feasibility analysis is a sort of probe that can be inserted in the gas mains from a home network connection. At the home-connection side, the probe system will connect to the electric energy grid and perhaps the existing network (e.g. telephone or internet). Inside the main pipe (typically under the street) a small docking-connection mechanism will be able to attach to the robot and make a connection (electrically, data).

3.5 Conclusion

Based on the observations in this chapter, in the following chapters three realisations of the given conceptual design will be discussed. The focus for realisation of the robot will be on the following points:

- modular design using clamping V-shapes and a rotation module
- wheel design optimised for friction contact with the pipe wall
- distributed control architecture minimising wiring
- internal sensing and monitoring system
- (optical) sensor for navigation and pipe assessment
- both a tether system and short-range wireless communication system for battery operated tests
- operator control interface.

Design of the docking station, realising a network (swarm) of robots, full autonomy (both software- and power system wise), have been given a lower priority in the remainder of this thesis.

This chapter discusses the work on the first mechanical design which originated at DEMCON and has been completed at the University of Twente.

4

Mechanical Design: Prototype I

This chapter discusses the first design of a mechanical structure of a miniature pipe inspection robot¹ capable of moving through very small pipes. The requirement to negotiate bends, T-joints and steep inclinations poses another set of strict design constraints. The proposed robot consists of a modular design (7 modules) with a relatively low number of active degrees of freedom. The system is using a novel clamping mechanism with a series-elastic drive. The design of this mechanism has resulted in a high spreading factor allowing the system to operate in a wide diameter range of standard components in the gas distribution network (63 mm to 125 mm outer diameter). In this chapter the mechanical design requirements and control system will be discussed. Preliminary test results will be given.

4.1 Introduction

The majority of current robot designs for pipe inspection use a clamped, wheeled design: Explorer by CMU [109] the MRINSPECT [36] and many others [108] [48] [10] [43]. They have been discussed in detail in chapter 3.

When ‘network’ components are discussed, i.e. the physical tubes and connection pieces that are used in the network, it is normal to use the standard outside diameters (63 mm, 75 mm, 110 mm, 125 mm, see table 2.3). For the design of the robot the inside diameters are important, which depend on material properties, wall thickness and the presence of welds on the inside.

In the PE pipe of 63 mm the welds have a height of 3 mm. In PE(125) heights of 5 mm are

¹This chapter has been published at the ICRA 2011 [21]. The master’s thesis by Jeroen Vennegoor [104] and internship project by Jos Anskink [4] on this work have been conducted at DEMCON. The work has been continued at the University of Twente with the master’s projects of Harm de Boer [18] and Harwin Reemeijer [75].

possible. The welds have a length varying from 6 - 11 mm. In a 63 mm pipe of PE, SDR 11 (which means the wall thickness is 5.7 mm) the inner diameter is 51.5 mm. With a combination of a protruding weld on the inside of 3 mm and deformation of 10% the absolute minimal diameter for the robot to pass through is 41 mm. The question is whether this worst-case value should be leading, or the situation that *either* a weld or a 10 % deformation has to be dealt with.

None of the existing systems discussed in chapter 3 are capable of taking a sharp (mitre) joint in a 63 mm pipe - which has been established as one of the key criteria for being able to operate in the given (Dutch) urban low pressure network [72]. Another requirement for this robot is a high spreading factor (maximum/minimum pipe diameter) which has to be higher than in existing robots. Depending on wall thickness and possible deformation, the inner pass-through diameter of a 63 mm pipe can be as low as 41 mm (worst case). The inner diameter of a 125 mm pipe can be as large as 120 mm. Therefore the spreading factor should be high: $120/41 = 2.95$.

The focus of the design of the discussed first prototype is on the capability of manoeuvring through these small diameters and sharp bends. Besides the mere capability of moving through bends and small diameters the design is optimised and intended for long (autonomous) operation. A schematic image of the developed robot is given in figure 4.1.

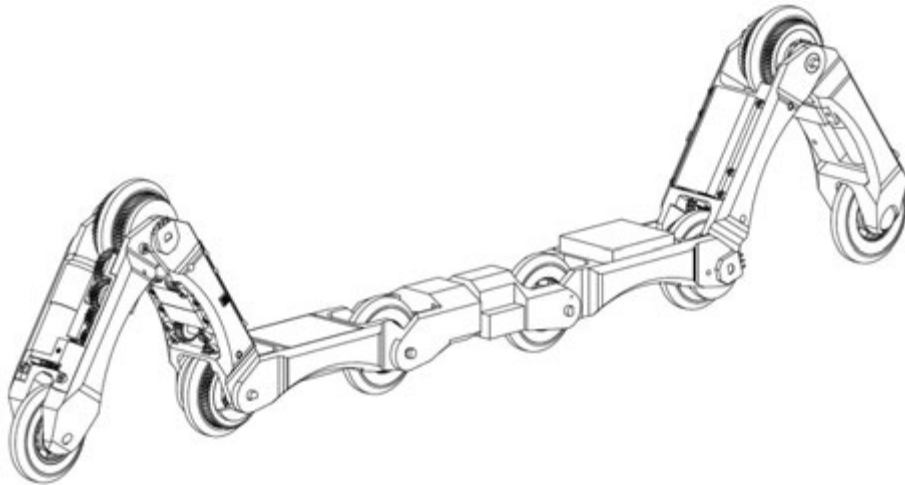


FIGURE 4.1 Schematic drawing of the pipe inspection robot - *image from [104]*

4.2 Requirements

The requirements have been discussed in detail in chapter 2. In this section some of the important requirements for the mechanical system will be repeated shortly. These requirements have led to the robot design that will be presented in the section thereafter.

4.2.1 Goal

The final aim of this project is to realise a platform capable of autonomously inspecting a certain area of the gas distribution network, detecting leaks and recording the exact location and status of the pipe. The most stringent requirements are posed by the environment the robot has to operate in: the layout and makeup of the gas distribution network.

4.2.2 Environment

The mechanical properties of the environment regarding size and shape can be listed in order of increasing complexity for a mobile robot system and are listed in table 2.1. The inside diameter for a pipe follows from the SDR number. Typically, SDR 11 or SDR 17 pipes are used. Besides the network components (welds, sleeves, bends, T-joints) the environmental temperature, moisture and contamination are also important with respect to toleration and robustness. The criteria, sizes and network elements have been selected in close cooperation with gas network operators².

Material

In general the robot has to move around in a PE/PVC pipe of 63 mm with a smooth surface and in a pipe of grey cast iron of 100 mm with possible corrosion. These two inner surfaces are very different. In the PE/PVC situation it is likely for the robot propulsion module to lose traction because of slip due to the smooth material properties. In the case of a grey cast iron pipe, it is likely for the robot to lose traction because of contaminants (rust, dust).

Connections between pipes

Connections occur in the network with an average frequency of once per 12 m. Two methods for connecting pipes are used: by *welding* and with *sleeves*. Welds have an inner height of roughly the pipe wall thickness. The inside diameter minus the inner height of these welds, together with the allowed external deformation (dents) of the pipe, specify the maximal height and width of the robot system.

²Liander, <http://www.liander.nl>

T-joints and corners

Although the somewhat flexible PE/PVC pipe allows (gentle) curves, normally for corners and bends special connection pieces with varying radius (curvature) are being used. They are connected to the pipes with sleeved connection pieces. Also T-joints are mostly connected with sleeves. In these T-joints and sharp (mitre) bends we find the parts imposing the severest space- and morphological constraint on the robot design (see figure 4.2). By other systems such as the MRINSPECT [36], this problem has been partially solved by using T-joints and elbow joints with a smooth radius. For this project, however, changing the network is outside its scope.

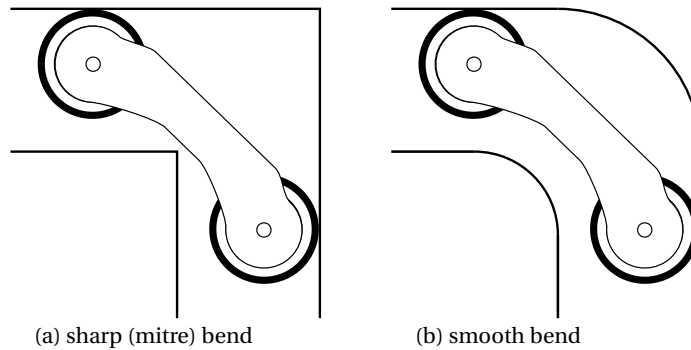


FIGURE 4.2 Schematic drawing of robot module in sharp (mitre) bend besides a smooth bend

4.3 Design

4.3.1 Design concept

The requirements for the mechanical design can be summarised as:

- high spreading factor: clamp in 41 - 120mm inside diameter
- take a mitre bend
- actively select the route in a T-joint
- move efficiently through long straight segments of the network
- move through tilted pipes (climb up and down a 30° angle)

A clamping V-shape as presented schematically by Neubauer et al. [66] (see figure 3.7) has been chosen as base concept. In order to be able to select and steer into T-joints a rotation mechanism has been designed in between (a number of) these clamping V-shapes.

4.3.2 Modular Design

The proposed structure of the robot allows for a separation in *modules* with each its specific function. Regarding maintenance and operation a modular design has advantages: when the interface (both mechanical and electrical) between modules is well chosen, modules can be interchanged or swapped for repairs or maintenance and modules can be added or removed for specific missions, adding functionality. Also the manufacturability of the system increases when it consists of modules using an identical shape and identical parts.

Therefore a modular design has been chosen for the robot system. The robot consists of seven modules with specific functions: two propulsion- or driving modules, two modules to clamp the robot in the pipe, two payload modules and one central rotation module. The payload modules contain the power system, control electronics and sensing equipment.

This concept has been extended even further in subsequent prototypes (see the following chapter 5) where the functions of propulsion, clamping, control and power have been combined in identical modules, much more similar to a 'snake like' modular approach [44].

As can be seen in figure 4.1 the robot has a symmetric layout around the central rotation module. The maximum module size is determined by the pipe diameters and obstacles as stated in table 2.1. At least at one of the surface planes, the size of a module cannot exceed the size of the minimal pipe diameter (see figure 4.3) Moving through sharp elbow joints and T-joints poses another constraint, besides being able to clamp into both 63 mm and 125 mm pipes. These constraints have resulted in a curved module shape, using a wheel diameter of 40 mm and an inter-wheel distance of 90 mm.

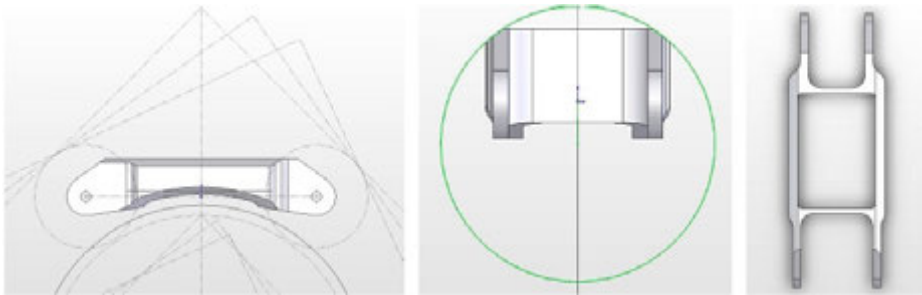


FIGURE 4.3 Module size and shape - *image from [104]*

Bending module

It is possible for the robot to clamp itself in a pipe using the V-shape. The orientation in the pipe can be arbitrarily chosen. In order to avoid contaminants and dust on the bottom of the pipe, it is advantageous to clamp and drive *sideways* through the pipe, in the horizontal plane, as illustrated in figure 4.5 and 4.4.

Most of the drawings and pictures of the robot system in this thesis show the robot aligned in the vertical plane with respect to the earth, at least from the viewpoint of the observer. Although this is a useful orientation to display the robot, for taking corners, bends and omitting contaminants and dust on the bottom of the pipe, a horizontal orientation might be preferred. This means that in that respect most of the drawings and pictures show a *top* view of the system.



FIGURE 4.4 Top view and side view of robot model in 125 mm pipe - *image from [104]*



FIGURE 4.5 Top view and side view of robot model in 63 mm pipe- *image from [104]*

To drive sideways through a pipe, the robot always needs to exert a certain force on the wall in order to keep itself in the centre. It can generate this clamping/preloading force through a torque between the first two modules and the last two modules of the robot. Two geared motors with a spring connected acting as series elastic actuator or SEA [70] are used to generate this clamping torque.

SEA

A spring in series with the motor that is used for generating the clamping torque has the advantage that small bumps and welds can be taken by the robot without having to adjust the control mechanism. Also from the point of view of conserving power (as discussed further in the work on the V2E2 actuator by Stramigioli et al.

[95]) a spring can be used for storing energy especially when dealing with periodic motions. The primary choice for using a spring in case of the clamping module is that a certain clamping torque can be maintained without providing energy to the motor. This is a result of the self-locking properties of the chosen worm gear. The complete drive is shown schematically in figure 4.8.

Figure 4.7 shows the assembly of the spring mounted inside the driven wheel. Two potentiometers are used as displacement sensors. In this configuration one of the sensors measures the angle between the modules. Since the other is connected on the same physical body, only separated by the spring, this sensor measures the spring deflection directly, independent of the angle between the modules. An other function of these motors is to bend the entire robot shape along the curve of a bend or T-joint.

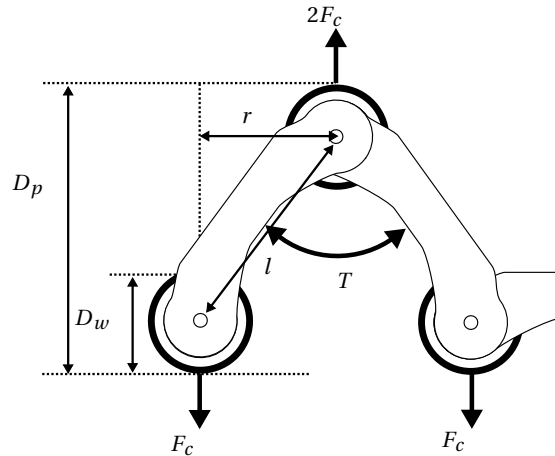


FIGURE 4.6 Geometric relation for calculating the clamping torque

A torque T is generated between the two modules and this results in a clamping force F_c on the wall, as shown in figure 4.6. At one side there is only one wheel. This wheel has twice the clamping force of the other two wheels ($2F_c$). Because of this fact this wheel is used for traction in this prototype. *In the prototype discussed in chapter 5 all wheels will be driven.*

This means that the same torque creates a larger clamping force in a big pipe than in a small pipe. The driving torque also influences the preload torque: the reaction torque of the driving torque actually adds up or subtracts from the bending torque generated by the bending module:

$$T_{preload1} = T_{bend1} + T_{drive1}$$

Using data from table 4.1 the clamping force depends on the diameter D_w in which the robot is clamped:

$$F_c = \frac{T}{r} = \frac{T}{\sqrt{(l^2 - (D_p - D_w)^2)}}$$

The clamping force needs to generate enough friction between the tires and pipe wall to allow the drive motors to move the robot. The weight of the robot which has to be moved is the limiting factor. Considering a slope α , a robot with an estimated weight m , for the total traction force F_{tr} holds

$$F_{tr} = mgsin(\alpha)$$

The necessary clamping force F_c depends on the necessary traction force F_{tr} and tire friction coefficient μ :

$$F_c = \frac{F_{tr}}{\mu}$$

In the case of moving up the slope, considering a situation where two clamping V-shape sections are used, each of the sections need to deliver half of the required traction force. Using an estimated mass m of 1.4 kg and a slope of 30° , (see table 4.1) the traction force per section is $1/2F_{tr} = 1/2mgsin(\alpha) = 3.1N$. With a worst case assumption of $\mu = 0.3$ this means a clamping force F_c of $3.1/0.3=10.6$ N is necessary per clamping V-shape.

In the smallest diameter (a pipe diameter of 51.5 mm inside diameter) arm r is $\sqrt{(0.09^2 - (0.0515 - 0.04)^2)} = 0.089$ the torque required to produce this force is 1.44 Nm. Since the V-shape yields twice the clamping force at the wheel depicted in figure 4.6 the necessary torque for the joint is 0.720 Nm.

The bending actuator contains a position actuator in series with a spring, so it can be considered a torque actuator. As stated earlier, compliant behaviour of the bending module can compensate for small bumps and diameter changes when driving through a pipe, without using the bending actuators.

A torsion spring capable of handling the required torque appeared too large to fit in the bending module. For that reason the torsion spring is placed inside the main drive wheel. As DC motor Faulhaber 1016 has been chosen with a 1:64 gearbox. For further reduction a worm gear with a single start and a small lead angle is used. The total reduction used is 1:5486, realised as shown in figure 4.9.

Because of the use of a worm gear, the expected efficiency in generating the clamping torque is very low; in the order of magnitude of 20 %, severely limiting the maximum torque available. However, the worm gear has the advantage of *self locking*

behaviour. The motor does not need to be powered to maintain a certain clamping torque which is an important concern when considering battery powered operation, especially since the clamping torque needs to be provided continuously during operation.

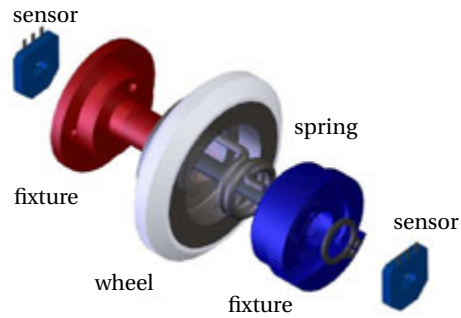


FIGURE 4.7 Assembly drawing of spring mounted in wheel - *image from [104]*

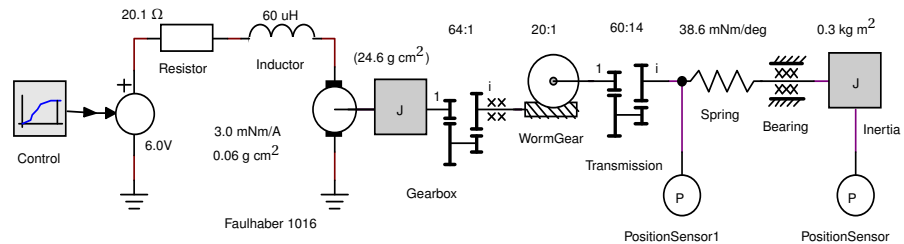


FIGURE 4.8 IPM of the bend drive, drawing from 20sim

Traction Module

The propulsion mechanism is one of the most defining parts of the system design. Not only has the robot to move into two directions inside the pipe, also direction has to be chosen at T- and Y-junctions. Theoretically a minimum of two actuators is necessary: one for propulsion (forward and backward) and one for selection between two directions. A wide variety of propulsion mechanisms is available for in-pipe navigation, as summarised in [36]. For this system the choice has been made for wheeled propulsion since wheeled locomotion promises the best energy efficiency in a structured environment.

The robot will drive sideways through the pipe, to avoid dust and contaminants on the bottom of the pipe. The length of the modules has been chosen such that the

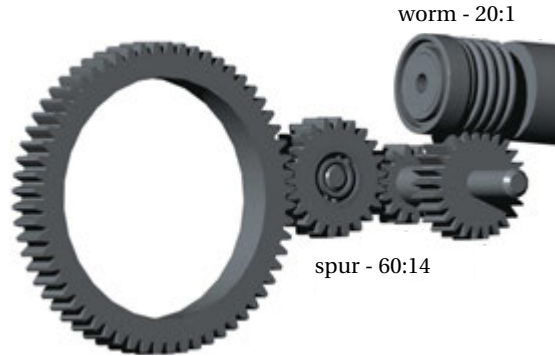


FIGURE 4.9 CAD drawing of gearing in bending module - *image from [104]*

robot can generate a suitable clamping force in both a 125 mm pipe (119 mm inner diameter) and 63 mm (57 mm inner diameter), as shown in figures 4.4 and 4.5. Note that these figures give a ‘top view’ of the robot with respect to the ground.

The robot has to be able to drive up a slope of 30° . Using the assumptions listed in table 4.1 the necessary torque for the used DC motor is determined.

TABLE 4.1 Estimate values for design parameters

mass per module(m):	0.2 kg
number of modules:	7
length of a module, axle to axle(L):	90 mm
total mass(m):	1.4 kg
slope(α):	30°
wheel diameter(D_w):	40 mm
pipe diameter (D_p):	51.5 mm
friction coefficient (μ):	0.3
	F_c : clamping force
	F_t : traction force

The traction force required to ‘push’ the robot up the slope is used for determining the necessary torque for the motors in the traction module. Not taking into account the friction due to bearings and plastic deformation of tires, the required torque for both the motors is:

$$mg \sin(\alpha) \cdot \frac{D_w}{2} = 0.194 \text{ Nm}$$

with parameters as specified in table 4.1. This torque can be divided over two motors, so each motor should deliver at least 0.103 Nm. Note that in the prototype described in chapter 5 the choice has been made to implement a drive in every wheel

increasing the amount of available drive torque.

A Faulhaber³ 1717 motor and the transmission of 1:186 yield a maximum theoretical torque at wheel of 0.157 Nm which is sufficiently larger than the required 0.097 Nm (safety factor of 1.5). The maximum driving velocity of this module is 56 mm/s. However, when performing manoeuvres which require one module to unclamp (for example taking a T-joint), all necessary driving torque has to be delivered by one of the two motors.

This means that with the chosen configuration (0.157 Nm) taking a corner cannot be executed whilst driving up a slope. Although it is not clear how often this situation arises in practice, in the next prototype (chapter 5) the system will be dimensioned such that the robot has sufficient driving torque in the situation where only one module can provide clamping force (and traction).

Rotation module

The motor in the rotation module should be strong enough to rotate one half of the robot with regard to the other half. When the rotating half is completely detached from the wall, it will be very easy to rotate. The motor then only has to overcome the friction in its own gearbox and the sliding bearing. If some wheels of the rotating half of the robot touch the wall, the required rotation torque has to be much larger.

The friction with the pipe wall depends on clamping force F_c and friction coefficient μ . Considering a clamping force of 6 N (caused by gravity, considering a robot section weighing 600 g (three modules) in vertical orientation and no additional torque in the clamping module) and $\mu = 0.5$ (rubber tire in a rough pipe) in a pipe with radius $r = 119/2$ then the friction torque is

$$r \cdot \mu \cdot F_c \approx 0.3 \text{ Nm}$$

Note that a more detailed stick-slip model is required to estimate the effects of the chosen material of the tires (rubber) with more precision both on driving (traction and deformation) and friction (during rotation). One of the problems here is that the inner surface of the pipe can be both very rough (rusty metal, ideal for traction, bad for rotation) or very smooth (PE - also used as sliding bearing material) or even smoother (PE with remnants of lubricant). The choice has been made to test the robot in a lab environment using smooth PE and PVC pipes, so regarding traction also iron (grey cast iron) pipes should be possible.

In the measurements shown in the section 4.5 all rubber wheels have been replaced with

³<http://www.faulhaber.com>

nylon wheels (except the two driven wheels) in order to facilitate axial rotation in the pipe. The friction tangent to the pipe wall is a serious problem for clamping and rotation. A radical solution for this problem has been implemented in the third prototype in chapter 6 using omnidirectional wheels.

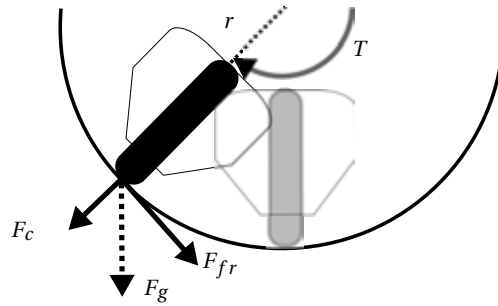


FIGURE 4.10 Friction force on the rotation module

For the rotation module a Faulhaber 1516 with a 1:809 gearbox is selected plus an incremental encoder. This combination has a maximum output torque of about 0.380 Nm.

4.3.3 Payload

The robot contains two payload modules which can be used for power (batteries), sensors and control hardware. The electronic system will be discussed in more detail in chapter 7.

Distributed control

distributed

Because of the modular approach of the design and the space limitations a *distributed control system* has been designed. Every joint is equipped with a small local motor-controller, connected as 'slave' to the central 'master' controller. For communication between the main control board and the local motor control boards I²C (TWI) has been chosen with a data rate of 400 kbps.

Master board

As main control board of the robot a small controller board with an *LPC2148* ARM 7 processor by NXP has been developed. The board fits together with a battery in one of the payload modules (see figure 4.11). The board communicates with a host PC system using a Nordic *NRF24L01* 2.4 GHz radio transceiver, USB or 115 kB serial link. Extra memory for data logging or navigation data is added with a 1 GB flash microSD card.

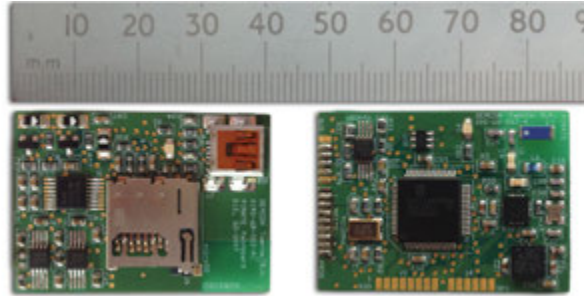


FIGURE 4.11 Main controlboard

Sensors

On the master board a *LIS3L02 3D accelerometer* is used to determine the robot's orientation with respect to the earth. Also a *TC77 ambient temperature sensor* for protection and monitoring of the environment is added. All used sensors are further discussed in chapter 8.

Power

Two switching power supply IC's convert and monitor the board's main supplies. The main board and motor section are powered using separate LiPo batteries in order to make the system rechargeable - and eventually energetically autonomous. In one payload module space is allocated for the battery for the motor section. This is a 7.4 V 350 mAh LiPo battery yielding maximum 2.2 Wh storage. The battery measures 20 mm x 30 mm x 10 mm and completely fills the available payload module space (see figure 4.12).



FIGURE 4.12 7.4V LiPo battery and payload module

The battery for the main board is a 3.7 V 350 mAh LiPo battery measuring 20 mm x 30 mm x 5 mm which fits the module space together with the main board.

Slave nodes

microcontroller

Every slave on the bus consists of an 8-bit *microcontroller* and 1 W *H-bridge* (shown on the top side of the board in figure 4.13). It interfaces with local position sensors, both incremental encoders on motor-side and analog absolute position sensors on joint angles. In each slave node one or two PID controllers are implemented, running locally at 1 kHz. PID controllers can be selected to do speed, position or torque control, first ones based on position sensor information, the latter based on current measurement and position difference using the series elastic joint:

$$\tau_{joint} = (\theta_{module} - \theta_{spring})k_{spring}$$

As position sensors potentiometers have been used. The slave node also monitors current consumption and protects the motors from overheating.

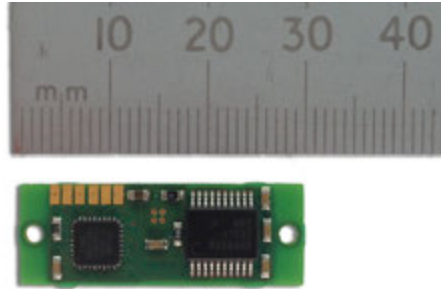


FIGURE 4.13 Motor driver capable of controlling two DC motors

4.4 Control

The robot consists of seven segments with a total of eight wheels. The construction (see figure 4.7) is such that one potentiometer measures the bend angle of the module, the other sensor measures the spring deflection relative to this position (and has a linear relation with the clamping torque).

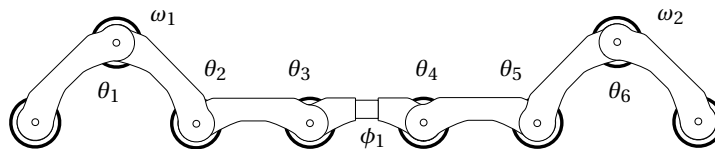


FIGURE 4.14 Degrees of freedom for control of the robot

Joints θ_1 , θ_2 , θ_5 and θ_6 are actively controlled using this serial elastic drive (and have two position sensors in each joint (see figure 4.14). The joints θ_3 and θ_4 have a passive spring and are not being controlled. Two wheels, denoted with ω_1 and ω_2 , are used for propulsion in the pipe. The rotation module angle is denoted by ϕ_1 .

The control software offers an interface (GUI) between the robot operator and the robot hardware. All functionality (motors, sensors) should be accessible through this interface. Secondly the control software runs the robot's state machine for operation inside the pipe. Three levels of control are currently implemented

1. slave control: distributed PID control using force (torque), position or velocity set-points
2. master control: takes care of initialising, configuring and communicating with the distributed slaves.
3. user interface: A PC system communicating with the robot with a GUI for scheduling motion sequences and giving direct commands.

The first two levels are implemented on the robot. An operator can manoeuvre the robot through the pipe by commanding *Motion Primitives*. Each robot action can be broken down to a series of these motion primitives being *clamp*, *unclamp*, *drive*, *bend*, *rotate*. For communication between the operator system and the robot both wired and wireless (2.4 GHz short range radio) have been implemented.

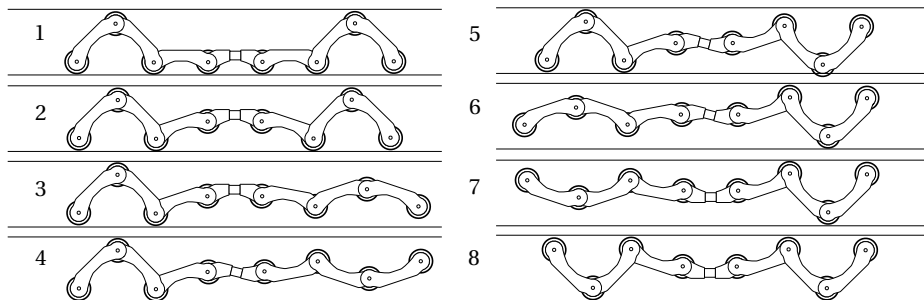


FIGURE 4.15 Sequence for axial rotation

The basic robot actions split in motion primitives:

- *drive straight*: clamp front, clamp rear, drive front, drive rear
- *axial rotation*: clamp rear, unclamp front, rotate 180°, clamp front, unclamp rear, rotate 180°, clamp rear, clamp front (see figure 4.15)
- *take bump*: unclamp front, drive, clamp front, drive, unclamp rear, drive, clamp rear

One of the complex manoeuvres for the robot is to *take the sharp (mitre) bend* in a T-joint. For this sequence we use a robot with one payload module less, (so θ_3 is missing). Note that neither of the centre angles ($\theta_{3,4}$) can be actively controlled. A breakdown in motion primitives (illustrated in figure 4.16) can be described as follows:

1. clamp front ($\theta_{5,6}$), clamp rear ($\theta_{1,2}$), drive ($\omega_{1,2}$).
2. unclamp front ($\theta_{5,6}$), clamp rear (θ_1), drive rear (ω_1), bend front (θ_5)
3. unclamp front ($\theta_{5,6}$)
4. drive (ω_1).
5. bend payload (θ_2)
6. clamp front ($\theta_{5,6}$)
7. unclamp rear ($\theta_{1,2}$)
8. unbend payload module (θ_2)
9. drive (ω_2)
10. clamp rear ($\theta_{1,2}$), continue to drive ($\omega_{1,2}$).

Note that the degrees of freedom of the robot have been numbered from left to right, the definition of front and rear has been chosen based on driving direction.

4.5 Results

The robot has been put through a series of preliminary experiments, testing the driving capabilities, joint control and overall control. In these experiments the robot has been controlled with a user interface (see figure 4.17) programmed in Matlab which allows manual setting of every motor setpoint. The tests have been conducted with a tether cable for power supply and communication.

The robot can manoeuvre through pipes with different diameters, drive under angles of 30° and rotate around its central axis. The robot can move forward with a velocity of 5.6 cm/s. These manoeuvres have been shown in a video⁴ at ICRA 2011 [20]. In the image sequence displayed in figure 4.18 the robot successfully negotiates a sharp (mitre) bend in a 90 mm pipe following the motion sequence described in figure 4.16. Angles, torques and velocities during this sequence are given in figure 4.19.

⁴<http://eprints.eemcs.utwente.nl/20661/02/ICRA2011.mp4>

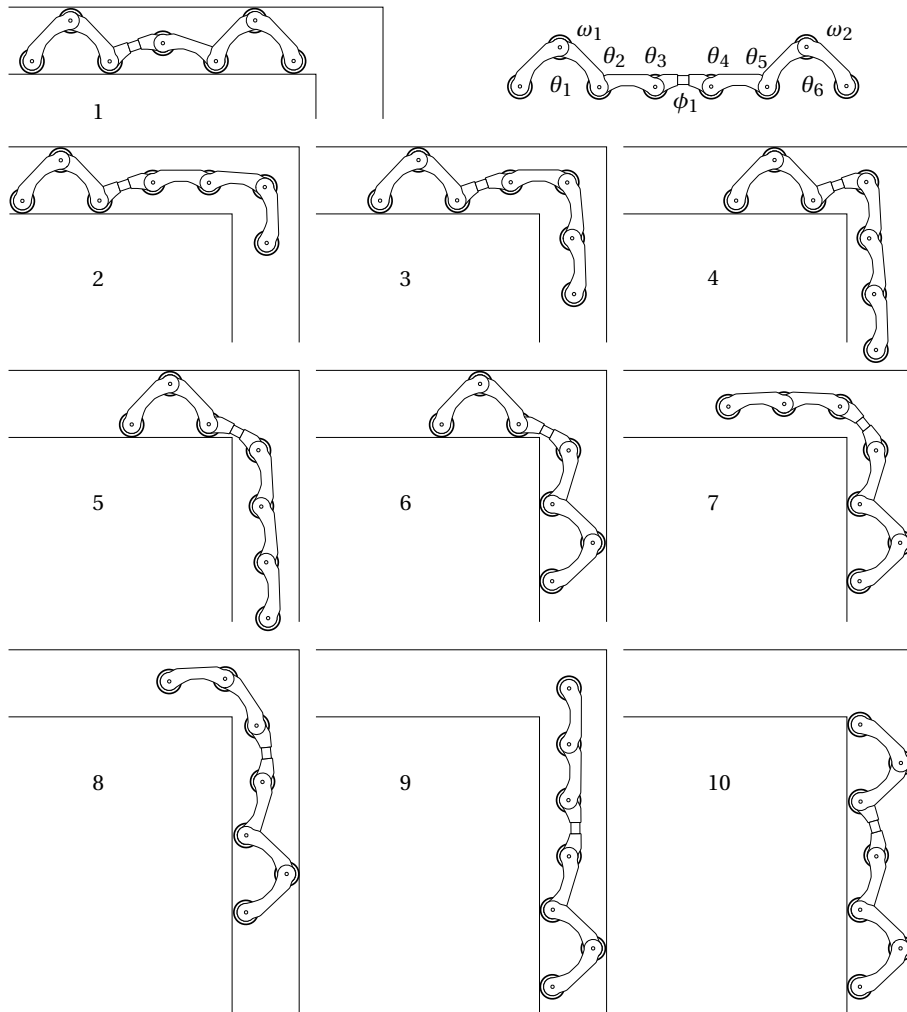


FIGURE 4.16 Sequence for the robot moving through sharp corner

The prototype described in this chapter has seven modules. Two clamping V-shapes, one rotation module and two passive payload modules. These passive payload modules lead to an ‘underactuated’ design. Passive springs have been implemented to yield a preferred bending orientation. During the tests described in this sections one of the payload modules has been removed. Partially because the robot has been operated using a tether so the module space has not been necessary, partially because the passive springs which have to facilitate a preferred bending orientation in the two payload modules (which are not actuated) were not strong enough. In

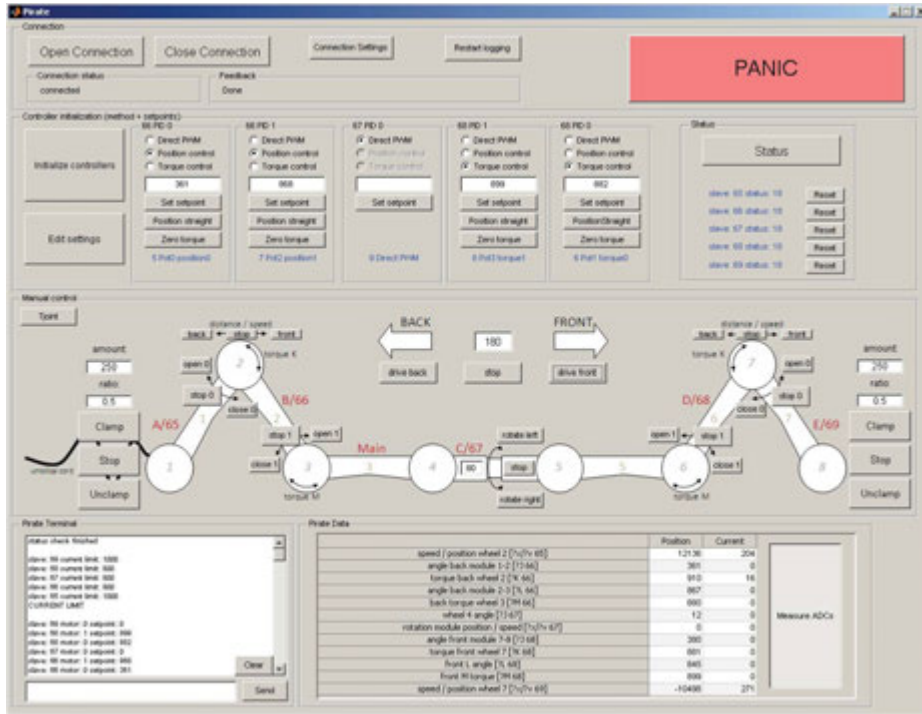


FIGURE 4.17 User interface in matlab

the next prototypes described in the following chapters, it will be tested whether it is possible to reduce the amount of modules even further as shown in figure 4.20. The minimum configuration consisting of five modules (two clamping V-shapes, one rotation module) should also be capable of taking a corner in a mitred bend, but a different control sequence might be needed.

4.6 Conclusions

4.6.1 System design

The research questions which have been stated in chapter 1 aim at finding the best methods for propulsion, energy provision, sensing, control and communication - given the intended environment. In the prototype described in this chapter the focus lies on propulsion and control.

The first prototype is capable performing the desired manoeuvres, showing the most complex (negotiating a sharp bend) in figure 4.18. Other manoeuvres like the rotation inside a pipe have been showed in a video [20], proving the concept viable and encouraging further study.

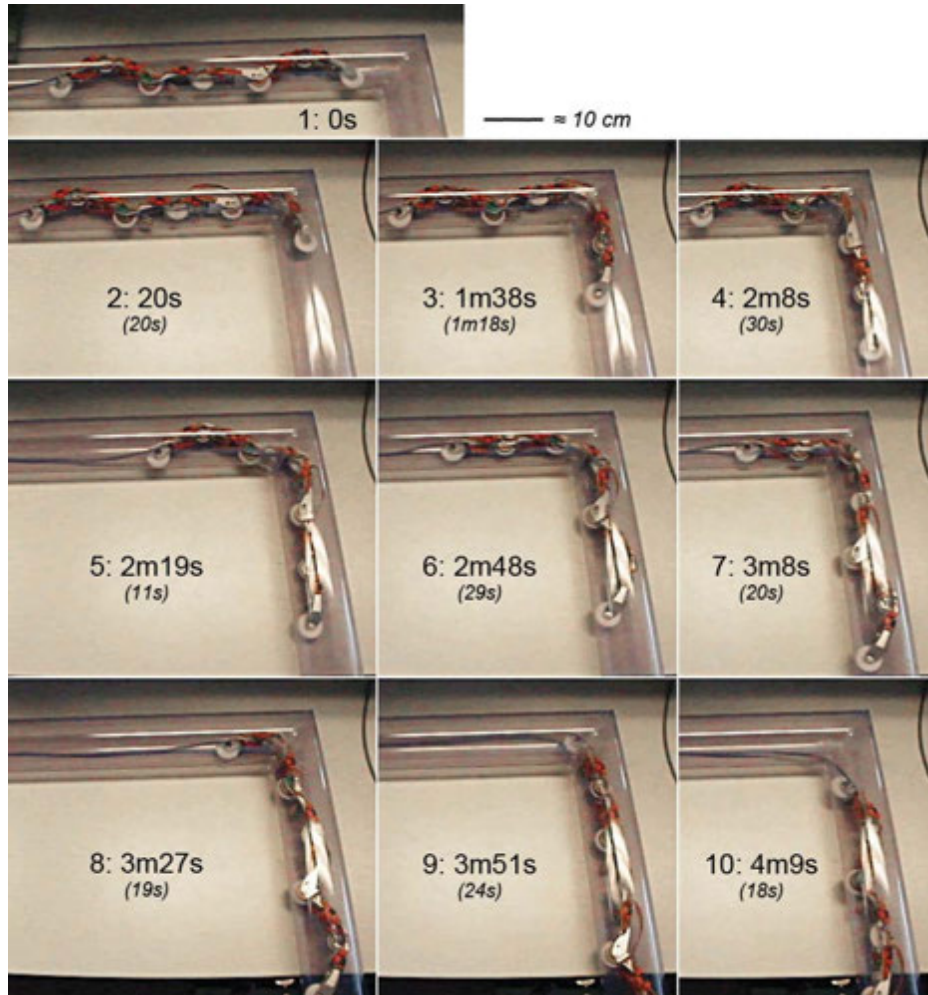


FIGURE 4.18 Robot moving through a sharp corner - *image from [75]*

4.6.2 Discussion

Although the capability of the desired manoeuvres has been shown, especially negotiating the bend is hampered by the loss of traction of one of the modules. Providing more wheels with traction power (all wheel drive) would be a possible option. Also the forward velocity of 5.6 cm/s does not match the secondary requirement listed in chapter 2 of 8.0 cm/s. It matches the desired primary requirement of 4.0 cm/s.

In order to allow for re-engineering the prototype, one of the size requirements needs adaptation. The minimal pass-through (41 mm) and the resulting wheel size

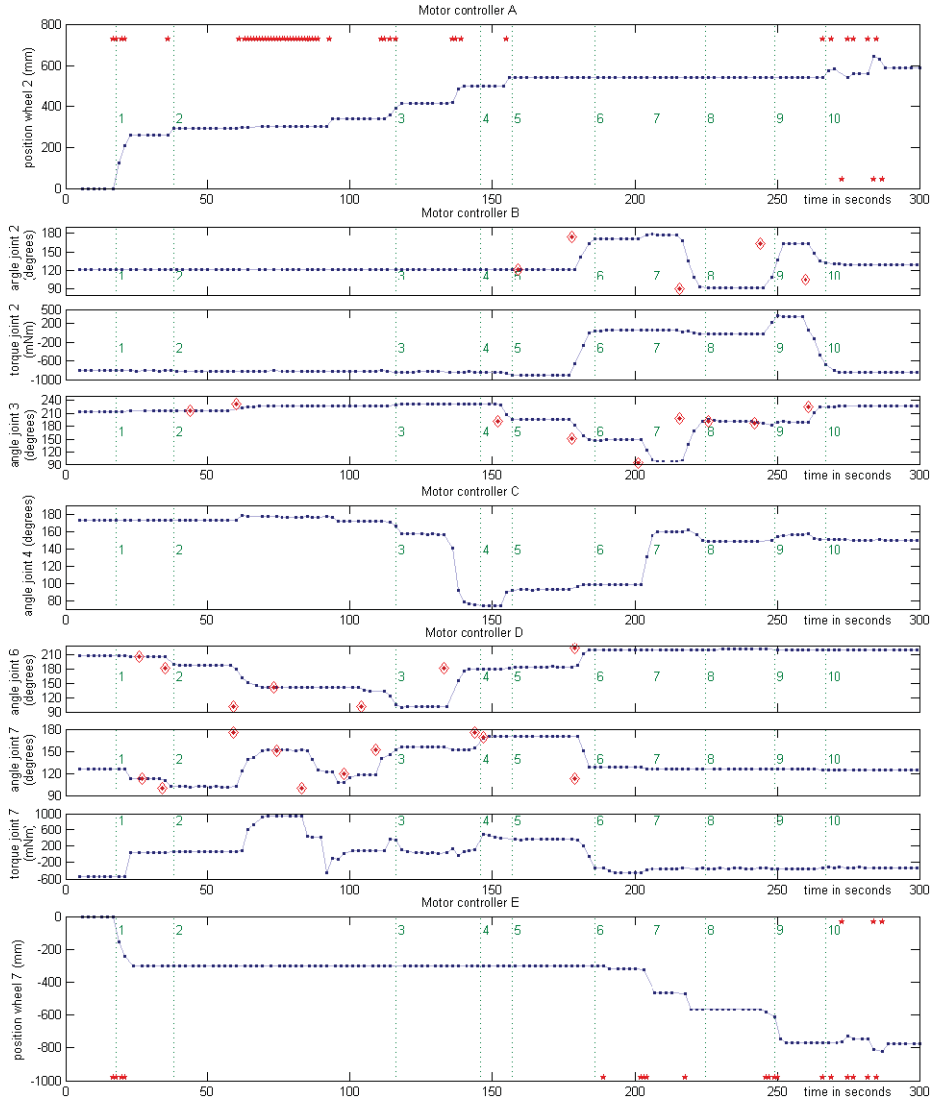


FIGURE 4.19 angle, torque and position measurements during cornering-
image from [75]

(40 mm) are based on the worst-case situation where there is a thick walled 63 mm pipe, SDR 11 resulting in an inner diameter of 51.5 mm. The combination of *both* a 3 mm weld and a 10% deformation require a minimal pass-through of 41 mm. Since it is hard to state the frequency of the occurrence of this situation, instead the choice is made to require a pass-through of *either* the weld or deformation, resulting in a minimal pass-through of 46 mm.

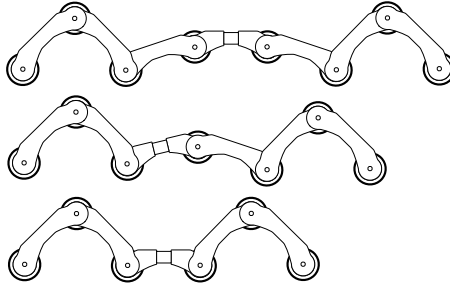


FIGURE 4.20 Reduction of the number of modules

The discussed prototype is relatively heavy due to the choice in materials (bronze, aluminium, steel). Decrease in weight would allow for steeper angles to climb, larger than the tested 30° .

The used electronics system works reasonably well, but is not very robust. Also the process of developing software, (re)programming, interchanging boards is not very convenient. The chosen position sensors suffer from play and electrical noise. Finally the chosen Matlab user interface is elaborate, but not user friendly.

The results of this work and the discussed improvements lead to a set of new requirements for a second prototype, as discussed in the projects described in [18] [75] [7]. The implementation of these requirements will be discussed in detail in chapter 5.

For the *propulsion system* the following improvements are desired:

- increase total robot drive torque, preferably by having every wheel driven
- decrease the weight of the robot
- decrease the number of gears, increase the efficiency
- allow for an increase in wheel size up to 46 mm instead of 40 mm.

For the *electronics and control* part also a number of requirements can be added:

- use a different, more robust protocol instead of the used I²C bus
- use different, interchangeable wiring and smaller connectors
- use different position sensors, solid state sensors instead of potentiometers
- use a more intuitive and complete user interface suitable for operator control.

This chapter discusses in which a fundamentally different method production and development has been chosen, described in more detail in chapter 11.

5

Mechanical Design: Prototype II

This chapter discusses design and construction of the second prototype¹. The new design is fully actuated using identical modules for facilitating ease of production and maintenance. It maintains the high spreading factor from the previous design (63 mm - 125 mm outside diameter) using series elastic driven clamping mechanism. The new mechanism proves to be able to take a vertical climb, broadening the general application range and facilitating entry in the gas distribution network by means of vertically drilled holes. The robot is produced using additive manufacturing technology, having a large impact on both the development process and the robot performance.

5.1 Introduction

One of the most restricting design requirements is being capable in manoeuvring in a relatively wide diameter range of 63 mm to 125 mm while at the same time being able to take a sharp (mitre) bend. An added (or changed) requirement is the possibility of climbing vertically inside a pipe. In chapter 2 as first requirement an inclination of 45° has been specified enabling the robot to move through ‘sunken’ pipes. Although different designs exist for climbing vertically inside a pipe such as the designs by Hirose et al. [43] none of these designs target the large spreading factor, capability of moving through T-joints and capability of a vertical climb.

A prototype capable of manoeuvring through a T-joint and rotation inside a pipe has been shown in chapter 4. This robot uses a modular structure consisting of modules with a dedicated function: payload modules, bending modules, drive modules and one rotation module. Two bending modules form a clamping v-shape which generates the necessary friction force on the tires. Two driven wheels have been used for propulsion.

¹This work has been presented at the GERG 2010 [23] and has partially been carried out during the bachelor’s project by Bram Burkink [11], internship project by Systze Spijksma [91] and the master’s project by Dian Borgerink [7]

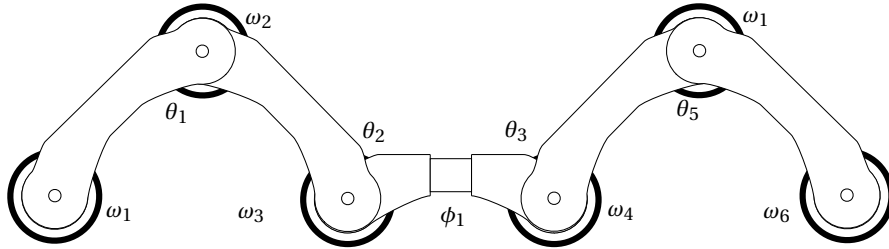


FIGURE 5.1 Overview of the robot using 5 modules

The previous model of the robot proved capable of negotiating a mitre bend in a 90 mm pipe. The amount of available traction force proved to be insufficient; the robot was only capable of taking a 30° inclination, not meeting the 45° requirement. Also taking bends took a lot of time, due to the lack of traction power.

The goal of the prototype described in this chapter is increasing the drive torque with respect to the prototype described in chapter 4, eventually allowing the robot to perform a vertical climb with the same morphology. One novel aspect of the design process is the structural use of additive manufacturing methodology (3D printing). This allows an unprecedented rapid iterative design cycle and has yielded a lightweight design with a relatively small number of parts. The impact of this process will be discussed in chapter 11

5.2 Analysis

In this section the main considerations for adapting the previous design will be given, focusing on the clamping mechanism, the propulsion, sensing and modularity.

5.2.1 Clamping

The robot uses a V-shaped section consisting of two modules to generate friction force on the tires. The tires are in this case neoprene rubber O-rings of 3 mm diameter. The amount of friction force that can be generated using this V-shape depends on the diameter of the pipe. The maximum attainable clamping force (F_c) on the pipe wall is given by (repeated from [21] and section 4.3.2):

$$F_c = \frac{T}{r} = \frac{T}{\sqrt{(l^2 - (D_p - D_w)^2)}}$$

where l is the length of a module, D_w is the wheel diameter, D_p the pipe diameter

and T the exerted torque by the clamping module (see figure 4.6). The relation is graphed in figure 5.2 with $l = 0.09$ m and $D_w = 0.046$ m.

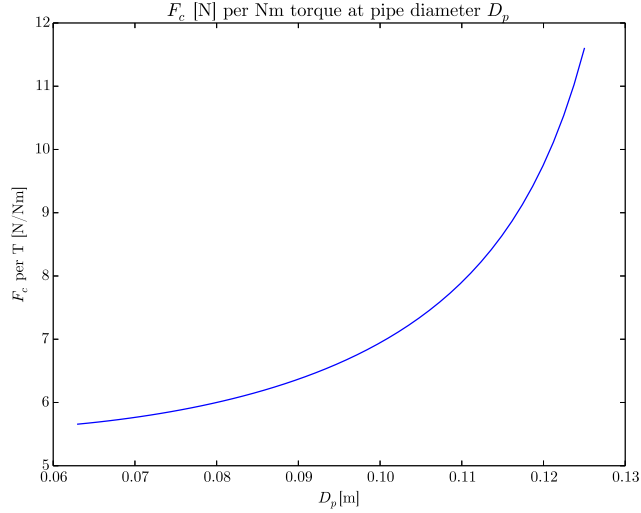


FIGURE 5.2 Clamping force on the pipe wall per Nm clamping torque for different pipe diameters

As already mentioned in chapter 4, the reaction torque of the wheels used for propulsion also adds to clamping torque T , depending on the driving direction.

$$T = T_{clamp} + T_2 - T_1 - T_3$$

In forward direction (in figure 5.1 from right to left) the torque T_2 of the second drive motor ω_2 adds to the clamping torque while the torque T_1 of first motor ω_1 and T_3 of the third motor ω_3 subtract from the effect. The same holds for the rear clamp, but mirrored.

The clamping torque is generated through a DC motor using a worm gear. Power of this motor is transferred to the joint through a spring (series elastic[70]) and worm gear which enables the joint to keep a clamping force without powering the motor, even compensating for small bumps in the pipe wall without any intervention.

The motor responsible for generating torque T_{clamp} has to be able to deliver the desired torque in the first place. After setting the angle θ_{spring} the torsional spring with constant $k = 3.5 \times 10^{-3}$ Nm/° takes care of maintaining this torque. The angle θ_{spring} is depending on the bend drive motor position reduced by the motor gearbox (64:1) and the worm gear (24:1).

$$T_{clamp} = \theta_{spring} * k$$

The effective stiffness k_{joint} felt between the modules is determined by the spring constant and the gear ratio between spring and module angle:

$$k_{joint} = \left(\frac{58}{16}\right)^2 k = 46 \times 10^{-3} \text{ Nm/}^\circ$$

The clamping module requires a gear train to transfer power from the self-locking worm gear via the spring to the joint. An IPM of the system (without controller) is given in figure 5.3. The CAD design of the system is given in figure 5.4. Note that each mechanism drives the geared edge on the *next* module.

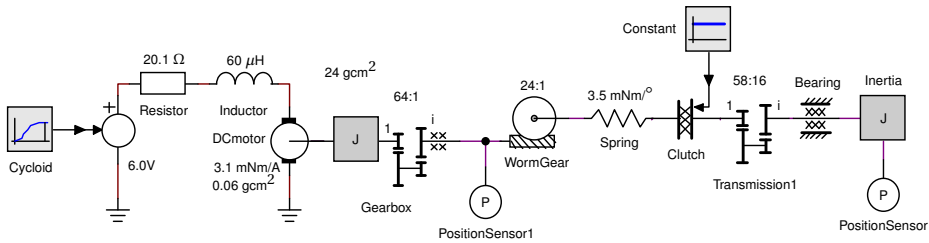


FIGURE 5.3 IPM of the bend drive

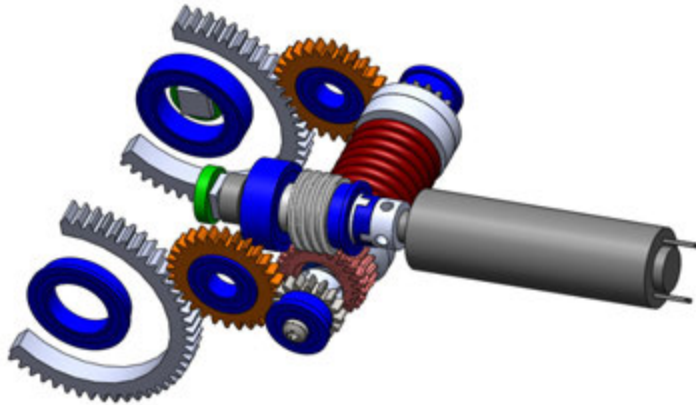


FIGURE 5.4 CAD drawing of complete bending gear system showing worm gear, spring and clutch.

For vertical climbing, the amount of clamping torque necessary depends on the tire friction and traction force. The tire friction is depending on the materials: smooth PE or PVC for the pipe wall and NBR70 rubber O-rings as tires. The force necessary

to hold the robot in the pipe F_h

$$F_h = \mu * F_c \geq mg \sin(\alpha)$$

with α the inclination of the pipe. Since the prototype discussed in this chapter will be lighter we assume total weight. The robot loses traction when $F_c \leq 9.8 \cdot 0.45 \text{ kg} = 4.41 \text{ N}$ with $\mu = 0.5$ the supplied normal force has to be at least 8.81 N, divided over the three wheels.

Deformation of the tires due to hysteresis in the material causes a considerable amount of rolling friction F_r , depending on the exerted amount of clamping force. To let the robot climb, a traction force of at least $mg = 4.41 \text{ N}$ has to be delivered by three motors, resulting in 0.1 Nm per motor. The force loss is given by

$$F_r = C_r \cdot F_c = \frac{C_r}{\mu} \frac{T_m}{r_w}$$

and is depending on wheel radius r_w and estimated friction constant $C_r = 0.01 - 0.015$. The resulting friction torque is about 5% of the motor torque per wheel.

5.2.2 All wheel drive

The propulsion torque in the previous prototype was generated using two wheels. In the situation where the robot has to navigate through a corner, only one wheel is available for propulsion, since the other half of the robot has to un-clamp. In the case with just two wheels the available amount of torque proved barely sufficient. In the new design the location of the motors has changed; every wheel has a motor mounted inside - a so called 'in wheel drive'. A coupling between motor shaft and wheel has to be implemented which decouples five of the degrees of freedom while connecting only one (traction). Figure 5.5 shows the wheel with decoupling, bearing, connector shaft and geared DC motor. The O-ring which is used as tire is not shown in the figure.

The chosen motors (Faulhaber 2619 SR series with included 112:1 gear box) can deliver up to 0.1 Nm. Due to space restrictions these were the only motors available capable of delivering the required torque without additional gear reduction.

Figure 5.6 shows the CAD design of one complete module, including the driven wheel of figure 5.5 and the clamping mechanism.

5.2.3 full modular concept

Since now every wheel has an in-wheel mounted drive system, and every joint has to be able to bend in one plane, every module of the robot can have the same design, except for the rotation module in the centre. The minimal robot configuration consists of two clamping V-shapes with one centre rotation point as shown

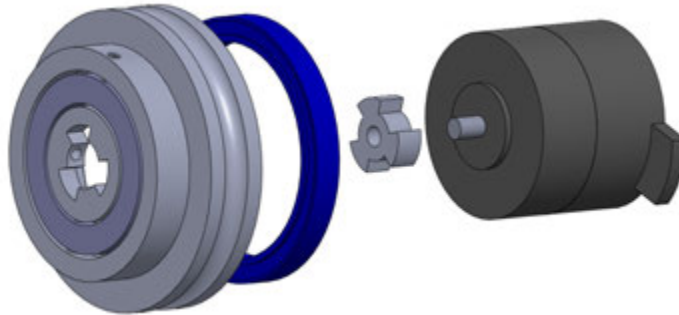


FIGURE 5.5 exploded view of in wheel drive mechanism showing (from left to right) wheel with rotational decoupling, bearing, linear decoupling and motor

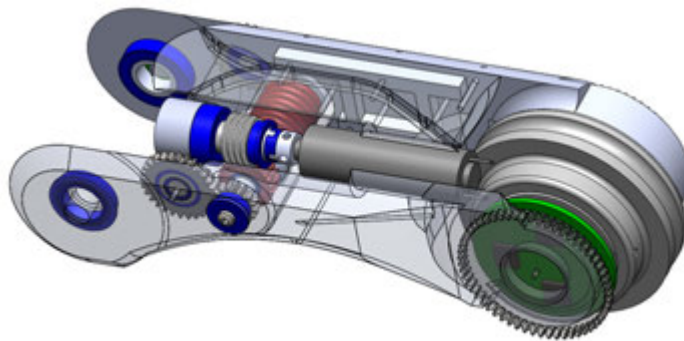


FIGURE 5.6 CAD drawing of one robot module

in figure 5.1. This configuration can be made using four exactly the same modules (encompassing bend and drive) and one different rotation module. This setup has advantages not only for production but also for maintenance, and offers flexibility in choosing the right robot layout for a certain task.



FIGURE 5.7 CAD drawing of three identical modules

5.2.4 position sensing

In the previous prototype potentiometers have been used as position sensors for joint angles and spring deflection. In this prototype rotary hall-effect based sensors have been used. These absolute position sensors have a resolution of 12 bit and can be interfaced digitally (using an SPI protocol). This results in a resolution of 0.09° per bit. For the bend angle range $[80..200^\circ]$ and the spring deflection $[0..85^\circ]$ this resolution is enough.

The wheel motors have 16 ppr incremental encoders on the motor shaft. With a reduction of 1:112 and a wheel diameter of 46 mm this results in a resolution of 0.083 mm per pulse which is more than sufficient.

5.3 Implementation

For realising the prototype extensive use has been made of an Objet Eden 250 3D printer. This printer uses a photopolymer (VeroWhite™) which is advertised as 'simulated plastic'. Although some of the material properties are insufficient for final (industrial) use, the realised mechanical parts prove strong and durable enough for laboratory experiments.

The advantage of using a 3D printer is the way it facilitates a rapid design cycle. While with our previous prototype basically one design cycle of Simulation, CAD, CAM and production was taken over a period of one year, in the described project at least four cycles were run through in a period of half a year.

The choice for this production method for the prototype leads to restrictions on the design for future producibility. Since a 3D printer can print virtually any shape no consideration has been given to the restrictions that apply with methods like CNC milling or injection moulding. For that reason the only available production method for this design will be 3D printing. Other 3D printing processes can however use stronger materials than the used photopolymers, so the choice to proceed with this limited manufacturing option has been made.

However, not all functional parts can be made using the described photopolymer based process. Eventually a prototype has been made using a SLS (selective laser sintering) process in fibre reinforced nylon (PA). Also an experiment has been done on printing a number of the drive parts (axles and bushes) using 3D printing in stainless steel. These experiments are described in chapter 11.

5.3.1 Clamp system

The clamp motor has a (self breaking) worm gear reduction (see figure 5.4 which allows for a high clamping torque at the joint. The total realised reduction is 1:5500 with a maximum rotational velocity of 1.0 rpm. The maximum output torque of 0.615 Nm allows for a clamping torque F_c of 25 N in an average pipe diameter of 80mm. The series elastic drive is also equipped with a clutching mechanism as over-torque protection. Rough handling of the robot can be expected, so it is important that bending the robot using external torques will not lead to defects in the gearbox or cause plastic deformation of the spring. The maximum spring deflection that is allowed (with maximum allowable external torque):

$$\theta_{max} = T_{max}/k = \frac{0.3 \text{ Nm}}{3.5 \times 10^{-3} \text{ Nm}/^\circ} = 85^\circ.$$

The spring is located in between the gear stages; in front of the gear a 1:1536 reduction acquired by the build in gearbox (64:1) and the worm gear (24:1) is situated. The power from the torsional spring is transferred using a 1:3.8 ratio (see for the construction details figure 5.4). This means that the torsional spring should handle a maximum of 0.23 Nm (at an estimated gear efficiency of 70%).

A Faulhaber 1016 series micromotor is used to drive the clamp system. With a maximum torque of 8.7×10^{-4} Nm and a reduction of 1:5500 (with a total efficiency of 20%) a theoretical maximum torque of 0.957 Nm is possible. The motor has a torque constant of 3.0×10^{-3} Nm/A with a maximum current of 300 mA. A measurement of the normal force using a digital scale and current sensor is displayed in figure 5.8. The maximum measured value (11N) corresponds well with the calculated maximum necessary clamping torque at 60 mm in figure 5.2.

The over-strain protection is designed to slip when the torque at the spring exceeds 0.3 Nm. This is implemented using a set of disc springs on the same axle as where

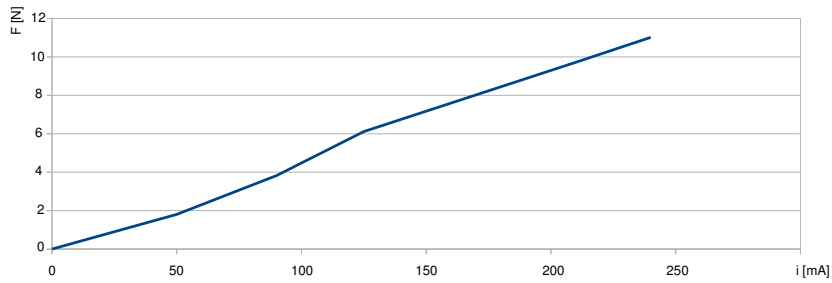


FIGURE 5.8 Measured clamping force versus motor current in a 63 mm pipe

the spring is located. Figure 5.9 shows a measurement of this protection system in action. At a motor current of 250 mA a sudden drop in current and change in position of the spring can be seen. The accompanying torque is close to the intended value:

$$0.25\text{A} \cdot 3.0 \times 10^{-3} \text{ Nm/A} \cdot 1536 \cdot 0.36 \% = 0.414 \text{ Nm}$$

The maximum torque for the spring where plastic deformation takes place is 0.800 Nm.

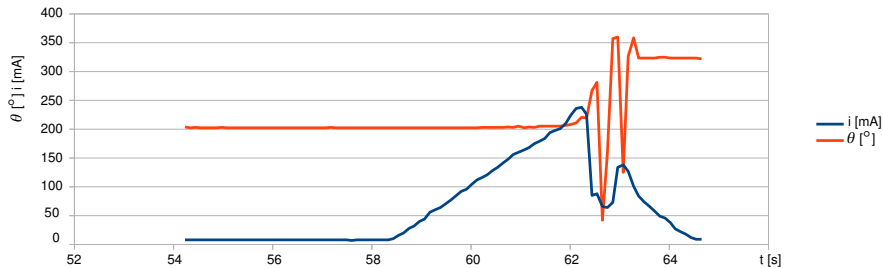


FIGURE 5.9 Clamp test where over strain protection slips at $t = 62$ s. θ is the bend angle measurement in $^{\circ}$ using the same scale as the current in [mA]

One problem with this protection system which becomes apparent from figure 5.9 is that the difference between the two angle sensors is no longer a reliable measure for the clamping torque: re-calibration is necessary at this point. The motor current can still be used as measure, so a combination of both should be implemented to gain maximum accuracy.

When a passive robot is entered into a pipe, allowing for 'rough' handling, the robot

should always start its operation with the calibration procedure. During normal clamping operation, the situation where re-calibration is necessary can be recognised by change in sign in the clamping torque with respect to the clamp motor current. In this case the mechanical protection acts before the current limit protection.

5.3.2 Drive motor

The in-wheel drive design has to accommodate a 5DOF decoupling between motor shaft and wheel, while 1 DOF (the driving rotation) needs to be coupled. A gimbal design combined with a sliding coupling as displayed in figure 5.5 has been printed directly. Small sliding axles allow translation in directions tangent to the motor axis.

5.3.3 Design iterations

The following design iterations were produced with stepwise increasing complexity over a course of a number of weeks. The first test in VeroGray - see figure 5.10 - (a) was printed as initial test with limited functionality. In this model space is left for motors and driven wheels. This first test model is deliberately oversized for testing basic strength.

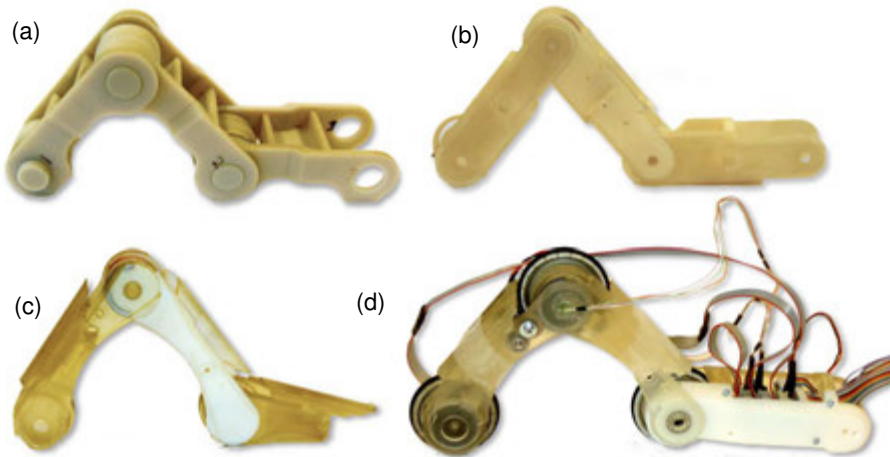


FIGURE 5.10 Design iterations in 3D print

The second iteration (b) has the same layout, but is scaled down to a shape approaching the desired robot's size. The material thickness is now at a limit (3mm) which starts to bend under influence of moisture. The material's heat deflection

temperature (HDT) is specified at 40° and a water absorption quotient of 1.5%. This data can be found on the website of Objet² Using the material itself as rotational joint did not prove sufficient so bearings and metal inserts have been added in model (c).

The third model (c) is also displayed without motors and approaches the necessary curved shape. Material thickness proves fairly robust. Two types of material (VeroWhite and transparent FullCure) have been used. Also space for the bending motor and spring joint is present.

The final prototype discussed in this chapter (d) contains three driven wheels, one bending motor. The position sensors are mounted in place, for connection however not the final distributed electronic system as described in [21] has been used, but a connection board to a separate electronic system with microcontroller and motordrivers.

5.3.4 Material

The materials used in for the prototypes are photopolymers Objet VeroWhite and Objet FullCure720. The transparent FullCure720 gave the best results and has been used in the motorised prototype. It has a strength and weight comparable to nylon (PA) although the tensile strength is less (50 MPa vs. 76 MPa). A larger problem might be the tendency to react (deform) under influence of moisture. The water absorption percentage of the printed material is at least twice as high as nylon. The reason to compare with nylon is because this material is also available for 3D print, be it using a different (SLS) process. The model used for the final testing is printed using fibre reinforced nylon (see chapter 11).

5.4 Results

Experiments were done with a sub-section of a complete robot consisting of one clamping V-shape with one additional module containing wires and connections. The robot has been controlled through a flat-cable using an *Arduino Mega*³ board with additional H-bridge drivers. The electronics of the previous prototype have also been based on the same Atmel⁴ microcontroller family which is used on the *Arduino* boards. All measurement signals were obtained through this microcontroller: for every driven wheel (3) a current measurement and encoder position is available. For the bend motor two AS5055 magnetic absolute encoders are used measuring the bend angle and spring deflection. The chosen sensors and drive electronics are discussed in chapter 7.

Arduino

² <http://www.objet.com>

³ <http://arduino.cc/en/Main/arduinoBoardMega>

⁴ <http://www.atmel.com>

The clamping mechanism is tested using digital scales while sensing current and displacement of both sides of the torsional spring. These results have been presented in the previous section and were used to set a predefined clamping torque on the module before driving it inside a pipe. Simple pulling experiments, using a spring scale and the robot in a horizontal pipe, yield pulling strengths of 14 N before wheels start to slip.

The most surprising outcome was that the robot is capable of a vertical climb. Due to the use of light (3D printed) materials instead of heavier brass and aluminium in the previous model, the shown half of the robot weighs 450 g, resulting in a complete robot of (estimated) 900 g. If batteries and sensors are included (amounting to another 100 g) the total weight will be approximately 1.0 kg. The previous version without batteries did weigh 1.4 kg.

Experiments have been done in three different pipe diameters with a considerably smooth surface (transparent polycarbonate). Since PE and PVC pipes are very common in the targeted gas distribution network, these pipes provide a realistic test situation. Figure 5.11 shows the test setup.

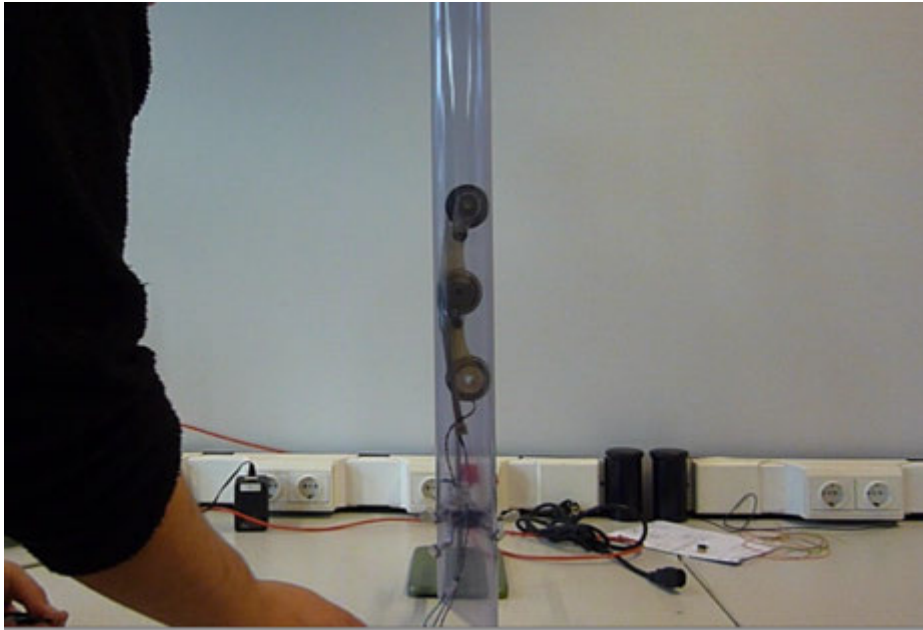


FIGURE 5.11 Climb in 63 mm pipe (57 mm inner diameter)

Figure 5.12 shows measurements of a climb in a vertical pipe of 63 mm (57 mm inside). In the first part of the graph the motor current is gradually increased up to the moment where the robot starts to move. This point can be seen at $t = 7$ sec. in the graph. After climbing 270 mm the current is reversed and the robot drives back.

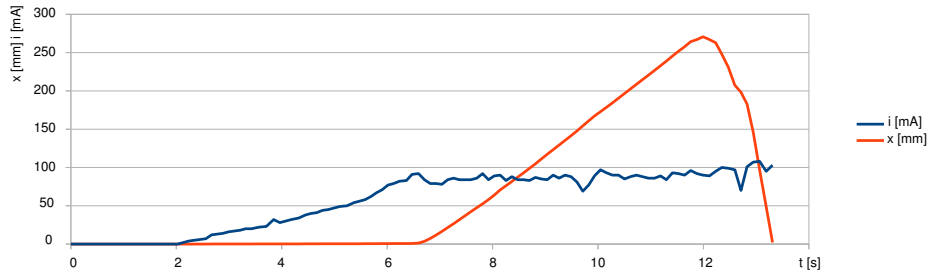


FIGURE 5.12 Climb in 63 mm pipe, current and height

Note that only the absolute current through a motor can be measured, not the direction.

Figure 5.13 shows measurements of a climb in a vertical pipe of 90 mm (86 mm inside). When the robot starts to move, the current consumption required for the propulsion torque is fairly constant. Tiny dips in the current signal show that the wheels do occasionally slip. However, since chances are low that all three wheels slip simultaneously, the climbing velocity remains constant. After the current is reduced at $t=13$ s, the robot falls back passively starting at $t=15$ s. The current after $t=16$ s is probably generated through the back EMF in the motors.

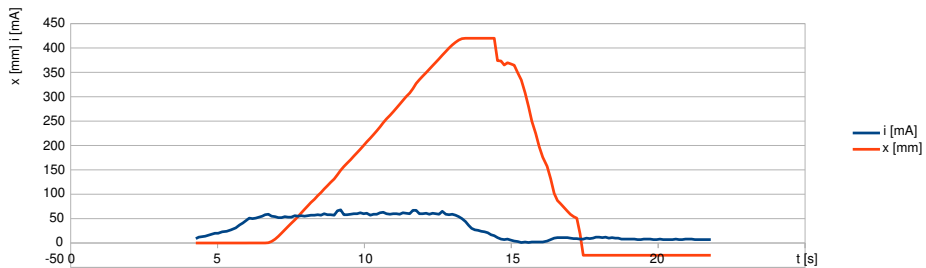


FIGURE 5.13 Climb in 90 mm pipe, current and height

Both experiments have been done with (smooth) manual motor control, keeping the motor power as low as possible. Note that the 63 mm pipe requires in these series approximately 100 mA per motor, the 90 mm pipe requires 50 mA per motor. In a next series of experiments the drive motors were set to full power (after a predefined clamping force was applied). The graphs of figures 5.14 and 5.15 show runs in 63 and 110 mm pipes respectively. In the shown series in 63 mm the measure-

ment is stopped before the robot can fall back. In figure 5.15 the robot falls back passively after cutting the current.

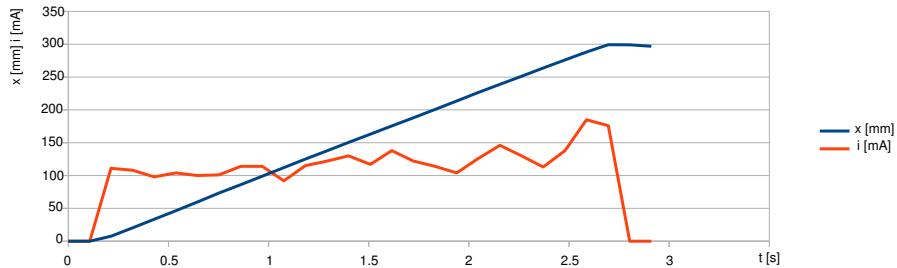


FIGURE 5.14 Climb in 63 mm pipe, current and height, full power

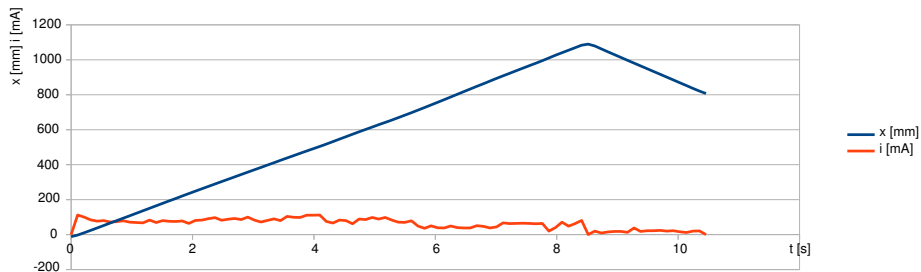


FIGURE 5.15 Climb in 110 mm pipe, current and height, full power

In all three diameters the climbing velocity is approximately 116 mm/sec. Since the original target for the robot was 80 mm/sec (horizontally) this velocity is considered sufficient. The results furthermore show that the required current for the 63 mm pipe is higher than for the 110 mm version. This might be a result of the used clamping force, which requires an almost twice as big clamping torque than with the 110 mm pipe. Therefore it is harder to find the necessary amount, it might be that the clamping torque was simply too large, causing too much friction. Another possible extra source of friction are the cables and wiring which touched the pipe wall only in the 63 mm pipe (quite a tight fit).

5.5 Conclusion

This chapter presents a re-design of the propulsion system, capable of climbing vertically. Although the results have not been obtained using a complete robot (only one section of the symmetric system) it can be concluded that the robot can perform a vertical climb. Furthermore the use of a 3D printer increased the development speed dramatically compared with the development of the previous prototype (4 months instead of two years for a fully functional prototype).

The design that is yielded using this methodology is both lightweight and mature, since many of the multidisciplinary design choices necessary in mechatronics have been dealt with in rapid design iterations, such as the placement of the sensors, selection and placement of motor configuration (gearbox, sensors, size), dimensioning and placement of the control electronics, integration of channels and routing points for wiring, etc.

This chapter discusses a modification of our main design using omnidirectional wheels. It is a novel concept which might solve some difficulties in the rotation move which has been described in chapter 4.

6

Mechanical Design: Omniwheel Prototype

This chapter discusses a different propulsion mechanism using omnidirectional wheels (or omni-wheels) which allows direct control of the orientation in the pipe¹. A quick study model using rapid prototyping techniques has been developed, tested and evaluated. The prototype can move and rotate inside 125mm pipe and large bends but needs active control of the V-clamp in order to take sharp bends as well.

6.1 Introduction

With most of the peristaltic or crawler-type robots no attention is paid to the orientation (or rotation) of the system inside the pipe - or is not actively compensated for. The CMU snake makes explicit use of the rotation movement inside a pipe and compensates the generated CCTV image so the operator has a level horizon view. Other systems such as the MRINSPECT or Roboscan design have a preferred orientation but can change their orientation also by a series of (un)clamping and rotation movements.

The chosen curved shape of the robot modules (see section 3.4.2) enforces a preferred orientation for taking bends and corners, i.e., they can only be taken in one plane or orientation, dictated by the curve. One of the prerequisites of taking a corner is that this orientation or rotation in the pipe can be selected or controlled. In the proposed design this is facilitated by a separate rotation module which allows one section of the robot to unclamp and rotate with respect to another module which stays clamped.

The rotation using a rotation module whilst clamping one of the modules causes

¹This prototype has been realised together with Mohammad Mozzafari Fomashi. The text of this chapter has been presented at ICRA 2014 [24]

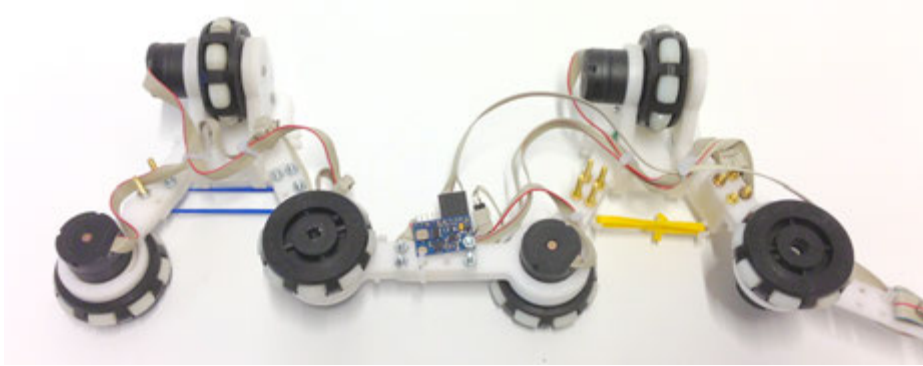


FIGURE 6.1 Design with two clamping V-shapes using omnidirectional wheels

an amount of friction of the module that is rotating in the pipe, as can be seen in de video's [20]. An alternative has been found in using smooth plastic (nylon) wheels instead of the rubber wheels [75], but in the second prototype with all-wheel-drive described in the previous chapter this solution was no longer an option.

A possible solution for this problem is explored in this chapter, using *omni-wheels*² or mecanum wheels³. These wheels have been used in many robot platforms mainly aimed at a flat floor. They have been deployed in other pipe inspection robots, such as commercially exploited by helical robotics⁴. SHK⁵ demonstrated a clamping inspection robot for a 100 - 200 mm pipe diameter using omniwheels at ICRA 2013, but no further references have been found. One reference of using omni-directional tracks in the context of pipe inspection had been found in the works of Tadakuma et al. [99].



FIGURE 6.2 Transwheel image - *image from Kornylak.com*

In the following section the analysis of the design considerations will be given, followed by implementation details, results and conclusions.

²Wikipedia on OmniWheels, http://en.wikipedia.org/wiki/Omni_wheel

³Sometimes also called 'Swedish wheels'.

⁴Helical Robotics, <http://www.helicalrobotics.com>

⁵<http://www.shk-k.co.jp>

6.2 Analysis

In this section the main considerations for adapting the previous design will be given, focusing on the clamping mechanism, the propulsion, sensing and modularity. The realised robot is shown in figure 6.1 for reference. The implementation of this design will be discussed in the next section.

The clamping V-shape used in the previously described prototypes needs to unclamp before a rotation in the pipe can be made. This clamping and unclamping is realised using a series of pre-programmed movements (basically unclamp-rotate-clamp).

6.2.1 Orientation

Due to irregularities in the pipe surface, weight distribution, pulling of the tether the robot will not remain in the chosen plain, but its orientation can deviate over time. Periodically unclamping, rotating and re-clamping is the only possible solution with the previously described prototypes. For semi-autonomous control, used by an operator, this behaviour will slow down the robot since this sequence of motions cannot be performed while driving.

In this chapter a mechanism is discussed without this nonholonomic constraint around the system's principle axis, so that continuous control of the mechanism's orientation is possible. Although eventually autonomous control is intended with the mechanism, also for user controlled operation this mechanism has advantages, especially since selection of entering bends and T-joints is depending on the orientation of the system.

For forward propulsion, traction (resistive force or friction) in the driving direction has to be maximised by the wheels. The chosen wheels have small inset wheels consisting of rubber.

However, for the rotation manoeuvre, it is necessary that the robot has as little friction with the pipe wall as possible. In the first prototype this has eventually been solved by replacing most of the rubber wheels by nylon wheels. The same problem has been solved on a different (conceptual) level by the RoboScan design [108] where wheels have been employed which can rotate round a vertical axis. This concept has also been used in many other designs described by [82]. The solution explored and proposed here makes use of the properties of an omnidirectional wheel to provide friction necessary for traction in the driving direction while allowing free motion in a direction orthogonal to the wheel.

6.2.2 Wheel choice

Robots with omnidirectional wheels are mainly used on flat floors. Different wheel designs exist, the main difference lying in their *roll-off shape*. A typical mecanum wheel can have a continuous motion on a flat floor providing traction in a different orientation with respect to the driving direction. The rollers typically each have an axis of rotation at 45° to the plane of the wheel.

In the chosen wheel the roller wheels have an axis of rotation at 90° to the plane of the wheel. On flat floors normally a double set of these wheels is used, however space constraints only allow for one. The number of roller wheels used inside one omniwheel influence the 'bumpiness' of the roll-off shape.

6.2.3 Clamping

For simplicity sake the clamping force has been provided using a linear spring (implemented as a series of rubber bands). To keep the robot centred in a 125 mm pipe a clamping force of at least 5 N needs to be provided (experimentally validated). The force provided by the joint in this pipe is 13.5 N per Nm according to figure 5.2. A torque of $5/13.5 = 0.37$ Nm is necessary, which can easily be provided using the chosen rubber bands.

Although the deformation of the roller wheels due to hysteresis in the material is very small, it still causes a considerable amount of rolling friction F_r , depending on the exerted amount of clamping force. To let the robot drive (uphill) a traction force of at least 4.41 N has to be delivered by three motors (from results of the measurements on the previous robot prototype), resulting in 100 mNm per motor. Note that in this case only two motors are used for propulsion, the third motor per clamping V-shape is used for the rotation in the pipe and cannot be used for propulsion.

The chosen motors (Faulhaber 2619 SR series with included 112:1 gear box) are the same as used in the model described in the previous chapter and can deliver up to 100mNm. Due to space restrictions these are the only motors available capable of delivering the required torque without additional gear reduction.

The wheel motors have 16 ppr incremental encoders on the motor shaft. With a reduction of 1:112 and a wheel diameter of 52 mm this results in a resolution of 0.083 mm per pulse which is more than sufficient for velocity measurement and position control.

6.2.4 Orientation control

For the orientation control a straightforward PID controller will be used. Since odometry data is likely to be influenced by slip with the pipe wall, especially considering the makeup of the wheels (with a very small contact area with the pipe

wall) a sensor using external input to measure orientation is necessary. An accelerometer has been chosen which measures accelerations in three directions. At relatively low linear accelerations the direction of gravity is the dominant signal. Using the formulae stated in section 8.4 the orientation can be determined.

6.3 Implementation

6.3.1 Mechanical design

In order to quickly evaluate the design and test the orientation control a mechanical prototype has been designed using flat 3 mm Delrin sheet and a limited number of extra parts. Using flat plate has the advantage that the design can be manufactured quickly using a laser cutter, allowing for short development cycles. The CAD design is shown in figure 6.3, the final implementation in figure 6.4.

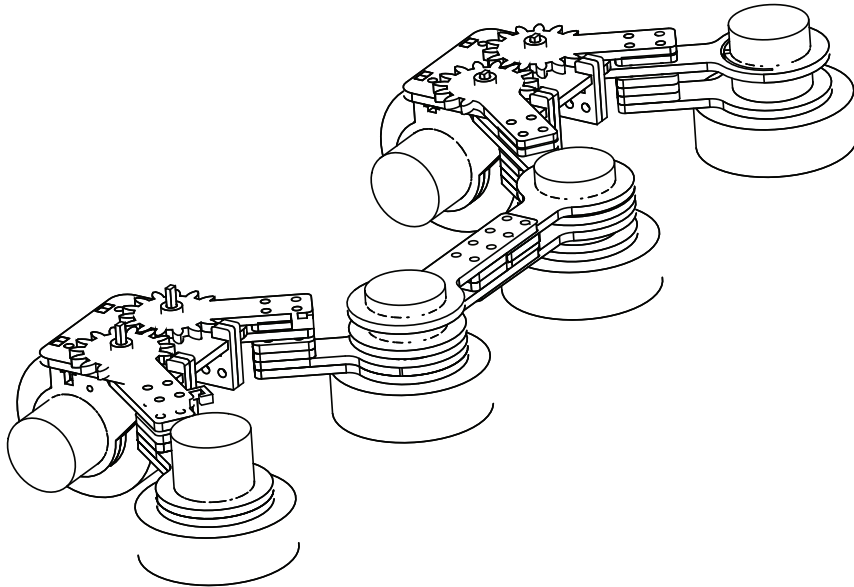


FIGURE 6.3 CAD sketch of the proposed robot mechanism

The design uses six motorised wheels using the earlier described Faulhaber 2619 SR series with included 112:1 gear box. The omni-wheels have been mounted to the output shafts directly.

In order to keep the orientation of the rotation motor perpendicular to the pipe wall, the joint in the clamping V-shape consists of two geared branches. The V-shape forms an equilateral triangle. The gears make sure that the piece holding the rotation motor is always orthogonal to the base of this triangle. Both legs of the triangle have a length of 75 mm, the wheels have a diameter of 52 mm. In theory a range of diameters between 80 mm and 125 mm should be possible using this setup, where it not for the size (length) of the motors. Only when they are mounted inside the wheels (the 52mm wheel allows for a 26mm motor to be mounted within) this minimum diameter can be ranged using this prototype.

One clamping V-shape has three contact points with the pipe wall. In order to fully define its position a fourth contact point is necessary. This point is provided by having not one but two clamping V-shapes attached symmetrically. However, when all contact points are aligned in the same plane (as drawn in figure 6.3) the system is still undefined (except for infinitely high clamping forces). Therefore, instead of building the robot totally symmetric in one plane, an offset has been chosen between the wheels in driving direction, to have them intermittently at both sides of the central plane.

As described in the previous section, instead of the active clamping mechanism for this prototype a passive system is used. The rubber bands extended 86 mm inside the pipe with the diameter of 125 mm. The force exerted from the rubber bands when the module is inside a pipe with the diameter of 120 mm is between 7.0 N and 7.2 N (measured with a spring balance).

6.3.2 Electronics

The control electronics for the experiments consist of an embedded micro controller (Atmel ATmega328) controlling the DC motors through a number of H-bridge driver chips (L298) measuring current through shunt resistors and a low-pass filter. Two incremental encoders, one on a drive motor and one on a rotation motor have been connected for measuring position. Finally an ADXL345 accelerometer shown in figure 6.5 has been connected through an I²C bus for measuring orientation.

Since for the time being only one rotation is considered (and allowed by the setup) just one axis of the accelerometer has been used, using $\phi = \arcsin(a_y)$ as value for the angle. Note that this axis is the most accurate to use for deviations in the horizontal plane.

6.3.3 User interface

The user interface has been kept to a bare minimum for this proof-of-principle. An analog joystick has been connected to the control electronics, where one of the axes gives the control set point for the translation (the four drive-motors) and the other



FIGURE 6.4 Model inside a 125mm pipe

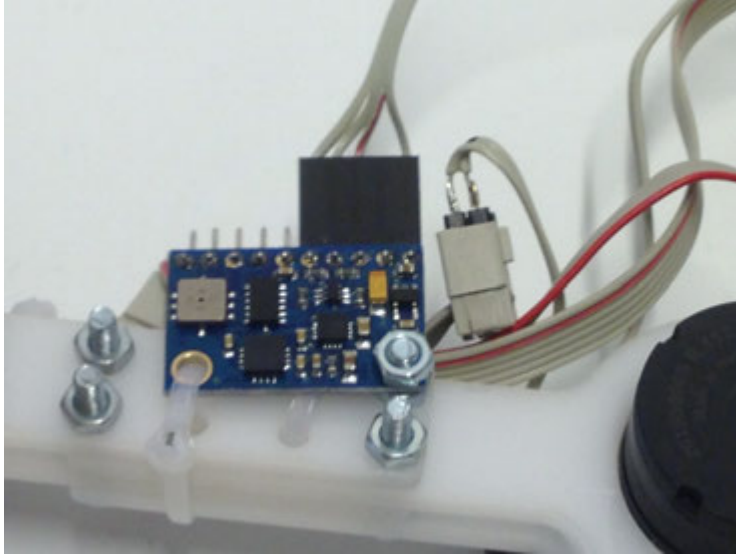


FIGURE 6.5 Accelerometer on a multi-sensor interface board mounted centrally in the mechanism

axis gives the set point to the rotation (the two motors tangent to the pipe axis) as an offset for the orientation control.

6.3.4 Orientation control

A PID controller has been used to control the robot's orientation. Since damping in the system due to friction is very high and the first-order behaviour is dominant, additional damping of the controller (D-action) might not be necessary. The velocity of the rotation motor can be controlled (PWM controls voltage, for a running motor which can be seen as a pure gyrator) equivalent to the velocity) while position (orientation) is measured. Hence the encoder acts as a 'hidden' integrator. Instead of deriving a velocity signal (with the possible added noise by adding a differentiator) the choice has been made just to use the controller with position feedback and a reasonably large feedback gain.

$$\phi = \arcsin(a_x)$$

$$output = K_p * (setpoint - \phi)$$

With a desired motor signal in the [-255..255] range and an error in radians ($-\pi.. \pi$) a feedback gain $K_p = 150$ is sufficient for the first experiments. As stated in the introduction, goal of this chapter is not to design an optimal controller for the discussed

prototype, but rather a working proof-of-principle in order to investigate possibilities.

All data (timestamp, set points, motor current, accelerometer data and encoder data) are sampled with a frequency of 50 Hz and send through the serial port to a PC application. At the PC side the data is recorded, processed and is shown in the graphs in the next section.

6.4 Results

The passive clamping mechanism has been tested using a spring balance and digital scales. The force exerted by the passive spring equals 7.2 N inside the 125 mm pipe. Experiments show that this is enough force for traction but still slip occurs in both translation as rotational direction. Three tests in short 125 mm pipe segments are described here. The robot mechanism drives through a straight section with minimal disturbance, followed by a test drive in a straight section with a large disturbance. The last test is a bend with large radius.

6.4.1 Straight section

The robot is entered in the pipe drives 80 cm forward and back. Figure 6.6 shows the experimental setup. Figure 6.7 and figure 6.8 show the measurement data obtained in this drive. The forward velocity is quite high compared with previous prototypes: $0.8\text{m}/4\text{s} = 0.20\text{m/s}$. The accelerometer data shows a lot of noise. These might be contributed to the uneven surface of the wheels caused by the individual rollers. The deviation between the encoder data (purple) and the accelerometer data (green) is caused by the slip of the roller wheels.

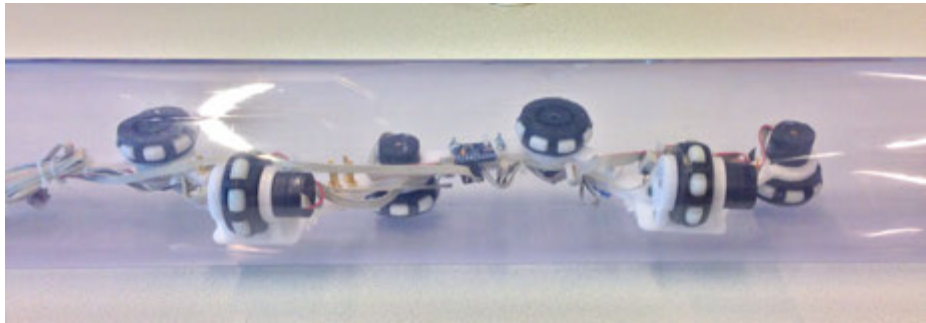


FIGURE 6.6 Robot in a 125 mm transparent pipe

In a next experiment two times a large disturbance of 90° is introduced by rolling the pipe with the robot over the table (shown in figure 6.9 at $t = 4.5$ s and $t = 8$ s).

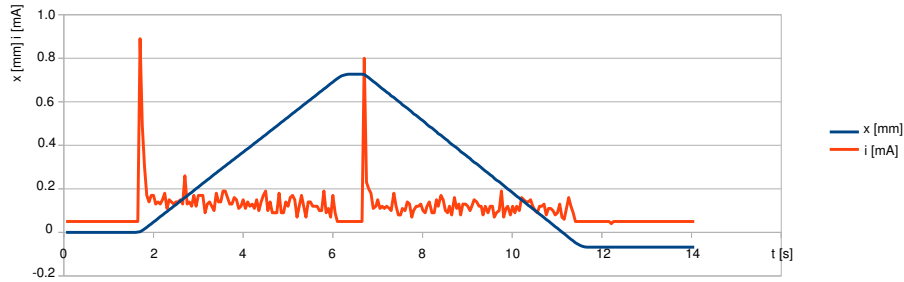


FIGURE 6.7 Straight drive with minimal disturbance, translation of the robot including total motor current

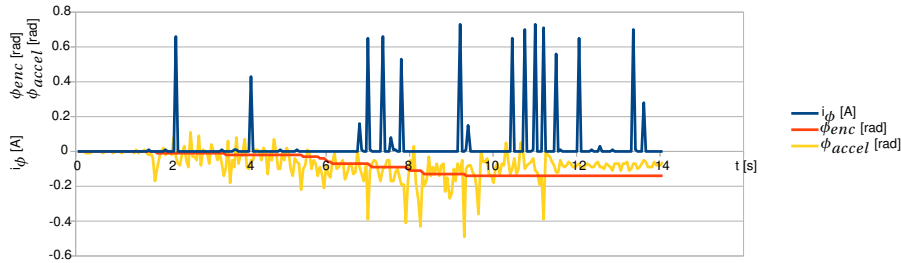


FIGURE 6.8 Straight drive with minimal disturbance, rotation of the robot

This is of course a disturbance highly unlikely to occur in real life, however, it shows the correction of the orientation of the system. The accelerometer data shows the error introduced by rolling the pipe and the return to a 0 rad orientation of the system. The encoder data shows the correction the robot performs on the disturbance.

Finally a test run has been made in a bend in a 125 mm pipe with a radius of $4 \times D_p$ (4D) shown in figure 6.10. As to be expected, for this range the mechanism does not behave any differently from driving in the straight pipe. However, rotation becomes more difficult since the mechanism has a preferred orientation.

6.5 Conclusion

In this chapter a third prototype has been presented showing experiments with omnidirectional wheels. One of the advantages of this approach is the ‘continuous’ control: this setup allows for a very intuitive mapping to user control (rotation and

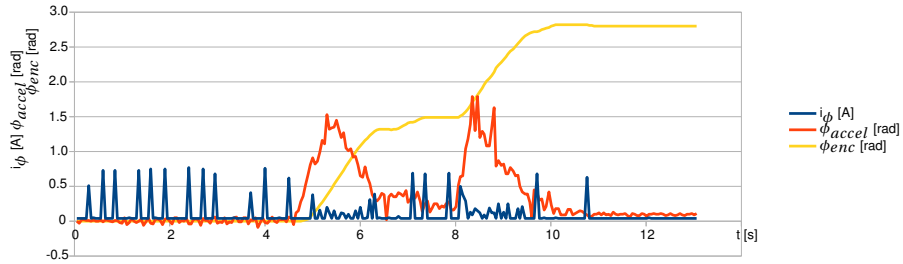


FIGURE 6.9 Rotation in a 125mm pipe with two large disturbances

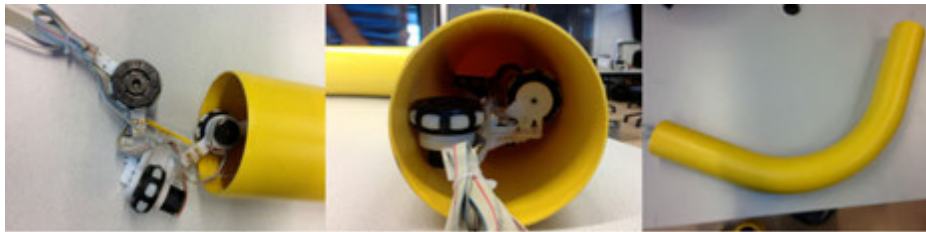


FIGURE 6.10 Robot concept in 125 mm bend with radius of 4D

translation in the pipe). The prototype has shown the possibilities of the control, as well as manoeuvring in a straight 120mm pipe and a smooth bend with a radius of 4D. Experiments have been done with the outline of the robot finding the most suitable distribution of contact points.

The major issue, however, is the fact that per segment one omniwheel is used perpendicular to the driving direction. This would pose no problems in a perfectly smooth pipe. However with a weld, a dent or a coupling piece at regular intervals this would require the robot to stop, unclamp, move along, reclamp and continue.

The question that has to be answered now is whether the need for continuous control of the orientation is more important than continuous control of the longitudinal motion in the pipe (driving forward and backward). For the scope of this project eventually the latter has been given priority.

7

Electronic (embedded) system Design

7.1 Introduction

The electronic system of the robot is responsible for powering, controlling and communicating with the robot. Some parts of the electronic designs and the choices made in the specific prototypes have been discussed in the previous chapters. This chapter will give an overall overview discussing the modular setup using master/slave nodes, internal communication bus, protocols, external hardware, power supply and battery technology.

7.2 Embedded system design

The choice for a modular approach of the electronic system design as opposed to a central computer with dedicated hardware drivers has been primarily motivated by the issues present with wiring and the real-time constraints necessary for a central control system.

Suppose a central controller in the middle of the robot. For one clamping V and half of a rotation module three drive motors, one rotation motor and two bending motors have to be interfaced. The wire count (shown in tabel 7.1) yields a total of $28 + 18 + 6 = 52$ wires per side. Power, tethering and communication has not been taken into account, which might increase the number. Multiplexing for sensor signals on the other hand can reduce the number.

Needless to say that an amount of wires in this order of magnitude would pose a severe mechanical limit on the robot design. Therefore, for all prototypes a modular architecture has been chosen using in case of the first prototype five wires (chapter 4) and in case of the second prototype (chapter 4) four wires.

TABLE 7.1 Wire count per module

device	number of wires
drive motor	6
bend motor	2
module angle position sensor	6
spring deflection position sensor	6
rotation motor	6

A decentralised (distributed) control architecture has, besides the reduction of wiring, the advantage of reducing the computational load. Instead of a central processor which has to execute more than 10 control loops in real time, the central processor can operate in ‘soft’ real-time sending set-points and commands to modules executing the ‘hard’ real-time control loops.

Since the implementation of the electronics of the first prototype has been discussed in chapter 4, this chapter will focus on the implementation of the system for the second prototype. The discussion on the general outline is valid for both implementations.

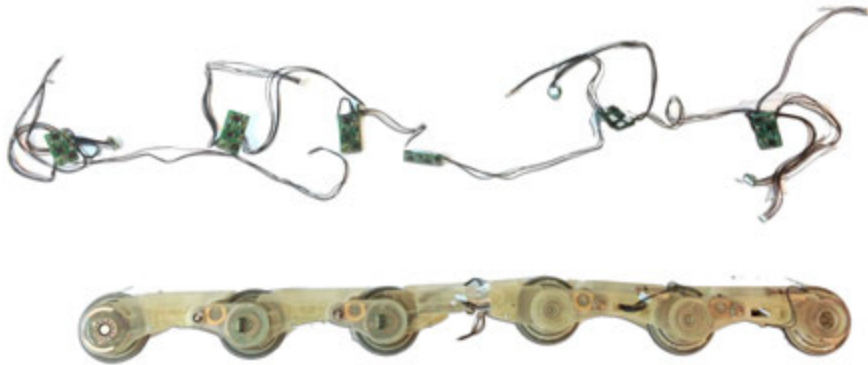


FIGURE 7.1 Robot with its ‘nervous system’

7.2.1 Master Slave setup

In the minimal configuration (see figure 5.1), two clamping V-shapes and one rotation module, a total of six drive motors, four bending motors and one motor for axial rotation need to be controlled. The advantages of the identical, interchangeable

modules of the second prototype (chapter 5) are high with respect to the modules with dedicated functionality as used in the first prototype (chapter 4), especially when it comes down to building the physical hardware and performing tests.

The modular setup for the electronic system facilitates these advantages. Every module has an identical control board, controlling both the drive motor and the bend motor located in that module. The only exception in this case is the rotation module which houses two drive motors and one motor for axial rotation. Since the control boards have been designed to interface a maximum of two motors, two control boards are necessary in the rotation module.

7.2.2 RS485 bus

In the first prototype an I²C¹ has been implemented as communication method between master module and slave modules. I²C has a number of aspects making it a suitable candidate:

- two wires (data and clock)
- logic levels (no level shifters)
- large number of nodes on the bus (up to 128)
- reasonable high baud rate (400 kbit/s)
- flexible configuration (multiple masters)
- simple protocol, hardware support in many microcontrollers

I²C is meant as communication standard on a PCB between logic circuits. As physical bus (wires with a certain length) it suffers from noise. Also when the length of the wires increases, the bus capacitance also increases, dramatically reducing the possible baud rate.

For the second prototype the choice has been made to migrate to the RS-485 communication standard². The bus uses a differential signalling protocol which can be interfaced using a single driver chip. It offers data transmission speeds of 35 Mbit/s up to 10 m and 100 kbit/s at 1200 m. The maximum number of supported nodes on a bus is 32 or 64, depending on the chosen driver chip.

The standard itself offers just the physical layer of the OSI reference model³, the datalink layer has to be implemented according to desired behaviour. In the case of this project the choice has been made to implement simple packetised data without implementing a transport layer (so no retransmission of packets). The network

¹Inter IC Bus - a standard by Philips, also know as two-wire interface(TWI) bus

²also known as the ANSI/TIA/EIA-485 standard

³http://en.wikipedia.org/wiki/OSI_model

layer is pretty straightforward: every node has a unique address on the bus, every node receives all data broadcasted on the bus - and is programmed simply to ignore data addressed at other nodes.

The protocol that has been used, has been inspired by the protocol implemented for Dynamixel⁴ servo's which are used widely in (hobby) robotics but also in rapid prototyped robotic setups or the robot soccer competitions.

The chosen RS-485 transceiver can switch between transmitting and receiving data. When a transceiver is transmitting, all other nodes should be switched to receiving ('listening') mode, otherwise collisions might occur.

A bus protocol is considered with one master which dictates the communication. Slave nodes can only communicate on the bus on request of the master (depicted schematically in figure 7.2. In this way collisions can be avoided, although it is possible that a slave node blocks the bus. In every slave node a timer will reset its communication status to 'listening' when for a certain period (20 ms) no data has been received from a master.

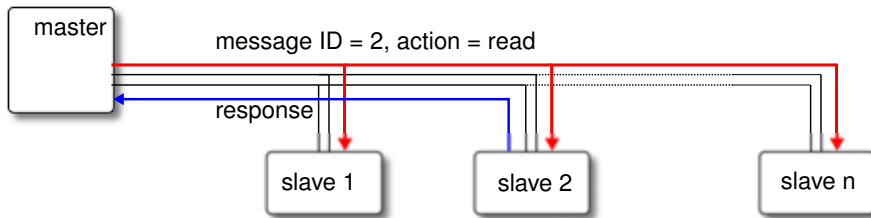


FIGURE 7.2 Master requesting data from a single slave

A data frame consists of a header $[0xff\ 0xff, ID, n, cmd, data\ 0, data\ \dots\ n, checksum]$. A standard data frame sent by the master will consist of one command, (i.e. read or write or special status messages) At a baud rate of 57600 sending an average data frame (10 byte) will take 1.7 ms allowing 500 messages per second. The delay between receiving an instruction by the slave node after receiving a 'read' instruction by the master can be adjusted. Figure 7.3 shows a data request and response from a slave node with a delay of 0.4 ms. A read instruction returns all requested values from memory from a certain start address for a given length.

In order to address 7 slave nodes on the bus, the following protocol is applied. The length of each communication frame or time slot is depending on the necessary sampling frequency. The example in figure 7.4 shows an update frequency of 9

⁴<http://www.robotis.com>

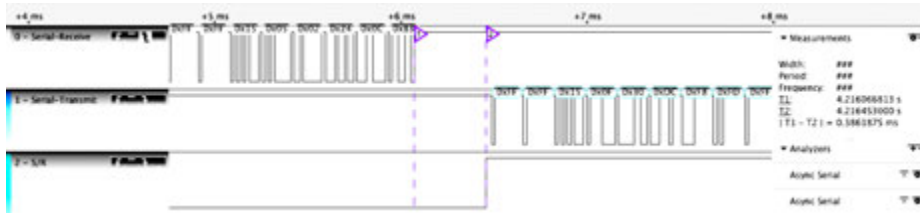


FIGURE 7.3 Measured delay in slave node response using *Saleae* Logic analyser

Hz. At the beginning of each frame, data is being sent to all slave nodes, consisting of the setpoints for drive motor and bending motor. After that, each slave is addressed with a read instruction each slave responds immediately with all its available sensor- and status data. Figure 7.4 shows the large block of setpoints transmitted at the markers 1 and 2. It shows the responses of two slave nodes at to different lines.

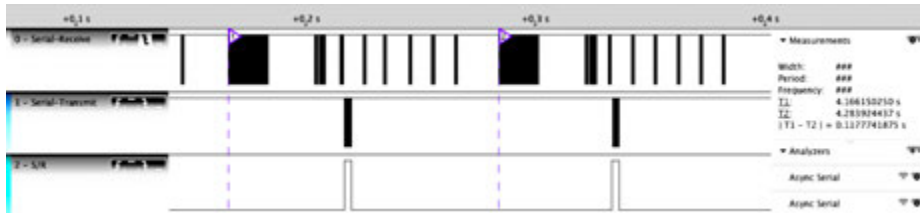


FIGURE 7.4 Measured communication frame using *Saleae* Logic analyser

7.2.3 Slave node design

Both the first and second prototype of the robot make use of the described master-slave system. A number of improvements of the slave node of the first prototype (described by Ansink [4]) have been discussed in the projects by Reemeijer [75] and Borgerink [7]. The functions that need to be implemented on the slave boards are listed in table 7.2.

TABLE 7.2 Specifications for the motor control board

item	implementation
motor amplifier	dual H-Bridge
current sensing	2 motors, shunt resistor
communication	RS-485
position sensors	2 absolute rotary encoders
velocity sensor	incremental encoder
tasks	communication, 2 (PID) control loops safety functions (watchdog timer) update firmware

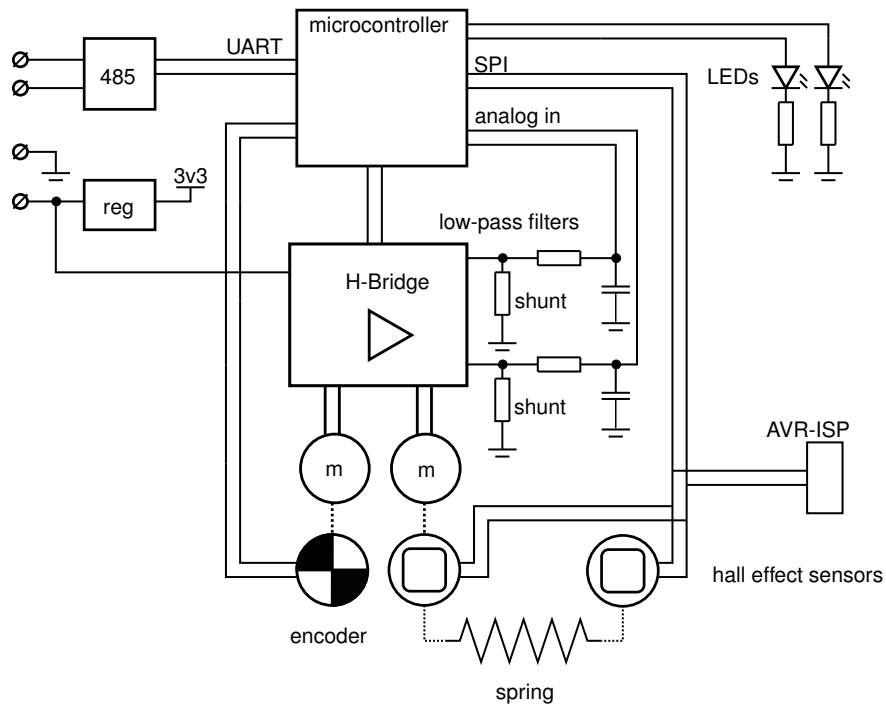


FIGURE 7.5 Schematic overview of the motor control board

Bridge amplifier

The choice of the motors has been described in chapter 5. The drive motor is a Faulhaber 2619 flat motor with built-in 112:1 gear box and 16 ppr incremental encoder. The motor operates at 6.0 V and has a maximum current draw (stall current) of 750 mA. The bending motor is a Faulhaber 1016 with 64:1 gear box. Only on the drive motor an encoder can be mounted due to size constraints in the design. For the bend motor two position sensors are added. The maximum current draw is 298 mA and the motor operates at 6.0 V.

The selected H-bridge, the A3906 by Allegro Microsystems, can deliver up to 1.0 A per channel and operates between 2.5 V and 9.0 V. The chip allows for separate shunt resistors for sensing the current through each motor individually. An internal over-current protection circuit reduces the output power when the voltage over the shunt resistor exceeds 200 mV. A shunt resistor of 0.5 Ω effectively limits the current to 400 mA.

Since direct measurement of the voltage over the shunt resistor contains noise generated by commutation of the motor, per channel a low-pass filter is implemented before the signals are fed into the AD converter of the chosen microcontroller. The PWM frequency used is 31.4 kHz. In order to filter this (and commutation effects) out, the low pass filter has a cut-off frequency of $1/2\pi RC = 1/(2\pi \cdot 1.5 \times 10^3 \cdot 1 \times 10^{-7}) = 106$ Hz, the bandwidth of both the drive motor and bending module will not exceed this frequency.

Microcontroller

On both the motor controllers in prototype 1 and prototype 2 microcontrollers have been used of the AVR series by Atmel. These controllers have been supported by a the GCC⁵ (GNU compiler collection) tool chain for a long time, which has fuelled the popularity of boards (and de-facto-standard) of the Arduino family. Arduino boards are currently widely spread in education, creative design and engineering. The impact of using open source hardware like Arduino will be discussed further in chapter 11.

As microcontroller the ATmega328p has been chosen, which is the most common controller on Arduino boards. It is a controller with a good balance between internal memory, hardware peripherals, size and pin count. For the motor control boards in prototype 1 the ATmega168 was chosen, at that time the most powerful controller in the 8 bit range with relatively low pin-count (28 pins). The controller executes instructions at 8 MHz using an external clock.

Implementation

A small board measuring 15×27 mm has been realised, shown in figure 7.6. One side of the board contains the components, the other side the connectors for motors and sensors (Hirose DF57 standard). In the implementation described in chapter 4 and [4] all electrical connections were soldered. In the following experiments [75] this proved to be an unworkable situation. First MicroMatch connectors were added, and later on also Harwin connectors were used. Both of these connector systems were relatively large and proved unreliable. The DF57 connectors are smaller and come with pre-crimped wires, improving the reliability.

Although it seems very trivial, during development, manufacturing and experimentation flexibility in use of hardware is very important. Being able to quickly swap a module might save an entire series of experiments during a field test. Choosing the right connectors enhances the modularity of the system. On the other side, the use of connectors also increases the risk of faulty connections and loose contacts.

⁵<http://gcc.gnu.org/>

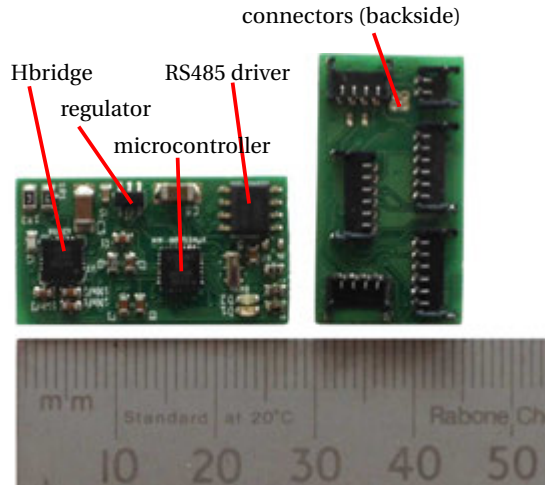


FIGURE 7.6 Motor control board (slave node)

Position sensors

In the first prototype due to space constraints Murata potentiometers have been used as position sensor. Since the signals are interfaced using a 10 bit ADC, the available resolution is in theory $270^\circ/1024$. This theoretical resolution is never utilised due to mechanical play and the amount of (electrical) noise.

Since the production method for the second prototype allows much more flexibility (see chapter 11) in each module two AS5055 12 bit magnetic rotary encoders have been integrated into the design. A sensor consists of two parts: a diametrically polarised magnet (as opposed to the standard axial polarisation) and an integrated circuit containing the hall effect sensors and processing electronics. The sensor can be interfaced using a standard SPI bus. The resolution for measuring the angle θ between two modules is 0.088° or 1.53 mrad. The sensors have been mounted on individual PCBs (shown in figure 7.7 and can be connected using a DF57 connector.

The faulhaber geared DC motors come with integrated incremental encoders. These encoders have a resolution of 16 ppr. The drive motor has a 112:1 gearbox, so the total resolution for the drive motor is 1792 ppr. With a wheel diameter of 46 mm the resolution is 0.08 mm. The pulse transition time is measured in software to calculate the rotation velocity. The rotation motor is equipped with a 809:1 gearbox, yielding a resolution of 12944 ppr or 4.85×10^{-4} rad.

Communication

A low voltage (3.3 V) version of the standard RS-485 bus driver has been used to connect each module to the communication bus. A driver (ST3485) has been cho-



FIGURE 7.7 AS5055 Position sensor PCB

sen allowing up to 64 units on one bus. The driver has also a built in 15 kV ESD protection making it less sensitive to damage by static electricity.

The communication bus is used both for exchange of information and reprogramming the slave nodes by accessing a bootloader. The bootloader is activated upon reset (or power-up) and will listen for 0.5 s to incoming data. Only if in that time slot the escape character is received (0x1b) the node will enter the bootloader.

Furthermore a watchdog timer is implemented on every slave node. When communication fails - and a node 'freezes' the bus, eventually (after 0.5 s) these nodes will reset and resume functioning.

Power

For the first prototype a bus layout was chosen with two separate supply voltages: a 3.7 V battery as 'logic' supply and a 7.4 V battery source as 'motor' supply. In the version of the motor driver board for the first prototype two switching regulators were chosen: one buck converter to generate the 3.3 V logic supply from the 3.7 V battery source, and a boost converter generating 5 V from 3.3 V especially for the use of incremental encoders. These two switching converters generate noise on the power supply lines which did influence the measurements of the used potentiometers in the first prototype.

In order to minimise switching noise, in the version for the second prototype a standard linear regulator has been chosen. A single supply source is used for the motors, the logic supply (3.3 V) is derived from this 6 V supply using a LP2985 linear regulator capable of 150 mA and a very low dropout voltage(0.28 V). Note that with a linear regulator all excess power $(V_{out} - V_{in})i$ will be converted to heat. The average power consumption of an ATmega328 at 3.3 V and 8 MHz is 4.0 mA⁶.

⁶see ATmega328-PU datasheet by ATMEL

Two indicator LED's consume $i = (3.3 V - V_F)/100\Omega$ which for blue ($V_F = 2.9 V$) yields 4 mA and for red ($V_F = 2.0V$) 13 mA. Although they blink with a duty cycle less than 50 % their consumption (8.5 mA) is more than the controller. The H-bridge draws current directly from the unregulated bus supply. The average current consumption of the absolute encoders is 5 mA when being read at a 1 ms interval. The current consumption of the incremental encoders is 8 mA.

device	average current consumption at 3.3 V
microcontroller	4 mA
2 LEDs	8.5 mA
2 hall effect sensors	10 mA
1 incremental encoder	8 mA
total	30.5 mA

Per module $(6 - 3.3) \cdot 0.0305 = 82.5$ mW is being dissipated by the regulator (worst case). For the entire robot with six of these slave nodes this amounts to 0.5 W being dissipated to heat. Note that the LEDs are only used for lab experiments, testing and debugging.

The power consumption can be reduced when the robot is not moving, by turning off the hall effect sensors, LED's and putting the microcontroller in sleep mode. Only for the incremental encoder no facilities have been included in the design to switch it off or reduce the power consumption.

The linear regulator is the cause of most of the heat dissipation (and power loss). An efficient switching regulator as implemented in the first design can solve this, but has a larger footprint, increasing the size of the PCB. Also the increase in electrical noise and the need for larger capacitors using switching power supplies have been reasons to use a linear regulator instead.

The power which is dissipated is small with respect to the total power consumed by the robot. Each of the motors draws an average of 200 mA during operation (maximum 300 mA) which amounts to $10 \cdot 0.2 = 2.0$ A (during complex manoeuvres using all motors at once) At 6.0 V this amounts to 12.0 W. The dissipated energy by the boards is just 4.2 % of the total power.

7.2.4 Master node design

The implementation of options for control of the robot can be categorised in levels of increasing complexity as shown in table 7.3.

TABLE 7.3 Hierarchy in control implementation

level	control implementation
1	Hardwired setup - sensors and motors connected through a cable to a switchboard. This is the first and simplest option: motors are directly switched to a power supply (turn on/off), sensors are monitored with (lab) equipment.
2	Direct IO setup - sensors and motors are wired directly to a computer control system using an interface such as a NI Labview system, XPC target or custom designed microcontroller board.
3	Serial bus control - motors and sensors are connected using local interfaces (motor control boards), used in transparent mode: all values are being generated from a host system using a serial bus protocol. The host system implements the (PID) control. Power can be obtained through a tether cable or internal battery.
4	Local (PID) control - motors and sensors are connected with local interfaces (motor control boards), using local (PID) control. Set-points are being given by a host system (PC or microcontroller) directly through the serial bus. Power can be obtained through a tether cable or internal battery.
5	Transparent master - a master controller on the robot generates signals for the local motor control boards and provides a mapping between the set-points it receives from a host system and the internal serial bus on the robot. Power can be obtained through a tether cable or internal battery.
6	Intelligent master node - a master controller sends data to local motor controllers based on sensory information and stored mission data. Power can be obtained through a tether cable or internal battery.

First prototype

Three physical versions of a bus master have been implemented. For the first prototype a control board using an ARM7 32 bit microcontroller was implemented which has been described in chapter 4. In experiments this board has been used in transparent mode (table 7.3, option 5), simultaneously logging measurement data on external memory. The set-points are generated from a user interface programmed in *Matlab*, visualisation of the data (and comparison with simulation) has been implemented in *20sim*.

The master control board has been designed as 4-layer board using the components described in table 7.4. The board is shown in figure 7.8. The NRF24L01 radio transceiver has been used for wireless state feedback and control (described in chapter 10). The accelerometer has been used to measure orientation of the robot with respect to the direction of gravity. As development environment the GNU-GCC port for ARM (available as 'WinARM') has been used. For programming and debug-

TABLE 7.4 Specifications for the master control board of prototype 1

item	implementation
size	30mm * 40 mm
controller	ARM7 LPC2148 at 60 MHz
power	Low Power <300mW 3.7 V Li-ion battery stabilisation circuit
memory	expandable 1 GB SD card
sensors	orientation LIS3L02AL accelerometer temperature TC77
communication	NRF24L01 2.4 GHz wireless P82b96 I ² C driver mini USB to host PC RS232 connection Philips ISP programming

ging USB, RS232 and the Philips ISP programming connection have been used.

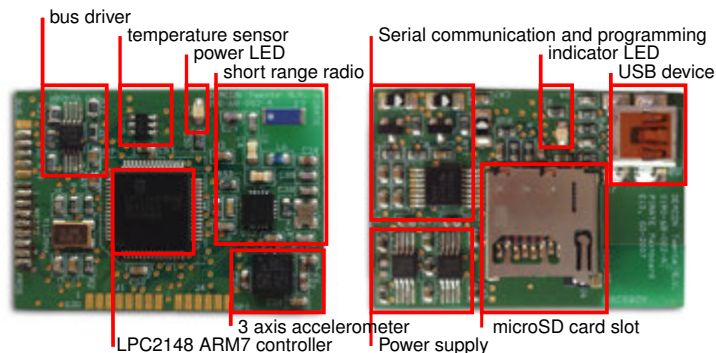


FIGURE 7.8 Master control board used in the first prototype

Second prototype

For the second prototype no on-board master controller has been implemented. During experiments by Borgerink [7] implementation 2, listed in table 7.3, has been used: an Arduino Mega⁷ board acts as interface between host PC and the robot prototype. All robot hardware is directly wired through a large multi-pole cable to this board.

During the experiments and measurements with the second prototype described

⁷<http://arduino.cc/en/Main/arduinoBoardMega>

in chapter 12 implementation 4 has been used: all slave nodes run local PID control loops, set-points are transmitted over the serial bus from a host PC system. In the software running on the host system a mapping of user control inputs and set-points is made. Although the timing transmitting these set-points is not very critical, still a latency (or worse, missed control events) could lead to unexpected and undesired behaviour.

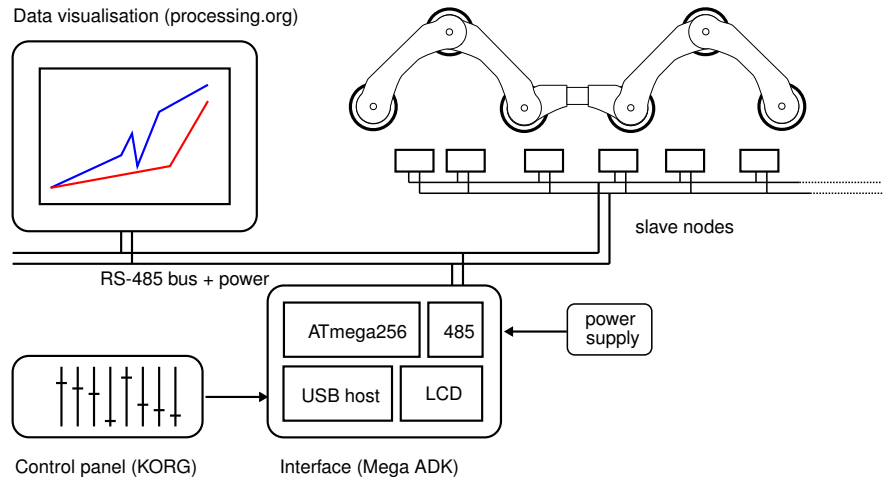


FIGURE 7.9 Schematic overview of control setup implementation

Since the communication bus allows only for a half-duplex implementation (one node can transmit at a time, simultaneously transmitting and receiving is not possible) it is vital that the synchronisation of the communication is continuous. Every node has the possibility to ‘freeze’ or block the communication on the bus.

An interface program for controlling and monitoring the robot’s behaviour written in Processing⁸ (a shell and set of java libraries aimed at easy development, see chapter 11) proved a simple way to get started, but has difficulties in fulfilling the timing-critical tasks. Eventually the mapping and interfacing of user inputs has been done on a separate system, an Arduino Mega ADK board⁹, capable of meeting the real-time constraints while using the application in Processing for visualisation and recording of the robot data.

A measurement setup using this hardware is shown in figure 7.10. A USB-host implemented on the Arduino Mega ADK board interfaces the USB-MIDI control panel (Korg nanoKONTROL2) which is used for user input. The board sends set-points

⁸<http://www.processing.org>

⁹<http://arduino.cc/en/Main/ArduinoBoardADK>

over RS-485 through a separate adapter to the connected slave nodes. Also in this picture is a measurement bench containing a strain-gauge sensor for measuring clamping force of the module. This sensor is interfaced using an instrumentation amplifier circuit (INA122) to the analog input of the board. Measurements are discussed in chapter 12.

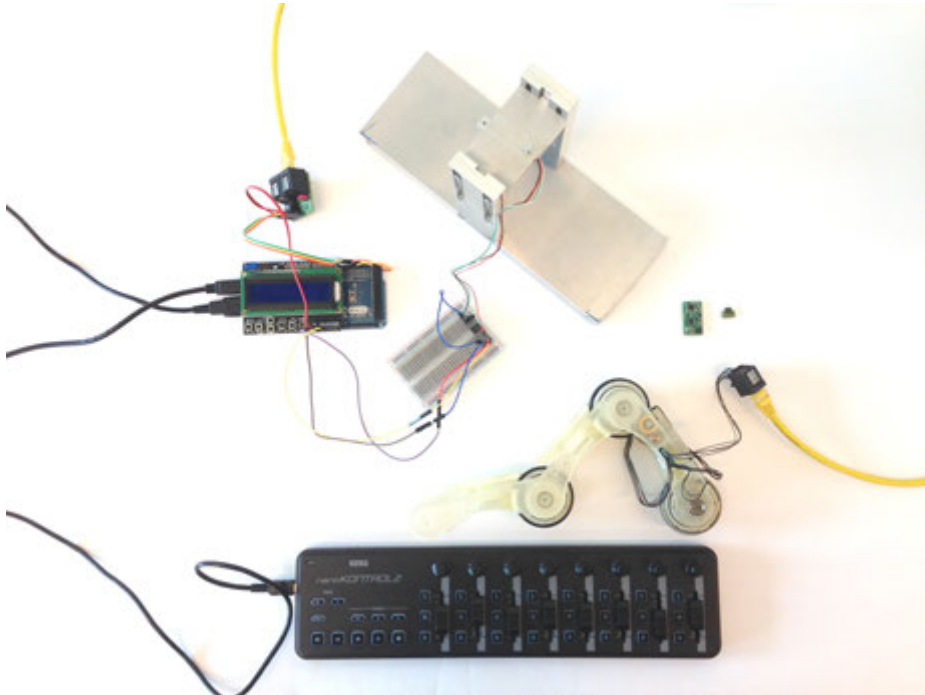


FIGURE 7.10 Measurement setup using control panel, robot segment and Arduino Mega board

Final prototype

The final implementation of the master control board for the robot aims to integrate both the control of the robot's slave nodes and the vision system. The implemented hardware consists of an Overo Water Com ARM Cortex A8 embedded target running realtime linux capable of doing both user input mapping and vision processing. The software implemented on this version is documented in chapter 10 on robot control and in chapter 8 on sensing hardware. The setup is schematically shown in figure 7.11.

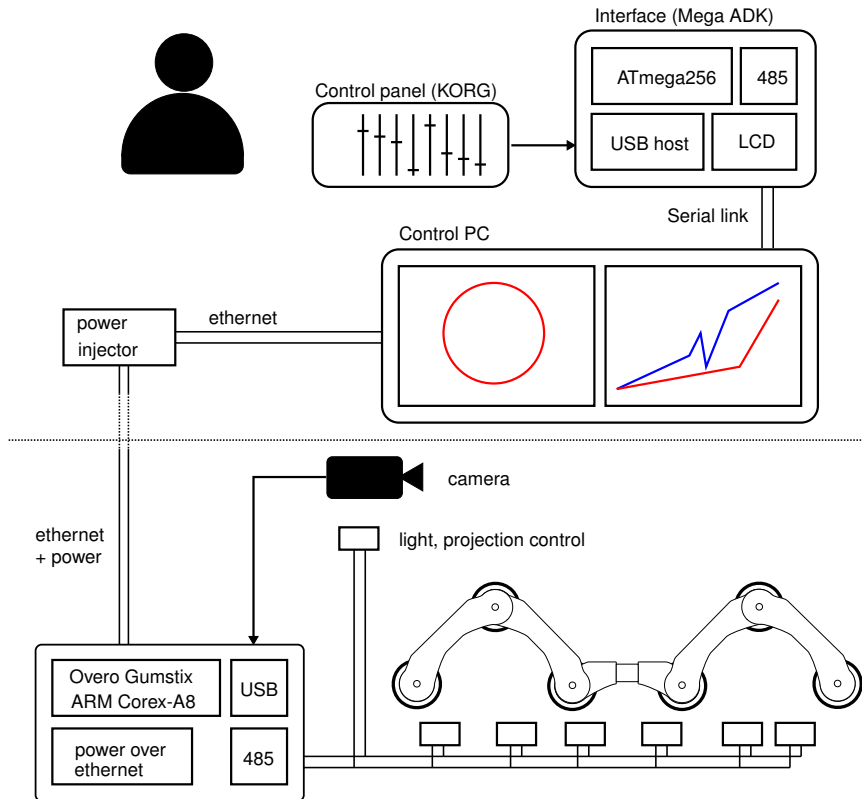


FIGURE 7.11 Setup with Overo Water Com ('gumstix'), power over ethernet and host PC

7.3 Power system

7.3.1 Battery considerations

As described in chapter 4 two separate lithium polymer batteries have been used to power the robot, one battery for the sensing- and control hardware, the other battery for motion. The 7.4 V 350 mAh LiPo battery for driving has a total capacity of 2.2 Wh. The 3.7 V 350 mAh logic battery holds 1.1 Wh which is roughly enough for 20 minutes of autonomy (without powering additional sensing equipment).

These batteries have only been implemented and used in the first prototype. For the second prototype the choice has been made to focus primarily on tethered operation, so no further experiments using batteries have been done. All experiments

described in chapter 5 have been performed using a flatcable as tether following control implementation 2 described in table 7.3. The experiments with the final prototype described in chapter 12 use a twisted pair cable with one pair for RS-485 signals and three pairs for power. In both cases an external power supply is used providing power through the tether cable to the robot.

7.3.2 Tethered power supply considerations

During a number of first tests a multi-pole (flat) cable has been used (table 7.3 level 2) or a twisted-pair wired version of the RS-485 bus (table 7.3 level 3). For the final design a CAT5 ethernet cable is proposed using power over ethernet (PoE) described in the IEEE 802.3at-2009¹⁰ standard (also known as 802.3at Type 2) allowing a supply of up to 25.5 W of power, using both the 'free' CAT5 cable pairs and an added power offset to the signal pairs.

7.4 Conclusion

In this chapter a number of realisations of the distributed control architecture for the robot have been discussed. All systems have in common a master controller communicating over a (serial) bus with a number of slave nodes. A hierarchy in levels of complexity of control architecture can be distinguished. On the different prototypes different levels of control have been reached.

For all of the discussed prototypes different versions of the embedded control system have been realised. Each of these systems has been realised with the specifications for the final system in mind, however, the capability of performing the necessary experiments has been given priority during implementation.

The first version of the embedded control system described in this chapter consists of an master control board (ARM7) communicating over an I²C bus to five slave nodes (AVR) on the bus. This setup has been used for control through a user interface on a host system written in Matlab and for data acquisition using an application written in 20sim.

The version of the embedded control system used for the experiments described in chapter 12 uses a master controller (ATmega256) as base-station, controlling seven slave nodes (AVR) through an RS-485 bus. Data acquisition has been realised using an application in Processing. Although a design for an on-board master controller (containing an Overo Water Com ARM-Cortex A8 controller) has been made, the final implementation has not been realised within the scope of this project.

¹⁰IEEE 802.3at-2009 at <http://standards.ieee.org>

8

Sensing

8.1 Introduction

This chapter discusses the sensor systems used on the robot. The platform has to be capable of manoeuvring inside a pipe environment and assess the pipe condition. A vision system will be discussed capable of both qualitative measurements for navigation and quantitative measurements for pipe assessment.

A second sensor system which is tested for pipe assessment is an audio sensor ‘listening’ for gas leaks.

Furthermore a number of internal ‘state’ sensors have been implemented which are mainly used for control of the robot, such as temperature sensors and sensors for measuring current consumption. For navigation (and partially for assessment of the pipe network layout) a set of sensors comprising an inertial measurement unit (IMU) have been added.

8.2 Stereo Camera System

8.2.1 Introduction

This section discusses the design of a vision system¹ capable of providing qualitative information of the pipes in order to aid navigation and quantitative information for pipe assessment. For navigation the system has to identify the position of obstacles such as bends and T-joints. For pipe assessment the system needs to detect deformation of the pipe (caused by external stress or load) and, if possible, tiny defects (i.e. cracks) on the inside.

The proposed system consists of an active stereo vision system using a laser projector and camera sensor. The system has to be very small and lightweight, both

¹The master’s project by Eric Drost [28], Twan Mennink [60] and Mark Reiling [76] and the bachelor’s project by Maarten Brillman [8] have contributed to this work.

in size and power consumption in order to fit the requirements for (autonomous) navigation by the robot.

Related research

Many sensor systems exist for assessment of the quality of pipes. The two systems which are most widely implemented are eddy current (EC) and ultrasonic sensing (US). Since eddy current sensing only works in metal pipes, it is unsuitable for a robot assessing mainly PE and PVC pipes. Ultrasonic sensing needs a coupling medium (liquid), therefore it is unsuitable for use in a live gas distribution mains. Therefore optical imaging sensors are considered the most viable candidates for this project.

Most of the existing robots for pipe inspection use a closed-circuit television camera system (CCTV) as discussed in the overview of inspection systems given by Duran et al. [29]. In order to facilitate interpretation and assessment of the images by operators, automated computer vision systems utilising image analysis, pattern recognition and neural networks have been developed, for example in the work on inspecting sewer pipes to detect surface defects by Xu et al. [111] or deformation of pipe joints by Moselhi et al. [64].

Stereo imaging systems

A problem, however, is the absence of reference points in the CCTV images, which makes it difficult to perform quantitative measurements. A solution is the use of a stereo vision system, in which two cameras are employed to capture an image of the same illuminated scene from a different viewpoint. Optical triangulation can be used to reconstruct points of interest in the images in three dimensional space, that in turn can be used to determine the dimensions of interesting objects as used by Rome et al. [81] and Ahrary et al. [1].

Active stereo vision

A stereo camera system requires that points of interest are clearly visible in the images, such as the bricks in the sewer pipe wall. Since the PE and PVC pipes in a gas distribution network have a smooth surface these points are lacking. A solution for this problem is to use an active stereo vision (ASV) system; instead of two cameras this system uses one camera and a projector. The projector projects a well-defined light pattern onto the inner pipe wall so that features of interest or the shape of the pipe become visible; optical triangulation is again used to reconstruct them. Furthermore, the light pattern simplifies the detection and extraction of the features.

In the works by Zhang et al. [115] and Duran et al. [30] circular laser patterns are used to calculate diameters and deformations of pipes. Other patterns that have been used for shape measurement and obstacle detection are point grids as used by

Tsubouchi et al. [101] or cross-hair patterns used by Kolesnik et al. [54]. A more recent example is the Kinect™ gaming interface by Microsoft² which uses a random dot pattern. One of the goals of this part of the project is to select a pattern which has a small computational load so that it can be executed on a small (embedded) target.

8.2.2 Analysis

Active stereo vision system

When a point of interest is viewed by two camera's, using optical triangulation the position in space can be determined. The same holds when one of the cameras is replaced by a source of structured light. As illustrated in figure 8.1, a point X defines two corresponding points u_c and u_p in the camera and projector planes; these three points, or equivalently X , O_c and O_p , define a triangle. This triangle is determined by the corresponding points and other aspects of the system such as the distortion of the lens and field of view of the camera.

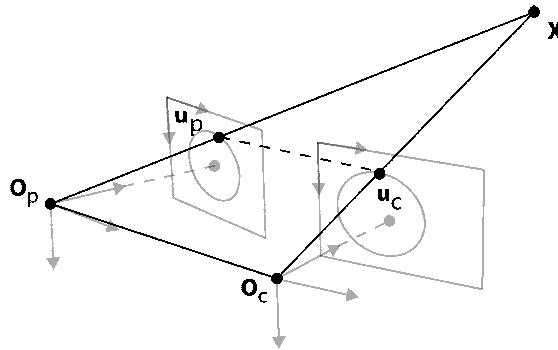


FIGURE 8.1 Optical triangulation.

The relations between the points in the camera and projector plane can be described using *epipolar geometry*³. These relations are derived based on the assumption that the camera and projector can be approximated by a pinhole camera model.

*epipolar
geometry*

The pinhole model (see figure 8.2) relates the camera frame coordinates $X_c = [X_c, Y_c, Z_c]^T$ with the image plane coordinates $u_c = [u_c, v_c]^T$ with the following intrinsic parameters:

- $f_{c,u}$ and $f_{c,v}$ are the camera normalised focal lengths expressed in number of pixels. Pixels are assumed square: $f_{c,u} = f_{c,v} = f_c$

²<http://electronics.howstuffworks.com/microsoft-kinect.htm>

³http://en.wikipedia.org/wiki/Epipolar_geometry

- $u_{c,0}$ and $v_{c,0}$ are the coordinates of the principal point p_c of the image sensor, expressed in pixels
- s_c , the skewness factor of the camera. The camera plane is assumed to be orthogonal: $s_c = 0$.

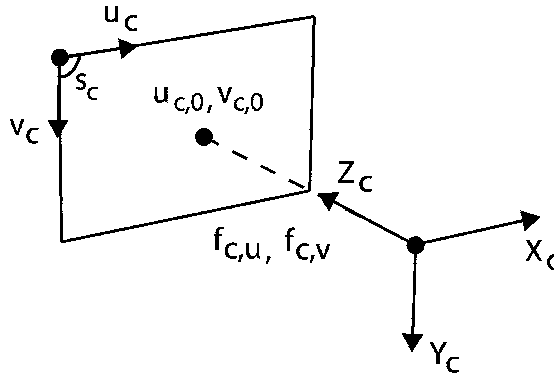


FIGURE 8.2 The pinhole model

Since (wide angle) lenses will have to be used, radial distortion of the image has to be taken into account, using for example a second order distortion model as given in (8.1), where k_1 and k_2 are the radial distortion coefficients. The principal point of the camera (x_c, y_c) is used as the centre of distortion. A point (x_o, y_o) of the original undistorted image in the pinhole model results in distorted coordinates (x_d, y_d) following:

$$\begin{aligned} x_d &= x_o(1 + d) \\ y_d &= y_o(1 + d) \end{aligned} \quad (8.1)$$

$$d = k_1((x_u - x_c)^2 + (y_u - y_c)^2) + k_2((x_u - x_c)^2 + (y_u - y_c)^2)^2$$

The field of view of the camera is an important measure for the (minimum) measurement range of the system. The field of view is determined by the dimensions of the image sensor, here denoted by $N_u \times N_v$ pixels, and the focal length f_c of the camera. Assuming $N_v < N_u$, the (half) field of view v is expressed as:

$$v = \arctan \frac{N_v}{2f_c} \quad (8.2)$$

Pattern

As described in section 8.2.1 many different patterns are used for vision systems. The circular pattern that is used for the pipe profiling system is generated by projecting a cone of light. This cone can be described in polar coordinates, defined by

u and θ , where α is the half fan angle of the cone (shown in figure 8.3). In the projector reference frame (x,y,z) it can be described by the following equations:

$$\begin{aligned}x &= u \tan \alpha \cos \theta \\y &= u \tan \alpha \sin \theta \\z &= u\end{aligned}\tag{8.3}$$

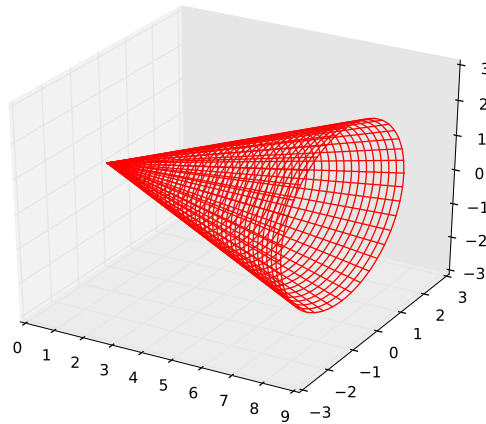


FIGURE 8.3 Cone with half fan angle $\alpha = 0.3$ rad

Configuration

A number of configurations of the camera and cone projector are possible. All can be used for the pipe profiling system, as long as the projected light pattern is in the FOV of the camera. However, since the system has to detect obstacles that are in front of the robot, the optical axes of camera and projector should be oriented in the same direction. The possible configurations are:

- planar system configuration, shown in figure 8.4 (a): for every point on the laser cone there are maximum two possible points (X_1 and X'_1) in the camera plane, so ambiguities exist when reconstructing the image
- centred system configuration, shown in figure 8.4 (b): in this case there is exactly one point in the camera plane which corresponds to a point on the laser cone. The configuration is symmetrical.
- the camera is in line with the projected laser cone (not shown): in this case

there are an infinite number of point correspondences. This is an undesired situation and should be prevented.

For the setup a centred configuration has been chosen, with camera and projector placed along the same optical axis. Although a planar configuration is easier to implement, it lacks symmetry resulting in differences in sharpness and measurement accuracy.

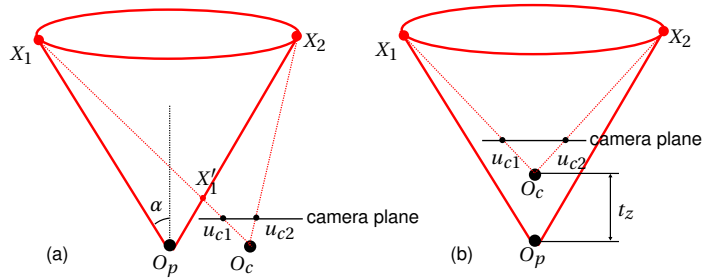


FIGURE 8.4 Camera configuration

Measurement range

The measurement range of the system is determined by the base distance t_z between camera and projector, the half fan angle α of the laser cone and the field of view ν of the camera. Note that if the camera is placed in front of the projector ($t_z > 0$), a constraint is imposed on the minimum radial distance to be measured (assuming that $\alpha > \nu$) and that if $t_z < 0$, a constraint is imposed on the maximum distance to be measured (assuming that $\alpha < \nu$).

The maximum distances to be measured are in theory infinite, but in practice limited by the amount of light reflected back to the camera and the sensitivity of the camera image sensor. PE/PVC pipe of 63 mm with a smooth surface has different reflection properties than a pipe of grey cast iron of 100 mm with possible corrosion. For the first tests PE pipes with a smooth surface are chosen, so the system is likely to work on a surface with a rough surface, inducing more scattering and backward reflection of the projected light.

Calibration

Let matrix \mathbf{R}_c^p describe the orientation of the projector in the camera coordinate frame and \mathbf{t}_c^p the translation of the projector in the camera coordinate frame. In the centred configuration the camera and projector are located in front of each other so that the triangulation base becomes parallel with the optical axes of the system. The parameters of the ASV system can then be written as:

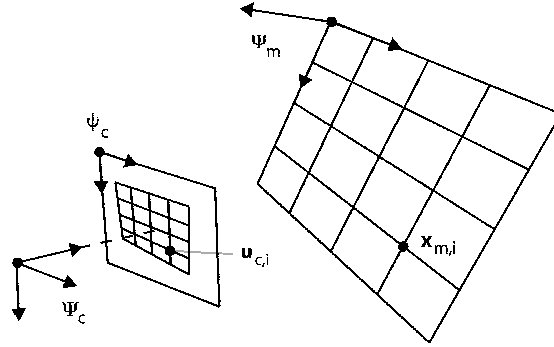


FIGURE 8.5 Schematic drawing of camera and model plane containing calibration features

$$\mathbf{R}_c^p = \mathbf{I} \quad \text{and} \quad \mathbf{t}_c^p = [0, 0, t_z]^T \quad (8.4)$$

The vision model is only useful if its parameters are established with sufficient accuracy. For this a calibration of the camera based on some known patterns must be performed first. A standard approach using a series of images (at least four) [32] has many example implementations in Matlab and OpenCV. A checkerboard pattern, see figure 8.5, has been used for finding the camera calibration data. A circle grid pattern (with four dots) has been used to calibrate the orientation of the laser, resulting in finding the combined parameters \mathbf{R}_c^p , \mathbf{t}_c^p and α .

Subsequently, the alignment of the laser has to be adjusted, shown in figure 8.6. The implemented mechanism for adjusting the mirror (see the following section on implementation) can only compensate errors in orientation (rotation) of the laser with respect to the camera. The translation errors have to be found and compensated for in software.

A circle is projected at a distance of 250 mm with a diameter of 150 mm, resulting in a circle in the image plane with a diameter of 665.7 ± 0.25 pixels, yielding a resolution of 0.22 mm. The centre of the laser projection in the image plane is (630.5, 480.5) px. The optical centre of the camera itself is (636.6, 480.6) px.

Image processing

Goal of the image processing algorithm is to extract the location of the observed laser curve. A number of algorithms have been designed, eventually leading to the following steps being the most efficient (with respect to computational load) without sacrificing too much accuracy:

- capturing and filtering by using only the luminance channel (Y in YUV mode instead of using RGB mode)

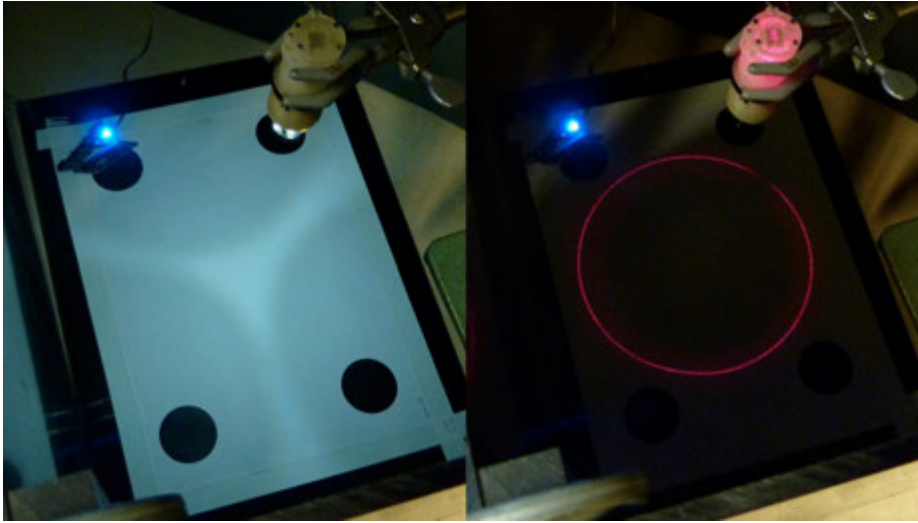


FIGURE 8.6 Calibration of the vision system using a circle grid pattern

- compensating for lens distortion
- polar transformation of the image
- filtering image
- select object (fit a line).

Pipe profiling

A polar transformation $R_p(\theta)$ is used to represent the data about the pipe. Deviations of the line with respect to R_0 can be seen as continuous deformations. Dis-junct features denote the presence of bends and T-joints.

$$R = \sqrt{(x - x_0)^2 + (y - y_0)^2}$$

$$\theta = \arctan\left(\frac{y - y_0}{x - x_0}\right)$$

The polar transform is also a beneficial reduction of the data set, so instead of a full image frame a linear data set, depending on angular and radial resolution needs to be transmitted or stored. Figure 8.7 shows a transformation in a captured image. A thin red circle is super-imposed on the original image locating the optical centre. Note that a segment at the bottom is missing because the camera (which is placed in front of the projector) gets in the way.

The extracted curves can be used for two purposes: profiling the pipe (quantitative measurement) and detecting obstacles, bends, T-joints (qualitative measurement).

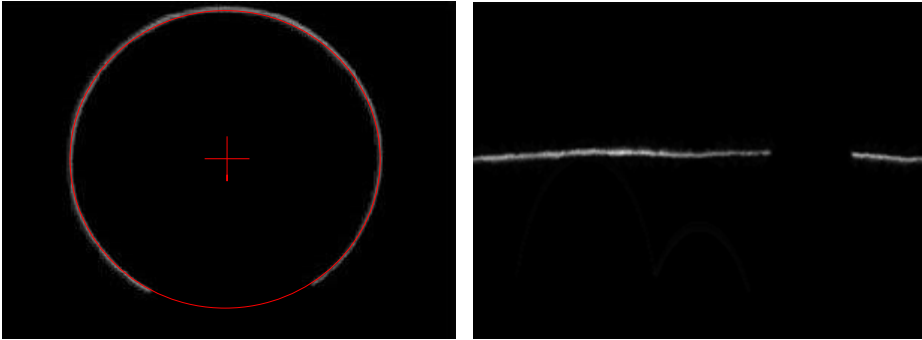
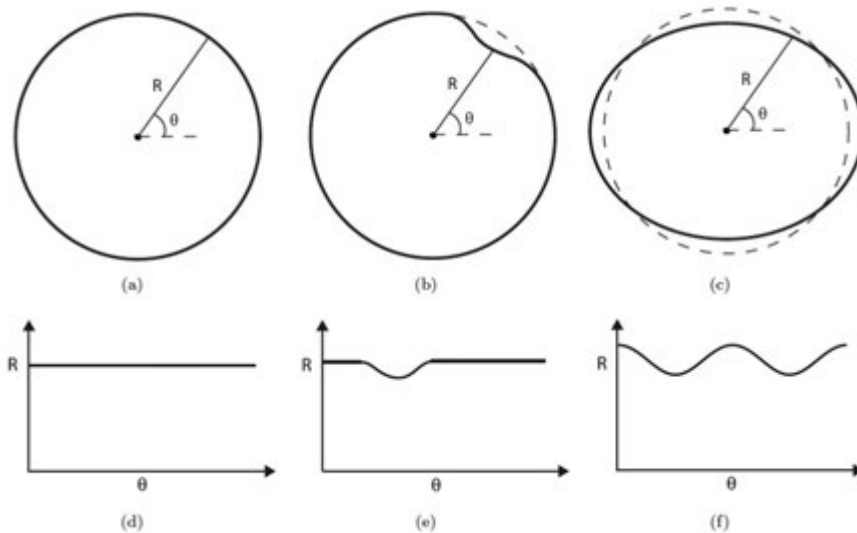


FIGURE 8.7 Polar transformation of a captured image

A number of basic deformations can be detected, as shown in figure 8.8. Images (d), (e) and (f) are the polar transformation of data obtained by the profiles of (a), (b) and (c).

FIGURE 8.8 Commonly found pipe cross sections, *image from [28]*

Using a series of captured circles the shape of the pipe can be reconstructed. Figure 8.9 shows a straight pipe section. The indents are caused by the points where the projected circle could not be captured due to the wires needed for camera and LED light in the construction.

When the robot is equipped with an accurate orientation sensor, combined with the internal state data of the robot (see chapter 10) this pipe reconstruction can be used to estimate stress on the pipe in longitudinal direction as well as in the de-

scribed cross section.

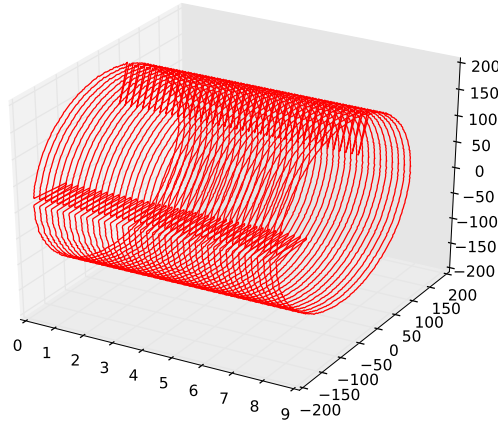


FIGURE 8.9 Reconstructed pipe profile

Obstacle detection

Obstacle detection has to be performed in real-time and processing requirements should be kept as low as possible. Drost [28] proposed an algorithm for obstacle detection which does not require the exact reconstruction of the illuminated pipe interior. Mennink [60] made an exact reconstruction of the pipe, which is subsequently compared with pre-generated maps. Since the computational power on the robot is expected to be small (see section 8.2.3) for now the method by Drost is best suited for implementation.

The system proposed by Drost uses low resolution images (160×120 pixels) for the part of obstacle detection. Eight lines in a radial symmetric configuration are used for obstacle detection in one image. They are denoted by \mathbf{l}_i and the intersections between \mathbf{l}_i and the captured laser curve is denoted by \mathbf{u}_i . The distance between \mathbf{u}_i and the principal point \mathbf{p}_c is given by $r_i = \|\mathbf{u}_i - \mathbf{p}_c\|$.

In a set of measurements a bend and a T-joint are approached. In figure 8.10 the measurements are shown schematically from the top. The bend can be compared to a T joint with one side junction. The behaviour of r_1 and r_5 over successive images captured by the system when it approaches the obstacles ($r_1(n)$ and $r_5(n)$) is shown in figure 8.11. From this figure, it is clear that sudden changes in $r_i(n)$ contain information about the possible presence of an obstacle. From the sequences also the orientation of the obstacle becomes apparent; the bend in 8.11(a) curves

towards the right, the branch of T-junction I in 8.11(b) is located at the left and the two branches of T-junction II in 8.11(c) are located in a plane perpendicular to the camera image plane.

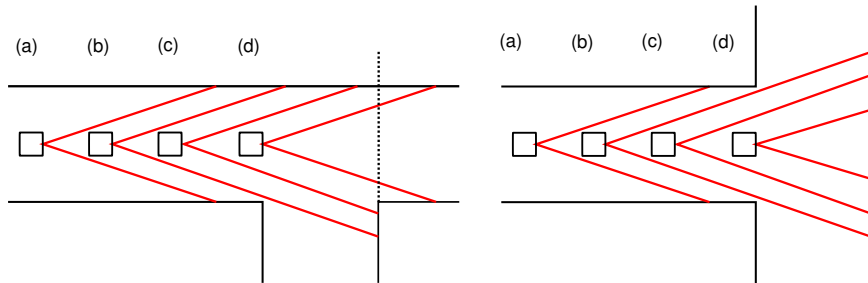
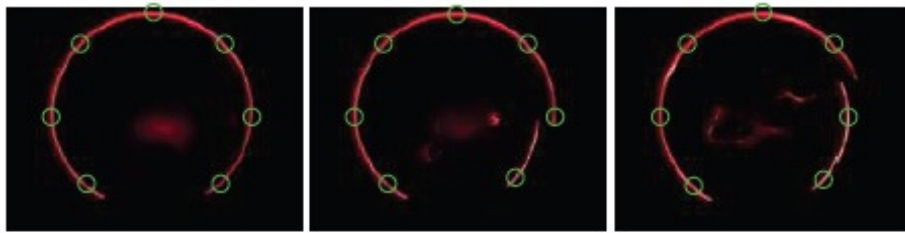
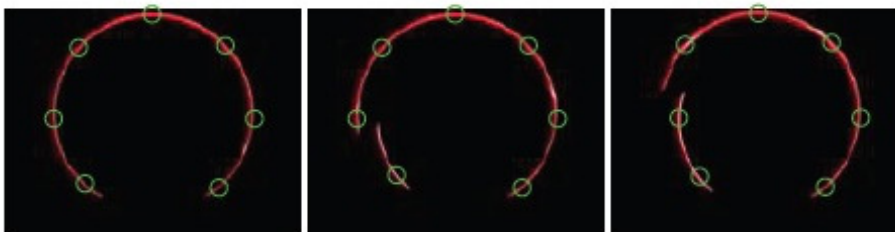


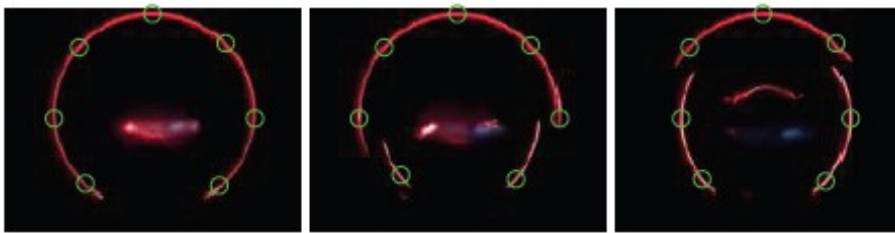
FIGURE 8.10 Schematic view of cone projection in a T-joint in two orientations



(a) Bend



(b) T-junction I



(c) T-junction II

FIGURE 8.11 Sequences of measurements for three types of obstacle - *image from [28]*

Alignment error

The alignment error is defined as the error on the cross-sectional profile when the optical axis of the measurement system is used as the pipe axis. These errors occur when the system is misaligned with the pipe.

The pipe is assumed to be defect-free, $R_0(\theta) = R$, and the errors are calculated by determining the intersection curve $\mathbf{X}_p(\theta)$ of the laser cone and the pipe. Note that for the radial symmetric configuration, $R_c(\theta) = R_p(\theta)$. The relative alignment error on the cross-sectional profile $R_c(\theta)$ is then computed as:

$$\rho_{R_c}(\theta) = \frac{|R_0(\theta) - R_c(\theta)|}{R_0(\theta)} \quad (8.5)$$

This means that the system cannot distinguish between an elliptical deformation of the pipe and a misalignment. The alignment of the ASV system is depending on the orientation of the robot and the accuracy of clamping exactly in the centre of the pipe. One possible solution would be a calibration procedure in a known deformation-free section of the pipe such as a T-joint or bend segment (which have a considerably higher stiffness than the pipes themselves).

8.2.3 Implementation

In order to function on the robot the imaging system has to work in a diameter range between 63 mm and 125 mm. For navigation purposes a setup is considered where the focal point of the system is located inside, or close to the first robot module. The half fan angle needs to be chosen such that for these pipe diameters the projection will be inside the camera's field of view. With $\alpha = 0.3$ rad and an inner pipe diameter of 51 mm the projected cone touches the pipe at $25.5 \text{ mm} / \tan(0.3) = 81 \text{ mm}$. When an obstacle occurs at maximum robot speed of 80 mm/s, at least 1 frame/s is necessary to be able to detect this.

TABLE 8.1 Parameters of the implemented vision system

Parameter	Value
Camera focal distance f_c	3.85 mm
Camera resolution	1280 × 960 pixels
Image sensor size $N_u \times N_v$	4.54 × 3.42 mm
Pixel size	3.54 × 3.56 μm
Camera field of view v	1 × 0.8 rad
Triangulation base distance t_z	12 cm
Laser cone half fan angle α	0.3 rad

A number of implementations of this system has been realised. In the work by Drost [28] a vehicle has been realised shown in figure 8.12 using a rotating mirror,

a camera with a resolution of 1280×960 pixels. The image processing is done (not strictly realtime) in Matlab. The properties of the system are listed in table 8.1.



FIGURE 8.12 First prototype ASV system by Drost [28] consisting of frame, mirror, laser and camera

Mennink [60] replaced the mirror by a diffractive lens⁴. The vision system was used for a number of experiments, described in [60], implementing recognition of basic features such as bends and T-joints in the image data, which is a basic requirement for performing SLAM (simultaneous localisation and mapping). In the subsequent versions of the vision system the diffractive lens has remained the method for producing the laser cone.

⁴DE-R 219 by <http://holoeye.com/>

Embedded control

During the project of Brillman [8] a small embedded target board has been selected to check whether the image processing can be done on board.

When the robot works in tethered operation, of course there is the option to do all vision processing on a host computer. However, all implementation steps were chosen with the autonomous robot in mind, so an embedded control board is needed with a small footprint (size and power consumption) so it can fit the robot module size, but with enough computational power to do the vision processing necessary for navigation (vision processing for qualitative assessment can be done based on a pre-recorded data set, so that part is not necessary on the robot)

The *Overo Water Com board*, also known as 'gumstix', is a very small board ($17 \times 58 \times 4.2$ mm) using an ARM Cortex-A8 family design based on the Texas Instruments OMAP 3530 processor, an application processor that is specifically designed towards video, image and graphics processing. It supports high-level operating systems such as Linux. It operates at 720MHz with 256MB DDR RAM and 256MB Flash memory on board. Also a DSP is placed on top of the processor: a TMS320C64x+ DSP (digital signal processor) core running at 520 MHz, which can eventually be used to perform certain vision processing tasks.

The same company produces a vision board using an Aptina MT9V022 image sensor which can connect directly to the Overo board using a 10 bit parallel connection. The sensor has Wide-VGA resolution: 752×480 pixels at a maximum framerate of 60 fps. This board has been used for an experimental setup, but is eventually replaced by a standard USB camera with higher resolution.

Final setup

The final system as realised by Reiling [76] is shown in figure 8.13 and consists of a 1280×960 camera with an added wide-angle lens. The laser projection is realised using the diffractive element. The laser diode is mounted with its back to the camera, so the cone has to be projected via a mirror. In the centre of the mirror a *beam dump* has been added preventing the reflections from the direct laser output.

The mirror and beam-dump have been mounted on a flexible structure which allows for calibration by adjusting the angle of the mirror with respect to the laser. A ring with three white-light LED's has been mounted round the camera lens in order to illuminate images for inspection by an operator. The camera module is mounted together with a control board and IMU sensor board at the front of the robot, shown in figure 8.14.

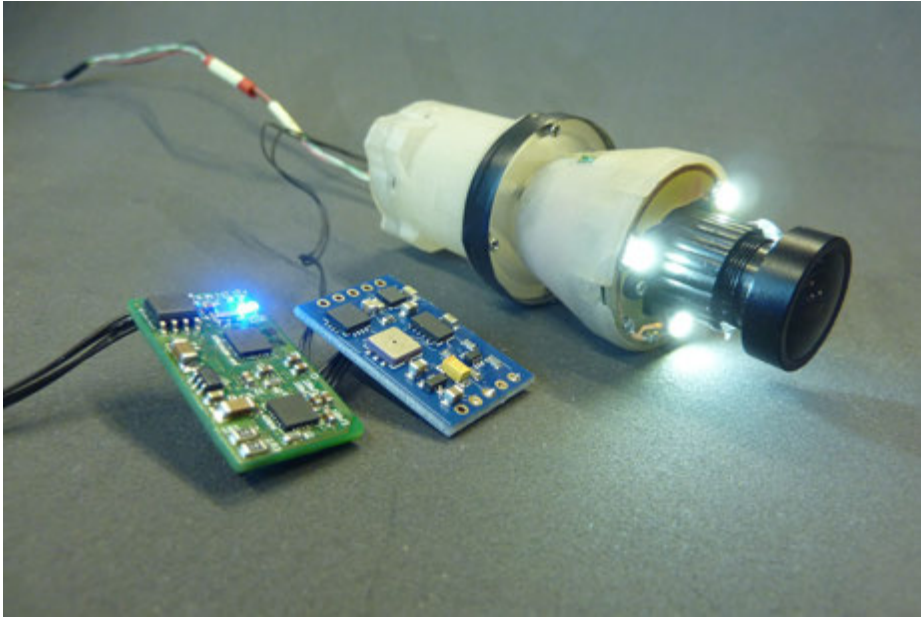


FIGURE 8.13 Camera system in 3D printed housing with sensor- and control board

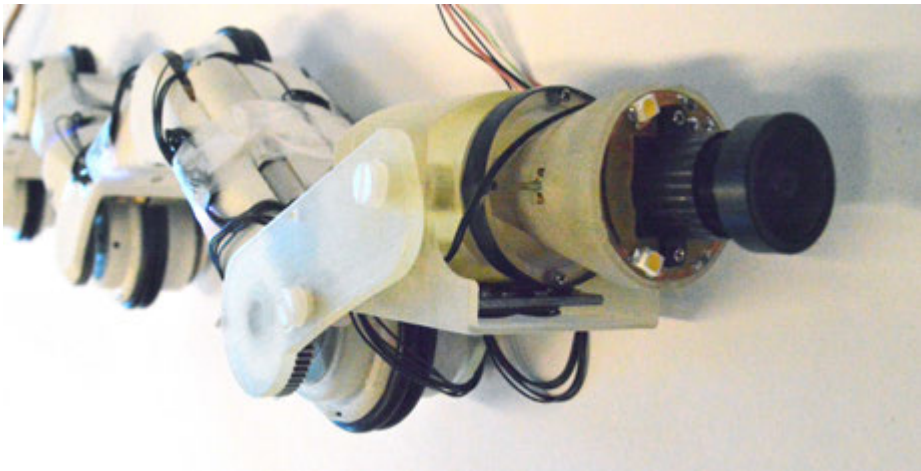


FIGURE 8.14 Camera system mounted on the robot

8.2.4 Results

To verify the resolution of the system a number of tiles with a thickness of 3 mm have been placed inside a 125 mm pipe. Every tile has a milled out slot with varying depth ranging from 0 to 1 mm in 0.2 mm increments. Figure 8.15 shows the mea-

surement data from a 0.2 mm groove inside the bigger 3mm slate at 0° . The overall deviation from the straight curve of ± 1 mm is caused by misalignment in the pipe.

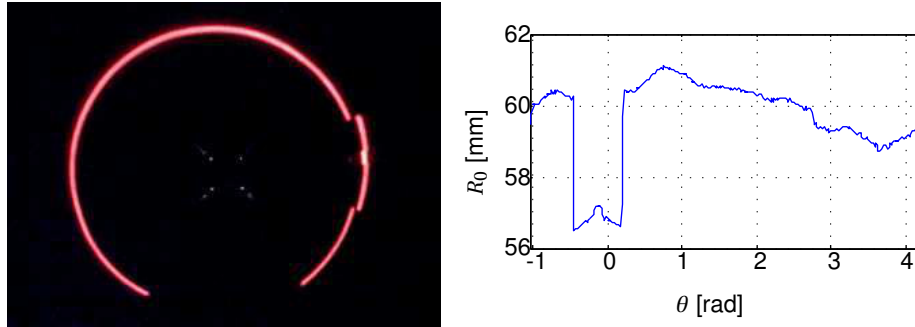


FIGURE 8.15 Measurement of a 0.2 mm obstacle

8.2.5 Conclusion

Based on the results discussed in this section the chosen principle of active stereo vision using a conical projection has been developed for the pipe inspection robot. The accuracy in measuring deformations of 0.2 mm should prove satisfactory for quantitative inspection. Also the performance of the sensor for navigation and obstacle detection proves to be satisfactory.

A housing for the camera, laser projector, adjustable mirror and beamdump has been designed and implemented using a 3D printer (see chapter 11). The design can be mounted on the robot and is small enough to satisfy the size restrictions for passing a mitre-bend in 63 mm. Two actuated degrees of freedom are necessary in order to adjust the camera with respect to the centre of the pipe, which have not been implemented yet.

The used vision algorithms have been scaled and optimised so they can run on an embedded target which can be placed on the robot. A design has been made for a carrier board fitting inside the available space of one module (explained in chapter 3).

8.3 Acoustic sensor

8.3.1 Introduction

In chapter 2 a number of conventional methods for leak searching have been explored. Only sensor systems with a small size and power budget that can work from the inside of a pipe might be suitable for the robot. Ultrasonic sensors are used on an industrial scale for detecting cracks and defects in the pipe wall. These systems however require a medium (fluid) for acoustic coupling which is the main reason this system can not be used in a 'live' gas distribution mains. Therefore a solution is investigated where one (small) acoustic sensor is taken into a pipe to detect leaks by their sound characteristics alone⁵.

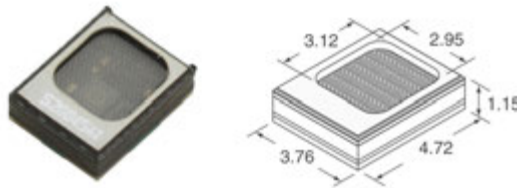


FIGURE 8.16 Ultrasonic MEMS microphone

8.3.2 Analysis

Acoustic sensors are widely used for leak searching in pipe systems for water, oil and gas, and are standard systems in the overview of leak-searching systems in overviews by for example Terry et al.[100] or Geiger et al.[35]. An overview of specifically the use of acoustic sensors for leak searching has been given by Fuchs et al. [33]. Most of the acoustic setups use multi-point sensing: for detecting a leak in a main water line acoustic sensors are placed on different end points, some distance from the spot where a leak is suspected. By cross-correlating the received 'noise' signals, differences in travel time from the leak to the sensing points can be calculated and thus the exact location of the leak.

There are however not many examples for using a single acoustic sensor in detecting gas leakage from the inside of a pipe. The characterisation and detection is normally done in the frequency domain, and even further by the use of a Kalman filter as shown by Zhang et al. [88] or a neural network as described by Shibata et al. [89].

⁵This research has been executed as part of an internal project at KIWA by Kees Pulles, Matthijs Kippers and Gert Woutersen

8.3.3 Implementation

An experimental sensor setup for leak searching has been developed at KIWA eventually suitable for mounting on the robot. Goal is to detect the sound of the gas-flow through a leak in the pipe. The flow is strongly dependent on the size of the leak, but also on the damping qualities of the material on the outside of the pipe, the shape of the hole (and the edge of the hole) causing the leakage and the gas pressure in the damaged pipe section.

The developed sensor system uses an ultrasonic acoustic sensor (SPM0404UD5 by Knowles Acoustics, shown in figure 8.16) which has a very small footprint and high sensitivity in the range of 20 kHz to 60 kHz.

A test setup is realised using an mbed LPC1768 microcontroller⁶. A signal conditioning circuit has been implemented using a band pass filter with a centre frequency of 30 kHz. The on-board 12 bit ADC has been used for sensing. The audio signal is sampled (undersampled) at 10kHz for a period of 1 second, subsequently the RMS value of these samples is measured.

8.3.4 Results

A number of measurements and tests in pressurised pipes has been done at KIWA [73]. Test conditions that have been varied are the diameter of the size of the leak, gas pressure inside the pipe, damping material (sand) around the pipe and direction of the microphone. Also experiments have been done measuring the effect of the digital signal processing setup by comparing the processed measurements with the measurement data obtained by a conventional oscilloscope.

Figure 8.17 shows a set of typical measurements of the microphone approaching a hole in the pipe. The environment of the pipe (sand) might have a dampening effect, so also experiments have been conducted using a pipe enclosed in a thick layer (10 cm) of sand. These results are shown in figure 8.18.

8.3.5 Conclusion

Although not all conditions are suitable for detecting a leak, in a large number of situations the change in audio data might be a good indication for the exact position of a leak. The distance range where a change in audio signal might be notified is however quite small, most measurements show a change in signal starting at 20 cm from the leak.

Since the sensing method is relatively low-cost, in terms of hardware, power budget, space and computational load, the method can be added to the existing methodology as extra indication. Since there might be a large number of other sources of

⁶<http://mbed.org/platforms/mbed-LPC1768/>

noise (traffic, other pipelines, junctions, strong gas flow due to internal components) it is unlikely that audio data alone will provide enough information for pipe assessment.

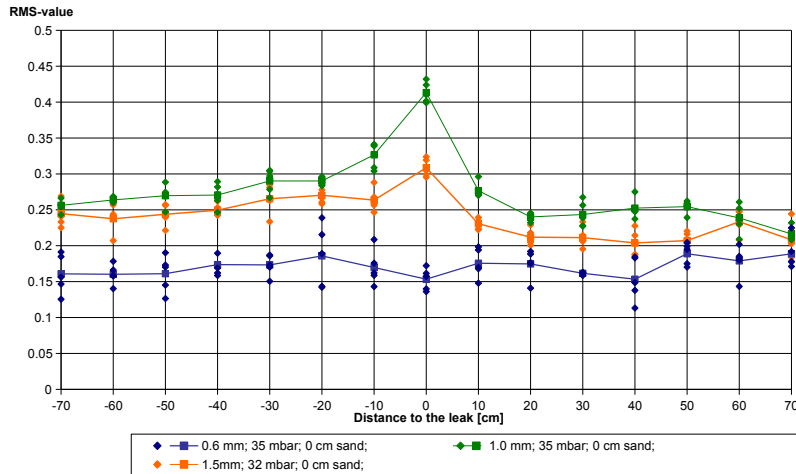


FIGURE 8.17 Measurement at varying leak sizes

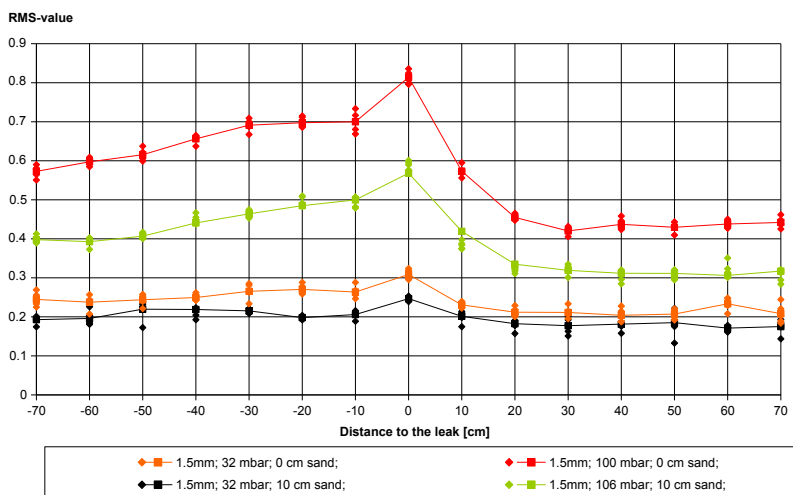


FIGURE 8.18 Measurements showing the effect of a layer of sand

8.4 Internal state sensing

A number of different sensors is used for measuring the internal positions of the joints, necessary for control. These sensors and a number of other sensors which will be discussed here are used for acquiring information on the robot's internal state.

In the first prototype a number of resistive sensors (potentiometers, shown in figure 8.19) have been used for sensing joint angles and spring deflection. These sensors have been chosen initially because of their size and because they were relatively easy to integrate in the mechanical design. Incremental encoders have been used to measure velocity and position of the drive motors and the motor for rotation around the centre axis.

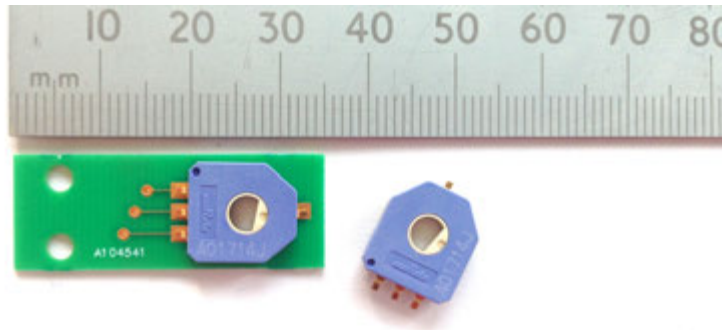


FIGURE 8.19 Murata potentiometers and the used connection PCB for the first prototype

In the second prototype high-precision absolute magnetic encoders have been used instead of the potentiometers for sensing the joint angles. Since these sensors need two components (a magnet and a sensor PCB) to be mounted, they have not been considered for the first prototype. The production method by using 3D printing (see chapter 11) of the second prototype offered enough flexibility to incorporate these sensors. For wheel revolution (both speed and position) again incremental encoders have been used - basically the only choice offered by the motor manufacturer and the only choice available which fits the available space.

Besides using the sensor data of angles and positions as feedback signals for controlling the robot's clamping torque, module angles and drive velocity, they can also be used for modelling the robot's environment which has been tested by Doggen [27]. When both the front and the rear module are clamping inside a pipe, the angles between both modules and the clamp diameter can be used to generate a model of the direct environment.

When the position of all modules relative to each other is known, the enveloping shape (reduced to cylindrical fits, since an environment of pipes and similar round

structures can be assumed) can be determined (or at least, a minimum structure in which the robot is placed. When this data is combined with other external measurements, the combined set of sensor data can yield an internal robot-state which can be used for modelling world/environment for navigation and control, but can also be used for classifying and measuring pipe diameters.



FIGURE 8.20 multi sensor board (IMU)

The IMU sensor board (see figure 8.20) uses an ADXL345 three axis accelerometer, an L3G2400D three axis gyroscope, a BMP085 barometric pressure sensor and an HMC5883L three axis magnetometer. Since the boards come as ready-made ‘building blocks’ (see chapter 11 there is not much choice in the specific selection or combination of available components. However, the same holds for the first design of the main controller board (described in chapter 4 and chapter 7) where at that time the amount of available and affordable miniature three-axis accelerometers was equally small.

The primary use of the multi-sensor board is the acceleration sensor used for orientation measurement⁷. When external accelerations are considered minimal, the accelerations measured are solely induced by gravity so the following condition must hold:

$$\sqrt{(a_x^2 + a_y^2 + a_z^2)} = 1g$$

The angles round the axis by convention are labeled pitch (ρ) for rotation around the x-axis, roll (ϕ) for rotation around the y-axis and yaw (θ) around the z-axis. Note that the yaw of the robot in world coordinates cannot be measured by acceleration only since only the x-axis and y-axis are influenced by gravity. In the following case the angles ρ, ϕ, θ are given in the sensor frame. For the angles holds:

$$\rho = \arctan\left(\frac{a_x}{\sqrt{a_y^2 + a_z^2}}\right)$$

⁷see AN-1057 by the ADXL345 manufacturer

$$\phi = \arctan\left(\frac{a_y}{\sqrt{a_x^2 + a_z^2}}\right)$$
$$\theta = \arctan\left(\frac{a_z}{\sqrt{a_x^2 + a_y^2}}\right)$$

For rotation around the z-axis (yaw) in the world frame, under normal conditions a magnetometer can be used. The HMC5883L also uses three axes, so under each rotation an indication of the direction of the earth's magnetic field can be given. For the pipe inspection robot this might only be relevant when the robot is operating in non-ferro pipes such as PVC or PE. Also the amount of influence of the rest of the electronics and the magnetic fields induced by the motors needs to be taken into account.

The IMU sensor board has been used for orientation control in the prototype described in chapter 6. The accelerometer (which was also implemented on the master controller of the first prototype) has also been used in the tests described in chapter 10 where a model of the robot's immediate surroundings is made using state information. The accelerometer data is in this case used for the correct orientation of the 3D visualisation of the robot in 20sim.

8.5 Conclusion

This chapter discusses all sensing systems realised for the robot. The limited power and limited size on board of the robot pose strong constraints on the choice in sensor hardware. These constraints affect both the sensor systems used for control and navigation and the sensor systems for pipe assessment.

A stereo vision system has been proposed which can be used both for navigation and pipe assessment. A number of implementations of this system have been realised demonstrating the capabilities of detecting small defects and detecting obstacles such as bends and T-joints. Although other pipe inspection robots have been using similar active stereo vision systems with circular projection, the system described in this chapter is unique because much attention has been paid to optimisation, both of the size and of the computational load.

The implemented version of the vision system consists of a USB camera with integrated projector using a beam dump for removing unwanted reflections in a 3D printed housing, small enough to fit the final prototype of the robot. The vision processing software has been implemented, optimised and tested on an embedded control board board.

A series of experiments have been done on using an ultrasonic microphone for acoustic leak detection. Although the usefulness of the signal is strongly depending on the size of the leak, the pressure in the pipe and the immediate environment of the pipe, the sensor is relatively inexpensive to add with respect to power consumption, computational load, size requirements and costs.

In all prototypes of the robot accelerometers have been used to measure orientation. The omniwheel prototype uses the signal for orientation control, in the first prototype it has been used for world modelling using robot state data. These sensors are also inexpensive to add with respect to power consumption, computational load, size requirements and costs. Furthermore, integrated sensor boards such as the described IMU board also use gyroscope sensors, magneto meters and barometric pressure sensors. In the future these sensor data could be merged (sensor fusion) to realise more accurate orientation data for measuring the exact orientation of the pipes through the robot.

9

Communication

9.1 Introduction

In chapter 2 the goal of realising a fully autonomous robotic inspection system for a pipe network is broken down into a number of smaller (partial) research goals leading to a series of prototype systems in order to develop and increase the system's functionality gradually over time.

In the case of a fully autonomous system, communication is only necessary for the exchange of the acquired pipe assessment data, which can be done for example at docking stations. Local communication on board of the robot, for example between a master controller and a number of local motor controllers can happen through a selected bus protocol, as described in chapter 7. In case of semi autonomous control, or full operator control as described in section 10.4.1, a communication link between a host system and the robot is necessary.

This chapter describes the communication systems which have been developed¹: a short-range radio system for tests in the laboratory, which eventually might be used for close range data exchange with a docking station and a long range tether system using an optical fibre.

For tests and measurements described in chapter 12 of this thesis the tether using standard CAT5 ethernet cable, as described in chapter 7 has been used.

9.2 Wireless communication

In the design of the main controller of the first prototype a 2.4 GHz radio transceiver has been used aimed at local (short range) communication. This system has been described both in chapter 4 and in chapter 7.

¹The Master's thesis by Corne Doggen[27] describes the development of a short-range radio communication protocol and the Bachelor's thesis by Jort Baarsma[5] describes the design of a spooling system for optical fibres

Due to the high path damping of amongst others the layers of (wet) sand around the pipes, radio transmission is difficult. In some cases however the piping (especially metal pipes) can act as a waveguide. Ultra wide band (UWB) systems, for example described in a patent by Allouche et al. [2] have been implemented for communication between a robot underground and a base-station above ground. Section 3.4.2 describes a number of projects which use radio communication from a robot underground to a number of receiver stations for localising the robot. The necessary amount of power is however large, in an order of magnitude not available on this robot.

The main goal of this 2.4 GHz transceiver system is to provide a wireless communication method for experiments above ground in a laboratory environment, as well as providing (eventually) a method for exchange of data between a robot and an underground docking station as shown schematically in figure 9.1.

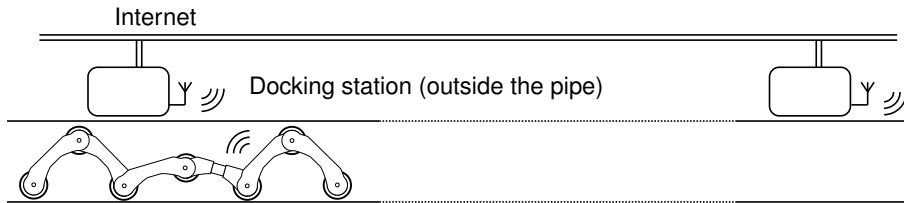


FIGURE 9.1 Schematic drawing of two wireless short-range docking stations

The chosen Nordic NRF24L01 chipset provides the low level ‘bit pipe’. Buffering, packetising and error checking is done on the chip, as well as channel selection (frequency hopping) and adjustment of the transmission power. Effectively for the end user in software a transparent 115.2 kbps serial link is offered. A number of simple serial protocols have been implemented, among which the transmission of the complete robot state for offline generation of a rudimentary world model as described in section 10.3.

9.3 Tether system

A tether system can provide the robot with both the means for *communication* and *power supply*. Although some experiments with batteries have been conducted (see chapter 7) in the majority of short missions for the robot a tethered operation might work equally well. In cases where sensing equipment will be used which requires more power, such as magnetic flux leakage (MFL) sensing, or when a coupling medium is necessary, for example the liquid which is used for ultrasonic (US) sensing, a tether might be the only available option. A tether can also be used as an extra precaution, combined with a tether for power and data a system can be in-

stalled which has the mechanical capabilities of *pulling back* the robot in case of an emergency or unrecoverable failure.

A tether cable which allows for pulling back the robot, providing electrical power and communication at the same time might be thick and heavy to pull. A tether can be pulled by the robot, which means that the robot needs to pull the entire weight of the tether, which can cause a serious amount of friction force, especially in bends - or can be wound on and off by a spooling system attached on the robot.

9.3.1 Spooling system

Since the space in a single, round module which can still be pulled through the mitre-bend in a 63 mm pipe segment is small (see chapter 3) an experimental design has been produced for checking the maximum length of a tether that can be taken with the robot using an active spooling system. This length is larger for a thinner tether material. The thinnest medium that could be found for communication (limiting the search to the more common off the shelf materials and excluding experimental materials such as carbon nano-tubes) is optical fibre.

In the design presented by Jort Baarsma [5] a length of 100 m (extrapolated) of 250 μm bend-insensitive fibre can be spooled on a spool with an inner diameter of 23 mm. The experimental model exceeds the maximum module length due to the choice in drive motor. Although the dimensions of the spooling mechanism allow for spooling of at least 133 m theoretically, in practice the signal loss due to bending the fibre limits the feasible length to 100 m. A special bend-insensitive fibre has to be used (as opposed to the standard fibres which are currently in use for home-network connections) due to the small diameter available for spooling.

The design is implemented using parts of a spooling system for fishing lines based on the spin cast reel design, combined with a housing printed on the lab's 3D printer. Figure 9.2 shows a cutaway drawing of the SolidWorks design. The double helix worm shaft (a) is used to shift the spool back and forth (not drawn) sliding over brass tube (b) which acts as a guidance for the spool. The fibre is wound on this shifting spool by axial rotation of the fibre guide (c). The module is completely enclosed (d) and driven by a Faulhaber 2619 motor (e).

The design is shown in figure 9.3. Unfortunately the fibre is very fragile; when the fibre is confronted with a radius smaller than 4 mm (verified by tests [5]) or when the fibre is scratched by a sharp edge in a corner, it is prone to break. Reinforcement or a protective coating would increase the thickness and reduce the maximum available length. The spooling mechanism proves to be working, although after a number of cycles the risk of entanglement both inside the mechanism or outside in the pipe increases.

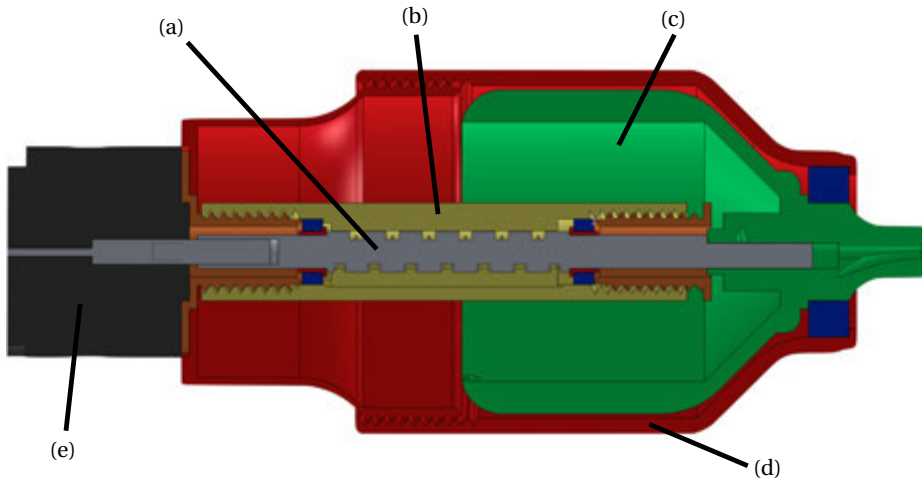


FIGURE 9.2 Schematic overview of the design of the spooling mechanism



FIGURE 9.3 'exploded' view of the parts used for the spooling system

9.3.2 Single use coil

Although in the mechanism described in the previous section the available space for spooling fibre is maximised, still a lot of room has to be reserved for the motor, shafts, gears and housing. The fibre is indeed the medium for data transfer with the smallest diameter, but it comes with a price of high fragility. A different solution might be to abandon the active spooling system and to choose a system that unwinds passively - and is not being rewound, at least not by a system attached to the robot.

During my internship at the Shadow Robot Company in London in 2004 I found a couple of spools of very smooth, teflon coated double stranded wire which came from a military surplus stock where it had been designed for torpedo control or airborne wire-guided

9.4 Ethernet cable

One of the requirements by *ALSTOM Inspection Robotics* is the use of (standard) CAT5 ethernet cable for tethering. The robots for turbine- or shaft inspection normally operate on short missions so ethernet has a number of advantages:

- standard cable, many varieties from office version to waterproof shielded versions,
- communication up to 100 m, longer ranges can be covered using repeaters,
- many protocols on different layers of the OSI reference present, it is easy to allow a number of applications use of the cable in parallel,
- power over ethernet (PoE) standard (802.3at Type 2) allows for injecting power up to 25.5 Watt (see section 7.3.2),
- RJ45 connectors which are normally used for CAT5 cable have already a simple mechanical lock. Also very strong and robust connectors are available for CAT5 cable.

The experiments described in chapter 12 have been carried out using a standard CAT5 cable, see figure 9.5. Not only using the above described ethernet and power connection, the twisted pair cable is also used directly for RS-485 - which allows even longer transmission length, up to 1200 m using 100 kbit/s.



FIGURE 9.5 Robot prototype with an ethernet cable as tether

9.5 Conclusion

During most experiments in the lab either the short-range radio or tethered operation proved to be sufficient.

Although an active spooling system has been developed capable of winding at least 100 metre of optical fibre for communication, probably single-use coils will be easier and more reliable in operation. With respect to optical fibre these coils of conducting wire can also provide power, communication and a mechanical pull-back option.

Ethernet cables are the standard used for many tethered systems. They are convenient for short range missions. When considering these cables for missions in pipes that contain a (large) number of joints and obstacles, probably an active tether guiding mechanism will have to be designed.

10

Control

10.1 Introduction

In this chapter the control of the robot will be discussed. On all the slave nodes local control loops are implemented. The data that can be obtained through these nodes is used to create a rudimentary world model, for now used for operator feedback. The operator interface maps user inputs to robot set-points. In the last section the design and implementation of a base station with control software will be discussed.

10.2 Slave nodes

The slave nodes in the bending modules are configured to do torque control for the bending joint and velocity control for the drive motor. All of these nodes are programmed equally, except for the ones in the rotation joint.

Since the rotation joint contains two drive motors and one motor for axial rotation, two slave nodes are used. One node only controls the velocity of a single drive motor, the other node controls both one drive motor and does position control with the motor for axial rotation.

Because of the limited space and the relatively high torques that are required, every motor that is selected is used in the range of its maximum permitted torque. This also means that most of the motors are equipped with a relatively high gearing, and are, therefore, moving slowly. This results in a 'well behaved' robot system in which the friction and damping are high. The risks of instability due to applying controller feedback are quite low. However, the risk of introducing instability due to the use of sampling (digital control) with a microcontroller board with very limited capabilities, is still present, and needs to be verified.

TABLE 10.1 System parameters used in simulation

parameter	quantity
motor constant K_m	3.01×10^{-3} Nm
motor induction	$60 \mu\text{H}$
motor resistance	20.1Ω
spring constant	0.181 Nm/rad
transmission ratio	64:1
transmission efficiency	0.7
transmission inertia	$6 \times 10^{-8} \text{ kg.m}^2/\text{rad}$
worm gear ratio	24:1
worm gear efficiency	0.36
module gear ratio	3.625:1
module gear efficiency	0.8

Torque control

In the four bending modules torque control is implemented using the spring deflection. An IPM of the drive train is shown in figure 10.1. This model is simulated in 20sim to verify the dynamic behaviour. A PID control loop is implemented in simulation using the spring deflection as controller feedback signal.

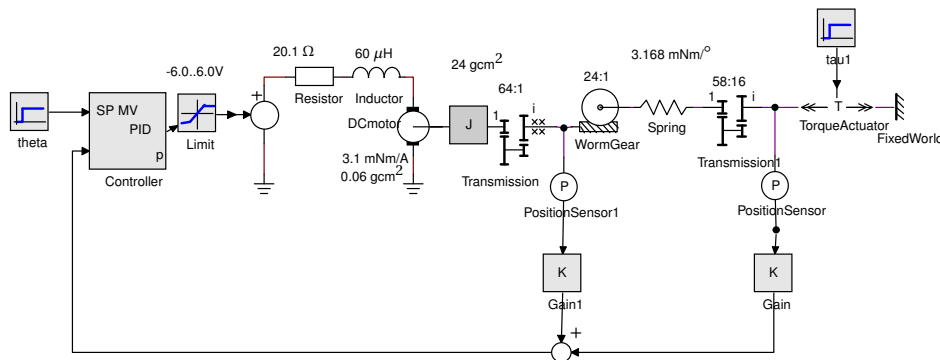


FIGURE 10.1 Schematic overview of the clamp control setup in 20sim.

The parameters which are used for the simulation are given in table 10.1

The spring is located between two gearboxes. The deflection is measured not on the spring itself but before and after the gearbox. In the simulation the clamp torque could be calculated by measuring the spring deflection. In the robot it is not possible to measure the spring deflection directly, the position sensors are mounted between motor gearbox and worm-gear and on the module itself.

This means that for accurately calculating the applied torque, besides the ratios of

the gearboxes also the efficiency of both gearboxes needs to be taken into account. In the model, gains K_1 and K_2 are used to derive the spring deflection from the two measured positions.

The stiffness felt at the end tip is $0.3625^2 \cdot 0.181$ [Nm/rad] $\cdot 0.8$ resulting in a gain $K_2 = 2.628$ [Nm/rad]. The deflection of the other side of the spring is measured through the 24:1 ratio of the worm gear. The effect of this position on the output depends also on the output gear stage and its efficiency, so for the gain K_2 holds: $(0.181$ [Nm/rad] $\cdot 3.625/24) \cdot 0.8 = 0.0218$ [Nm/rad].

A standard PID controller has been implemented in simulation to control the output torque based on the spring deflection. The controller is simulated in standard form (parallel form):

$$u(t) = K_p \left(e(t) + \frac{1}{T_i} \int_0^t e(\tau) d\tau + T_d \frac{d}{dt} e(t) \right)$$

Using the multiple run features of 20sim a numerical optimisation has been done minimising the error output of the controller using criterion $J = \int_0^t e^2$. The controller gains have been constrained to 'realistic' ranges.

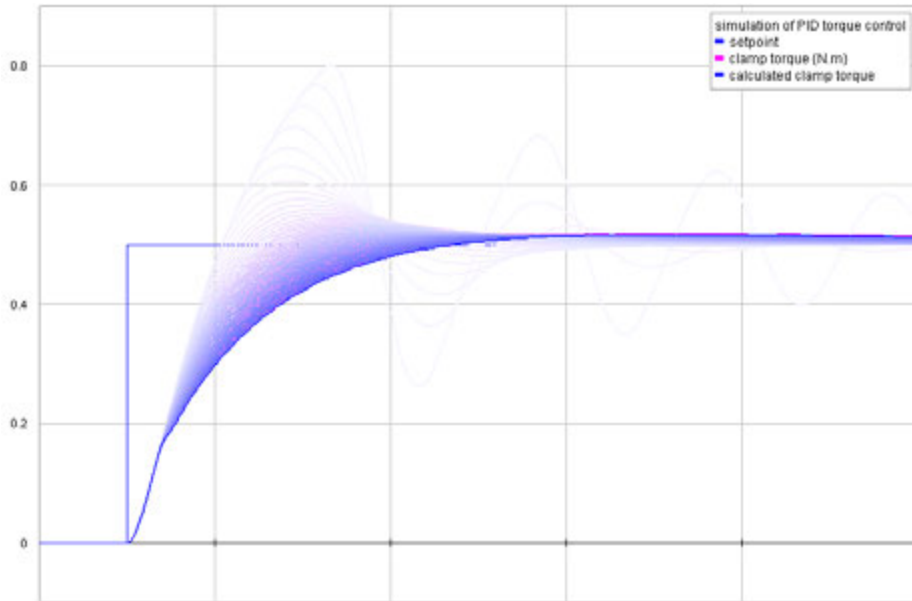


FIGURE 10.2 Multiple run simulation for determining controller gains

The power supply in the simulation is limited to -6 .. 6 V, reducing the maximum speed of the motor, so the time constant of the system is in the order of magnitude of seconds. The resulting values for the PID control are (taken from the simulation):

```

1 parameters
2   real K = 50.0 {}; // Proportional gain
3   real Td = 0.1 {s}; // Derivative time constant: Td > 0
4   real Ti = 4.0 {s}; // Integral time constant: Ti > 0

```

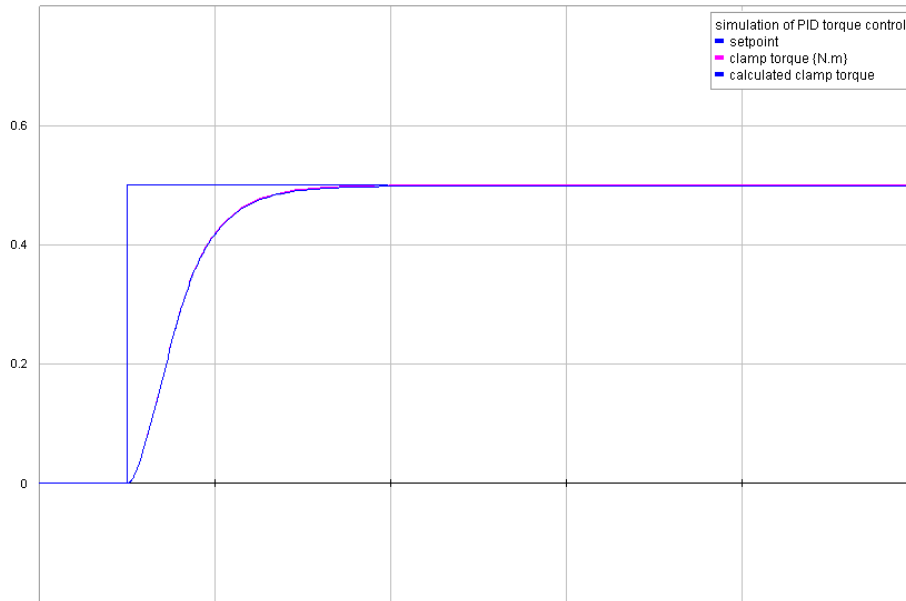


FIGURE 10.3 Step response with tuned controller

The controller is implemented in software. The maximum clamping force and control have been tested and measured in a test bench, shown in figure 10.4. The test bench can be adjusted in height (currently set at 83 mm) and is equipped with a strain gauge. The strain gauge sensor is calibrated using spring scales and interfaced using an instrumentation amplifier (INA122) directly to the Arduino Mega board which acts as ‘base station’ for the robot.

The output torque can be varied using the operator input. In a fixed position (clamped in 83 mm in the test bench) a relatively large range of clamping torque can be applied, see figure 10.5. The response of the strain gauge shows an exponential decay. This is probably caused by the deformation of the tires, which have some settling time. These deformations are too small to be measured on the angular displacement sensors (so the spring deflection does not recognise it), but they are clearly visible on the measurements of the strain gauge.

Although the range and the maximum clamping torque that can be supplied is sufficient (see figure 10.6 and matches the calculated values in chapter 5, the spring suffers from mechanical play, leading to hysteresis in the control. Since clamping

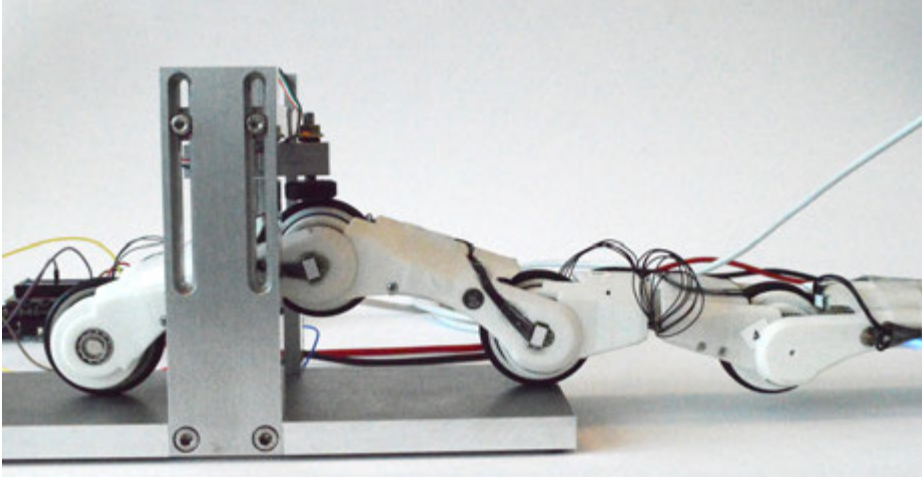


FIGURE 10.4 Robot in clamp setup

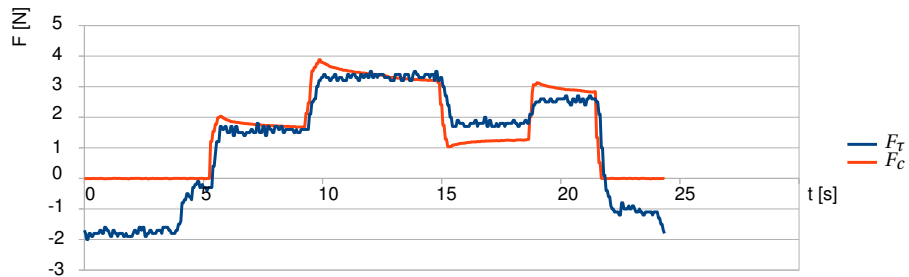


FIGURE 10.5 Torque measured with spring deflection compared with strain gauge data

torque is always in one direction (depending on the clamping direction, i.e. normal or reverse clamp) this is not a problem, but it prevents an accurate torque control using a standard PID controller. Figure 10.7 shows a mapping between the torque measured with spring deflection and the force measured with the strain gauge. According to the relation graphed in chapter 5 at 83 mm the ratio between torque and force should be 7 N per Nm torque.

In figure 10.7 two clamp - unclamp cycles are shown. The hysteresis is quite large, making continuous control difficult (but not impossible, even with PID control, see the work by Jayawardhana et al.[49]) However, since the main purpose of the clamping module is to provide a pre-set clamping force, simply starting the clamp, and stopping the motor when the desired clamping force is reached, is sufficient.

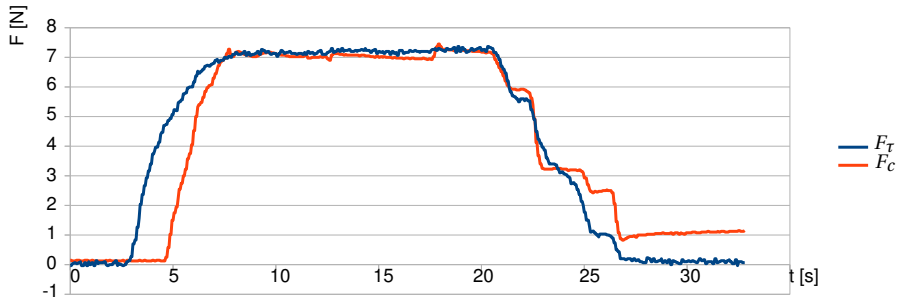


FIGURE 10.6 Maximum clamp torque

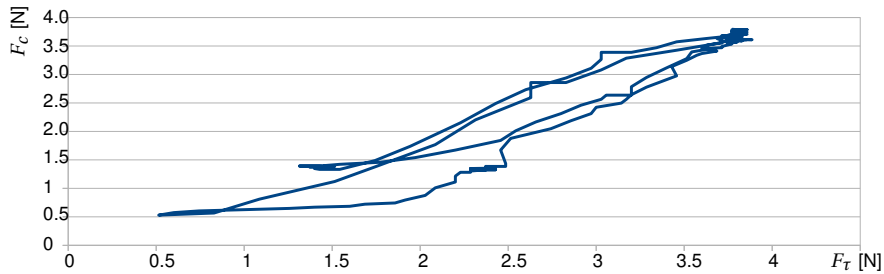


FIGURE 10.7 Hysteresis in the measured torque

A sudden decrease or increase in torque (for instance when meeting a bump or a diameter change) will be noticed (but the hysteresis and, perhaps more importantly, the maximum adjustment velocity of the bending motor) will prevent a direct response in control, at least not on the time-scale at which the robot is moving through the network. The controlled response will be too slow for compensating for a bump or a weld at the 80 mm/sec driving velocity.

10.2.1 Velocity control

The wheels are velocity controlled using a similar PID controller. There exist two basic approaches in measuring the velocity using an incremental encoder. In the sampling routine the encoder position can be differentiated in order to yield a measure of the velocity. Since the sampling frequency in the slave node is quite high, the resolution is very low. This is referred to as the ‘clock driven approach’ in the work by Merry, van de Molengraft en Steinbuch [61]. They propose an ‘encoder driven approach’ which is implemented here, by measuring the transition time of encoder pulses. In this case the resolution does not depend on the sampling frequency. However, the sample frequency itself is depending on the wheel velocity.

The maximum velocity of a wheel is (according to the datasheet) 44 rpm, or 4.6 rad/s. With a 1:112 gearbox and a 16 ppr encoder this means that the minimum pulse transition time (at maximum velocity) is 760 μs . A pulse transition triggers an interrupt. The Arduino function `micros()` is used to count the pulse duration in this case, it has a resolution of 8 μs .

Since the velocity is inversely proportional to the transition time, the resolution with which the velocity can be measured is non-linear. However, in worst case (maximum velocity) the resolution in wheel speed (calculating the resulting speed difference with a pulse transition difference of 8 μs) is 0.048 rad/s. At slower speeds the resolution increases, but the update frequency of measurements decreases. With a control loop with $f_s = 200$ Hz, the minimum speed should be larger than $200 / (112 \cdot 16) \cdot 4.6 = 0.5$ rad/s.

Figure 10.8 shows the no-load response of the PID controlled wheel. Results of the full robot are shown in chapter 12. In that case not only the inertia (mass) that has to be moved increases, but, due to the clamping force and the tires, also the friction increases dramatically.

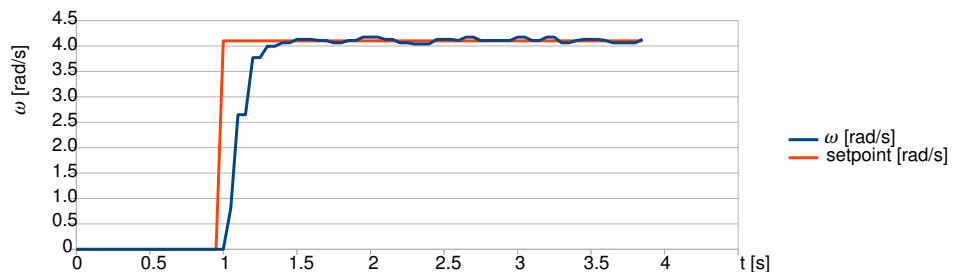


FIGURE 10.8 Velocity control of a drive motor

10.2.2 Position control

The rotation module consists of two drive motors and one motor for axial rotation which is position controlled. Since this motor also has a gearbox with a large (809:1) ratio and a lower efficiency (max 62%) the dynamics of the system does not require a controller with much additional damping.

A P controller has been implemented (no D action was necessary and the steady state error is small since a sufficiently large gain can be used) of which the response is shown in figure 10.9. In chapter 12 the same controller is used for the complete robot (with extra inertia, but also with a large amount of friction caused by rotating two modules with respect to the pipe wall).

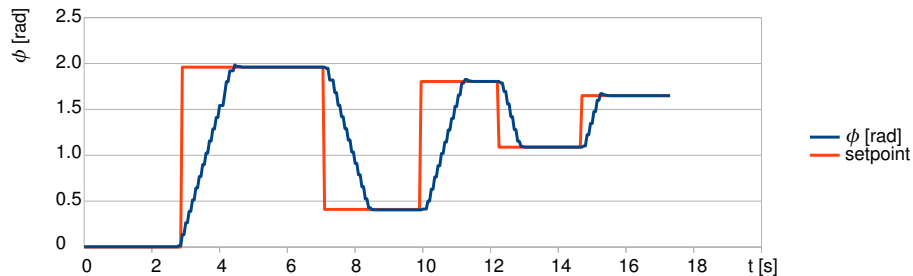


FIGURE 10.9 Position control of the rotation module

The control loop frequency implemented on every slave node is 200 Hz. The communication frequency between the master node and the slave nodes is 20 Hz. With the slow responses of the motors due to the high gearing ratios and the friction in the system, the control loop frequency satisfies the rule of thumb of being at least an order of magnitude (factor 10) higher than dominant time constant in the system. Even the master control loop, closed through the communication system, has a relatively high frequency with respect to the system.

10.3 World Model

The internal state data of the robot can be used to estimate the features of the network the robot is currently occupying¹. From the robot a state vector composed of all variables that can be measured internally is transmitted to the simulation package 20sim. Although this estimation can be done statically and offline, a setup is used which uses the wireless data transmission setup as described in chapter 9

¹This work is partially described in the Master's thesis by Corne Doggen[27]

shown in figure 10.10. The estimation is done in ‘soft’ realtime with an average update frequency of 20 Hz.

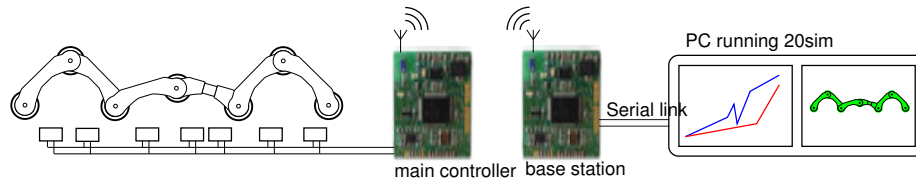


FIGURE 10.10 Setup using two main controllers for wireless data transmission

The state vector consists of the raw data of the accelerometer, clamping joint angles, drive motor position and velocity, motor current, hardware status and environment temperature. The procedure for determining the network features starts with determining whether one of the clamping V-shapes is -in fact- clamping. The (presence of the) clamping force can be measured using either the clamp motor current (during operation) or the deflection of the spring (which also works in a static situation).

Around one clamping V-shape an enveloping cylinder can be defined. It is assumed that the model has been clamped exactly centred in the pipe. Of this cylinder the diameter and the orientation with respect to the next module after the V-shape can be determined. If both V-shapes are clamped, two cylinders with two different diameters $D_{1,2}$ can be determined, as well as angle γ between both pipes.

Figures 10.11 show the real situation and the estimate made in simulation. Figures (a) and (b) show the situation with $D_1 = D_2 = 86$ mm and $\gamma = 45^\circ$. Figures (c) and (d) show the situation with $D_1 = D_2 = 86$ mm and $\gamma = 90^\circ$. Figures (e) and (f) show the situation where a diameter change is present. Note that the transition angle cannot be deduced exactly (only a maximum length of the transition can be given, depending on the distance between the two clamping V-shapes). Figures (e) and (f) show a transition from $D_1 = 86$ mm to $D_2 = 56$ mm, $\gamma = 0^\circ$.

The accuracy of the estimation is strongly dependent on the measurement of angle ϕ between the enveloping tubes. In the first prototype this angle is calculated by adding three module angles (the version of the robot uses six modules). Since these angles are measured using potentiometers which also suffer from mechanical play and electrical noise, the accuracy is low. The results in the described experiment are quite good since the implemented estimator uses a fixed set of available angles (0° , 45° , 90°).

For the final implementation this system might be used with a more complete set of available network components. It is not possible using only this approach to dis-

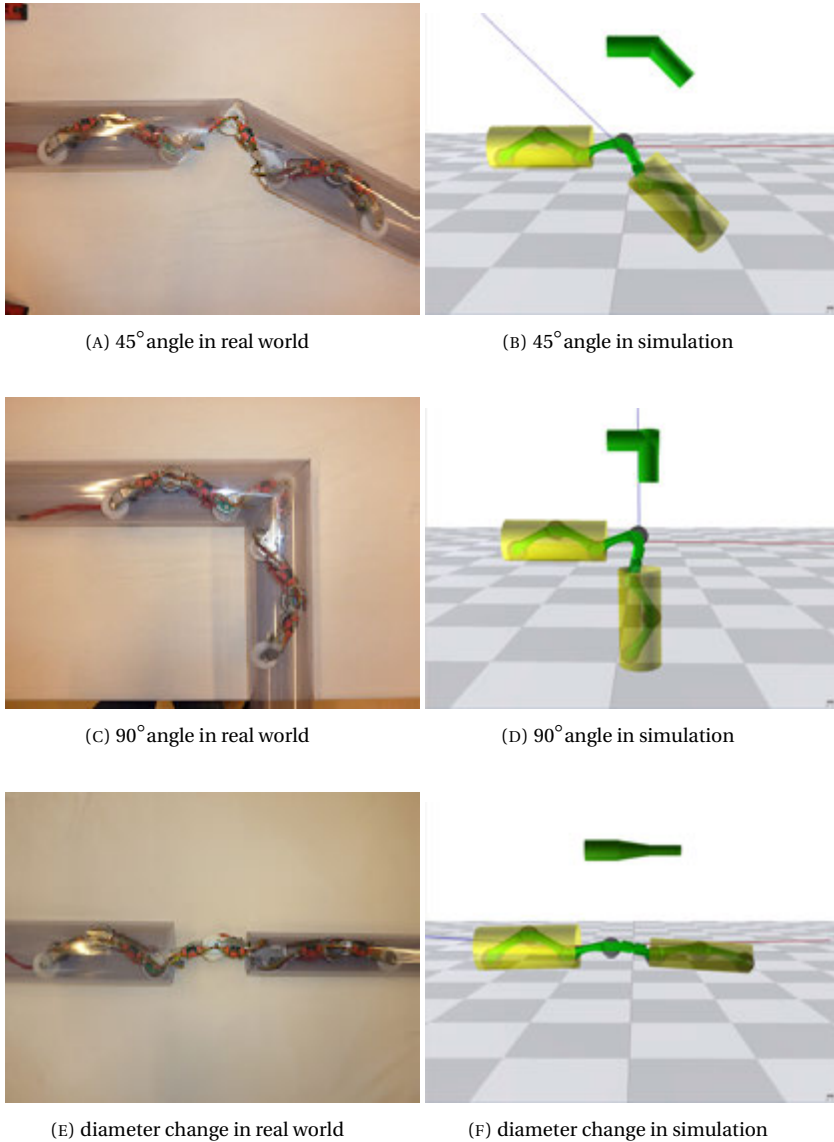


FIGURE 10.11 Experimental results where the robot's world is estimated in simulation - *images from*[27]

tinguish a mitre bend from a T-joint (in both cases the robot will exhibit a 90° angle between the front and rear clamp. In order to make a full estimate probably the vision system offers the most accurate results. The estimate based on robot state can be added as a 'sanity check' for those measurements

10.4 Operator interface

In chapter 7 in table 7.3 a hierarchy in complexity of control is described in relation to control software and operator interaction. With an increase in autonomy of the system, the number of degrees of freedom of the operator input decreases (up to the theoretical point where the operator input is just an on-off switch - or not even that)



FIGURE 10.12 Control setup used for experiments in chapter 12

In an environment consisting of one pipe with only bends, diameter changes but no branches and junctions, the operator control could be simply one-dimensional: the driving velocity - since the robot can only move forward at a certain speed, stop or move backward. Only when a branch or junction needs to be selected the operator has to make a choice. Since the robot has a preferred orientation for taking a corner (and is simply incapable of taking a corner, or even starting a cornering manoeuvre, when not properly aligned), the orientation around the pipe axis determines which junction the robot takes.

These two control inputs: driving velocity and rotation around the pipe axis are also incorporated in the prototype described in chapter 6. The control inputs are linked to an analog joystick. One of the axes gives an angular offset as input for the orientation control loop. The other axis controls the velocity of all drive motors simultaneously. Differences in timing of the bus control protocol can cause differences in synchronicity. The set-points are sent to all nodes within 5 ms, which is small compared to the dominant time constant in the system, so this effect is not noticeable. When communication errors occur (and a message is missed) a difference in synchronicity can occur. Re-transmission occurs in 50 ms which might be noticeable.

For the experiments with the first prototype a user interface had been developed in Matlab running on a host PC. The interface consisted of software buttons, sliders and input fields, one set for each motor. The interface is shown in chapter 4. Although it was possible to control the robot and to execute most of the necessary manoeuvres, the interface was hardly ‘user friendly’.

For the next prototype a more convenient human input device (HID) was sought. Since a standard joystick was lacking enough degrees of freedom, based on previous experience with animatronics² a fader panel was chosen which is normally used for music production. This panel was first coupled to a host PC running a *Processing* (Java) application. Since the required update rate of 20 Hz could often (and very irregularly) not be met, a stand-alone ‘base station’ for mapping user inputs and data acquisition has been designed.

For the experiments described in chapter 12 a ‘base station’ has been realised (shown in figure 10.12) using an Arduino Mega ADK. This board has an USB host chip which allows it to interface with dedicated USB devices such as the attached Korg nanoKONTROL2 panel. A USB-host library implementing support for MIDI devices has been used to interface the control panel. An LCD display for feedback of operation modes is added. Furthermore an RS-485 level shifter and 20 W power supply are added. This choice of hardware is discussed in more detail in chapter 11.

This ‘base station’ sends configuration and calibration data to the robot. In ‘polling mode’ it queries the attached slave nodes at 20 Hz, updating set points and collecting state information. The information which is collected is transmitted to a host PC for visualisation and analysis. Two formats are supported: data which can be visualised directly using a *Processing* sketch (optimised for quick response / ‘live view’) and a large *.csv data-set for later analysis.

The set-points which are transmitted to the robot are mapped to the operator inputs directly. The mapping is shown in figure 10.13. For the drive motors a similar coupling has been realised as described for the omniwheel prototype described in chapter 6. One slider controls all velocities simultaneously. Four sliders control clamping torque of the bending modules. They are grouped together, so they can be operated simultaneously (but not on the same slider since for some of the movements bending modules need to be controlled individually). One slider is giving the position set-point for the rotation module. A last slider is used for the controller in the vision system, adjusting the light intensity or turning on the laser projector.

A start has been made in grouping controller actions together and parameterising them. The necessary behaviour of the robot can be divided into combinations of motions or ‘motion primitives’, for which most of the names stated below come ‘naturally’ and have been used throughout this thesis.

²see the Dancing White Man project at TEDx - <https://www.youtube.com/watch?v=v1Eeg9KW-Co>

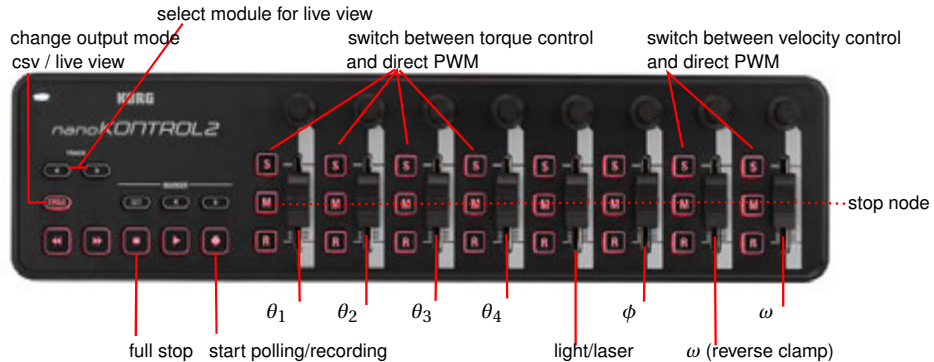


FIGURE 10.13 Mapping of the nanoKONTROL input device

TABLE 10.2 Motion primitives

motion primitive	parameter
drive	ω [rad/s]
clamp	τ [N]
rotate	ϕ [rad]
bend	γ [rad]

These motion primitives can be parameterised (see table 10.2): the motion *drive* has one parameter: the velocity. Whether wheels should turn clockwise or counter clockwise (depending on which side of the pipe they touch) can be determined on basis of joint angle information. *clamp* has also one parameter: the desired clamping force on the pipe wall. For the V-shape both bending modules are used which get the same set point, only in opposite directions. The clamping torque required should be compensated for the current pipe diameter which can be measured with the module angles. *rotate* has one parameter: the angle between both sides of the robot. *bend* has also one parameter: the desired radius γ for a certain module to curve along a gradual or sharp bend.

10.4.1 Control software

The function of the control software is twofold. First it should offer an interface between a user and the robot hardware. All functionality (motors, sensors) should be accessible through an interface for direct control. The options listed in table 7.3 can be implemented using different distributions over hardware platforms. A distinction can be made in tasks that are hard-real-time, such as the execution of a local control loop - and tasks that are 'soft' realtime, such as processing and visualising

robot data. The first implemented functions in the software of the described ‘base station’ are:

- low level access to all control parameters
- visualising and measurement of relevant data for tuning controllers
- mapping of user input, parametrizing motion primitives at the robot platform.

A schematic overview of the global design of the control software is given in figure 10.14. The higher levels have not been implemented in the current hardware setup.

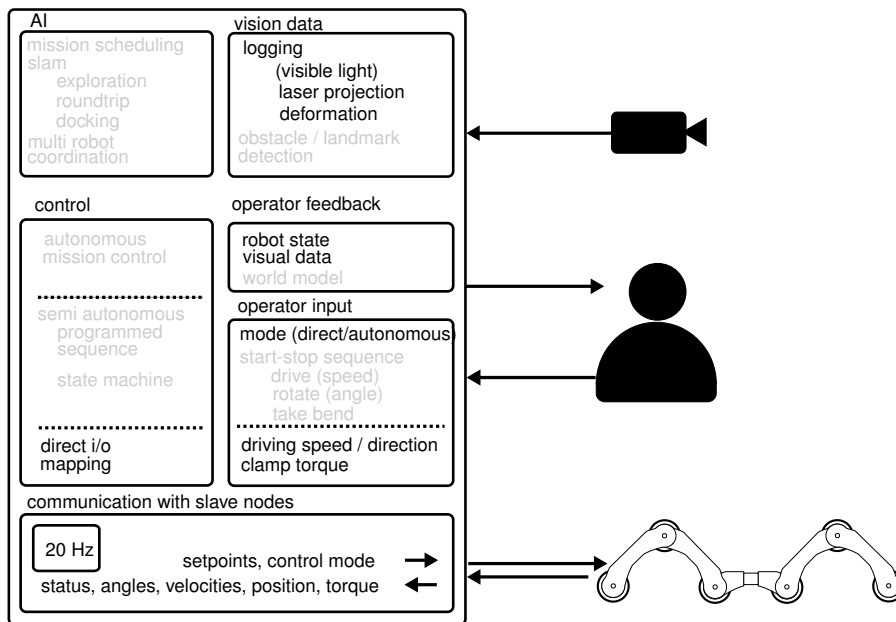


FIGURE 10.14 Schematic overview of the control software.

10.5 Conclusion

The control of the robot has been distributed over small local controllers and one master controller or 'base station'. The local controllers or 'slave nodes' are capable of position, velocity and torque control, although the latter not using a continuous control loop.

A first mapping of control actions to a human input device (fader panel) has been made which proves satisfactory for the experiments described in chapter 12. A stand-alone 'base station' has been realised meeting the real-time requirements and capable of executing the bus-control and data acquisition. Data is visualised on a host PC system.

Formulating further 'motion primitives' or combinations of controller actions is the next step to (semi) autonomous behaviour. After that the goal is executing some of the manoeuvres described in chapter 12 as autonomous sequences and formulating them as state-machines based on direct state information (clamping torque) or vision data.

Regarding the bending module control: ideally the controller would accept two parameters: a stiffness and a position, see figure 10.15. Clamping with a certain force would mean to give a position set point just outside the pipe wall and a desired stiffness as clamping force. To be totally passive (and, if control would permit, back drivable) any position set point with zero stiffness would do. Position control could be done by giving a high stiffness and a target position.

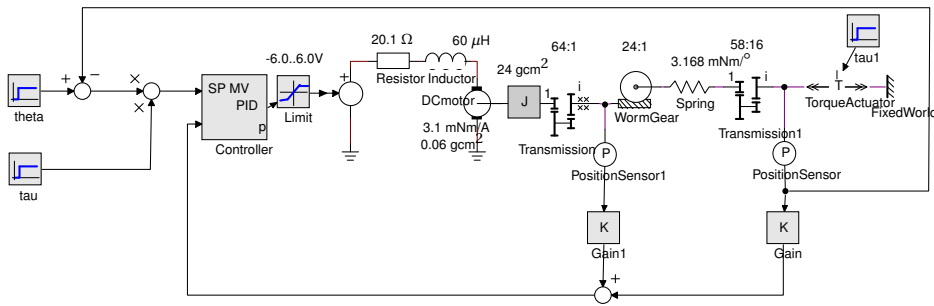


FIGURE 10.15 Desired controller implementation for the bend module

11

Prototyping and development

11.1 Introduction

This chapter describes the methods used for design, development and production of the discussed prototypes. During the development of the robot system described in this thesis a number of developments in other fields eventually allowed a radical change in the way the robot hardware, electronics and software have been developed.

The role of engineering as an academic discipline is discussed for example by Herbert A. Simon in his book ‘The Sciences of the Artificial’ [90], who describes the divide between teaching ‘design’ and teaching ‘analysis’. The method of engineering is investigated in further depth by, among others, Schön in ‘The Reflective Practitioner’ [87] and Vincenti in ‘What Engineers Know and How They Know It’ [105].

The engineering and design *process* influence the result. There is not just one right way to build a bridge, if there were, all bridges would look similar. (However, there are definitely *wrong* ways to build a bridge¹).

This chapter does not intend to contribute to the discussion on the differences between engineering and academia or to present a detailed analysis of how the choice of *method* of design and engineering influences the end result. Yet, during the course of this project, a major change in engineering process has taken place. This change might be the influence of the *zeitgeist* or a deliberate choice, or both. This chapter aims to describe and reflect upon this change and its effect on the engineering process of the robot.

The project underlying this thesis started out with the mechatronic design process as described by Schipper [86], but continued with a more ‘maker’ inspired methodology as described by Chris Anderson in his book ‘Makers, the new industrial revo-

¹Bridges are often referenced as example cases in engineering. One of the most notorious ones would be ‘*The Tay Bridge Disaster*’, recorded in a poem by William McGonagall, dated 1880, which has been subject of many works on disasters in both [engineering](#) and the [English language](#)

lution' [3]. The maker movement refers in this case to the large worldwide group of DIY enthusiasts, open hardware and open software designers, hobbyists and other people that 'build' things. O'Reilly media coined the term 'makers' with the start of their magazine 'Make:' in 2005 and the organisation of gatherings of makers and builders called 'Maker Faires' in the US².

Although strictly speaking many of the technologies that will be discussed in this chapter have been available for use throughout the entire span of this project, they have only recently been actually used for this project. This progression appears to coincide with the rise of aforesaid 'maker movement', but there might not be a strong causal connection that can be claimed. For example, in 2006 at the start of the project, a *Stratasys Dimension 3D printer*³ was located at the University in the modelling workshop used for industrial design students. The use of this machine was effectively never considered for production or prototyping of the robot, although it could have done the job equally well as the Objet machine currently in use at the RaM group.

The goal of this chapter is to compare the method used for the first prototype to the prototypes thereafter that have benefited from the available rapid prototyping techniques and open source hard- and software. Among other things, an additional level of creativity enters the way a product is designed when allowing other technologies and also different design methodologies to enter a hitherto 'linear' design process. At the University of Twente the Bachelor course Creative Technology tries to put different design paradigms to practice, sparking a discussion about the way chosen development methodologies influence engineering science as also for example discussed by Resnick et al. [77] of MIT.

The level of hardware detail in this chapter might seem out of place in a 'scientific' thesis. One of the points the author wishes to make is that the level of mechatronic engineering in this project - from the hardware point of view - is constantly bordering on what is still possible in a laboratory environment. In a 'normal' engineering project (and to do no-one injustice, I'll take for example a previous project of mine, the walking robot [22] as reference) for example the motor selection depends mostly on required torque and velocity, for which there is a large choice available. Since the robot is operated by a single motor, no further investigation for producibility of series production is necessary.

In this project in this thesis, however, size is always the limiting factor reversing the question to: find the motor which still fits the hardware and find out whether it can supply enough torque. The same holds for drive electronics, sensing, bearings etc.

Every detail, from the chosen material (the strongest 3D printable light-weight material available to us) to the connectors (DF75 have the smallest height for a standard footprint

²http://en.wikipedia.org/wiki/Maker_culture

³<http://www.stratasys.com/>

size available) to the wiring (which wires are readily available without time consuming tooling) up to the producibility (can the shafts be made using CNC tooling) need to be engineered on an almost 'industry ready' scale before being able to do a single laboratory test. The level of complexity (large number of degrees of freedom) and the high modularity caused a certain degree of 'mass production' per robot prototype, as illustrated in figure 11.1, showing some of the drive motors during production

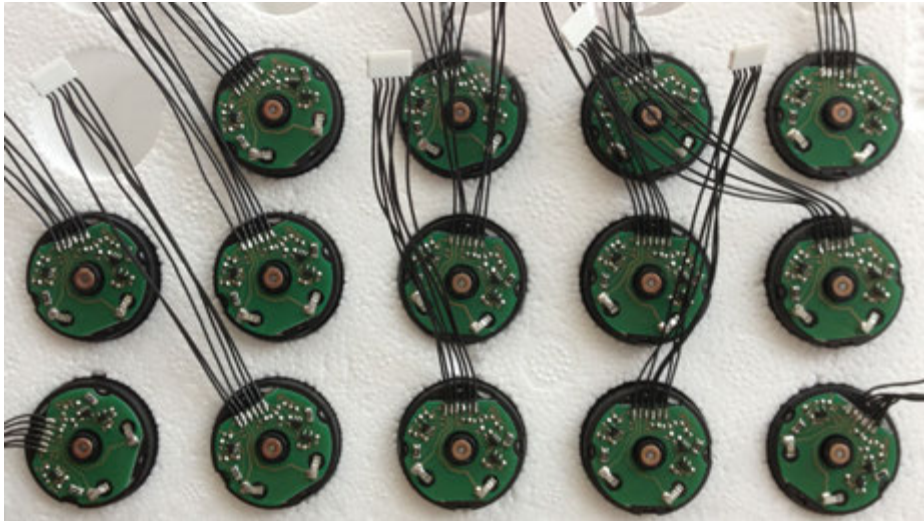


FIGURE 11.1 Series of pre-fabricated motors

The first prototype (described in chapter 4) has been designed using the mechatronic design method as used at that time at DEMCON, which underlying philosophy is described in the work by Schipper in his thesis [86]. Using a 'one room approach' the mechanical engineer (MSc student Jeroen Vennegoor op Nijhuis), electronic engineer (Jos Ansink) and systems engineer (writer of this thesis) designed the robot in a collaborative effort under supervision of two senior engineers. This initial project followed the classical engineering approach using decomposition, realisation of sub-components, integration and eventually testing and evaluation.

A modular design approach was in this case interpreted as designing separate modules with each their specific function. This allowed the engineers to narrow their focus 'per module' instead of focussing on an overall design. In later prototypes a setup using mostly identical modules has been chosen.

The approach was furthermore a 'first time right' approach, meaning that once all the mechanical design drawings had been fixed, the drawings were processed for manufacturing, the design drawings were shipped to a manufacturer (in this case a company in Malaysia) and after a relative long period (8 weeks) of production

and shipment a start could be made in assembling the robot. Note that the parts arrived long after Vennegoor op Nijhuis [104] completed his assignment on the design. Subsequently the robot was assembled by DEMCON and control hardware and wiring could be added.

Especially the amount of wiring necessary for the motor control boards and the inflexible installation (soldered connections) took a lot of time and effort. Eventually the wiring had been mounted at the outside of the modules as shown in figure 11.2, acting as obstacles during tight manoeuvres in pipe joints discussed earlier [75]. Although the placement of the wires had been discussed during the design phase, the choice had to be made to postpone this for later, since taking in the routing of cables and placement of connectors was a too large effort in this ‘first time right’ approach. All in all the ‘first time right’ approach takes a long time and lacks possibilities for quickly exploring alternatives.

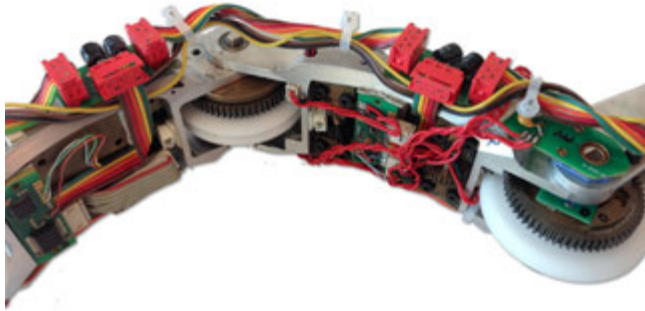


FIGURE 11.2 Close up picture of the wiring of prototype 1

11.2 Additive Manufacturing

During the course of the project a change took place in the world of desktop fabrication. Due to this maker movement and the FabLab⁴ concept, 3D printers, laser cutters and CNC routers have made a leap from the factory to the desktop. *Accessibility*, *visibility* and *availability* of production methods in a lab or at home increase the usage dramatically. This point has been made clear in the work by Mader and Dertien [58] in the context of student assignments for the bachelor track ‘Creative Technology’ at the UT.

Only when a tool or machine satisfies the following three criteria it will have a serious impact on the design process:

- the machine or tool needs to be *visible*

⁴http://en.wikipedia.org/wiki/Fab_lab

- the machine or tool needs to be *available*
- the machine or tool needs to be *accessible*.

The reverse is also true: when a machine is not visible (as in, present in the lab) the machine will not be taken into consideration. When a machine is not available (as in, constantly in use), other options will be sought. When the machine is not accessible (as in, difficult to use, steep learning curves, high threshold, no information) the machine will only be used by the happy few willing to learn and adapt.

All of these arguments might explain why in an earlier stage of the project the printer in the modelling workshop of Industrial Design was not considered: it was not visible (different building), the availability was unclear (sometimes days of work by Industrial Design students, sometimes nothing) and information on workflow, file types and necessary preparation was missing.

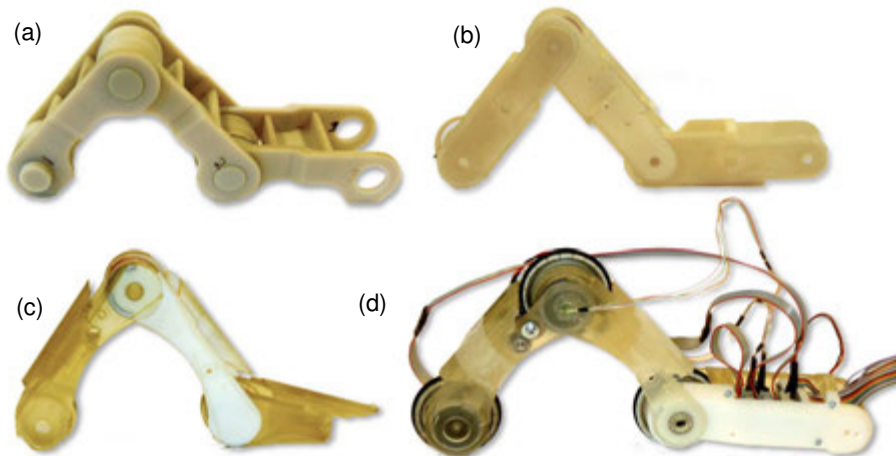


FIGURE 11.3 Three prototypes and the final model by Borgerink

11.2.1 Design iteration through 3D print

After the first successful experiments with the previously developed hardware described by De Boer [18] and the experiments together with Reemeijer [75] taking

mitre-bends, it was clear that no further progress could be made with the first prototype. The points listed at the end of chapter 4 explain the main reasons: the weight of the design, lack of traction torque, difficult (and erratic) control electronics.

An Objet Eden 250 machine was installed in the laboratory for Robotics and Mechatronics (RaM) lab in september 2010. This machine was bought and placed deliberately inside the working environment of the students (and not, perhaps more conveniently, in a closed cabinet, a soundproof room or one of the workshops in the building). The machine is not planned and scheduled for production (for third parties). This means that the machine is almost always immediately available for an overnight manufacturing run of new parts. The machine accepts standard STL drawings which can be generated directly from SolidWorks. No further post-processing of the drawings is necessary, so the accessibility is high.

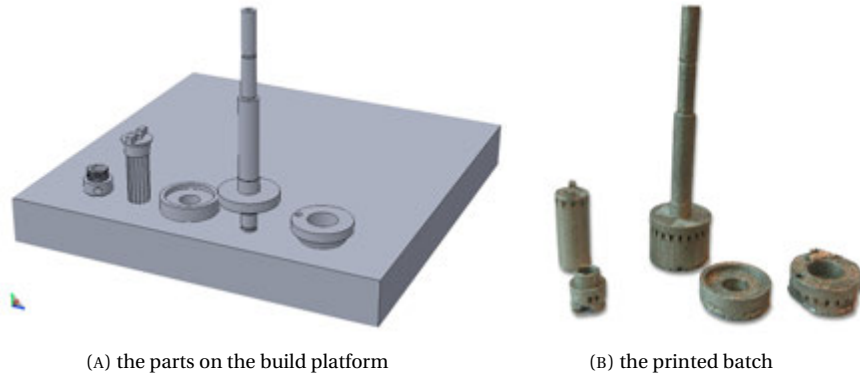
It took a long time before the first prototype (2006-2008) was ready for testing (first time right constraint). After manufacturing of the parts the assembly took also a long time due to small deviations in manufacturing, small errors in design, the lack of availability of necessary tooling and technicians, etc. This is in strong contrast with the process during the project by Borgerink [7] where prototypes have been produced on an almost two-weekly basis. Figure 11.3 shows three prototypes which have been subsequently designed and tested. It can be argued (and defended) that the final module design presented in this project has reached at least an equal level of complexity and completeness as the first prototype shown in chapter 4.

The first two models (a) and (b) in figure 11.3 used printed materials for joints, the third prototype (c) and the final model (d) allowed for metal inserts such as bearings and gears. While the first prototype shown is rather bulky and not capable of moving inside even the largest of the required pipe diameters, it still yields valuable information on necessary wall thickness, placement and aligning of the drive motors, available space for the bending drives, etc. Each iteration adds more functionality and solves more design constraints. The main merit of this process is that not all design constraints have to be solved in one go, but can be tackled incrementally.

11.2.2 Printed metal parts

In an experiment to bring the additive manufacturing technology even further in the design process, an attempt has been done to also produce the mechanical shafts and bushes on a 3D printer. At the 3D Print Company⁵ a *Concept Laser M3 Linear* machine capable of working with stainless steel is being used. Since the tolerances of the print quality were not quite specified (everything between 0.2 and 0.6 mm deviation) in both shape and thickness, an experimental batch of the needed mechanical parts has been produced.

⁵<http://www.3dprintcompany.nl>



(A) the parts on the build platform (B) the printed batch
 FIGURE 11.4 The five experimental metal drive parts

In order to compensate for size deviations, the shafts have been printed incorporating a number of grooves on the surface - which could act as both centring aid and 'compressible' structure for an axial fit of gears and bearings. The height of the grooves has been set at ± 0.4 mm with respect to the original diameter in order to accommodate for most of the specified deviation range.

The shafts have been printed in vertical orientation (the print-bed could be much lower and the process shorter) instead of printing the shafts horizontally. Due to the support material that needs to be printed, a shaft could turn out strongly imbalanced due to the added material.

Figure 11.4a shows the parts generated in SolidWorks in the desired orientation on the build platform for print. The resulting parts are shown in figure 11.4b. After the printing, the support material needs to be removed. Figure 11.5 shows an extensive section of cross-hatch printed support. Figure 11.6 shows the last bit of support that is removed. After removing the support, the remaining bit needs to be sanded and polished. Unfortunately this proved to be a very time consuming task, comparable to turning the complete parts by hand on a lathe (by a skilled technician).

The complete realised batch is shown in figure 11.8. The surface of the printed material remains quite rough, as can be seen in the pictures taken through a microscope (magnification set at 40x) in figure 11.7. Figure 11.9 shows a printed drive-shaft with mounted oldham coupling plate and mounted worm gear. The grooves allow a reasonable tight fit although for the final assembly gluing is necessary. Also with the (CNC) produced metal parts gluing is a necessary step in the final assembly.

Figure 11.10 shows the comparison of two shafts. The gears that are fitted are stock components of HPC. Note that the thread cut in the spring shaft (the long shaft shown in figure 11.10) had to be cut by hand after printing. The printing quality cannot offer enough level of detail to print a reliable thread, especially not when

after print some support material attached to this thread needs to be removed. To conclude, with the current printing technique the necessary level of precision for the drive parts cannot be reached. Also the price and the required time for printing and post-processing is too large to make it a part of a rapid-cycle iterative design process.



FIGURE 11.5 Shaft with the support material that needs to be removed

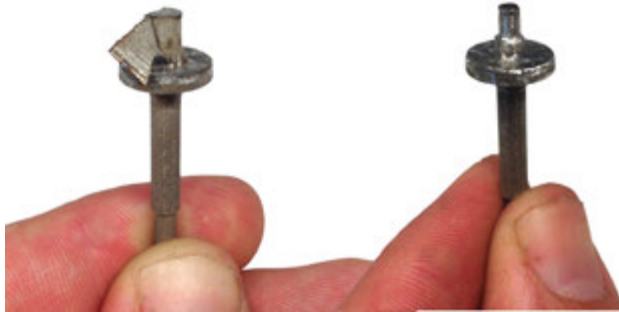


FIGURE 11.6 The final stage of preparing the shaft where the metal support material is 'peeled' off layer by layer

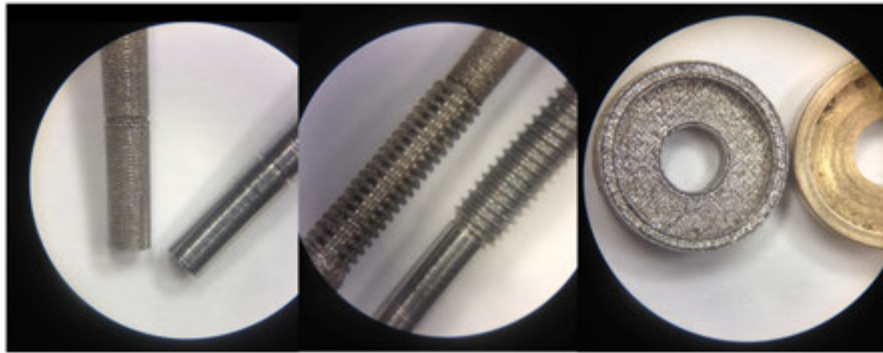


FIGURE 11.7 Comparison of the printed shafts and the parts produced on (CNC) lathe



FIGURE 11.8 Finished parts (after some considerable rework using a rotary tool)



FIGURE 11.9 Drive shaft with fitted oldham coupling plate and worm gear

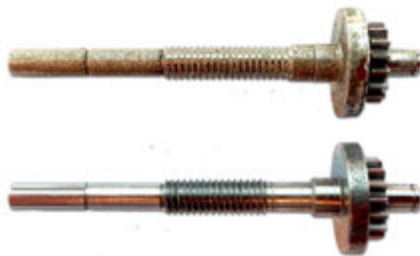


FIGURE 11.10 Two drive shafts, one printed, one produced on (CNC) lathe

11.2.3 Body material

The body structure which was originally printed in house on the *Objet Eden 250* machine has been printed for the final modules on a *FORMIGA P100 SLS* machine at the 3D Print Company. The main body parts are printed using PA3200: nylon reinforced with glass fibres, shown in figure 11.11. Since it is not easy to adapt or rework the fibre reinforced pieces, the parts which need some post-processing such as the wheels and the motor casing are printed with PA2200: 100% nylon which can be sanded and cut reasonably well.



FIGURE 11.11 Three modules printed in PA3200

11.3 Design for laser cutter

The prototype using omnidirectional wheels described in chapter 6 has been designed, constructed and tested in two weeks. As production method a ‘flat’ design which can be fabricated on a laser cutter has been chosen.

Following the ‘digital fabrication’ theme propagated by the Fablab movement, in 2010 the SmartXP lab at Univeristy of Twente (used by both Creative Technology and the Robotics and Mechatronics group) has acquired a *Trotec Speedy 100* laser cutter. This machine can cut and engrave most flat materials excluding metals and other good thermal conductors and materials containing PVC.

One remarkable feature of designing ‘flat’ robots is that the drawing functions both as design manual and CNC file at the same time. The drawing ‘is’ the design. One could select the vector drawing from the digital version of this thesis in figure 11.12 and send it directly to a laser cutter, resulting in almost all necessary mechanical parts for the frame.

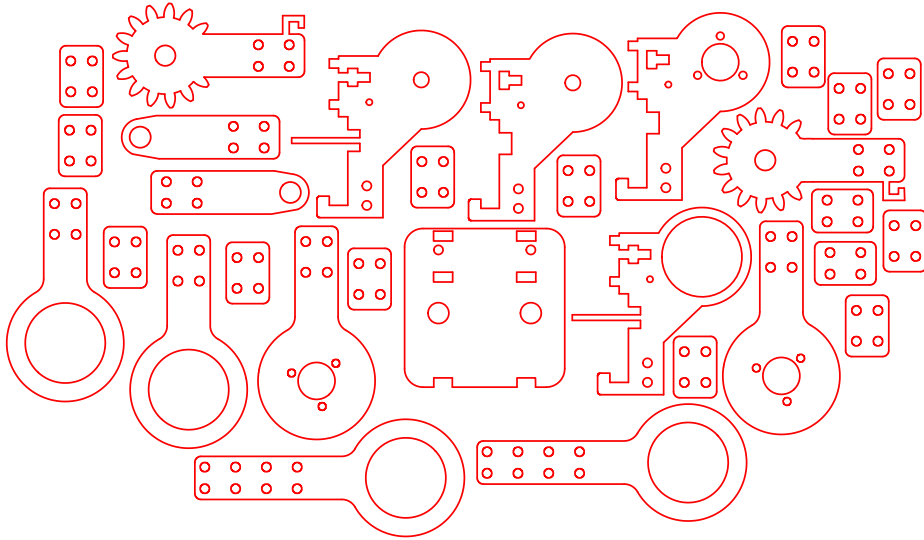


FIGURE 11.12 Drawing of the parts for the omniwheel prototype

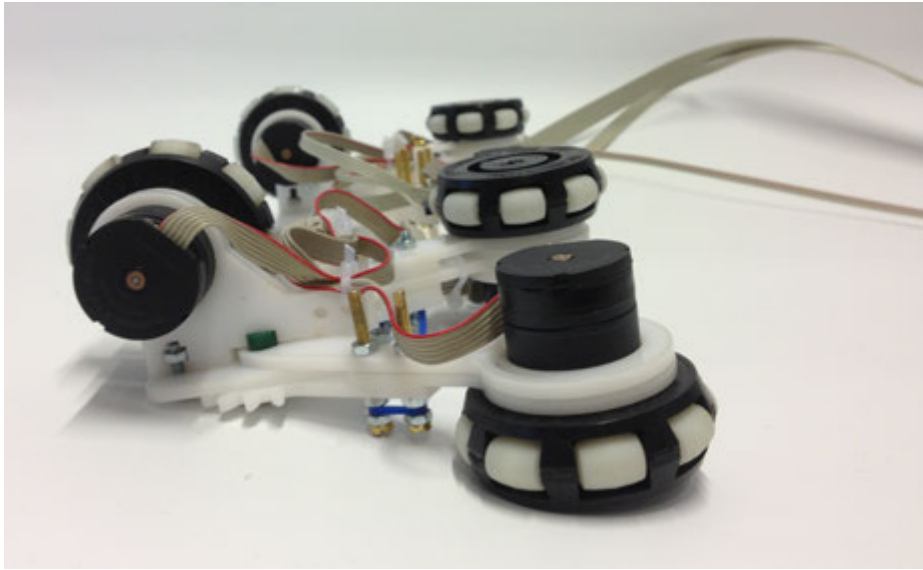


FIGURE 11.13 Detailed picture of the flat construction of the omniwheel prototype

11.4 Open micro controller design

The motor control boards for the first prototype have been developed using *Atmel's AVR studio*, using the GNU-GCC port for AVR wrapped and packaged in 'WinAVR'.

For the Main board a similar tool containing a cross compiler for ARM7 has been used called 'WinARM'. Although this worked fairly well, the development process was slow. Especially for the ARM7 controller resources and examples were sparse: a datasheet and a number of code examples for a slightly different controller version (that did not work right out of the box).

During the course of the project a different invention gradually took the world of education and design. *Arduino boards* and integrated development environment (IDE) have become a 'de facto' standard for Physical Computing and Interaction Design. Although primarily aimed at prototyping, hobbyists and 'makers', the board is also popular for rapid prototyping in engineering disciplines. The wide variety of available extension boards, software libraries and support materials allow the board to be used as quick, standard building block. As indication, all major online suppliers of engineering materials (Farnell, RS Components, Reichelt, etc.) ship Arduino boards and prototyping tools.

IDE

From wikipedia⁶: *'Arduino started in 2005 as a project for students at the Interaction Design Institute Ivrea in Ivrea, Italy. At that time the students used a "BASIC Stamp" at a cost of \$100, considered expensive for students. Massimo Banzi, one of the founders, taught at Ivrea. A hardware thesis was contributed for a wiring design by Colombian student Hernando Barragan. After the wiring platform was complete, researchers worked to make it lighter, less expensive, and available to the open source community. The school eventually closed down, so these researchers, one of them David Cuartielles, promoted the idea.'*

Normally an Arduino board contains either a single chip capable of direct USB connection or a dedicated USB converter for connecting the board to a (virtual) serial port. Since the developed board for motor control did not allow for an extra IC to be mounted (or the larger USB capable Atmega32U4 controller) the choice has been made to program the board through the available RS-485 bus. A scalable bootloader written by Alex Forencich called Xboot⁷ which is compatible with Atmel's AVR109⁸ flash programming standard has been adapted to be used on the board.

The Arduino IDE allows for adding new hardware targets. The motor control board is fully compatible with the IDE specifications. The bootloader can be programmed using a standard in system programmer (AVR-ISP) from the IDE. This only needs to be done once. One of the SPI ports on the motor control board doubles as AVR-ISP programming port. The reset signal (necessary for programming using AVR-ISP) can be routed to this connector by adding a wire bridge (0 Ω resistor or a pair of tweezers will do). After that a serial connection using a standard USB-RS-485 inter-

⁶<http://en.wikipedia.org/wiki/Arduino>

⁷<https://github.com/alexforencich/xboot>

⁸www.atmel.com/images/doc1644.pdf

face (for example the one used by Devantech⁹) is sufficient to update the firmware during development.

The change in development process of electronics with respect to the first prototype and the subsequent boards is large. Although in principle similar hardware (AVR familie microcontrollers) and similar software (GNU GCC) has been used, the change in development process of electronics by the Arduino system is comparable to the change in development process of the mechanical system by the 3D printer. The Arduino tool set (boards, bootloaders, IDE) makes the process very accessible. Many example projects are visible on the internet, libraries are readily available. This speeds up the development process dramatically.

11.5 PCB manufacturing

The modular design consisting of many identical modules and the large number of degrees of freedom (at least 11 motors per robot) have caused something which is normally rare in prototype development: series production. The simplest version of the robot described in chapter 5 needs, besides one centre module, four identical modules for clamp and drive. The robot uses six identical drive motors with identical wheels, bearings and couplings, four identical bend motors with four identical gear sets and spring shafts. The robot uses eight identical magnetic position sensors and six identical motor control boards (not counting the motors, sensor boards and motor control boards which have to be added for an active camera module). When a setup is used as proposed in chapter 2 with two double clamps (see figure 11.14 with additional payload module(s), all numbers have to multiplied by two.

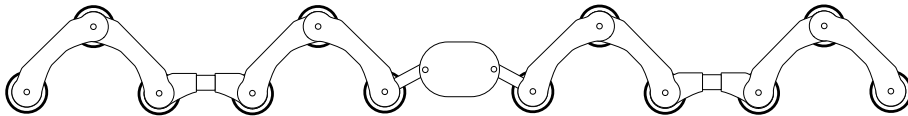


FIGURE 11.14 Set up consisting of two robots with a payload module in between

The PCBs have been designed using the open source package KiCAD¹⁰. There has been some study (and prior experience) with other software tools (among which UltiBoard, OrCAD, Eagle and the gEDA suite). Although an extensive research on PCB design tools is beyond the scope of this thesis, KiCAD proved to be a very fast and accessible design tool - besides being totally open source. Although KiCAD works together with online autorouter *Freerouter*, because of the size restrictions

⁹http://www.robot-electronics.co.uk/hm/usb_rs485_tech.htm

¹⁰<http://www.kicad-pcb.org>

the boards have been routed manually. Eagle, which is used widely in the open-hardware community is only free for limited 'educational' use. The choice for Ki-CAD allows the design to be totally free for the open-hardware community. Since it is inspired by - and borrows from - the open hardware Arduino project, this eventually allows for returning the board to the same community - while not inhibiting any commercial usage.

The boards have been designed as a standard two-layer PCB according to the smallest margins (track width, hole size) allowed by the chosen PCB pool service¹¹. Eventually the board size of 15 mm × 27 mm proved satisfactory for placement in every module. Special attention has been paid to the location of the connectors (all on the bottom side) so the PCB design allows for reflow soldering of all components (the connectors can be added by 'hand' later. An oven cannot conveniently solder double sided boards)

The PCB pooling service produces stencils for application of solder paste. A custom tool to fixate and outline the stencil with respect to the PCB has been produced on the laser cutter and is shown in figure 11.15.

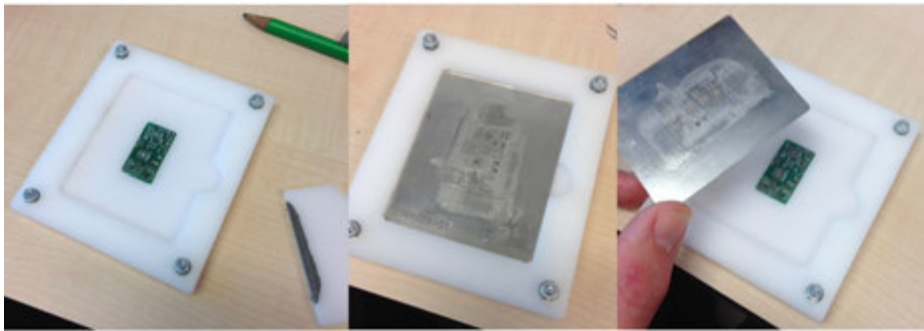


FIGURE 11.15 Applying solder paste to individual PCBs

11.6 Reflow oven

Populating PCBs using versions of SMD components (surface mount devices) which cannot be soldered by hand, has been previously the domain of specialised companies. The size of the board required a number these components (which were only

¹¹<http://www.eurocircuits.com>

available in QFN packages). Soldering these requires a re-work station or reflow oven¹². Especially for large series of boards the reflow oven is the preferred method for soldering. Instead of finding a specialised company (delaying the production and increasing the expenses), a standard toaster oven has been converted using an Arduino board, thermocouple and a MAX6675 thermocouple interface by Maxim, see figure 11.16.

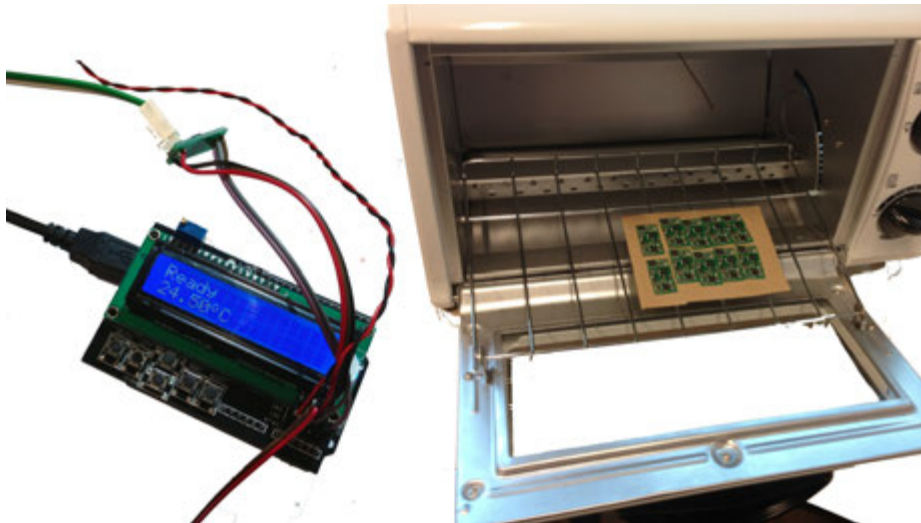


FIGURE 11.16 Converted toaster oven used for reflow soldering

The Arduino acts as PID temperature controller to follow closely the recommended thermal profile for soldering. Inspiration for this project came from the Ben Heck show¹³, using sources by Lim Pang Moh¹⁴. In this oven a number of batches of boards have been produced for various test models. Figure 11.17 shows a batch of 10 boards.

11.7 MEMS sensors

In order to measure the orientation of the camera head (and to extrapolate the robot's orientation based on the joint position sensors) a 'standard' IMU (Inertial Measurement Unit) board has been added using a number of custom sensors (custom as in Common Off The Shelf, sensors readily and inexpensively available in the open hardware community).

¹²http://en.wikipedia.org/wiki/Reflow_soldering

¹³<https://www.youtube.com/user/thebenheckshow>

¹⁴<http://www.rocketcream.com>

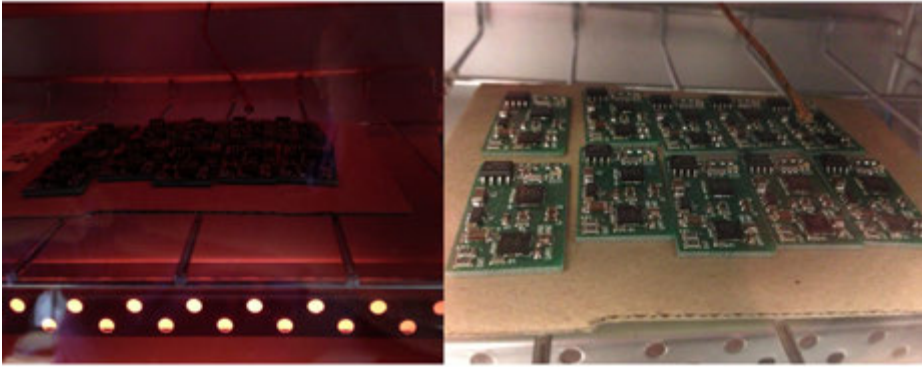


FIGURE 11.17 A batch of 10 motor control boards during the reflow process

While in 2000 the company XSens¹⁵ made their way as a startup in IMU sensing modules in a new market, currently the hardware (not their sensor fusion algorithms) can be obtained for very accessible prices due to the rapid progress in MEMS sensor technology development.

The chosen board uses an ADXL345 three axis accelerometer, a L3G2400D three axis gyroscope, a BPM085 barometric pressure sensor and an HMC5883L three axis magnetometer¹⁶. At the time the main board of the first prototype described in chapter 7 was realised, multi-axis MEMS gyroscopes were not available on the market yet. The ‘best’ option at that time was a single 3 axis accelerometer (LIS3L02a) and a separate temperature sensor (TC77). For a series of single axis gyroscopes and magnetometers was simply no space available.

The sensor board is connected through I²C to one of the motor control boards serving as ‘head’ controller. This board controls visible light, laser projection and angle of the vision system described in chapter 8.

Figure 11.18 shows the control board and the sensor board which is almost identical in size. The wire connection (four wires) is routed on the backside.

¹⁵<http://www.xsens.com>

¹⁶Note that at time of realisation this board costed 24\$ at <http://www.dx.com>

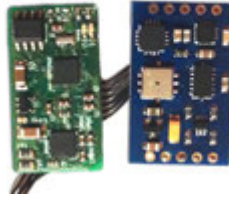


FIGURE 11.18 Motor drive board and the multi sensor board

11.8 Conclusion

In this chapter a wide number of techniques have been shown which are in itself not quite new and have been available throughout most of the course of this design project. Only in recent years techniques such as laser cut design, 3D printing techniques and open hardware (electronics) design, seem to have taken their place in the design process, at least, clearly visible in the design process of the product described in this thesis. Visibility, availability and accessibility are key ingredients in facilitating this upheaval in usage. It is interesting to realise how the tools shape the design process (and not only vice versa, i.e. that the design process can dictate the choice in tools).

Additive manufacturing (3D printing) has proved a technology with many benefits for the design process. The yielded design however is not immediately suitable for other production methods (CNC milling, injection moulding) since the printing process allows much design freedom than conventional techniques. Fortunately this didn't prove a problem, since the material available for print was not limited to the (hygroscopic) inkjet printed *VeroWhite* as described in chapter 5, but also glass fibre reinforced PA (nylon) which has enough strength and durability for 'real life' testing.

Printing the metal drive parts however proved not to be successful. Especially since the amount of post-processing after printing: removing the support material, polishing and doing the final modifications such as cutting thread and drilling holes, takes more time and man-hours than 'conventional' production on (CNC) lathe would take.

One of the major contributions to the *accessibility* of the tools listed in this chapter is the support by a large community of users, closely linked to various movements such as open-hardware, open source, FabLabs, MakerSpaces, HackerSpaces and other communities.

One of the major contributions to the *visibility* of the tools listed in this chapter is giving them a place directly in the space (the lab) where the design process takes place.

One of the major contributions to the *availability* of the tools is that they have not been installed to give a return in investment (money wise) regarding production costs, but that the machines are simply there, waiting for students, engineers and researchers to fill and fuel them with their ideas.

The design of the robot described in this thesis is crossing the boundary between a laboratory prototype and an 'industrialised' robot for real use. The complexity of the design required production and manufacturing on an almost industrial scale, since only a complete robot could act as 'proof of principle'.

Fortunately the tools for digital (desktop scale) fabrication which have been popularised through the 'maker' world in recent years, allow 'industrial' manufacturing within the lab environment, and even go a step further by offering an unprecedented level of flexibility and agility in the design process.

12

Evaluation

12.1 Introduction

In this chapter the final system is evaluated¹. A number of tests have been conducted demonstrating the capabilities. The tests that will be described in this chapter are an axial rotation in a 110 mm pipe, a vertical climb in a 63 mm pipe and taking a T-joint in a 110 to 90 mm joint.

The robot that has initially been used for the tests is based on the model described in chapter 5. However, during the evaluation a number of additional changes in the design was necessary. They will be described in the next section.

12.2 The complete robot

The model used for testing is largely based on the prototype described in chapter 5. The robot has been completed, adding two more clamping modules, the rotation module has been designed and realised and the distributed electronic setup has been added. This model is shown in figure 12.1.

The changes with respect to the model described in chapter 5 are:

- full robot setup including two clamping modules and one rotation module,
- all control electronics on board, full bus-control implementation,
- wheels using a smaller bearing, allowing for larger O-rings (46 mm) while keeping the same diameter,
- position sensors mounted on PCBs using connectors.

¹The presentation of these results has been accepted for publication at the IGRC 2014 [25]



FIGURE 12.1 Full system based on the design in chapter 5

During the tests and evaluation described in this chapter a number of changes had to be implemented, leading to some additions in the design². Although the chosen components, control and general specifications did not change with respect to the model shown in figure 12.1, these final changes were vital in taking the T-joint as described further on in this chapter. The changes with respect to the model in figure 12.1 are shown in figure 12.2 and are summarised here:

- fibre reinforced PA as main construction material,
- double O-rings as tyres to allow for traction when the module is not clamped exactly in the centre of the pipe,
- internal channels for cable routing, spaces inside the modules for mounting the PCBs,
- changed shunt resistors on motor drive boards from 1.0 Ω to 0.5 Ω to set the current limit at 400 mA instead of 200 mA per motor.

²Together with Mohammad Mozzafari Fomashi the design, which was initiated by Dian Borgerink, has been extended further and completed

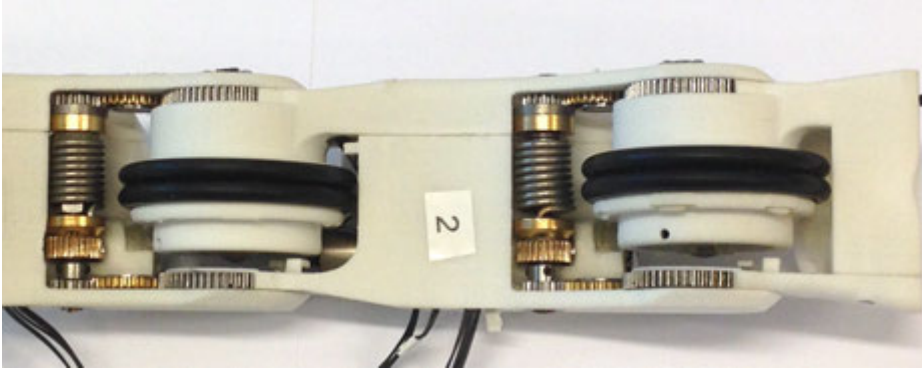


FIGURE 12.2 Image of the underside of two bending modules

These changes were necessary for being able to take the T-joint. The printed material by the Objet machine was not strong enough for the bending modules, causing the transmission in the bending module to separate during clamp at maximum torque. Also the wheels needed a wider contact surface for yielding traction force with respect to the pipe wall, also when the robot was not clamped totally in the centre of the pipe. The last improvement was additional space for the control boards and wiring. It is not possible to take any bend or joint when wires are sticking out of the robot.

12.3 Tests

The tests described in this chapter have been conducted in short pipe segments in the laboratory at the University of Twente. Although a much larger test network has been installed at KIWA in Apeldoorn, first the robot needs to prove to be able to reliably handle the individual obstacles before being subjected to a ‘real life’ situation.

The tests have been conducted in transparent pipes with the same outer- and inner diameters as pipes used in the network. The material has also a friction coefficient comparable to PVC and PE. Instead of constructing transparent (artificial) T-joints and bends, the standard yellow PVC components by Wavin³ which are frequently utilised in the existing network have been used. These components have ridges, bumps and unevennesses inside which hamper the robot. This is exactly the kind of situation the robot will encounter in reality and, therefore, should be introduced in the test conditions.

The measurements of angles, velocities and torques which are shown in this chapter are recorded using the robot’s own hardware. The slave nodes are queried by the master controller and their data is recorded on a host PC system. Visualisation of

³<http://nl.wavin.com>

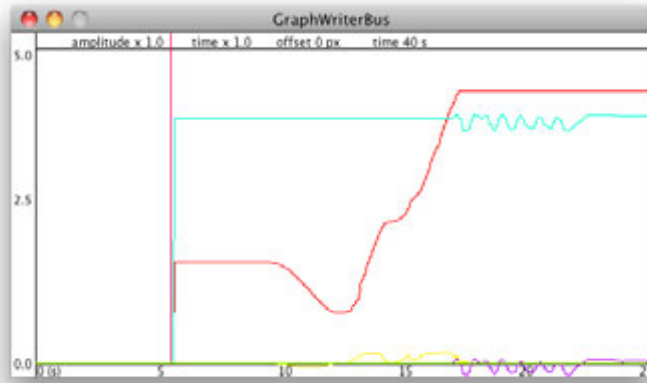


FIGURE 12.3 Data visualisation in Processing

data during the experiments has been implemented in *Processing*⁴, shown in figure 12.3. The data is stored as *.csv files and processed afterwards using *LibreOffice Calc*⁵.

During the described experiments the robot is connected using a short CAT5 cable to a ‘base station’ implemented using an Arduino Mega board. The CAT5 cable feeds power and RS-485 communication to the robot. The robot is supplied with an external 5 V (3 A) power supply. Although the robot allows supply of 6 V, the 5 V is used to provide another ‘worst case’ situation. In case of longer tether cables the voltage might drop even further, so operating the robot on a lower supply voltage than permitted gives some ‘headroom’ for further experiments.

By using the NanoKONTROL slider panel connected to the base station the operator can select the module that is individually monitored by the *Processing* application. Two data formats are supported: output which can be graphed ‘live’ by the application and a full *.csv data set in which all variables (angle, current, torque, velocity, distance) of every module are recorded.

⁴<http://processing.org/>

⁵<https://nl.libreoffice.org/>

12.3.1 Axial rotation in 110 mm

The axial rotation has been described in chapter 4. This manoeuvre is necessary in order to rotate the robot in the correct orientation for taking a bend. Although the maximum clamping force which can be produced is smaller in the 63 mm pipes, the manoeuvre has been carried out in a 110 mm pipe because the large diameter might require extra effort for re-clamping. Therefore, the 110 mm pipe is considered the ‘worst case’ for an axial rotation and should be validated by a test.

The maximum axial rotation ϕ is 4.0 rad. This is limited in software because of the maximum rotation the wires allow. In this sequence also an experiment is done with simultaneously clamping one side while unclamping the other. In the shown experiment the rotation is executed in three steps. In theory only two steps are required, but due to this simultaneous motion a correction step is also included.

Figure 12.4 shows the rotation in 12 steps, described in table 12.1. The images are all screenshots of a movie which has been captured during the experiments⁶.

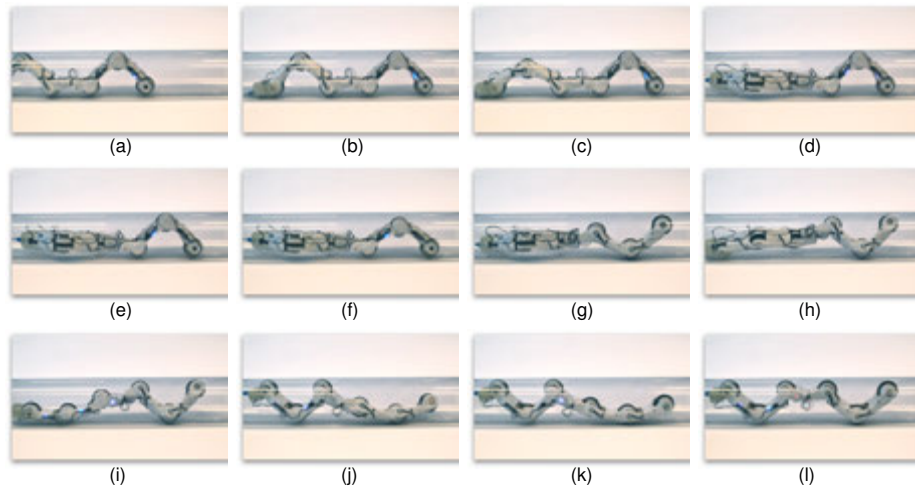


FIGURE 12.4 Rotation in a 110 mm pipe in 12 steps

This experiment is similar to the axial rotation described in chapter 4. In this case also the experiment has been done to test whether simultaneously clamping and unclamping, (h) and (j) in figure 12.4, gains time. Although the manoeuvre is pretty fast, an extra correction step (k) is necessary.

Figure 12.5 shows the velocity of the wheels during the manoeuvre. It shows that the driving velocity is 4 rad/s when entering and exiting the pipe, labeled with (a)

⁶<http://youtu.be/OasJQnYY600>

TABLE 12.1 Sequence for axial rotation

n	description
(a)	drive to the centre
(b)	stop
(c)	unclamp rear
(d)	rotate rear $1/2\pi$ rad
(e)	clamp rear
(f)	unclamp front
(g)	rotate front π rad
(h)	clamp front while unclamping rear (experiment)
(i)	rotate rear $1/2\pi$ rad
(j)	clamp rear while unclamping front (experiment)
(k)	rotate front 0.6 rad (correction)
(l)	clamp front

and (l) in the picture. During the rotation (g) there is no driving action. With a wheel diameter of 46 mm the velocity in the pipe is $4 \times 23 = 92$ mm/s which satisfies the criterion of being able to drive with a velocity of 8 cm/s.

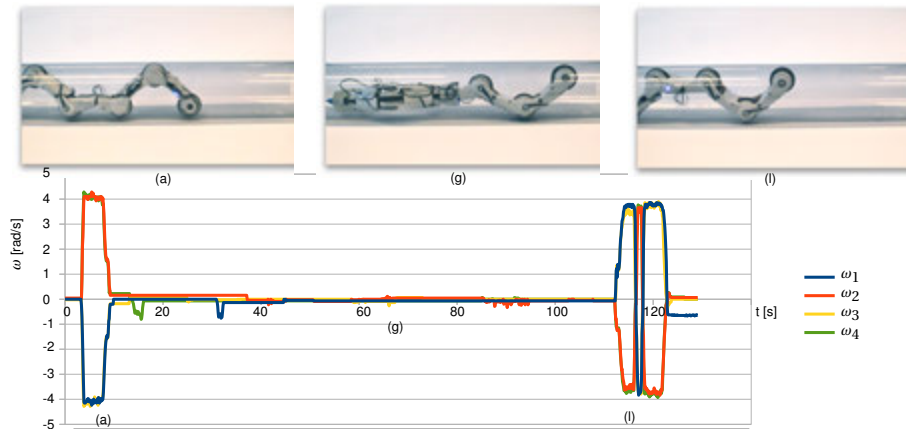


FIGURE 12.5 Drive wheel velocity during a rotation in a 110 mm pipe

Figure 12.6 shows angle ϕ of the rotation module. It is controlled in four steps listed in table 12.1: (d), (g), (i) and (k). It shows that the behaviour of the position control of the module does not differ significantly from the version without load shown in chapter 10.

The clamping torque is measured using spring deflection and expressed in 10^{-3} Nm. The modules have been clamped prior to the manoeuvre. The clamping torque

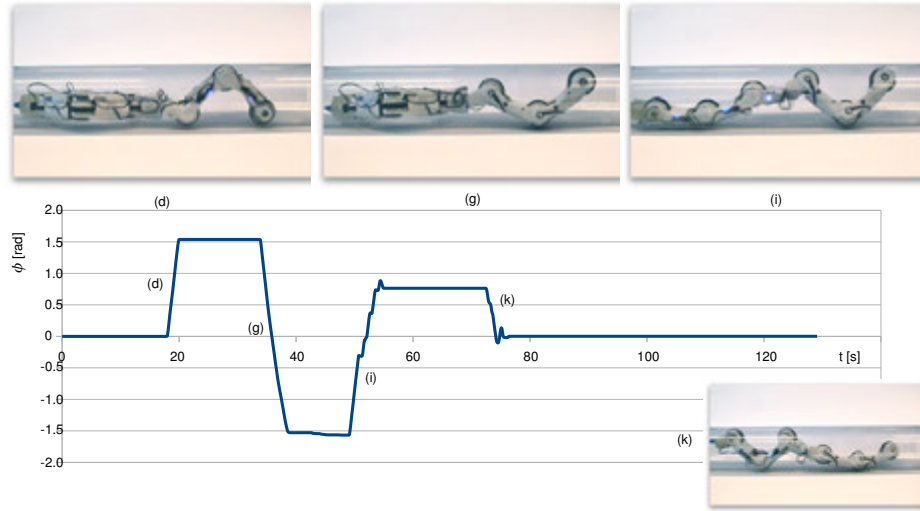


FIGURE 12.6 Rotation joint angle ϕ during a rotation in a 110 mm pipe

during the rotation is shown in figure 12.7 showing part of the clamping and un-clamping motions in the sequence (c), (e) and (f) from table 12.1.

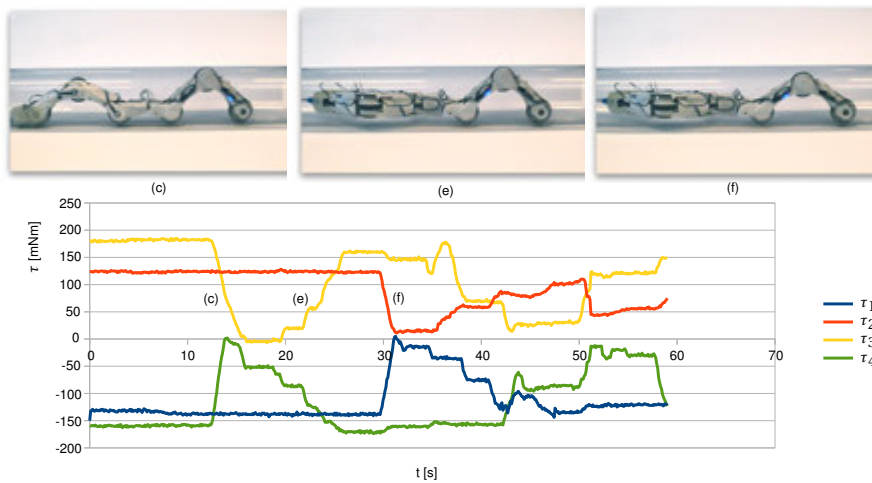


FIGURE 12.7 Clamp torque during a rotation in a 110 mm pipe

12.3.2 Climb in 63 mm pipe

Since the possible clamping force is the lowest in the smallest diameter, the vertical climb in a 63 mm pipe can be considered the worst case for climbing. In the experiment the robot is clamped in the bottom of the pipe and subsequently powered up to travel upwards and slowly back as well. Figure 12.8 shows the robot climbing 500 mm inside a pipe.

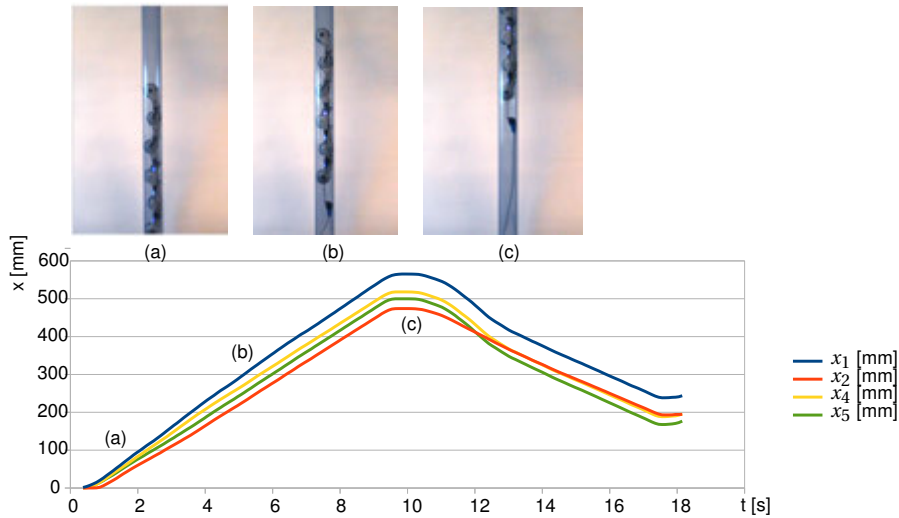


FIGURE 12.8 Position in the pipe during a climb in 63 mm

The distance is measured using the incremental encoders in every wheel. Since the clamping force is not distributed evenly across the wheels, the amount of slippage per wheel might deviate from the others. Motor ω_1 is the motor with the smallest amount of clamping force, so the slip is higher than the rest resulting in a higher measured distance. This can also be seen in the amount of current, which is less than the other motors.

Figure 12.9 shows the current used by drive motors ω_1 and ω_4 . In the figure it can be seen that the current i_4 is higher for ω_4 since this motor takes the full clamping force. The current is comparable to the measurements described in chapter 5. Since the shunt resistors have been decreased by a factor two (0.5Ω instead of 1.0Ω), the resolution for measuring the current is also reduced by the same factor. The Allegro 3906 motor driver has an active current protection which level is set using this resistor as well. The level of the current limiter has been increased to 400 mA. Note that in figure 12.9 the same scale refers to both, current in [mA] and position

in [mm].

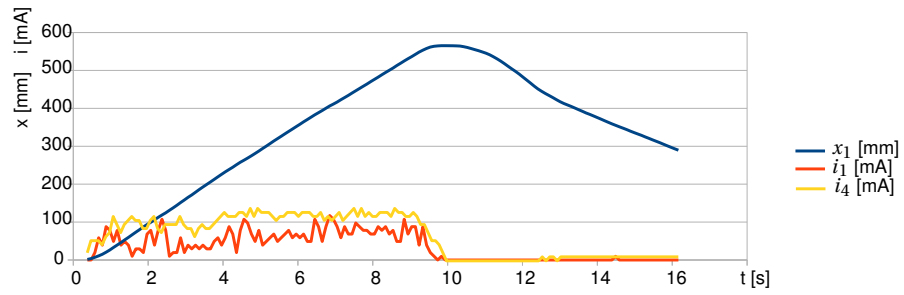


FIGURE 12.9 Used current during a climb in 63 mm

12.3.3 T-joint

In chapter 4 the first prototype takes a mitre-bend in a 90 mm pipe. The operation takes (when not taking in account the idle-time between motions) 4 minutes. The bend has been made by connecting to transparent pipes which have been cut off each at 45° .

In this experiment a standard T-joint with some edges and bumps inside has been used. An added disadvantage with respect to the constructed mitre-bend for the robot is the open side of the T-joint with which no contact is possible. The sequence the robot performs can be described in 11 steps and is described in table 12.2 and shown schematically in figure 12.10. This pre-planned sequence (on paper) is based on the experience with the previous experiments in chapter 4.

TABLE 12.2 Sequence for taking a t-joint

n	description
(1)	drive forward
(2)	stop when the front wheel ω_1 loses contact
(3)	unclamp θ_2 into the bend
(4)	unclamp θ_1
(5)	drive forward while unclamping θ_1 and θ_2
(6)	drive forward and unclamp θ_3
(7)	clamp the front $\theta_{1,2}$ and unclamp the rear $\theta_{3,4}$
(8)	drive forward, clamp θ_3
(9)	drive forward, unclamp θ_4
(10)	drive forward
(11)	clamp rear $\theta_{3,4}$

The resulting sequence is recorded using two camera's while all data is stored on the host PC. The resulting movie can be seen online⁷. The sequence is shown in figure 12.11. This image consists of captured stills of the recorded movies. A schematic drawing of the robot is superimposed on the pictures to show the position of the robot inside the joint.

The total sequence took 400 seconds (the movies used for generating the stills are both 7 minutes long) but during much of the time the robot was idle (while the position was evaluated, pictures are taken and the strategy was discussed). In the movie most of the idle time has been cut out, reducing the sequence to 2.35 minutes.

Figure 12.12 shows the angle of the rotation module during the entire sequence. Although in theory it has no function during the manoeuvre (see figure 12.10) since the robot has been aligned correctly for taking the bend, it is used at some crucial steps which will be discussed in section 12.3.4.

⁷<http://youtu.be/OasJQnYY600>

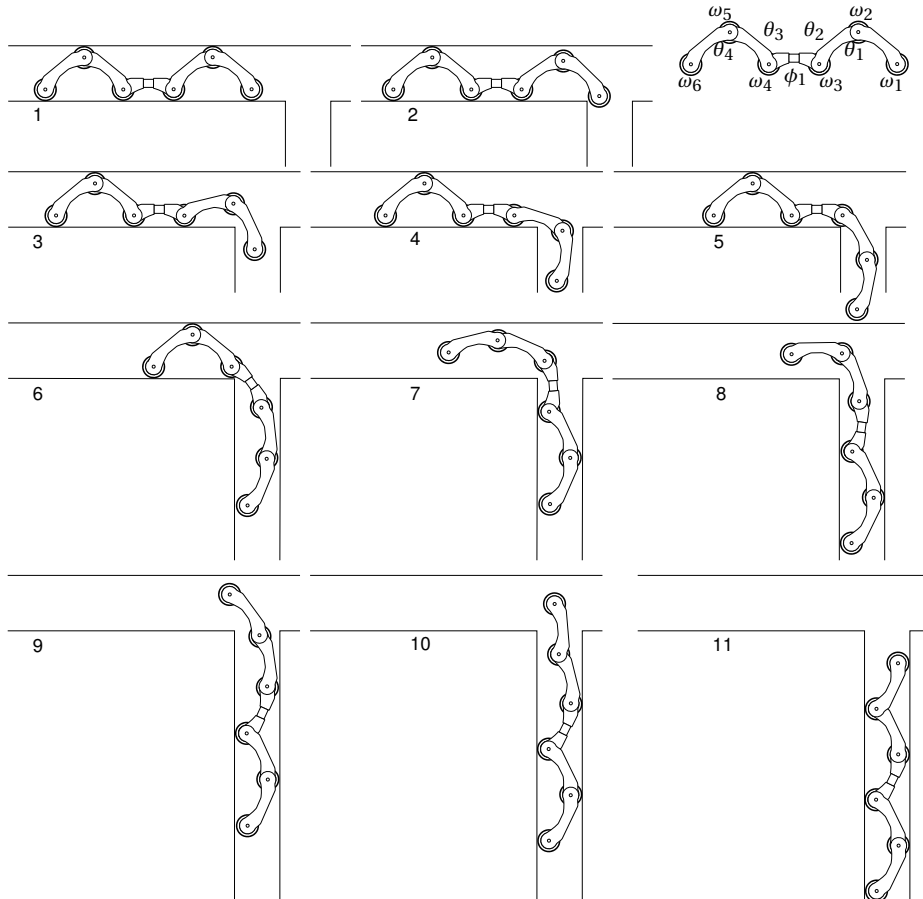


FIGURE 12.10 Sequence for taking a bend in a T-joint

Figure 12.13 shows the angles of the bending modules during the manoeuvre. The step numbers of the sequence have been added to the graph as points of reference. Between the red markers the robot is paused for 20 seconds. The spikes in the graph for θ_2 are caused by transmission errors which have not yet been filtered out by the communication software.

12.3.4 Wriggle and Squeeze

In the attempts to get the robot through the T-joint it happens sometimes that one of the edges of the robot gets stuck behind one of the edges inside a joint. When the complete robot is lying on the bottom of the pipe (both front and backside are not centred and sideways clamped in the pipe) it is difficult for the robot to regain

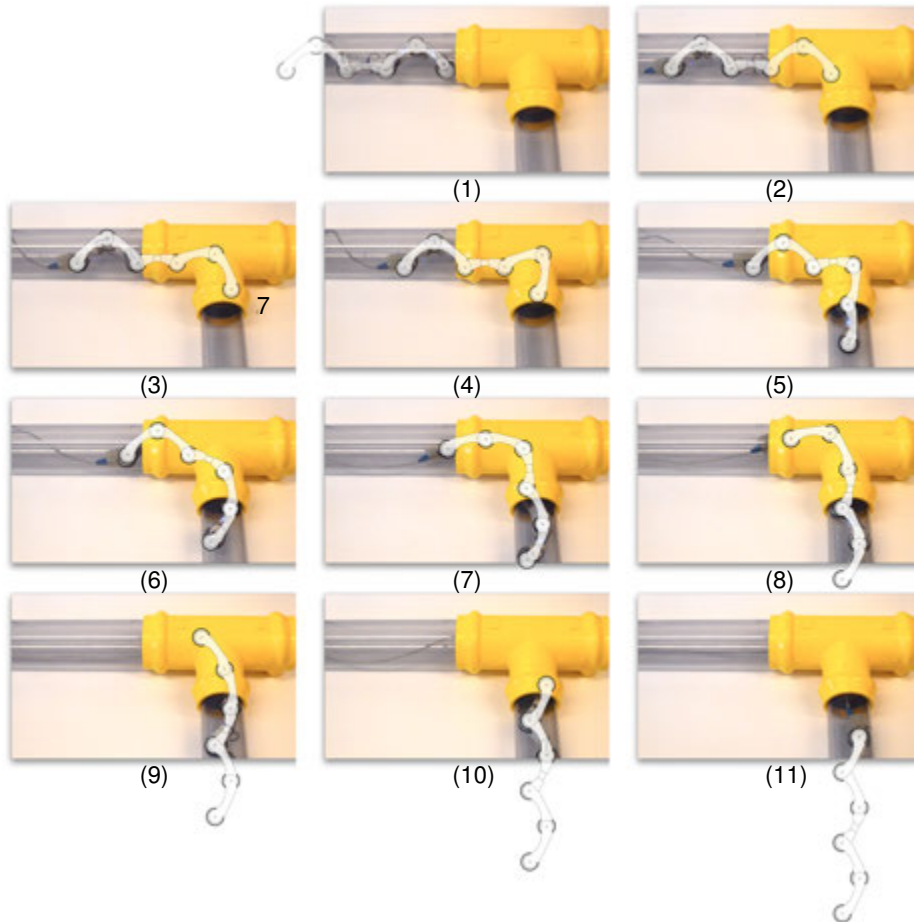
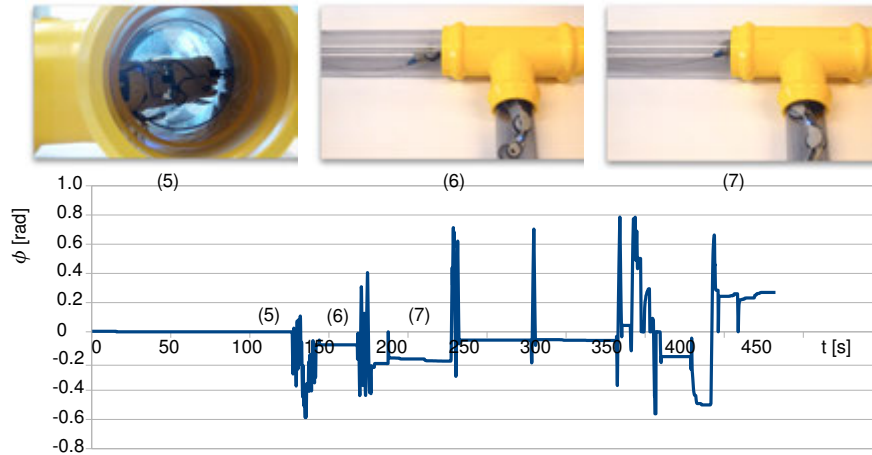
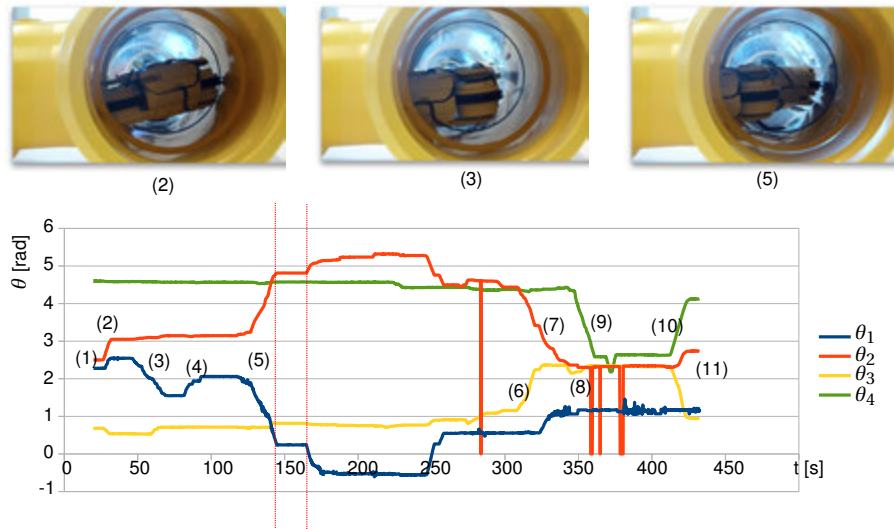


FIGURE 12.11 Sequence of stills showing the manoeuvre through a T-joint

traction with the front side. By using the back-side as lever, the front side can be twisted so that it can be clamped diagonally and regain traction once more. In this instance some 'wriggling' while starting the clamp procedure helps to regain enough clamping force for traction.

Wriggling, also referred to as dither, is frequently used in control, for example to overcome static friction. Bowl feeders⁸ use vibration motions (on a micro scale) to align components for a conveyor belt. Closer to the application described here are the walking robots by Mark Tilden [42] which cover an impressive variety of obsta-

⁸http://en.wikipedia.org/wiki/Bowl_feeder

FIGURE 12.12 Angle ϕ during the manoeuvre through a T-jointFIGURE 12.13 Angles θ during a manoeuvre through a T-joint

cles with simple (random) oscillatory motions as described by Rietman, Tilden and Askenazi in [78].

Figure 12.14 shows the robot in the situation where the front clamp needs to regain

traction. The graph shows an enlargement of a section of the graph showing the position of the rotational joint. The oscillations are fed into the system by operator control. At a certain point the front module regains traction and the oscillation can be stopped. In the complete sequence shown in figure 12.12 this procedure is repeated a couple of times.

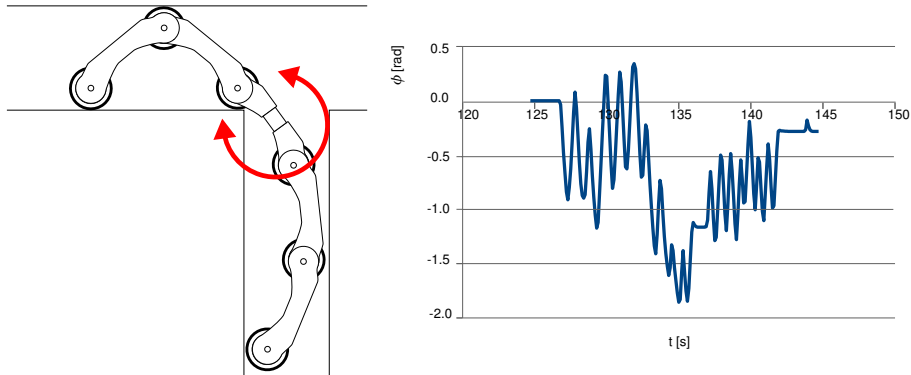


FIGURE 12.14 Dithering while moving through a corner

12.3.5 Reverse clamp

Up until now the robot has mainly been used in the previously described way, i.e. modules 1,2 and 4,5 form identical clamping V-shapes. As can be seen in figure 12.11 in the final two pictures (10 and 11) the rear module has not been clamped using the normal orientation, but is clamped in reverse. This was done deliberately, since this orientation followed logically from the position of the rotation module in step (9). Since the modules can generate an equal torque in both clamping directions (only the range is limited when clamping in reverse) this 'reverse clamp' can be an extension of the existing set of motion primitives.

12.3.6 Other manoeuvres

Other manoeuvres shown in the [movie](#) are different straight pipes ranging from 63 mm tot 125 mm, as well in horizontal as in vertical orientation. Also a diameter transition from 110 mm to 63 mm is successfully taken in a standard yellow PVC component by Wavin. Figure 12.16 shows stills from the movie.

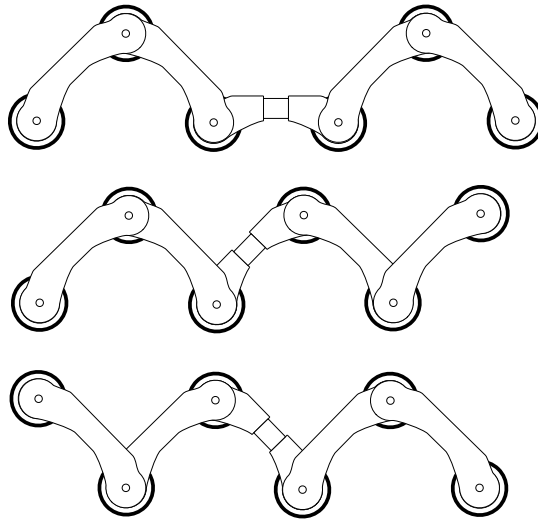


FIGURE 12.15 Normal and reverse clamping options



FIGURE 12.16 Robot taking a diameter change from 110 mm to 63 mm

12.4 Conclusion

The required manoeuvres for the robot have successfully been demonstrated in this section. The robot is capable of moving through a range of pipe diameters from 63 mm to 125 mm. Obstacles like welds or edges inside sleeves can be taken without any additional control input. The inside diameters in these pipes are 57 mm to 119 mm (the pipes have a wall thickness of 3 mm) resulting in a spreading factor (clamp range) of 2.08.

The capability of climbing vertically with a complete robot (instead of just one segment shown in chapter 5) has been demonstrated successfully in the same range of 63 mm to 125 mm. The current consumption is comparable with earlier measurements.

The manoeuvre through a T-joint has been shown in a standard Wavin segment which also incorporates a 110 mm to 90 mm diameter transition at the same time. The manoeuvre has been executed in 400 s, but when the idle time is disregarded, it should be possible to execute the manoeuvre in less than 120 s.

The bending modules have a preferred orientation for clamping which has been designed with the curved orientation through a bend or corner in mind. It is, however, possible for all modules to clamp equally well in the opposite direction (although with a limited range). This allows for new strategies to be considered for taking bends and joints.

The rotation module has been used differently than its originally intended use (i.e. for axial rotation manoeuvres only). During the manoeuvre in the T-joint it was necessary to use the joint as 'lever' to align the modules for re-clamping and to use dithering in the control input to pass some edges inside the joint. Although the torque the joint can supply is quite large due to the 1:809 gearbox, the joint is not implemented as force actuator like the bending modules. A re-design using a series elastic element (or at least an over-strain protection) might be desirable.

Due to the length of the rotation module it is not possible to demonstrate the manoeuvre through a bend in 63 mm. The current implementation is 4 mm too long to fit smoothly through the corner. While re-designing the joint to incorporate a series-elastic joint, also the length should be considered so that eventually also the bend in the smallest diameter can be taken.

13

Conclusion

13.1 Introduction

The gas distribution network in the Netherlands has a length of roughly 100 000 km in urban areas. This network needs to be monitored constantly and segments need to be replaced when the risks on leaks increase. Ageing is one of the most important reasons for monitoring the network. Since replacement is expensive it is important to know how long a segment of the network is still expected to offer reliable service.

This network is monitored by leak searching ('sniffing') above ground. The presence of leaks can be seen as indicator for the quality of the network, but accurate data from within the network is lacking. When pieces of the network are excavated they are often sent to KIWA in Apeldoorn for structural analysis, so that a prediction can be made on the estimated life time. Furthermore (endoscope) cameras are used for inspection inside, but they are not employed structurally.

A solution for the problem of getting 'inside information' which has been explored in this thesis is

the realisation of a swarm of autonomous robots that move constantly through the network, while collecting and storing data. The robots surface now and then for maintenance and exchange of data with the network operators.

This project can be seen as a feasibility study of a part of this goal: Is it possible to design a robot which can move (autonomously) through the gas distribution network?

This thesis is described a robot which has to inspect the gas distribution network from the inside, collecting measurement data which can be used to predict the life-time of the inspected section. Five partial questions were answered:

- What is the best mechanism for *propulsion* given the intended environment?

- What is the best way of providing *energy* to the system?
- Which *sensing methods* can be used for assessing the quality of the inspected pipes? How to represent and visualise the resulting measurement?
- What is the best method for *communication* with the system?
- How to *control* the designed mechanism? Which steps are necessary for autonomous or operator-based control?

In order to answer these questions, three prototypes have been realised. These designs focussed primarily on the question of finding the best mechanism for propulsion. Besides the propulsion mechanism for every prototype also a suitable implementation for energy supply, sensory system, communication and control has been realised.

The design of a propulsion mechanism is strongly depending on the construction of the gas distribution network. Based on data available on a number of representative urban distribution networks a list of elements has been made which will be the primary environment in which the robot has to operate. The most important aspects can be summarised as follows:

- long stretches of pipe (tens of metres)
- pipes with an outer diameter of 63 mm to 125 mm
- bends, mitre bends, T-joints
- inclinations of at least 30°

13.2 Conclusion

13.2.1 Mechanical design

The minimal pipe diameter (63 mm outside) is the most defining factor for the robot. In pipes with a high wall-thickness (and presence of butt-welded connections which protrude inside the pipe) this means that the robot has to move through an inner diameter of 51.5 mm. Most of the design requirements follow directly from the given network environment. The design choices that have been made can be summarised as follows:

- wheels (efficient propulsion for long straight stretches of pipe)
- clamping mechanism (to take inclinations in a smooth pipe)
- clamping V-shape (in order to have a spreading factor, to clamp in the smallest and largest diameters listed)

- curved module shape (as largest shape that can pass a mitre-joint in 63 mm)
- rotational joint (to align the clamping shape in orientation with a bend)
- second clamping V-shape (so one module can move freely with respect to the other, in taking a bend or rotating in the pipe)

The design which has been the basis of all of the realised prototypes is a wheeled robot 'snake' consisting of a number of modules (segments, minimum number is five) which can be used as two clamping V-shapes. The central module is a rotation joint which can be used to change the orientation of the robot in a pipe.

A number of prototypes has been realised with different numbers of modules. Although extra modules might facilitate the possibility of taking more payload (sensors, batteries), the reduced number of five modules has proven sufficient for making all necessary manoeuvres.

A prototype with omnidirectional wheels has been realised. Although this prototype is capable of limited manoeuvres (driving straight and axial rotation in pipes of 110 mm) the control is very intuitive due to the active orientation control.

The final design has shown to be capable of moving, climbing and rotating inside the required 63 mm to 125 mm pipes. The velocity with 9 cm/s is higher than the necessary 8 cm/s. The requirement of taking a 30° inclination has been exceeded with the possibility of climbing vertically. This allows for much simpler equipment for entry and exit to the network.

The design has shown to be capable of taking a T-joint in 110 mm to 90 mm. This manoeuvre can theoretically be executed in less than 120 s.

The clamping torque the system can provide is less than expected from calculations due to mechanical friction and efficiency of the used gearing. However, the clamping torque proves to be enough for all of the required manoeuvres, even the vertical climb.

13.2.2 Electronics

The design has many actuated degrees of freedom, so wiring is a serious issue. To reduce the amount of wiring, the electronic system has been distributed over the robot segments. In that way, the electronics is as close as possible to the motors and sensors necessary for propulsion. A master controller is added which communicates to this distributed 'slave nodes' via a serial bus. Also energy for propulsion has been provided through this bus. Energy is supplied through batteries or a tether cable.

13.2.3 Sensors

A camera system has been developed which can be used for both pipe assessment and navigation. The camera system uses a laser projector which projects a cone (circle) on the inside of the pipe. In a defect-free pipe the image captured by the camera will also be a circle. Deformations of the pipe show up as deviations of the captured circle shape. Also segments in the network such as bends and T-joints can be detected as sharp interruptions of the circular pattern. The camera system can detect deformations (indents in the pipe) up to 0.2 mm.

The camera system is small enough to be placed on the robot. The vision processing algorithms have been optimised so that they can be executed on a small, energy efficient embedded computer on the robot.

An experimental setup using an acoustic sensor has been realised. This system consists of an ultrasonic microphone which captures the noise of gas leaking out of a pipe. Although the relevance of this data is strongly dependent on the conditions of the leak (size, gas pressure, material surrounding the pipe), it is a relatively simple and inexpensive addition to the existing sensory system. In many cases a clear indication of the presence of a gas leak can be given.

For control of the robot a number of sensors has been implemented to measure joint angles and forces. Besides the incremental encoders which are integrated with the motors, a number of absolute magnetic position sensors is implemented. By measuring the angles between the modules while the robot is clamping inside a pipe, the diameter of this pipe can be determined. Using an accelerometer (of a more elaborate combination of accelerometer data with gyroscope, compass and barometric pressure) the orientation of the pipe can be determined and (eventually) a model (map) of the pipe network can be constructed.

13.2.4 Communication

Although wireless communication has been implemented with robots underground using Ultra Long Wave radio or Ultra Wide Band radio, the necessary amount of power exceeds the storage capacity on the robot design. The first prototype has been equipped with a short-range 2.4 GHz radio link which can be used for example for communication between the robot and a nearby docking station.

During experiments the robot has been mostly operated using a tether cable, which can be used both for communication and power supply. Also as mechanical fail-save can the tether be used for pulling the robot back in case of a technical failure. Eventually the autonomous robot should be able to operate without the need for continuous communication. Because dragging a tether cable reduces the operation range of the robot, a spooling system has been developed. This spooling system has the size of one module and is able to spool on (or off) 100 metre of glass-fibre which

can be used for communication. The system has not been used in the final tests.

13.2.5 Control

The robot has a number of degrees of freedom which all need different control inputs. The wheels are velocity controlled, the rotation joint is position controlled and the clamping V-shapes are controlled using a combination of position and force (stiffness). These controllers are implemented on the slave nodes as conventional PID controllers.

Although the overall goal of the project is to realise an autonomous robot, the focus during the project has shifted to creating a system that is capable of manoeuvring in the given network altogether. In simulation and on paper a number of strategies have been designed for control of the robot during complex manoeuvres like taking a T-joint. In order to test these strategies the robot has initially been controlled using a human operator. Because it is difficult to control the large number of degrees of freedom individually by an operator (at least 11 motors) a mapping, combining degrees of freedom to a reduced number of inputs, is necessary. In practice it appeared that different movements were necessary than those listed in the designed strategies.

Where in simulation or in (2D) drawings the robot is always clamped in the centre of the pipe, in practice the complex manoeuvres are taking place on the bottom of the pipe or even diagonally clamped. The rotation joint, which was primarily intended for axial rotation inside the pipe of one clamping V-shape with respect to the other) appeared to be a very useful source for 'wriggling' the robot over edges and bumps (ones that hardly show up in simulations). A next step in the research will be formalising these insights and adapting them for (autonomous) control.

13.2.6 Production

The chosen production methods had a large impact on the design process. The first prototype has been designed and produced in a 'conventional' mechatronic way. After a (long) design process the drawings were 'frozen' and prepared for production. A machine factory has produced the parts based on the drawings. Three months after finishing the drawings a mechanical prototype was ready for testing. Subsequently the electronics and wiring had to be added.

The second prototype has been designed and produced using a 3D printer. This approach has yielded a series of prototypes in a relatively short time, which, after a number of iterations, proved suitable for physical tests. The reduction of weight due to the printed material with respect to the metal (aluminium and brass) used in the first prototype, yielded a prototype capable of a vertical climb (instead of the requested 30°). Also in the design and production of the electronic systems extensive

use has been made of the developments in open hardware and open software in the recent years.

Although the described technologies for digital fabrication (3D printing, laser cutting) have been in use for a long time, the development in the ‘Maker’ communities (maker spaces, hacker spaces, FabLabs, DIY movement) allowed these tools to become increasingly accessible. The difference in design and production between the first prototype and the subsequent prototypes demonstrated the importance of *accessibility*, *visibility* and *availability* of these tools as a condition for fruitful usage.

13.3 Future Work

Two of the goals have not been reached completely: not all necessary obstacles were taken and the level of autonomy of the realised robot system is small.

The capability of taking a mitre-bend in 63 mm has not been demonstrated by the robot yet. The dimensioning of the modules is very critical. At the moment the rotation module is 4 mm too long to fit smoothly through this bend.

The length of this module is determined by the wheel sizes and the length of the rotation motor. The wheel size cannot be easily changed: no alternative combination of motor, bearing and tire could yet be found. Also no suitable alternative for the rotation motor has been found yet: a motor yielding the same torque but with a shorter length.

However, the coupling between the motor and the module might be replaced by a spring coupling. Currently, the same 5 DOF decoupling mechanism as used for the drive motors, described in chapter 5 has been used.

The experiments described in chapter 12 showed that the rotation module is used as a force actuator during the manoeuvre in the T-joint. A flexible coupling would protect the motor from being damaged through the applied forces and would also allow torque control, similar to the control implemented in the bending modules. The question is whether it is possible to implement this flexible coupling and reducing the module length at the same time.

The development of a certain level of autonomy in the robot has been moved to the background during the project, in favour of the focus on designing a capable robot mechanism.

The experience gained with operator control inputs should be formalised into more elaborate state-machine like structures (recipes) for moving through various types of obstacles. The discussed ‘motion primitives’ need to be elaborated, to such an extent that the robot can autonomously take a corner. For this it is necessary that the robot knows the position of the corner (through vision data) and relates this data to its own state information (like the front wheel losing traction).

The desired amount of autonomy will depend on the final application and the types of missions the robot will be used for. Also more experiments with operators 'in the loop' have to be conducted, in order to optimise the human-machine interface.

In the project by Mennink [60] a start has been made in 'fusing' data obtained by the vision system and an incremental encoder (a substitute for one of the encoders in the drive motors). By combining this data with more elaborate IMU orientation measurements and the robot's state data (angles, velocities, torques, traveled distance) a more complete world model (or map) can be derived. This map could be the basis of a SLAM (simultaneously localisation and mapping) algorithm, which is necessary for fully autonomous inspection missions.

Bibliography

- [1] A. Ahrary, Li Tian, S. Kamata, and M. Ishikawa. An autonomous sewer robots navigation based on stereo camera information. In *Tools with Artificial Intelligence, 2005. ICTAI 05. 17th IEEE International Conference on*, pages 6 pp.–633, 2005.
- [2] E. Allouche, A.P. Jaganathan, and N. Simicevic. Pipe survey method using uwb signal, January 8 2013. US Patent 8,350,570.
- [3] Chris Anderson. *Makers, The New Industrial Revolution*. Crown Business, 2012.
- [4] J. Ansink. Electronic design for a gas pipe inspection robot. Technical report, Control Laboratory, University of Twente, 2007.
- [5] Jort Baarsma. Tethering system for pirate. Master’s thesis, University of Twente, 2012.
- [6] Benjamin S Blanchard and Wolter J Fabrycky. *Systems engineering and analysis*, volume 4. Prentice Hall Englewood Cliffs, New Jersey, 1990.
- [7] D. J. Borgerink. Development of the second pirate prototype using rapid prototyping. Master’s thesis, Control Laboratory, Drienerlolaan 5, Enschede, 2012.
- [8] M. F. Brillman. Embedded vision system for pirate. Technical report, Control Laboratory, University of Twente, 2011.
- [9] Gido Brouns and Marco Poorts. Investing in the future, long-term optimization of asset replacement in the collective regional gas grids of the netherlands. In *25th World Gas Conference, Kuala Lumpur*, 2012.
- [10] A. Brunete, M. Hernando, and E. Gamba. Modular multiconfigurible architecture for low diameter pipe inspection microrobots. In *Robotics and Automation, 2005. ICRA 2005. Proceedings of the 2005 IEEE International Conference on*, pages 490–495, 2005.
- [11] B. Burkink. Pirate propulsion unit. Bsc thesis, Control Laboratory, University of Twente, October 2009.
- [12] Gilles Caprari, Andreas Breitenmoser, Wolfgang Fischer, Christoph Herzeler, Fabien Tâche, Roland Siegwart, Olivier Nguyen, Roland Moser, Patrick Schoeneich, and Francesco Mondada. Highly compact robots for inspection of power plants. *Journal of Field Robotics*, 29(1):47–68, 2012.
- [13] J. Carlson and R.R. Murphy. Reliability analysis of mobile robots. In *Robotics and Automation, 2003. Proceedings. ICRA '03. IEEE International Conference on*, volume 1, pages 274–281 vol.1, 2003.

- [14] Xubing Chen, Hanxin Chen, and Youlun Xiong. Passive ultrasonic rfid localization for pipeline pigs. In Ming Xie, Youlun Xiong, Caihua Xiong, Honghai Liu, and Zhencheng Hu, editors, *Intelligent Robotics and Applications*, volume 5928 of *Lecture Notes in Computer Science*, pages 279–287. Springer Berlin Heidelberg, 2009.
- [15] HR Choi and SM Ryew. Robotic system with active steering capability for internal inspection of urban gas pipelines. *Mechatronics*, 12(5):713–736, 2002.
- [16] Hyouk Ryeol Choi and Se gon Roh. *Bioinspiration and Robotics: Walking and Climbing Robots*, chapter 23, page pp. 544. I-Tech, Vienna, Austria, September 2007.
- [17] Lawrence B Conyers and Dean Goodman. *Ground-penetrating radar*. AltaMira Press, 1997.
- [18] H. E. de Boer. Analysis, optimization and evaluation of a pipe inspection robot. Msc thesis, Control Laboratory, University of Twente, August 2008.
- [19] E. Dertien. Dynamic walking with dribbel. *Robotics Automation Magazine, IEEE*, 13(3):118–122, Sept 2006.
- [20] E. Dertien and S. Stramigioli. Basic maneuvers for an inspection robot for small diameter gas distribution mains. In *Robotics and Automation (ICRA), 2011 IEEE International Conference on*, pages 3447–3448, 2011.
- [21] E. Dertien, S. Stramigioli, and K. Pulles. Development of an inspection robot for small diameter gas distribution mains. In *Robotics and Automation (ICRA), 2011 IEEE International Conference on*, pages 5044–5049, 2011.
- [22] Edwin Dertien. System specifications for pirate. Technical report, University of Twente, 2006.
- [23] Edwin Dertien. Development of an inspection robot for small diameter gas distribution mains, a mars mission underground. In *GERG academic network event 2010*, Brussels, 2010. GERG.
- [24] Edwin Dertien, Mohammad Mozzafari Foumashi, Kees Pulles, and Stefano Stramigioli. Design of a robot for in-pipe inspection using omnidirectional wheels and active stabilisation. In *IEEE International Conference on Robotica and Automation (ICRA) 2014*, 2014.
- [25] Edwin Dertien, Mohammad Mozzafari Foumashi, Kees Pulles, and Stefano Stramigioli. Development of an inspection robot for small diameter gas distribution mains. In *International Gas union Research Conference, IGRC 2014, Copenhagen, Denmark*, 2014.

- [26] R. Doctors. A systems approach to battery powered vehicles. In *Battery Conference on Applications and Advances, 1995., Proceedings of the Tenth Annual*, pages 117–122, 1995.
- [27] C. J. M. Doggen. Wireless state feedback and control of a pipe inspection robot. Msc report 029ce2010, University of Twente, December 2010.
- [28] E. H. Drost. Measurement system for pipe profiling. Msc report 003ce2009, University of Twente, March 2009.
- [29] O. Duran, K. Althoefer, and L.D. Seneviratne. State of the art in sensor technologies for sewer inspection. *Sensors Journal, IEEE*, 2(2):73–81, 2002.
- [30] O. Duran, K. Althoefer, and L.D. Seneviratne. Automated pipe defect detection and categorization using camera/laser-based profiler and artificial neural network. *Automation Science and Engineering, IEEE Transactions on*, 4(1):118–126, 2007.
- [31] C. Ekes and B. Neduczka. Pipe condition assessments using pipe penetrating radar. In *Ground Penetrating Radar (GPR), 2012 14th International Conference on*, pages 840–843, 2012.
- [32] Reyes Enciso and Thierry Viéville. Experimental self-calibration from four views. In Carlo Braccini, Leila DeFloriani, and Gianni Vernazza, editors, *Image Analysis and Processing*, volume 974 of *Lecture Notes in Computer Science*, pages 307–312. Springer Berlin Heidelberg, 1995.
- [33] H.V. Fuchs and R. Riehle. Ten years of experience with leak detection by acoustic signal analysis. *Applied Acoustics*, 33(1):1 – 19, 1991.
- [34] T. Fukuda, H. Hosokai, and M. Uemura. Rubber gas actuator driven by hydrogen storage alloy for in-pipe inspection mobile robot with flexible structure. In *Robotics and Automation, 1989. Proceedings., 1989 IEEE International Conference on*, pages 1847–1852 vol.3, 1989.
- [35] Gerhard Geiger. Leak detection and locating - a survey. Technical report, Pipeline Simulation Interest Group (PSIG), 2003.
- [36] Se gon Roh and Hyouk Ryeol Choi. Differential-drive in-pipe robot for differential-drive in-pipe robot for moving inside urban gas pipelines. *IEEE TRANSACTIONS ON ROBOTICS*, 21(1), 2005.
- [37] Se gon Roh, Do Wan Kim, Jung-Sub Lee, Hyungpil Moon, and Hyouk-Ryeol Choi. Modularized in-pipe robot capable of selective navigation inside of pipelines. In *Intelligent Robots and Systems, 2008. IROS 2008. IEEE/RSJ International Conference on*, pages 1724–1729, 2008.

- [38] R. M. Gooch, T. A. Clarke, and T.J. Ellis. A semi-autonomous sewer surveillance and inspection vehicle. In *Intelligent Vehicles Symposium, 1996., Proceedings of the 1996 IEEE*, pages 64–69, 1996.
- [39] Qi Haiming, Zhang Xiaohua, Chen Hongjun, Sun Dongchang, and Sun Yongtai. Global localization of in-pipe robot based on ultra-long wave antenna array and global positioning system. *Hightech Technology Letters*, 15(21):120–125, June 2009.
- [40] P. Hansen, H. Alismail, P. Rander, and B. Browning. Monocular visual odometry for robot localization in lng pipes. In *Robotics and Automation (ICRA), 2011 IEEE International Conference on*, pages 3111–3116, 2011.
- [41] K. Harigaya, K. Adachi, T. Yanagida, M. Yokojima, and T. Nakamura. Development of a peristaltic crawling robot for sewer pipe inspection. In *Mechatronics (ICM), 2013 IEEE International Conference on*, pages 267–272, 2013.
- [42] Brosl Hasslacher and Mark W. Tilden. Living machines. *Robotics and Autonomous Systems*, 15(1-2):143–169, 1995.
- [43] Shigeo Hirose, Hidetaka Ohno, Takeo Mitsui, and Kiichi Suyama. Design of in-pipe inspection vehicles for $\varphi 25$, $\varphi 50$, $\varphi 150$ pipes. In *Robotics and Automation, 1999. Proceedings. 1999 IEEE International Conference on*, volume 3, pages 2309–2314. IEEE, 1999.
- [44] James K Hopkins, Brent W Spranklin, and Satyandra K Gupta. A survey of snake-inspired robot designs. *Bioinspiration & Biomimetics*, 4(2):021001, 2009.
- [45] Mihaita Horodinca, Ioan Doroftei, Emmanuel Mignon, and André Preumont. A simple architecture for in-pipe inspection robots. In *Proc. Int. Colloq. Mobile, Autonomous Systems*, pages 61–64, 2002.
- [46] I.N. Ismail, A. Anuar, K.S.M. Sahari, M.Z. Baharuddin, M. Fairuz, A. Jalal, and J.M. Saad. Development of in-pipe inspection robot: A review. In *Sustainable Utilization and Development in Engineering and Technology (STUDENT), 2012 IEEE Conference on*, pages 310–315, 2012.
- [47] C.S. James and G.W. Henry. Control wire dispenser for a guided missile, May 16 1967. US Patent 3,319,781.
- [48] Anouar Jamoussi. Robotic nde: A new solution for in-line pipe inspection. In *3rd MENDT - Middle East Nondestructive Testing Conference & Exhibition, Bahrain, Manama*. www.ndt.net, November 2005.
- [49] B. Jayawardhana, H. Logemann, and E.P. Ryan. Pid control of second-order systems with hysteresis. In *Decision and Control, 2007 46th IEEE Conference on*, pages 4626–4630, Dec 2007.

- [50] Y. Kawaguchi, I. Yoshida, H. Kurumatani, T. Kikuta, and Y. Yamada. Internal pipe inspection robot. In *Robotics and Automation, 1995. Proceedings., 1995 IEEE International Conference on*, volume 1, pages 857–862 vol.1, 1995.
- [51] Ho Moon Kim, Jung Seok Suh, Yun Seok Choi, Tran Duc Trong, Hyungpil Moon, Jachoon Koo, Sungmoo Ryew, and Hyouk Ryeol Choi. An in-pipe robot with multi-axial differential gear mechanism. In *Robotics and Automation, 2013. Proceedings. ICRA '13. 2013 IEEE International Conference on*, 2013.
- [52] Tatsuya Kishi, Megumi Ikeuchi, and Taro Nakamura. Development of a peristaltic crawling inspection robot development of a peristaltic crawling inspection robot for 1-inch gas pipes with continuous elbows. In *Intelligent Robots and Systems, 2013. IROS 2013. IEEE/RSJ International Conference on*, 2013.
- [53] KIWA. Storingsrapportage gasdistributienetten 2012. Technical Report GT-130047, KIWA, April 2013.
- [54] Marina Kolesnik. Visual orientation and motion control of makro - adaptation to the sewer environment. In *in Proc. 7th Int. Conf. on Simulation of Adaptive Behavior*, pages 62–69. MIT Press, 2002.
- [55] D. Krysz and H. Najjaran. Development of visual simultaneous localization and mapping (vslam) for a pipe inspection robot. In *Computational Intelligence in Robotics and Automation, 2007. CIRA 2007. International Symposium on*, pages 344–349, 2007.
- [56] H. B Kuntze and H. Haffner. Experiences with the development of a robot for smart multisensory pipe inspection. In *Robotics and Automation, 1998. Proceedings. 1998 IEEE International Conference on*, volume 2, pages 1773–1778 vol.2, 1998.
- [57] G.W. LeCompte. High density filament winding and method for producing improved crossovers and inside payout, October 13 1992. US Patent 5,154,366.
- [58] Angelika Mader and Edwin Dertien. How to educate for creativity in creative technology. In Arthur Eger and Wouter Eggink, editors, *The 16th international conference on Engineering and Product Design Education (E&PDE2014)*, September 2014.
- [59] M. Maree and P. Moreau. Coil of very long optical fibre usable on a wire-guided missile, June 11 1991. US Patent 5,022,603.
- [60] T. Mennink. Self localization of pirate inside a partially structured environment. Msc report 027ce2010, University of Twente, December 2010.

- [61] R.J.E. Merry, M.J.G. van de Molengraft, and M. Steinbuch. Velocity and acceleration estimation for optical incremental encoders. *Mechatronics*, 20(1):20–26, 2010. Special Issue on Servo Control for Data Storage and Precision Systems, from 17th IFAC World Congress 2008.
- [62] Yunus A. Cengel Michael A. Boles. *Thermodynamics: And Engineering Approach*. McGraw-Hill, 1994.
- [63] Josep M. Mirats Tur and William Garthwaite. Robotic devices for water main in-pipe inspection: A survey. *Journal of Field Robotics*, 27(4):491–508, 2010.
- [64] Osama Moselhi and Tariq Shehab-Eldeen. Automated detection of surface defects in water and sewer pipes. *Automation in Construction*, 8:581–588, 1999.
- [65] A. A F Nassiraei, Y. Kawamura, A. Ahrary, Y. Mikuriya, and K. Ishii. Concept and design of a fully autonomous sewer pipe inspection mobile robot "kantaro". In *Robotics and Automation, 2007 IEEE International Conference on*, pages 136–143, 2007.
- [66] W. Neubauer. A spider-like robot that climbs vertically in ducts or pipes. In *Intelligent Robots and Systems '94. 'Advanced Robotic Systems and the Real World', IROS '94. Proceedings of the IEEE/RSJ/GI International Conference on*, volume 2, pages 1178–1185 vol.2, 1994.
- [67] Manabu ONO and Shigeo KATO. A study of an earthworm type inspection robot movable in long pipes. *International Journal of Advanced Robotic Systems*, 7(1), 2010.
- [68] Jungwan Park, Dongjun Hyun, Woong-Hee Cho, Tae-Hyun Kim, and Hyun-Seok Yang. Normal-force control for an in-pipe robot according to the inclination of pipelines. *Industrial Electronics, IEEE Transactions on*, 58(12):5304–5310, 2011.
- [69] F. Parrini, M. Pieraccini, Alessandro Spinetti, G. Macaluso, Gilberto Grazzini, G. De Pasquale, H. Scott, A.G. Yarovoy, P.J. Aubry, and D. Caratelli. Orfeus project: the surface gpr system. In *Radar Conference, 2009. EuRAD 2009. European*, pages 93–96, 2009.
- [70] G.A. Pratt and M.M. Williamson. Series elastic actuators. In *Intelligent Robots and Systems 95. 'Human Robot Interaction and Cooperative Robots', Proceedings. 1995 IEEE/RSJ International Conference on*, volume 1, pages 399–406 vol.1, 1995.
- [71] C. Pulles, E. C. Dertien, H. J. van de Pol, and R. Nispeling. Pirate, the development of an autonomous gas distribution system inspection robot. In *International Gas union Research Conference, IGRC 2008, Paris, France, USA, October 2008*. Curan Associates.

- [72] Kees Pulles. Programma van eisen robotinspectie gasdistributieleidingen. Technical report, KIWA, 2006.
- [73] Kees Pulles, Mathijs Kippers, and Gert Wouterse. Acoustic leak monitoring. Technical report, KIWA, 2013.
- [74] B.V. Ratnakumar, M.C. Smart, G. Halpert, A. Kindler, H. Frank, S. Di Stefano, R. Ewell, and S. Surampudia. Litium batteries on 2003 mars exploration rover. In *Battery Conference on Applications and Advances, 2002. The Seventeenth Annual*, pages 47–51, 2002.
- [75] H. W. Reemeijer. Control of a pipe inspection robot. Msc thesis, Control Laboratory, University of Twente, May 2010.
- [76] Mark Reiling. Implementation of a monocular vision system for pipe inspection robot pirate. Master's thesis, University of Twente, 2014.
- [77] Mitchel Resnick and Eric Rosenbaum. Designing for tinkability. In *Design, Make, Play: Growing the Next Design, Make, Play: Growing the Next Generation of STEM Innovators*, pages 163–180. Taylor and Francis, 2013.
- [78] Edward A. Rietman, Mark W. Tilden, and Manor Askenazi. Analog computation with rings of quasiperiodic oscillators: the microdynamics of cognition in living machines. *Robotics and Autonomous Systems*, 45(3–4):249 – 263, 2003.
- [79] Se-gon Roh, DoWan Kim, Jung-Sub Lee, Hyungpil Moon, and HyoukRyeol Choi. In-pipe robot based on selective drive mechanism. *International Journal of Control, Automation and Systems*, 7(1):105–112, 2009.
- [80] S.G. Roh, S.M. Ryew, J. H. Yang, and H.R. Choi. Actively steerable in-pipe inspection robots for underground urban gas pipelines. In *Robotics and Automation, 2001. Proceedings 2001 ICRA. IEEE International Conference on*, volume 1, pages 761–766 vol.1, 2001.
- [81] Erich Rome, Joachim Hertzberg, Frank Kirchner, Ulrich Licht, and Thomas Christaller. Towards autonomous sewer robots: the {MAKRO} project. *Urban Water*, 1(1):57 – 70, 1999.
- [82] Nur Shahida Roslin, Adzly Anuar, Muhammad Fairuz Abdul Jalal, and Khairul Salleh Mohamed Sahari. A review: Hybrid locomotion of in-pipe inspection robot. *Procedia Engineering*, 41(0):1456 – 1462, 2012. International Symposium on Robotics and Intelligent Sensors 2012 (IRIS 2012).
- [83] K. Sato, T. Ohki, and Hun ok Lim. Development of in-pipe robot capable of coping with various diameters. In *Control, Automation and Systems (ICCAS), 2011 11th International Conference on*, pages 1076–1081, 2011.

- [84] Hagen Schempf, Edward Mutschler, Alan Gavaert, George Skoptsov, and William Crowley. Visual and nondestructive evaluation inspection of live gas mains using the explorer™ family of pipe robots. *Journal of Field Robotics*, 27(3):217–249, 2010.
- [85] Hagen Schempf, Edward Mutschler, Vitaly Goltsbergm, and William Crowley. Grislee: Gasmain repair and inspection system for live entry environments. *The International Journal of Robotics Research*, 22(7-8):603–616, 2003.
- [86] Dennis Schipper. *Mobile Autonomous Robot Twente*. PhD thesis, University of Twente, 2001.
- [87] Donald A. Schön. *The Reflective Practitioner - How Professionals Think in Action*. Basic Books, 1982.
- [88] Zhang Sheng, A. Toshiyuki, and H. Shoji. Gas leakage detection system using kalman filter. In *Signal Processing, 2004. Proceedings. ICSP '04. 2004 7th International Conference on*, volume 3, pages 2533–2536 vol.3, Aug 2004.
- [89] A. Shibata, M. Konishi, Y. Abe, R. Hasegawa, M. Watanabe, and H. Kamijo. Neuro based acoustic diagnosis of gas leakage in pipeline. In *SICE Annual Conference, 2008*, pages 283–287, Aug 2008.
- [90] Herbert A. Simon. *The Sciences of the Artificial*. The MIT Press, 1996.
- [91] S. A. Spijksma. Redesign of the pirate bending module. Technical report, Laboratory for Mechanical Automation and Mechatronics - DEMCON, 2009.
- [92] Stephen Stancliff, John Dolan, and Ashitey Trebi-ollennu. Towards a predictive model of mobile robot reliability. Technical report, Carnegie Mellon University, 2005.
- [93] Stephen B. Stancliff. *Planning to Fail: Incorporating Reliability into Design and Mission Planning for Mobile Robots*. PhD thesis, Carnegie Mellon University, 2009.
- [94] J.P.M. Steeman. *Robot-besturing met uw homecomputer*. Elektuur, 1986.
- [95] S. Stramigioli, G. van Oort, and E. Dertien. A concept for a new energy efficient actuator. In *Advanced Intelligent Mechatronics, 2008. AIM 2008. IEEE/ASME International Conference on*, pages 671–675, 2008.
- [96] H. Streich and O. Adria. Software approach for the autonomous inspection robot makro. In *Robotics and Automation, 2004. Proceedings. ICRA '04. 2004 IEEE International Conference on*, volume 4, pages 3411–3416 Vol.4, 2004.

- [97] F. Tache, W. Fischer, R. Siegwart, R. Moser, and F. Mondada. Compact magnetic wheeled robot with high mobility for inspecting complex shaped pipe structures. In *Intelligent Robots and Systems, 2007. IROS 2007. IEEE/RSJ International Conference on*, pages 261–266, 2007.
- [98] Fabien Tache, Francois Pomerleau, Gilles Caprari, Roland Siegwart, Michael Bosse, and Roland Moser. Three-dimensional localization for the magnebike inspection robot. *Journal of Field Robotics*, 28(2):180–203, 2011.
- [99] K. Tadakuma, R. Tadakuma, Keiji Nagatani, Kazuya Yoshida, S. Peters, Martin Udengaard, and K. Iagnemma. Crawler vehicle with circular cross-section unit to realize sideways motion. In *Intelligent Robots and Systems, 2008. IROS 2008. IEEE/RSJ International Conference on*, pages 2422–2428, 2008.
- [100] Timothy M. Terry. Pipeline leak detection technology conference. Technical report, Alaska Department of Environmental Conservation, 2011.
- [101] T. Tsubouchi, S. Takaki, Y. Kawaguchi, and S. Yuta. A straight pipe observation from the inside by laser spot array and a tv camera. In *Intelligent Robots and Systems, 2000. (IROS 2000). Proceedings. 2000 IEEE/RSJ International Conference on*, volume 1, pages 82–87 vol.1, 2000.
- [102] Henk van Bruchem and Bert Wikkerink. De opbouw van het gasdistributienet. Technical Report 18, Gasnet, September 2004.
- [103] Pieter van Vollenhoven. Gasexplosie na breuk van gasdistributieleiding. Technical report, Raad voor de transportveiligheid, 2002.
- [104] J. J. G. Vennegoor op Nijhuis. Development of a pipe inspection robot. Master's thesis, Laboratory of Mechanical Automation and Mechatronics, University of Twente, 2007.
- [105] Walter G. Vincenti. *What Engineers Know and How They Know It*. Johns Hopkins, 1990.
- [106] Roy Visser. *Residual Lifetime Assessment of UPVC Gas Pipes*. PhD thesis, University of Twente, 2011.
- [107] P. van Vollenhoven. Grijs gietijzeren gasleidingen. Technical report, De Onderzoeksraad voor de Veiligheid, 2009.
- [108] George C. Vradis and William Leary. Development of an inspection platform and a suite of sensors for assessing corrosion and mechanical damage on unpiggable transmission mains. Technical report, Foster Miller, March 2004.
- [109] C. Wright, Austin Buchan, B. Brown, J. Geist, M. Schwerin, D. Rollinson, Matthew Tesch, and H. Choset. Design and architecture of the unified modular snake robot. In *Robotics and Automation (ICRA), 2012 IEEE International Conference on*, pages 4347–4354, 2012.

- [110] C. Wright, A. Johnson, A. Peck, Z. McCord, A. Naaktgeboren, P. Gianfortoni, M. Gonzalez-Rivero, R. Hatton, and H. Choset. Design of a modular snake robot. In *Intelligent Robots and Systems, 2007. IROS 2007. IEEE/RSJ International Conference on*, pages 2609–2614, 2007.
- [111] Kun Xu, A.R. Luxmoore, and T. Davies. Sewer pipe deformation assessment by image analysis of video surveys. *Pattern Recognition*, 31(2):169 – 180, 1998.
- [112] Wu Xue-Mei, Tuo Xian-Guo, Li Zhe, Liu Ming-Zhe, Zhang Jin-Zhao, Dong Xiang-Long, and Li Ping-Chuan. Radioactive source localization inside pipes using a long-range alpha detector. *Chinese Physics C*, 37(8):086201, 2013.
- [113] S. Yabe, H. Masuta, and Hun ok Lim. New in-pipe robot capable of coping with various diameters. In *Control, Automation and Systems (ICCAS), 2012 12th International Conference on*, pages 151–156, 2012.
- [114] Mures Zarea, Gael Pognonec, Christina Schmidt, Tilo Schnur, Josa Lana, Christoph Boehm, Marco Buschmann, Chabane Mazri, and Eric Rigaud. First steps in developing an automated aerial surveillance approach. *Journal of Risk Research*, 16(3-4):407–420, 2013.
- [115] Wen Wei Zhang and Bao Hua Zhuang. Non-contact laser inspection for the inner wall surface of a pipe. *Measurement Science and Technology*, 9(9):1380, 1998.
- [116] E. Zwicker, W. Zesch, and R. Moser. A modular inspection robot platform for power plant applications. In *Applied Robotics for the Power Industry (CARPI), 2010 1st International Conference on*, pages 1–6, 2010.

The Library didn't only contain magical books, the ones which are chained to their shelves and are very dangerous. It also contained perfectly ordinary books, printed on commonplace paper in mundane ink. It would be a mistake to think that they weren't also dangerous, just because reading them didn't make fireworks go off in the sky. Reading them sometimes did the more dangerous trick of making fireworks go off in the privacy of the reader's brain.

from 'Soul Music', Terry Pratchett, 1994

Ieder boek begint met een ander boek. Het verhaal in dit boek begint met een artikel van Steven Bolt in de 'KIJK' in 1984 over robotmuis 'Willie'¹, gevolgd door 'Robotbesturing met uw Homecomputer' van J.P.M. Steeman in de Elektuur series [94]. Ik kwam het tegen in 1988 in de bibliotheek in Drachten.

Van alle mensen die me hebben gestimuleerd om me met techniek bezig te houden zou ik dit werk vooral willen opdragen aan 'opa' Henk van der Weij, knutselaar, maker, techneut in hart en nieren. Hij overleed in 2008, maar de herinneringen aan de dagen dat we aan robots aan het sleutelen waren in de garage aan de Uthof zijn nog springlevend.

Via de wedstrijden voor 'Jonge Onderzoekers' leerde ik Gijs kennen. Vervolgens zaten we in 1995 samen achter de Acorn BBC (ok, ik liep technisch wat achter, de rest van de wereld had inmiddels tenminste een i486DX2) code te schrijven voor de brandblusrobot. Daarnaast hebben we ook samen de muziek als uitlaatklep: Drienerlalala, bruiloften, partijen en andere nootgevallen. Gijs, ik wil je bedanken voor je vriendschap, je vakmanschap waar het gaat om programmeren, problemen uitrafelen of sommen-maken-over-lopemde-robots-die-toch-niemand-begrijpt en het schrijven van liedjes die dat prachtig kunnen navertellen. Ik hoop in de toekomst nog (en weer) meer projecten samen met jou te kunnen doen. Robots doen het over het algemeen een stuk beter wanneer er een stuk van jouw code in zit...

In Enschede was de Parkweg een fijn thuis en ik vind het super dat we de tradities van het tot Sint-Juttemis uitgestelde Kerstdiner en de (intussen) kind-vriendelijke-vakanties overeind houden terwijl we inmiddels allemaal 'uitpandige inboedel' zijn. Gelukkig hebben we ook met de (huis)band de Gonnagles een excuus om elkaar regelmatig te blijven zien. Lieve Parkweg vrienden, 'Op de Poes, de Kat en de Kater!'

Dennis, ik wil je bedanken voor je fantastische timing bij het op stage gaan in 2001 zodat er aan de Parkweg een kamer vrij kwam (en jouw bereidheid om daarna maar in de bezemkast te gaan wonen). Daarnaast wil ik je bedanken als Vriend, als leidraad, bendelijder en bendeleider (ook bij de Gonnagles). Ik hoop dat onze wegen

¹http://sbolt.home.xs4all.nl/andere_robots.html#willie

elkaar blijven kruisen, bij muziek, (anti) sociaal robot gedrag en andere al dan niet wijselijk toegepaste creatieve technologie.

Stefano, volgens mij had je ons in 2003 nog amper gesproken voordat je Gijs en mij al wegstuurde naar een Summerschool bij EPFL. Ik wil je bedanken voor je betrokkenheid, inspiratie en bevologenheid, in situaties die met robots te maken hebben en vooral ook voor de fijne (en muzikale) situaties daarbuiten. Ik kijk met veel plezier terug op bijvoorbeeld de geweldige conferenties die we voor Dynamic Walking bezochten (die verder weinig meer met dit proefschrift te maken hebben, behalve dat de overgang van 2D naar 3D in geen van beide gevallen triviaal blijkt)

Job (en Gerda), hartelijk bedankt voor jullie grote vertrouwen, betrokkenheid en enthousiasme. Zowel bij het ontwikkelen van Creative Technology, dit proefschrift als de recente activiteiten met stichting ASSortiMENS. Bedankt voor al je commentaar en het gebruik van je mooie L^AT_EX template van het *Dynamical Systems* boek. Ik ben blij dat ik een aantal van de 40 jaar met je in de speeltuin heb mogen doorbrengen.

Angelika, dank voor de fijne zoektocht naar het hoe en wat van creatieve technologie, ontwerpmethodes onderzoeken, voor het bedenken van single value devices en het ons grondig afvragen of er iemand op zit te wachten. Er liggen nog prachtige paden open voor onderzoek en ik hoop er een flink aantal met jou te kunnen bewandelen.

Veel van de ontwikkelingen die ervoor hebben gezorgd dat de robot onderdelen nu gefabriceerd worden op lasersnijders en 3D printers komen uit de bijzondere wereld van de 'Makers'. Harmen en Diana, jullie zijn voor mij een bron van inspiratie, een ankerpunt en mijn voorbeeld bij het opzetten en doen van 'grassroots' onderzoek.

Wout, ik zou ook jou willen bedanken voor je inspirerende 'eigen' experimentele inslag. De experimenten met de eerste 3D printers die we deden hebben uiteindelijk via een omweg weer terug geleid tot het materiaal waarmee de huidige robot geprint wordt (PA) dat we ook in de eerste zelfgebouwde printkop (in de vorm van een nylon trekveer) hebben omgesmolten.

Kees, ik wil je bedanken voor de lange en plezierige samenwerking aan dit project. Vanuit KIWA ben je de motor binnen deze ontwikkelingen, en hoewel we er nog lang niet zijn hoop ik dat je met een goed gevoel terug kunt kijken op de ontwikkelingen tot nu toe.

Dear Ekki, I would like to thank you for offering the opportunity to take this project to a next level, for believing in this concept and defending it within AIR. I would love to see our lab prototype to be turned into something 'robust' and 'industrial'.

Mohammad, thank you very much for the pleasant collaboration (and also for the nice get-togethers with Neda and Nikan). It has been a joy working with you, bringing the 'one room approach' to mechatronics to life. I really appreciate your dedi-

cation and talent for improvisation. I hope we can continue to realise this beautiful (and sometimes impossible) project together.

Meteen daar achteraan hoort dan ook een bedankje voor (en excuus aan) onze kamergenote: Ditske, bedankt voor je onophoudelijke tolerantie jegens alle luide en thousiaste gesprekken, binnenvallende studenten, video opnames, lijm, experimenten met robots en andere zaken die volgens Jan (terecht) in het lab thuishoren en niet in ons kantoor. Ik ben heel blij dat we zo'n leuke (en speciale) periode in het leven als kersverse ouders met elkaar hebben kunnen delen.

De vakgroep RaM (vh Control Engineering) is een fijne plek om robots tot leven te wekken. In wil graag iedereen bedanken die deze groep tot zo'n prettige en productieve werkplek maakt. In het bijzonder wil ik Jolanda, Gerben, Marcel en Alfred bedanken voor de samenwerking. Niet alleen bij dit project, maar ook bij alle activiteiten die we ondernemen om de groep op de kaart te zetten (te houden) en de volgende generaties van het nut en de noodzaak van kennis over techniek te door-dringen. Daarbij ook Douwe, Geert, Dian, Jos, Eamon en alle andere usual suspects waar het gaat om Techniek en Kinderen, voorlichtingsdagen, demo's en Experimenten in het Bos, hartelijk bedankt!

Erik, ik wil jou bedanken voor het optreden als 'achtervang' voor het CreaTe gerelateerde werk tijdens de laatste weken van het schrijfwerk. Volgens mij kunnen we nog een mooie tijd tegemoet zien vol van nieuwe experimenten met onderwijs en het uitvinden wat het studeren van Creative Technology eigenlijk zou moeten betekenen. Gerrit, bedankt voor het vertrouwen in deze onderneming en het mogelijk maken om een mooie kruisbestuiving te laten ontstaan tussen de robotica en creatieve technologie. Daarnaast ook alle andere collega's bij Create: hartelijk bedankt voor jullie betrokkenheid en de fijne samenwerking tot nu toe!

Voor de robot hebben we maar zelden 'gewone' aankopen kunnen doen. Bij bijna alle componenten hadden we speciale wensen of moest het onderste uit de kast of het achterste van de plank geleverd worden. Daarom wil ik graag een aantal mensen (en hun bedrijven) speciaal bedanken: Marjan en Vincent (3DprintCompany) voor het prettige meedenken en de bereidheid om aan experimenten mee te doen. Eric Jan (Parts&Tools); PIRATE is je blijven achtervolgen. Ik geloof dat je bij DEMCON al de eerste versie in elkaar hebt gezet, en na alle prototypes die in dit boekje beschreven staan vast nog niet het laatste onderdeel hebt geproduceerd voor dit project. Ook Fred van Roest (Hankamp Gears) en Hein Vos (Minimotor Benelux) hartelijk bedankt voor alle 'specials' die voor dit project geproduceerd moesten worden. Hoewel het alweer een tijd geleden is wil ik ook graag Jan Leideman, Henk Jan van der Pol, en alle andere (oud) collega's bij DEMCON bedanken voor de leuke tijd daar en de prettige samenwerking bij dit project. Ook Rob Nispeling (Continuon) en Hans van der Vegt (Liander), hartelijk bedankt voor jullie inbreng in de beginfase van dit project!

Ook alle studenten die hebben meegewerkt aan dit project: Jeroen Vennegoor op Nijhuis, Jos Ansink, Harm de Boer, Sytse Spijksma, Eric Drost, Harwin Reemeijer, Bram Burkink, Corne Doggen, Twan Mennink, Jort Baarsma, Maarten Brilman, Dian Borgerink en Mark Reiling, allemaal enorm bedankt voor jullie positieve inzet en constructieve bijdragen aan het project.

Evelien en Magda, ik wil jullie graag bedanken voor de fijne samenwerking en het in stand houden van een dubbel-leven als muzikant. Zonder de ongestoorde momenten met laptop op de achterbank, in de kleedkamer of backstage was dit proefschrift een stuk leger geweest.

Lieve mama, papa, Anjolieke en Jeroen, bedankt voor alle ondersteuning, interesse, gezelligheid en fijne afleiding op zijn tijd!

Lieve Debbie en Bas, bedankt dat jullie mijn thuis willen zijn! Bas, jij verwoordde het laatst heel goed: 'Mama heeft altijd goede ideeën, papa bouwt robots, en ik heb altijd gelijk...'

Edwin Dertien, 19 april 2014

About the Author

Edwin Dertien builds robots and makes music. He was born April 19th, 1979 in Drachten (Smallingerland) and was raised on a diet of LEGO, Fischer Technic and broken television sets. His coming out as roboticist was marked by participation in the International Competition for Young Scientists in Helsinki, 1996. Fortunately this technical side of his personality could be balanced by making music in a large number of bands on keys and bass and by participating regularly in the 'KunstBende' art festival.

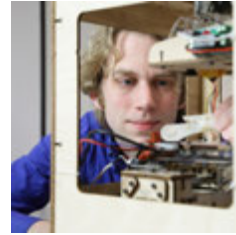


photo by G. van Ouwewerk

The studies Electrical Engineering which he started in 1997 were frequently interrupted with gigs and longer jobs in improv theatre music. He still makes part of his living playing (improv) piano for theatre groups.

During his internship In 2004 at the *Shadow Robot Company* in London, he worked at walking robot spiders for stage performances and miniature pneumatic valve manifolds for the famous Shadow Robot Hand. He also worked as piano player for the *London Theatre Sports group* during that period.

In 2005 he finished the *passive dynamic* walking robot 'Dribbel' and obtained his M.Sc. degree Electrical Engineering, with specialisation in mechatronics, at the Control Engineering group (now Robotics and Mechatronics group) of the University of Twente, under supervision of Stefano Stramigioli.

In the beginning of 2006 he started his own company 'Kunst- en Techniekwerk', since 2008 located in 'het Roombeek' in Enschede, which specialises in (control) systems for art and theatre, such as big robotic sculptures and light installations. An internship of an engineer diagnosed with ASD resulted in the start of a FabLab inspired workshop tailored for people with ASD in 2013 - and the start of the *ASSortiMENS* foundation of which he is technical director.

In september 2006 he started working on the design of a pipe inspection robot at DEMCON, which he continued as PhD project in 2008 at the University of Twente. In the same year he was also invited by Job van Amerongen to participate in the development of the new Creative Technology bachelor programme at the same university, for which he has been working as lecturer since.

He is a very enthusiastic 'maker' and co-organiser of the MakerFaire in Twente (2013). He was invited to give talks at TEDx Amsterdam (2012) and TEDx Zwolle (2013).

Universiteit Twente ontwikkelt gasbuisrobot

We hadden die automatische lasfunctie voor reparaties achterwege moeten laten...

